Title
Regulation of Glucocorticoid Receptor Function by the Coordinated Actions of the Hsp90 and Hsp70 Chaperone

Author
Kirschke, Elaine Colleen

Publication Date
2015

Peer reviewed|Thesis/dissertation

Regulation of Glucocorticoid Receptor Function by the Coordinated Actions of the Hsp90 and Hsp70 Chaperone Cycles

by

Elaine Colleen Kirschke

DISSERTATION

Submitted in partial satisfaction of the requirements for the degree of

DOCTOR OF PHILOSOPHY

in

Biophysics

in the

GRADUATE DIVISION

of the

UNIVERSITY OF CALIFORNIA, SAN FRANCISCO

[redacted]

Acknowledgments

First and foremost, I would like to thank David Agard. Working with David has been a phenomenal scientific experience. I cannot thank him enough for all his guidance, encouragement and mentorship throughout the years. I have thoroughly enjoyed the unique scientific environment that he creates which fosters excellence, creativity, and fun.

For my thesis committee Keith Yamamoto and Robert Fletterick, I would like to thank them for all their guidance and tremendous support. I could not have asked for a better set of expertise to help guide me through this project.

Daniel Southworth deserves special thanks for all his guidance and scientific insight, especially during my first 4 years in the lab. My success would not have been possible without his intellectual contributions and encouragement during critical points in the project.

The Hsp90 subgroup throughout the years has been a brilliant and supporting group. The success of this project is in part due to the pioneering work on Hsp90 in the lab carried out by Daniel Southworth, Kristin Krukenberg, Christian Cunningham, Ulrike Boettcher, and Timothy Street. Of the Hsp90 subgroup, I would like to express special thanks to Laura Lavery and Daniel Elnatan for the hours of insightful and enjoyable in-depth scientific discussions.

Much of the EM would not have been possible without the help and guidance of Daniel Southworth, Justin Kollman, Elizabeth Montabana, and Klim Verba.

Samuel Pfaff was the brave graduate student in the Fletterick lab who pioneered the apo GRLBD purification. He was very supportive in helping me get started with GR and provided many helpful discussions.

I am grateful to Derishi Goswami and Patrick Griffin, for their efficiency in generating the high quality HDXMS data that turned out to be incredibly insightful. The collaboration was both productive and a pleasure.

I express my gratitude to Mariano Tobias and Joyce Ramponi for both being a pleasure to work with and for ensuring that the lab is always running at optimal efficiency. Also, thanks to Mariano for seeing to my nutritional needs, it is likely because of him that I didn't get scurvy during graduate school.

To the ladies of UCSF, Laura Lavery, Elizabeth Montabana, Rebeca Choy and Rose Citron, you are delightful, brilliant and inspiring women, all in your own special ways. I consider myself blessed to have had such a strong support group and to have made such good friends during my time at UCSF.

To Brian Koch, not only have you been a loving and supportive spouse, you have also given me so much helpful advice throughout my graduate career. Thank you for keeping me grounded and helping me keep the big picture in perspective. Even though your puns are terrible, you were always able to make me laugh after those long days in the lab when I felt like I was never going to get my project to work. Thank you for always believing in me.

Regulation of Glucocorticoid Receptor Function by the Coordinated Actions of the Hsp90 and Hsp70 Chaperone Cycles

Elaine Colleen Kirschke

Laboratory of Dr. David Agard

Hsp90 is a ubiquitous ATP dependent molecular chaperone with numerous "client" proteins that depend on Hsp90 for activation. In eukaryotes, Hsp90's ability to hydrolyze ATP is essential, yet it is entirely unclear how hydrolysis is promoting client activation. One of Hsp90's clients, the Glucocorticoid Receptor (GR), is a ligand activated transcription factor that regulates many biologically important genes. Although Hsp90 is required for GR ligand binding *in vivo*, purified apo GR is fully capable of binding ligand with no enhancement from Hsp90. We reveal that Hsp70, known to facilitate client delivery to Hsp90, inactivates GR through partial unfolding of GR in a region important for ligand binding. Hsp90, with the cochaperones Hop and p23, reverses this inactivation, promoting ligand binding.

Recovery of ligand binding requires ATP hydrolysis on Hsp90. This indicates that energy from ATP hydrolysis on Hsp90 regulates client transfer from Hsp70, likely through the coupling of the two chaperone's ATP cycles. Such coupling is embodied in novel contacts between the ATPase domains of Hsp90 and Hsp70 in the GR:Hsp70:Hsp90:Hop complex by cryo-EM. This complex reveals that not only

does Hop precisely recruiting and orienting Hsp70's substrate binding domain such the GR is delivered to the client binding site on Hsp90, but Hop also coordinates the direct contact between the ATPase domains by inducing a specific conformation on Hsp90 required for the Hsp90:Hsp70 interaction.

Comparison of Hsp90's release function with release by a traditional Hsp70 nucleotide exchange factor, Bag-1, reveals that GR release initiated with Bag-1 also results in GR ligand binding recovery. However, while GR function is both recovered and maintained by the Hsp90 system, for Bag-1, rapid ligand binding recovery is accompanied by a gradual loss of function due to aggregation. This provides evidence for a refolding event occurring on Hsp90 after Hsp70 release. The loss of function observed with Bag-1 illustrates the need for coupling the release of the partially folded GR from Hsp70 to Hsp90's chaperone abilities, with precise coordination during client handoff protecting against aggregation.

Furthermore, cycling with the entire chaperone system results in enhanced GR function in the form of faster ligand association and dissociation rates, with an overall increase in ligand affinity. This indicates that the unfolding and refolding with the chaperones increases the accessibility of the ligand binding pocket, enabling the receptor to more rapidly respond to sudden changes in cellular ligand levels, while being protected from aggregation. Together, this work illustrates how the coordinated chaperone interactions can enhance stability, function and regulation.

Table of Contents

List of Tables

Appendix Section 2:

List of Figures

Chapter 1:

Chapter 2:

Chapter 3:

Chapter 4:

Chapter 5:

Chapter 6:

Chapter 7:

Chapter 8:

Appendix Section 3:

Appendix Section 4:

Chapter 1

Introduction

Hsp90

Hsp90 is a ubiquitous ATP-dependent molecular chaperone with numerous client proteins that depend on Hsp90 for activation (Taipale et al., 2010). While most canonical chaperones, such as Hsp70, recognize unfolded proteins by binding stretches of exposed hydrophobic residues, Hsp90 is unique because it acts in the later stages of folding by binding to partially folded intermediates (Jakob et al., 1995). Extensive biophysical and structural studies on Hsp90 have revealed a complex ATP hydrolysis cycle in which Hsp90 undergoes dramatic conformational rearrangements during its ATP cycle (Figure1) (Krukenberg et al., 2011). Hsp90 is a high affinity homodimer that is dimerized in the apo state through its C-terminal domains (CTD) and adopts a flexible and extended v-shaped conformation (Krukenberg et al., 2008). The N-terminal domains (NTD) contain the nucleotide binding sites to which ATP binding stabilizes rearrangements of the domains such that the arms come together in a closed conformation with a secondary dimerization interface between the NTDs (Ali et al., 2006). NTD dimerization then promotes ATP hydrolysis (Wegele et al., 2003). In general, Hsp90 is a relatively weak ATPase limited by slow NTD dimerization (Hessling et al., 2009). While Hsp90's ATPase activity is essential (Obermann et al., 1998), it is unclear how ATP hydrolysis promotes client folding and activation. Given the number of biologically important Hsp90 clients involved in the

progression of cancer and other diseases, understanding the mechanism of client activation will have significant therapeutic benefits.

In the eukaryotic system, there are several cochaperones that facilitate the progression of Hsp90's chaperone cycle by stabilizing specific conformations of Hsp90 along the pathway. Two of the better-characterized cochaperones relevant to this study are Hop and p23. Hop assists the client loading stage of the cycle by binding to the open state of Hsp90 and facilitates the delivery of the client bound Hsp70 complex to Hsp90. While Hop was originally thought to act solely as an adaptor protein that facilitates client delivery by providing a physical link between Hsp70 and Hsp90 (Chen and Smith, 1998), a recent cryo-EM reconstruction of the Hsp90:HOP complex revealed that Hop forms an extensive complex with an alternate open conformation of Hsp90 (Southworth and Agard, 2011). More specifically, Hop stabilizes both a more compact MD-CTD orientation seen in the apo crystal structure (Shiau et al., 2006), and promotes an upward rotation of the NTD relative to the MD such that the NTDs are pre-organized for ATP hydrolysis, but blocked from proceeding to closure. Simultaneously, these motions cause the alignment of the hydrophobic regions along the cleft in a way that could facilitate client binding.

The second important Hsp90 cochaperone, p23, has been identified to play a role in the later stages of the pathway by binding to the Hsp90 complex in which GR is in its ligand binding competent state (Dittmar et al., 1997). Like Hop, p23 inhibits ATP hydrolysis by binding and stabilizing a non-catalytic state in the cycle. However, while Hop and p23 bind to distinct regions on Hsp90, their binding is competitive. Hop binds to the open state, while p23 requires the closed nucleotide bound state of Hsp90. However, biophysical

investigations with cochaperones have lacked clients, thus their actions in the context of GR are still uncertain.

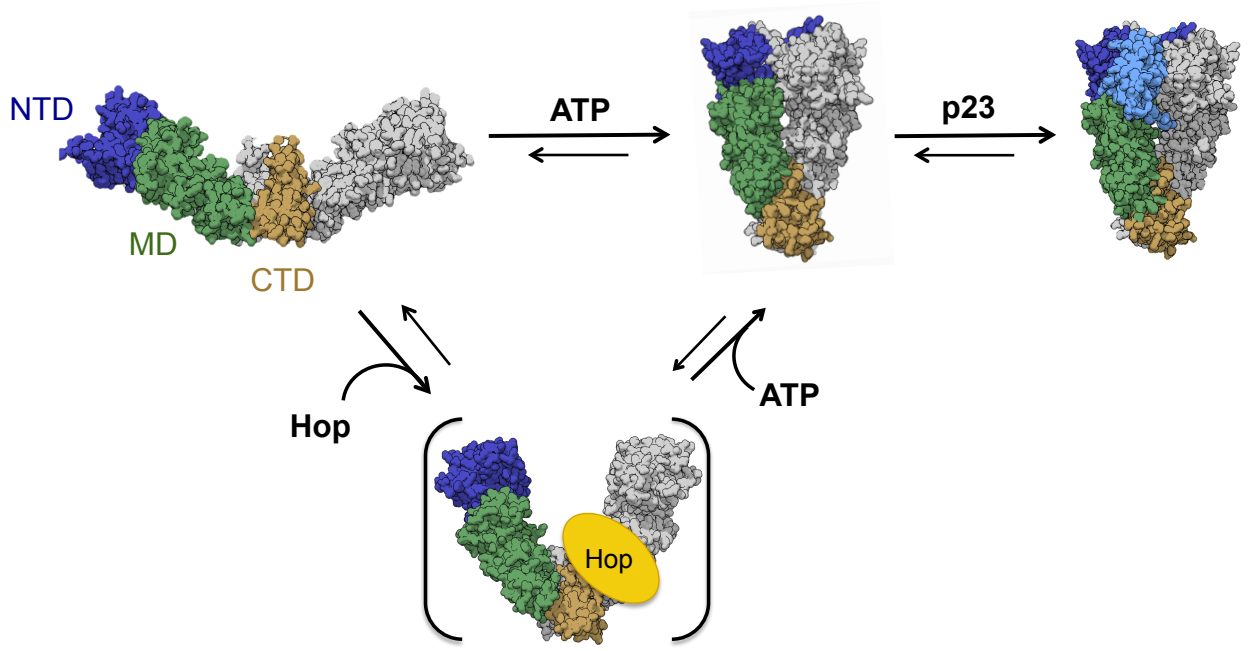

Figure 1. Hsp90's ATP driven chaperone cycle.
Hsp90's chaperone cycle involved dramatic structural rearrangements. In the absence of nucleotide, the Hsp90 homodimer is dimerized at its C-terminal domain (CTD) in brown. and exists in an extended flexible state. ATP binding to the N-terminal nucleotide binding domain (NTD) in dark blue stabilizes a compact state with a second dimerization interface formed between the NTDs. The cochaperone p23 (light blue) binds to and stabilizes the closed state. The cochaperone Hop (yellow) stabilizes an intermediate state between the open and closed state in which there is a compaction of the v-shape resulting from movement of the middle domain (MD) (green) about the MD-CTD interface. Additionally the NTD rotate upward about the MD interface such that the secondary dimer interfaces in the NTDs are aligned.

The Glucocorticoid Receptor

The Glucocorticoid Receptor (GR) is a well-known obligate Hsp90 client. GR is a ligand activated transcription factor that regulates transcription of numerous genes involved in critical biological processes such as glucose metabolism and immune function (Chrousos and Kino, 2009). *In vivo* it has been clearly shown that Hsp90 is required for GR

to bind ligand and become active (Picard et al., 1990). To varying degrees, Hsp90 interacts in a similar fashion with other steroid hormone receptors, a subclass of the nuclear receptor superfamily that includes the progesterone receptor (PR), the mineralocorticoid receptor (MR), the androgen receptor (AR), and the estrogen receptor (ER). Like most nuclear receptors, GR is a modular protein with three major functional domains; a highly variable N-terminal modulation domain, a conserved DNA binding domain (DBD), and a moderately conserved C-terminal ligand binding domain (LBD) (Figure 2A).

The DBD localizes the receptor to the response elements (RE) by recognizing specific DNA sequences. For transcription activation, this involves two DBDs cooperatively binding to palindromic DNA sequences as a head to head homodimer (Luisi et al., 1991; Watson et al., 2013) (Figure 2B). Once on the DNA, the N-terminal modulation domain, which contains the activation function 1 (AF-1), interacts with the transcription machinery at the RE to regulate transcription. In addition to being highly variable in sequence and length, these domains are intrinsically disordered (Chandra et al., 2008), and thus not well understood. Between the DBD and the LBD is a short sequence referred to as the hinge. While the role of the hinge is mostly unclear, insight into its function is emerging from crystal structures of intact DBD-LBDs of other nuclear receptor constructs bound to DNA. Several structures reveal that at least one of the hinges makes extensive interactions with DNA and coordinates contacts between domains (Chandra et al., 2008; 2013; Lou et al., 2014). Yet, the overall arrangement of the hinge and the different domains while bound to DNA differs dramatically between all the structures solved so far, with the quaternary structure dictated by non-conserved surface residues. Therefore, the domain organization of GR bound to DNA and the exact structural role of GR's hinge is still unknown.

The receptor activity is regulated through its LBD. All LBDs have a similar mostly helical structure with the ligand binding pocket located in the core of the protein (Figure 2D). In the absence of ligand, LBDs are thought to be dynamic, with the ligand providing both structural stability and allosteric control of the LBD's ability to interact with co-regulator proteins to modulate transcription (Bain et al., 2007). More specifically, the most dramatic change in the LBD upon ligand binding is in the C-terminal helix12, with agonists stabilizing the packing of helix12 in a way that forms the hydrophobic groove recognized by co-activators (Bledsoe et al., 2002). Reciprocally, antagonist bind such that the ligand protrudes from the ligand binding pocket and prevents the packing of helix-12 as in the agonist state (Kauppi, 2003). In this case, helix 12 can reposition and bind within the hydrophobic co-activator groove, thus occluding co-activator binding (Schoch et al., 2010). In the first reported crystal structure of the GRLBD, the agonist form of GRLBD bound with dexamethasone (dex) and a co-activator peptide crystalized as a dimer, with a novel dimer interface centered on the β-sheet region. This dimer interface was shown by mutagenesis to be functionally relevant for transactivation *in vivo*, however, later crystal structures indicate that the dimerization state and interface varied among different agonist crystal structures (He et al., 2014; Kauppi, 2003). Furthermore, while the first publication of the GRLBD dimer structure reported a dimerization affinity of 1.5μM, measured by analytical centrifugation in the presence of dex and co-activator peptide (Bledsoe et al., 2002), later reports indicate the purified ligand bound GRLBD is mostly monomeric, with only a small fraction (~10%) of dimer population detected during the purification (Schoch et al., 2010).

Hsp90 interacts directly with GR through its LBD (Howard et al., 1990). It is unclear why Hsp90 is required nor how Hsp90 activates GR for ligand binding. A likely explanation

is that GR's cognate ligand, cortisol (Figure 2C) is very hydrophobic, and the vacant hydrophobic binding pocket would be inherently unstable and prone to aggregation. Hsp90 is proposed to bind to and stabilize the apo binding pocket, allowing it to exist in a state that can both readily bind ligand and is protected from aggregation. A more detailed model for how Hsp90 might be stabilizing the apo GRLBD is discussed in the following section.

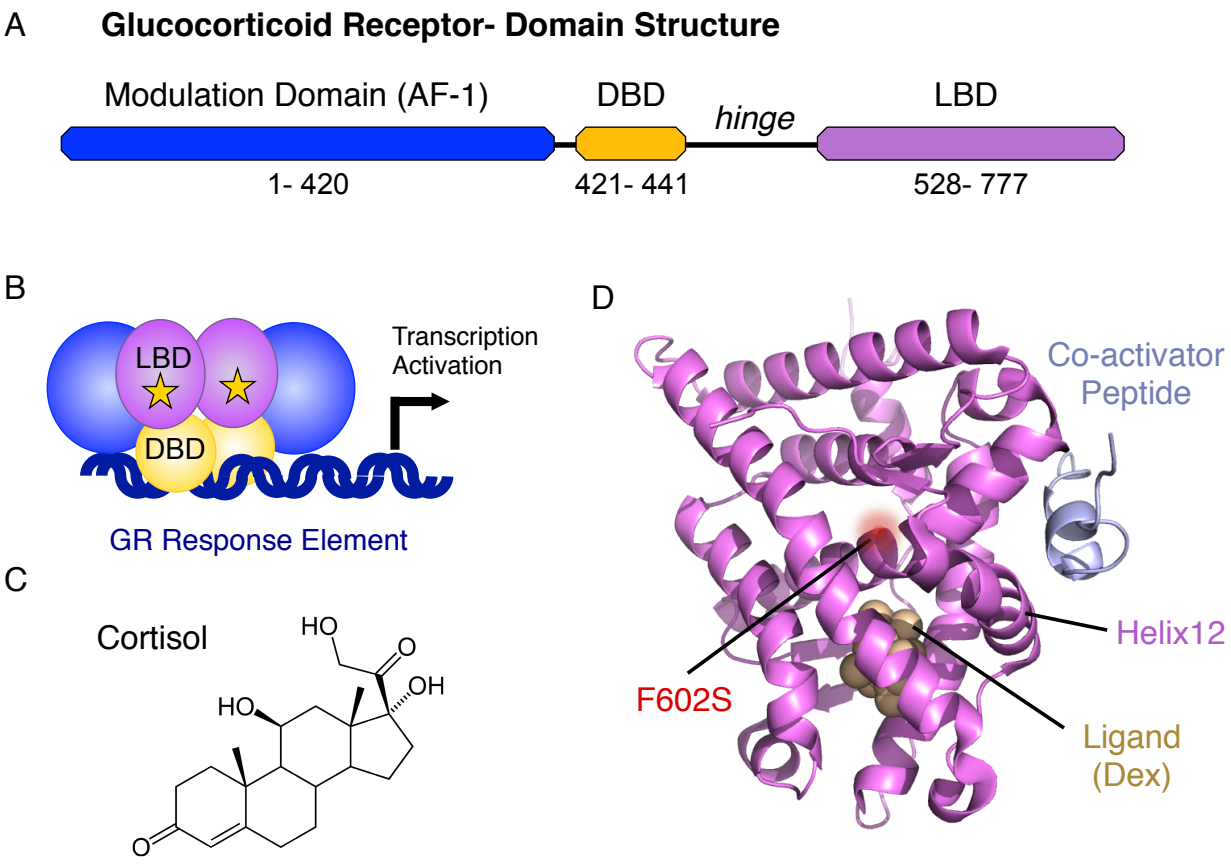

Figure 2. GR Structure and Function.
A) Domain structure of GR.
B) GR binds DNA as a dimer to promote transcription activation.
C) GR's cognate ligand, cortisol.
D) Crystal structure of GRLBD in agonist conformation bound to ligand (dexamethasone) and co-activator peptide (Pdb 1M2Z).

GR F602S mutation is required for recombinant expression of GRLBD

The ability to bacterially express and obtain working quantities of GRLBD for rigorous *in vitro* characterization has to date required the mutation of an internally buried phenylalanine, F602S (Figure 2D). This mutation first turned up in a yeast genetic screen for GR mutants with enhanced ligand efficacy since it has significantly elevated signaling (M J Garabedian, 1992). This mutation was later instrumental in obtaining sufficient expression of recombinant protein for the first reported crystal structure of the GRLBD (Bledsoe et al., 2002). In this case, the F602S mutation was identified by searching for hydrophobic residues in GR potentially contributing to aggregation that are not in closely related hormone receptors, PR and AR, that could be successfully expressed and purified in *E. coli*. Of the 14 residues identified (mostly surface residues), solubility was only enhanced when the buried F602 was mutated to the corresponding residue in PR, serine.

In the F602S ligand bound agonist crystal structure, the serine at position 602 has its side chain is oriented into a small hydrophilic cavity and coordinates an extensive hydrogen bond network including three water molecules with in the small cavity. This suggests that the hydrophobic phenylalanine would be energetically unfavorable at this location, and could be causing local instability responsible for the solubility issues associated with the wild type (WT) GRLBD. However, contrary to this, an unreleased crystal structure of WT GRLBD purified from sf9 cells, indicates that the WT structure is rearranged in the vicinity of F602 in an energetically favorable way, with the F602 forming π-stacking interactions with a neighboring tyrosine (Kauppi, 2003). This suggests that F602 is not necessarily destabilizing the structured agonist state but could be promoting aggregation while GRLBD exist in some other state.

This mutation was more thoroughly investigated when it was independently identified in a yeast genetic screen designed to identify variants of GR that were less dependent on Hsp90 (Ricketson et al., 2007). In this study, the enhanced signaling of GR F602S was found to not be due to an increase in hormone affinity. Instead, the F602S mutation shifts GRLBD's conformational equilibrium towards an agonist state as seen in the co-activator peptide bound crystal structure, indicating that enhanced signaling likely results from an increase in conformational stability. In fact, all of the less Hsp90 dependent mutants identified in the screen shifted GRLBD's equilibrium either to the agonist or antagonist state, suggesting that Hsp90 functions in a comparable way. From this work, the proposed model (Figure 3) is that in the absence of agonist or antagonist, the receptor's helix12 is highly dynamic, and in equilibrium between various conformations. This movement of helix12 results in temporary exposure of the hydrophobic ligand-binding pocket to solvent, allowing for "collapse" or aggregation of the apo receptor. Hsp90 would function to protect the receptor by stabilizing either the agonist or antagonist state.

Further supporting this model, a separate report suggests that Hsp90 has two different modes of interacting with GRLBD, one with the apo and the other with the holo forms of GR (Fang et al., 2006). Here, Hsp90 was found to stabilize an antagonist state of the apo receptor through an interaction mediated by Hsp90's CTD amphipathic helix (CTD helix 2). In this case, Hsp90 amphipathic helix was proposed to displace GRLBD helix 12, preventing it from packing in the agonist conformation (Figure 3). In the presence of ligand, Hsp90 utilizes a different amphipathic helix, CTD helix 1, to stabilize the agonist conformation in a comparable way to the co-activators. The main caveats to this work is

that the *in vitro* experiments were carried out using peptides corresponding to the sequence of Hsp90's interactions sites and not full length Hsp90.

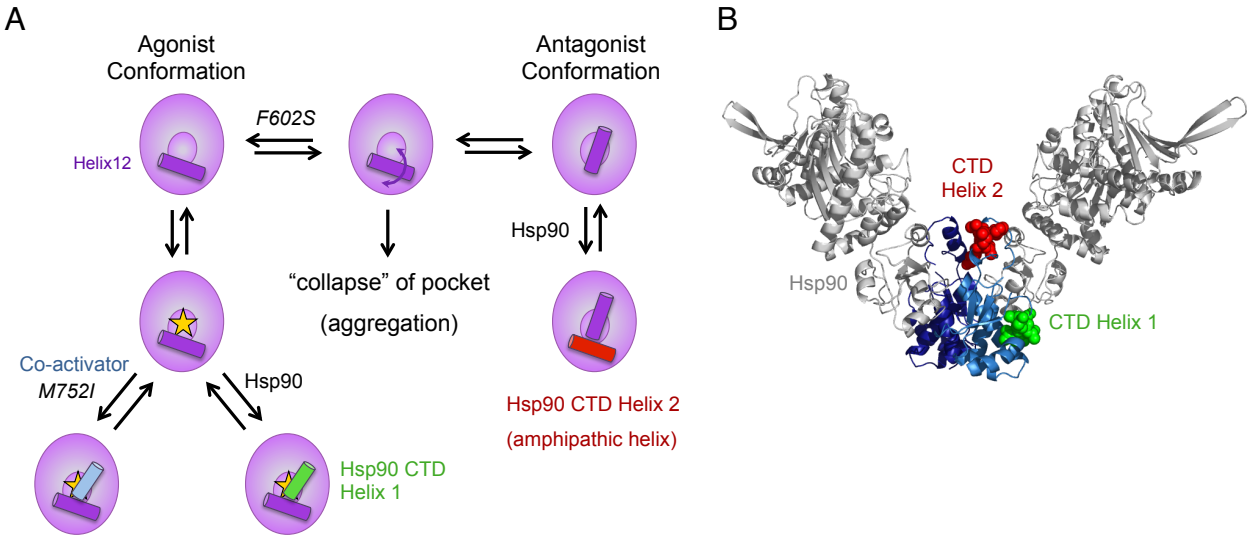

Figure 3. Hsp90 stabilizes GR by shifting GR's equilibrium either to the agonist of antagonist state using two different modes of interaction
A) GRLBD (purple) exists in a conformational equilibrium between multiple states that includes the agonist state (left) and antagonist state (right) defined by the position of helix 12 (dark purple). Stabilization of either conformation reduces the risk of "collapse" of the ligand-binding pocket during transitions between conformations. The F602S is less dependent on Hsp90 because it the mutation stabilizes the agonist state. Hsp90 binds apo GR with its CTD amphipathic helix 12, and stabilizing the antagonist conformation. The ligand bound agonist state is further stabilized by either co-activators, binding to the hydrophobic groove accessible in the agonist state, or by Hsp90, with Hsp90's CTD helix 1 binding in the same fashion as the co-activator. The M752I mutation that was also identified as being less Hsp90 dependent was characterized as stabilizing the agonist co-activator bound conformation of GRLBD. Figure adapted form previous reports (Fang et al., 2006; Ricketson et al., 2007).
B) Crystal structure of Hsp90 (pdb 2IOQ) with CTD (blue), and with the GR interaction sites for GR in (A) mapped onto the structure. The CTD helix 1 which interacts with the holo GR is in green and CTD helix 2 that interacts with the apo GR is in red.

Early hormone receptor reconstitution experiments

Early reconstitution experiments with GR by Pratt and coworkers, and with PR by Toft and coworkers established the central proteins in the hormone receptor maturation pathway and has been extensively reviewed (Pratt et al., 2006). In early investigations,

purified GR stripped of chaperones rapidly lost ligand-binding ability, but could be reactivated in an ATP dependent manner by the addition of cell lysate. GR's ability to bind ligand was then linked to its association with Hsp90, with a direct correlation between the dissociation of Hsp90 and the loss of ligand binding (Bresnick et al., 1989). Reconstitution experiments from the 1990's determined that the minimal system required to obtain efficient Hsp90 association and recovery of ligand binding activity consisted of a five component chaperones system that included Hsp40, Hsp70, Hsp90, Hop, and p23 (Dittmar et al., 1996; Hutchison et al., 1994), with Hsp70 and Hsp90 being the essential components. Unlike GR, PR could be stripped of chaperones and purified in a ligand binding competent state, however, if heat inactivated, PR could then be reactivated in a comparable way to GR with the same chaperone components (Kosano et al., 1998; Smith, 1993). In these reconstitution experiments, Hsp70, Hsp90 and p23 were required in stoichiometric amounts, but catalytic ratios (~1:10) of Hsp40 and Hop were sufficient (Kosano et al., 1998).

Due to the complexity and the number of cofactors involved, it has proved extremely challenging to dissect this system and assign specific functions to the individual components. Additionally, like most obligate Hsp90 clients, in depth biochemical investigation of GR has been greatly hindered by difficulty obtaining stable and functional apo protein for *in vitro* investigation. As a result, previous studies investigating GR's chaperone interactions have been carried out with proteins of variable quality and homogeneity and were limited to rather basic characterization. Nevertheless, early reconstitution experiments were able to defined a general order in which the chaperone components enter and exit the pathway (Morishima et al., 2000b; Smith et al., 1992). The

reactivation process could be broken up into two distinct steps (Figure 4). The first step involves an ATP hydrolysis dependent process on Hsp70 in which GR is converted to a state that can bind to Hsp90. Hsp40 facilitates this step (discussed further in Chapter 3). In the second step, an ATP dependent process on Hsp90 reactivates the receptor.

While not essential, Hop and p23 facilitate the reactivation process (Morishima et al., 2000a). Hop gets incorporated with Hsp90 into the cycle, and facilitates the delivery of the client bound Hsp70 complex to Hsp90. While Hop enhances GR activation, it is not essential in that partial recovery is achieved without Hop (but with p23) (Morishima et al., 2000a). Similarly, partial recovery was seen without p23 (with Hop) (Dittmar and Pratt, 1997). However, without p23, GR ligand binding activity is rapidly lost, indicating that p23 acts after GR activation to stabilize the Hsp90-GR complex in which GR is held in a ligand binding competent state (Dittmar et al., 1997). Molybdate was found to help stabilize and prolong the lifetime of the p23 bound state (Johnson and Toft, 1995), and is even reported to work on its own almost as well as p23 (Dittmar and Pratt, 1997). The molybdate effect was discovered by an historical coincidence (Pratt and Toft, 1997), with the mechanism of action still not well understood. Nevertheless, molybdate proved a useful tool in many of the early reconstitution experiments.

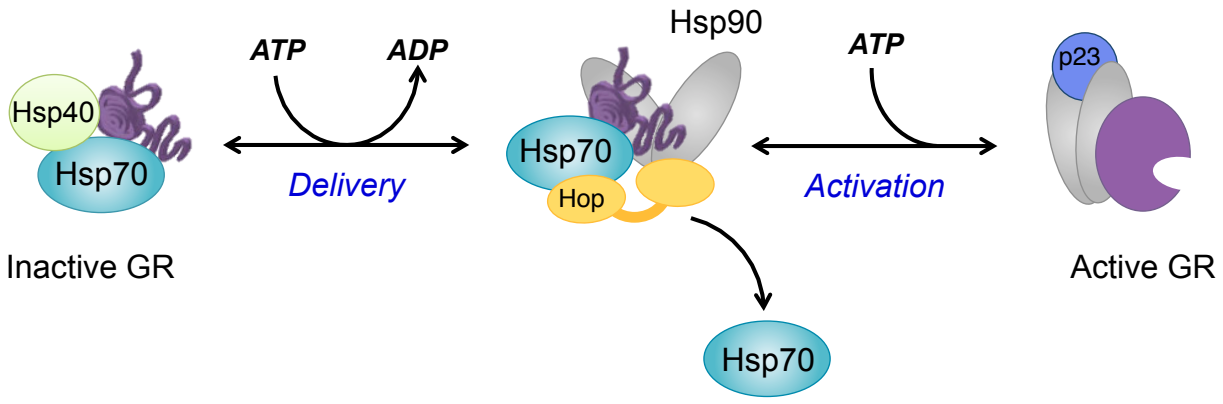

Figure 4. Minimal five-component chaperones system required for GR reactivation. In early reconstitution experiments, GR stripped of Hsp90 was inactive and could not bind ligand. Ligand binding recovery required a five-component chaperone system in which Hsp70 and Hsp90 were essential in a two-step activation process. In the first step, Hsp40 facilitates an ATP hydrolysis dependent process on Hsp70 that is required to convert GR into a state that can be reactivated by Hsp90. Hop facilitates the loading of the GR bound Hsp70 complex onto Hsp90. In the second step, ATP is required for Hsp90 to convert GR to a ligand binding competent state. Sequentially, p23 acts to stabilize the Hsp90:GR complex, prolonging the life time of the complex in which GR is held in an active state.

Pratt's Model for Ligand Binding Cleft Opening

Hsp90's clients consist of many proteins in which activation involves opening of a buried binding cleft that bind ligands such as steroids, ATP, and heme. In the absence of chaperones, ligand-binding proteins are highly dynamic and can access open cleft conformations during molecular breathing. However, while in the open cleft conformation required for ligand access, the protein would be inherently unstable as a result of the hydrophobic residues lining the pocket becoming solvent exposed and prone to aggregation. Pratt and co-workers proposed that Hsp70 and Hsp90 work cooperatively to assist in the opening of such ligand binding clefts, with Hsp90 and p23 stabilizing the cleft once open (Pratt et al., 2008).

In the first step of cleft opening, Hsp70 "primes" the receptors ligand-binding cleft, putting the receptor in a state that can then interact with Hsp90. Pratt and coworkers were unable to provide direct evidence for any structural changes occurring on the receptor during this "priming" step other than it being required for Hsp90 to be able to bind the receptor. Making the correlation to Hsp70's ability to promote dissociation of clathrin-coated vesicles (Schlossman, 1984), which was speculated to involve unfolding, it was postulated that priming of the receptor involved a comparable mechanism that resulted in unfolding of the receptor by Hsp70 (Hutchison et al., 1992). In both cases, ATP hydrolysis

on Hsp70 is essential, as deduced from the dependence of these processes on monovalent cations, such as potassium (K^+), which is specifically required for ATP hydrolysis on Hsp70 (O'Brien and McKay, 1995; Wilbanks and McKay, 1995).

In the second step, binding of Hsp90 is rapid, with the following Hsp90 dependent cleft opening being the rate limiting step in the whole cycle (Kanelakis et al., 2002). Evidence for GR having an open cleft is provided by thiol reactivity of GR's buried cysteines, and was specific to the molybdate stabilized state (Stancato et al., 1996). For cleft opening to occur, Hsp90 must assume its ATP dependent conformation. While Pratt and coworkers do not address the requirement of ATP hydrolysis on Hsp90, work from the Toft lab showed hydrolysis on Hsp90 is necessary for receptor reactivation. This was first evident in that AMPPNP could not support receptor reactivation (Johnson and Toft, 1995; Smith et al., 1992) and was further supported by the use of hydrolysis dead mutants of Hsp90 (Grenert et al., 1999). While ATP binding was sufficient to form Hsp90 cochaperone complexes and for Hsp90 incorporation into the receptor complex, hydrolysis on Hsp90 was required in the reconstituted system to progress to the p23 state of the receptor complex and to obtain hormone binding (Grenert et al., 1999).

Surprisingly, the second Hsp90 dependent step was also found to be partially K^+ dependent with the presence of Hsp40 optimizing the second step (Morishima et al., 2001). Since Hsp90 does not exhibit K^+ dependence, this suggests that Hsp70 undergoes an additional ATP hydrolysis events during the cleft opening, raising the possibility that Hsp70 and Hsp90 collaboratively open the receptors cleft (Morishima et al., 2001). However, given the crude nature of the techniques employed and the relatively long time scale of the experiments, it is unclear if the enhancement associated with ATP hydrolysis

on Hsp70 in the second step is actually due to the reentry of dissociated GR back into the cycle during the experimental time course (~20min) of the second step.

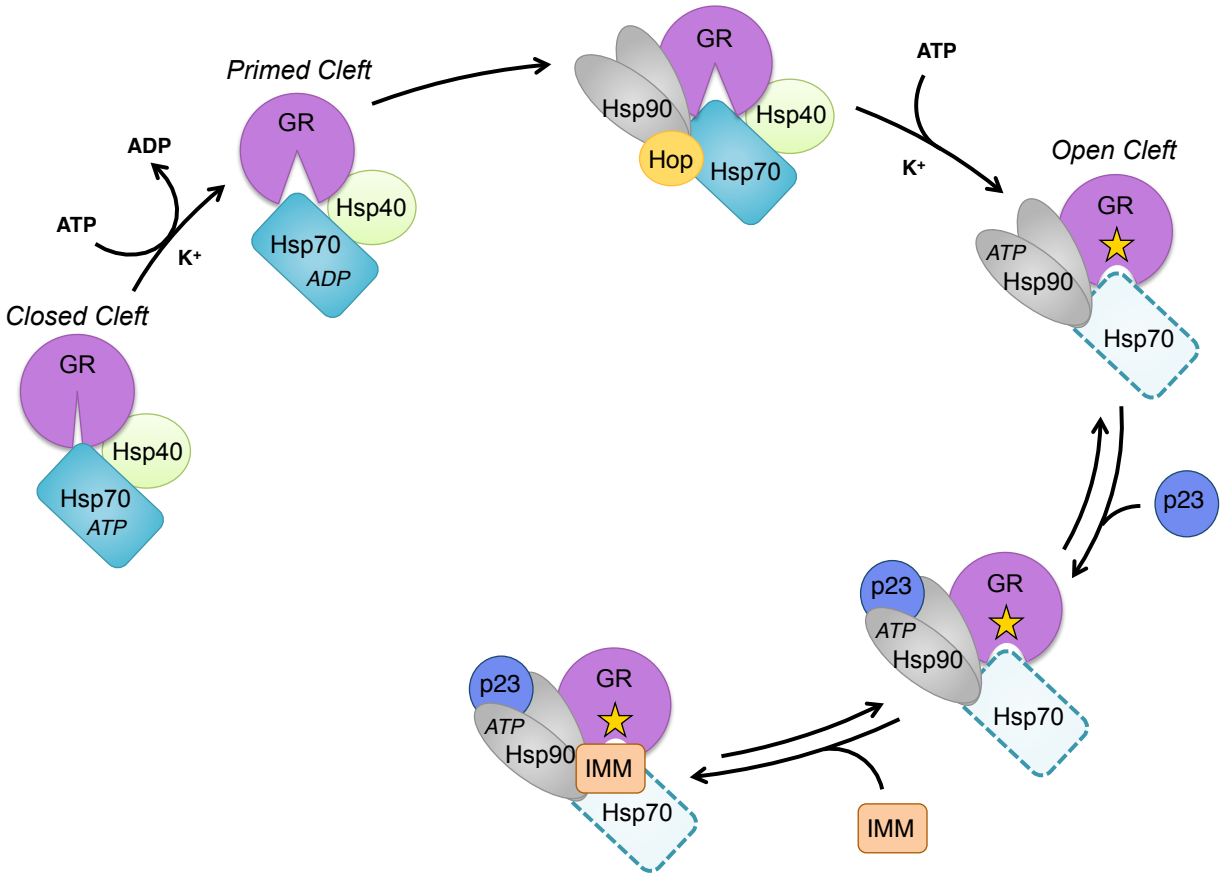

Figure 5. Pratt's mechanism for chaperone dependent ligand binding cleft opening Hsp70 interacts first with GR, and in an ATP hydrolysis dependent process that is facilitated by Hsp40, Hsp70 "primers" the ligand binding cleft such that Hsp90 can bind to the receptor. The rate-limiting step of the activation process is then the opening of the ligand-binding cleft by Hsp90, which require Hsp90 to be bound to ATP. Once open, ligand can access the ligand-binding site. P23 acts after cleft opening, and stabilizes the ATP state of Hsp90 that is required for Hsp90 to remain associated with GR and for GR to maintain ligand association. Immunophilin (IMM) proteins such as FKBP52 bind to the mature ligand bound GR complexes and are thought to facilitate receptor translocation to the nucleus (discussed in Chapter 6). Figure adapted from previous review (Pratt et al., 2008).

Apo GRLBD and other client proteins reported to stimulate Hsp90's ATP hydrolysis

In one of the first rigorous *in vitro* investigations, denatured and refolded WT apo GRLBD in the presence of the zwitterionic detergent, zwittergent 3-12, apo GRLBD was

shown to significantly stimulate Hsp90's hydrolysis, indicating a direct interaction between purified Hsp90 and GRLBD (McLaughlin et al., 2002). In this case, the apo GRLBD was reported to be a dimer and had a very poor binding affinity for ligand (46μM) (McLaughlin and Jackson, 2002). Since then, the stimulation of Hsp90's ATPase activity by client proteins have also been reported for the bacterial Hsp90 by the ribosomal protein L2 and by a partially folded model client; the synthetic variant of staphylococcal nuclease (Δ131Δ) (Motojima-Miyazaki et al., 2010; Street et al., 2011). Together, this suggests that the ability to stimulate Hsp90's hydrolysis cycle is a common feature of Hsp90 client proteins and potentially an integral aspect of the Hsp90 chaperone cycle. Furthermore, it implies that Hsp90 can interact directly with its client proteins *in vitro*, and does not necessarily require other chaperone proteins as suggested by the early nuclear receptor reconstitution experiments.

Thesis Project Objective

The aim of this thesis project was to determine in mechanistic detail how Hsp90 promotes GR ligand binding, and in so doing, provide much needed insight into how Hsp90 activates a bona fide client. My approach was to use highly purified recombinant proteins, allowing direct and precise measurements of ligand binding to GRLBD in an entirely *in vitro* system.

References

Ali, M.M.U., Roe, S.M., Vaughan, C.K., Meyer, P., Panaretou, B., Piper, P.W., Prodromou, C., and Pearl, L.H. (2006). Crystal structure of an Hsp90–nucleotide–p23/Sba1 closed chaperone complex. Nature *440*, 1013–1017.

Bain, D.L., Heneghan, A.F., Connaghan-Jones, K.D., and Miura, M.T. (2007). Nuclear Receptor

Structure: Implications for Function. Annu. Rev. Physiol. *69*, 201–220.

Bledsoe, R.K., Montana, V.G., Stanley, T.B., Delves, C.J., Apolito, C.J., McKee, D.D., Consler, T.G., Parks, D.J., Stewart, E.L., and Willson, T.M. (2002). Crystal Structure of the Glucocorticoid Receptor Ligand Binding Domain Reveals a Novel Mode of Receptor Dimerization and Coactivator Recognition. Cell *110*, 93–105.

Bresnick, E.H., Dalman, F.C., Sanchez, E.R., and Pratt, W.B. (1989). Evidence that the 90-kDa heat shock protein is necessary for the steroid binding conformation of the L cell glucocorticoid receptor. J. Biol. Chem.

Chandra, V., Huang, P., Hamuro, Y., Raghuram, S., Wang, Y., Burris, T.P., and Rastinejad, F. (2008). Structure of the intact PPAR-gamma-RXR- nuclear receptor complex on DNA. Nature *456*, 350–356.

Chandra, V., Huang, P., Potluri, N., Wu, D., Kim, Y., and Rastinejad, F. (2013). Multidomain integration in the structure of the HNF-4α nuclear receptor complex. Nature *495*, 394–398.

Chen, S., and Smith, D.F. (1998). Hop as an adaptor in the heat shock protein 70 (Hsp70) and hsp90 chaperone machinery. J. Biol. Chem. *273*, 35194–35200.

Chrousos, G.P., and Kino, T. (2009). Glucocorticoid Signaling in the Cell. Annals of the New York Academy of Sciences *1179*, 153–166.

Dittmar, K.D., Demady, D.R., Stancato, L.F., Krishna, P., and Pratt, W.B. (1997). Folding of the glucocorticoid receptor by the heat shock protein (hsp) 90-based chaperone machinery. The role of p23 is to stabilize receptor.hsp90 heterocomplexes formed by hsp90.p60.hsp70. J. Biol. Chem. *272*, 21213–21220.

Dittmar, K.D., Hutchison, K.A., Owens-Grillo, J.K., and Pratt, W.B. (1996). Reconstitution of the steroid receptor.hsp90 heterocomplex assembly system of rabbit reticulocyte lysate. J. Biol. Chem. *271*, 12833–12839.

Dittmar, K.D., and Pratt, W.B. (1997). Folding of the Glucocorticoid Receptor by the Reconstituted hsp90-based Chaperone Machinery. THE INITIAL hsp90 p60 hsp70-DEPENDENT STEP IS SUFFICIENT FOR CREATING THE STEROID BINDING CONFORMATION. Journal of Biological Chemistry *272*, 13047–13054.

Fang, L., Ricketson, D., Getubig, L., and Darimont, B.D. (2006). Unliganded and hormone-bound glucocorticoid receptors interact with distinct hydrophobic sites in the Hsp90 C-terminal domain. Proc. Natl. Acad. Sci. U.S.a. *103*, 1847–18492.

Grenert, J.P., Johnson, B.D., and Toft, D.O. (1999). The importance of ATP binding and hydrolysis by hsp90 in formation and function of protein heterocomplexes. J. Biol. Chem. *274*, 17525–17533.

He, Y., Yi, W., Suino-Powell, K., Zhou, X.E., Tolbert, W.D., Tang, X., Yang, J., Yang, H., Shi, J.,

Hou, L., et al. (2014). Structures and mechanism for the design of highly potent glucocorticoids. Cell Res. *24*, 713–726.

Hessling, M., Richter, K., and Buchner, J. (2009). Dissection of the ATP-induced conformational cycle of the molecular chaperone Hsp90. Nat. Struct. Mol. Biol. *16*, 287–293.

Howard, K.J., Holley, S.J., Yamamoto, K.R., and Distelhorst, C.W. (1990). Mapping the HSP90 binding region of the glucocorticoid receptor. J. Biol. Chem. *265*, 11928–11935.

Hutchison, K.A., Czar, M.J., Scherrer, L.C., and Pratt, W.B. (1992). Monovalent cation selectivity for ATP-dependent association of the glucocorticoid receptor with hsp70 and hsp90. J. Biol. Chem. *267*, 14047–14053.

Hutchison, K., Dittmar, K.D., Czar, M.J., and Pratt, W.B. (1994). Proof that hsp70 is required for assembly of the glucocorticoid receptor into a heterocomplex with hsp90. J. Biol. Chem. *269*, 5043–5049.

Jakob, U., Lilie, H., Meyer, I., and Buchner, J. (1995). Transient Interaction of Hsp90 with Early Unfolding Intermediates of Citrate Synthase. Journal of Biological Chemistry *270*, 7288–7294.

Johnson, J.L., and Toft, D.O. (1995). Binding of p23 and hsp90 during assembly with the progesterone receptor. Mol. Endocrinol. *9*, 670–678.

Kanelakis, K.C., Shewach, D.S., and Pratt, W.B. (2002). Nucleotide binding states of hsp70 and hsp90 during sequential steps in the process of glucocorticoid receptor.hsp90 heterocomplex assembly. J. Biol. Chem. *277*, 33698–33703.

Kauppi, B. (2003). The Three-dimensional Structures of Antagonistic and Agonistic Forms of the Glucocorticoid Receptor Ligand-binding Domain: RU-486 INDUCES A TRANSCONFORMATION THAT LEADS TO ACTIVE ANTAGONISM. Journal of Biological Chemistry *278*, 22748–22754.

Kosano, H., Stensgard, B., Charlesworth, M.C., McMahon, N., and Toft, D. (1998). The assembly of progesterone receptor-hsp90 complexes using purified proteins. J. Biol. Chem. *273*, 32973–32979.

Krukenberg, K.A., Förster, F., Rice, L.M., Sali, A., and Agard, D.A. (2008). Multiple Conformations of E. coli Hsp90 in Solution: Insights into the Conformational Dynamics of Hsp90. Structure *16*, 755–765.

Krukenberg, K.A., Street, T.O., Lavery, L.A., and Agard, D.A. (2011). Conformational dynamics of the molecular chaperone Hsp90. Quart. Rev. Biophys. *44*, 229–255.

Lou, X., Toresson, G., Benod, C., Suh, J.H., Philips, K.J., Webb, P., and Gustafsson, J.-Å. (2014). Structure of the retinoid X receptor α-liver X receptor β (RXRα-LXRβ) heterodimer on DNA. Nat. Struct. Mol. Biol. *21*, 277–281.

Luisi, B.F., Xu, W.X., Otwinowski, Z., Freedman, L.P., Yamamoto, K.R., and Sigler, P.B. (1991). Crystallographic analysis of the interaction of the glucocorticoid receptor with DNA. Nature *352*, 497–505.

M J Garabedian, K.R.Y. (1992). Genetic dissection of the signaling domain of a mammalian steroid receptor in yeast. Molecular Biology of the Cell *3*, 1245.

McLaughlin, S.H., and Jackson, S.E. (2002). Folding and stability of the ligand-binding domain of the glucocorticoid receptor. Protein Science *11*, 1926–1936.

McLaughlin, S.H., Smith, H.W., and Jackson, S.E. (2002). Stimulation of the weak ATPase activity of human Hsp90 by a client protein. J. Mol. Biol. *315*, 787–798.

Morishima, Y., Kanelakis, K.C., Murphy, P.J., Shewach, D.S., and Pratt, W.B. (2001). Evidence for iterative ratcheting of receptor-bound hsp70 between its ATP and ADP conformations during assembly of glucocorticoid receptor.hsp90 heterocomplexes. Biochemistry *40*, 1109–1116.

Morishima, Y., Kanelakis, K.C., Silverstein, A.M., Dittmar, K.D., Estrada, L., and Pratt, W.B. (2000a). The Hsp organizer protein hop enhances the rate of but is not essential for glucocorticoid receptor folding by the multiprotein Hsp90-based chaperone system. J. Biol. Chem. *275*, 6894–6900.

Morishima, Y., Murphy, P.J., Li, D.P., Sanchez, E.R., and Pratt, W.B. (2000b). Stepwise assembly of a glucocorticoid receptor.hsp90 heterocomplex resolves two sequential ATP-dependent events involving first hsp70 and then hsp90 in opening of the steroid binding pocket. J. Biol. Chem. *275*, 18054–18060.

Motojima-Miyazaki, Y., Yoshida, M., and Motojima, F. (2010). Ribosomal protein L2 associates with E. coli HtpG and activates its ATPase activity. Biochem. Biophys. Res. Commun. *400*, 241–245.

O'Brien, M.C., and McKay, D.B. (1995). How potassium affects the activity of the molecular chaperone Hsc70. I. Potassium is required for optimal ATPase activity. J. Biol. Chem. *270*, 2247–2250.

Obermann, W.M.J., Sondermann, H., Russo, A., Pavletich, N., and Hartl, F.U. (1998). In vivo function of Hsp90 is dependent on ATP binding and ATP hydrolysis. The Journal of Cell Biology *143*, 901–910.

Picard, D., Khursheed, B., Garabedian, M.J., Fortin, M.G., Lindquist, S., and Yamamoto, K.R. (1990). Reduced levels of hsp90 compromise steroid receptor action in vivo. Nature *348*, 166–168.

Pratt, W.B., Morishima, Y., and Osawa, Y. (2008). The Hsp90 Chaperone Machinery Regulates Signaling by Modulating Ligand Binding Clefts. Journal of Biological Chemistry *283*, 22885–22889.

Pratt, W.B., Morishima, Y., Murphy, M., and Harrell, M. (2006). Chaperoning of Glucocorticoid Receptors. In Molecular Chaperones in Health and Disease, (Berlin/Heidelberg: Handbook of Experimental Pharmacology), pp. 111–138.

Pratt, W.B., and Toft, D.O. (1997). Steroid Receptor Interactions with Heat Shock Protein and Immunophilin Chaperones 1. Endocrine Reviews *18*, 306–360.

Ricketson, D., Hostick, U., Fang, L., Yamamoto, K.R., and Darimont, B.D. (2007). A Conformational Switch in the Ligand-binding Domain Regulates the Dependence of the Glucocorticoid Receptor on Hsp90. J. Mol. Biol. *368*, 729–741.

Schlossman, D.M. (1984). An enzyme that removes clathrin coats: purification of an uncoating ATPase. The Journal of Cell Biology *99*, 723–733.

Schoch, G.A., D'Arcy, B., Stihle, M., Burger, D., Bär, D., Benz, J., Thoma, R., and Ruf, A. (2010). Molecular switch in the glucocorticoid receptor: active and passive antagonist conformations. J. Mol. Biol. *395*, 568–577.

Shiau, A.K., Harris, S.F., Southworth, D.R., and Agard, D.A. (2006). Structural Analysis of E. coli hsp90 Reveals Dramatic Nucleotide-Dependent Conformational Rearrangements. Cell *127*, 329–340.

Smith, D.F. (1993). Dynamics of heat shock protein 90-progesterone receptor binding and the disactivation loop model for steroid receptor complexes. Mol. Endocrinol. *7*, 1418–1429.

Smith, D.F., Stensgard, B.A., Welch, W.J., and Toft, D.O. (1992). Assembly of progesterone receptor with heat shock proteins and receptor activation are ATP mediated events. J. Biol. Chem. *267*, 1350–1356.

Southworth, D.R., and Agard, D.A. (2011). Client-Loading Conformation of the Hsp90 Molecular Chaperone Revealed in the Cryo-EM Structure of the Human Hsp90:Hop Complex. Mol. Cell *42*, 771–781.

Stancato, L.F., Silverstein, A.M., Gitler, C., Groner, B., and Pratt, W.B. (1996). Use of the thiol-specific derivatizing agent N-iodoacetyl-3-[125I]iodotyrosine to demonstrate conformational differences between the unbound and hsp90-bound glucocorticoid receptor hormone binding domain. J. Biol. Chem. *271*, 8831–8836.

Street, T.O., Lavery, L.A., and Agard, D.A. (2011). Substrate binding drives large-scale conformational changes in the Hsp90 molecular chaperone. Mol. Cell *42*, 96–105.

Taipale, M., Jarosz, D.F., and Lindquist, S. (2010). HSP90 at the hub of protein homeostasis: emerging mechanistic insights. Nat Rev Mol Cell Biol *11*, 515–528.

Watson, L.C., Kuchenbecker, K.M., Schiller, B.J., Gross, J.D., Pufall, M.A., and Yamamoto, K.R. (2013). The glucocorticoid receptor dimer interface allosterically transmits sequence-

specific DNA signals. Nat. Struct. Mol. Biol. *20*, 876–883.

Wegele, H., Muschler, P., Bunck, M., Reinstein, J., and Buchner, J. (2003). Dissection of the contribution of individual domains to the ATPase mechanism of Hsp90. J. Biol. Chem. *278*, 39303–39310.

Wilbanks, S., and McKay, D.B. (1995). How Potassium Affects the Activity of the Molecular Chaperone Hsc70. J. Biol. Chem. *270*, 2251–2257.

Chapter 2

Purified GRLBD Binds Ligand without the Aid or Enhancement from Hsp90

Preface

Based on the observations from the Jackson lab that GRLBD could be obtained in an apo state that stimulated Hsp90's ATP hydrolysis cycle and could not efficiently bind ligand, it was expected that Hsp90 would bind directly to this apo form of GRLBD and promote ligand binding. The initial objectives were to purify apo GRLBD in a comparable way utilizing the zwittergent detergent, and to reproduce the stimulation in ATPase activity to ensure that the apo GRLBD obtained interacts with Hsp90. From there, the goal was to develop a ligand-binding assay to dissect out the mechanism by which Hsp90 promotes GR ligand binding.

Summary

The previous account reporting the stimulation of Hsp90's ATP hydrolysis cycle is at least in part due to detergent artifacts. The detergent alone stimulates Hsp90's hydrolysis, and small angle x-ray scattering (SAXS) revealed that the detergent was concentrated to undeterminable amounts along with the protein during the purification procedure. A new purification strategy was developed to obtain well-behaved apo GRLBD in which GRLBD is expressed and purified without detergents in the presence of ligand, followed by ligand removal by extensive dialysis. Both SAXS and hydrogen deuterium exchange detected by

mass spec (HDXMS) indicated that the apo GRLBD is mostly folded. Surprisingly, this apo GRLBD was found to bind ligand without the aid or enhancement from Hsp90. The lack of Hsp90 dependence could not be attributed to the use of the F602S mutant of GRLBD that is less dependent on Hsp90 *in vivo*, since wilt type (WT) GRLBD binds ligand with higher affinity than GRLBD F602S mutant. While no effect on ligand binding was detected, GRLBD (F602) at high concentration can inhibit ATP hydrolysis on Hsp90.

Results

Stimulation of Hsp90's ATPase activity likely results from excess detergent

Using a GST-GRLBD(F602S/C638D) construct obtained from the Fletterick lab, the stimulation in Hsp90's ATP hydrolysis rate with apo GRLBD purified with 0.1% zwittergent 3-12 could be detected. However, the degree of stimulation was found to vary between GRLBD purifications. Insight into the source of this issue was obtained while analyzing GRLBD by Small Angle X-ray Scattering (SAXS) (Figure 1). The first peak at ~10Å in probability distributions (P(r)) obtained form the SAXS scattering data could not easily be explained as originating from GLRBD (**Figure 1** A-C). However, an equivalent scattering signal arose from zwittergent 3-12 (**Figure 1** D and E), indicating that the P(r) peak at ~10Å likely results from excess detergent in the protein samples compared to the sample buffer. This indicates that the detergent was concentrated along with the protein during protein concentration by centrifugation. This is a common issue for detergents with low critical micelle concentration (CMC), such as zwittergent 3-12. Concentration of the detergent is problematic because zwittergent 3-12 by itself was found to stimulate Hsp90's ATP hydrolysis (not shown). With zwittergent 3-12 both stimulating Hsp90's ATP

hydrolysis, and being concentrated to undeterminable amounts, it is impossible to determine if and to what degree the GRLBD purified with the detergent stimulates Hsp90's ATPase activity.

The SAXS analysis with the apo GRLBD obtained from the zwittergent purifications proved very challenging, with aggregation dominating the scattering. Aggregation that was clearly detected by the non-linear upward curve in the Guinier plot (not shown) resulting in the inability to determine an accurate D_{max} and the rippling tail observed in the P(r). Moreover, the zwittergent 3-12 (and likely detergent micelles) were potentially interfering with other assays being developed, such as the ligand binding assay. Together, preliminary investigations with the zwittergent 3-12 purified apo GRLBD revealed issues related to protein stability and detergent artifacts that would greatly hinder rigorous biophysical investigation. For these reasons, it was decided to move away from purifying GR in detergent and to develop new approaches for obtaining apo GRLBD.

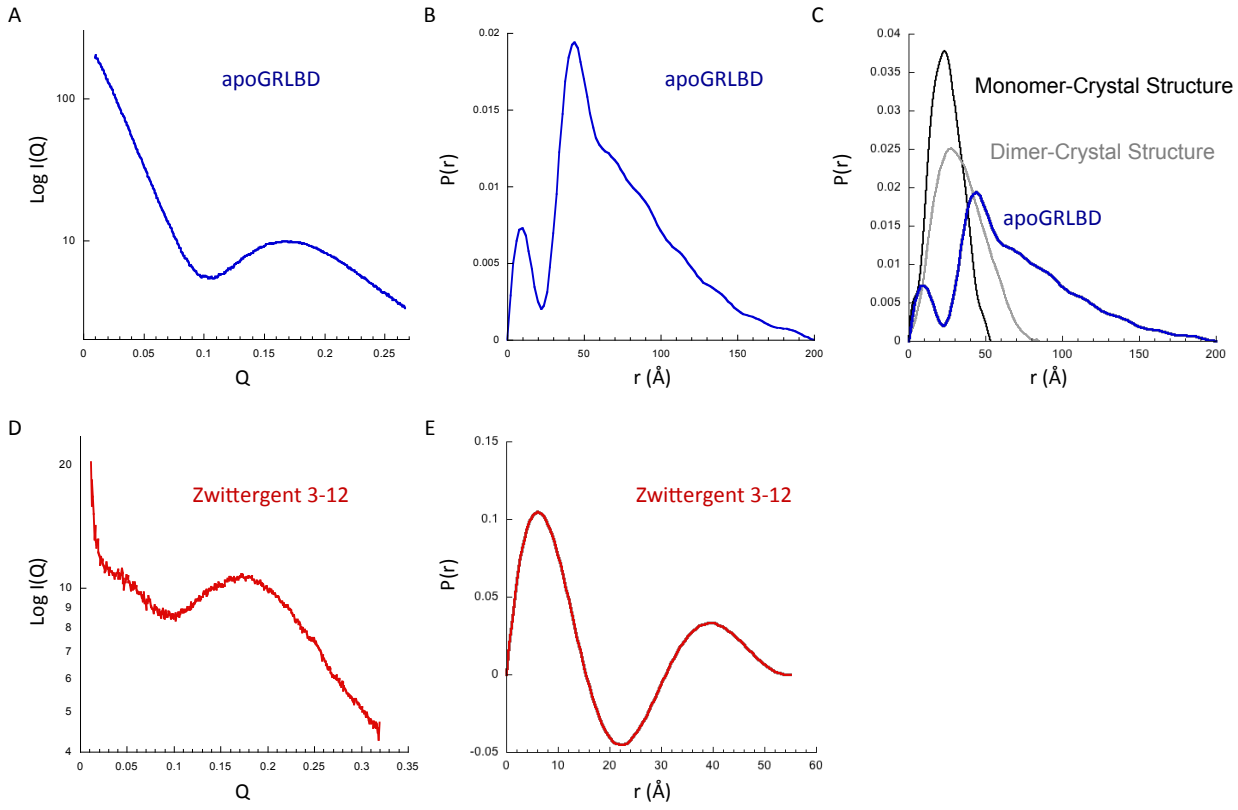

Figure 1. SAXS reveals zwittergent 3-12 is concentrated in the apo GRLBD sample.
A) SAXS scattering curve of apo GRLBD(F602S/C638D) subtracted with sample buffer containing 0.1% zwittergent 3-12.
B) P(r) of GRLBD from (A).
C) Comparison of P(r) of apo GRLBD(F602S/C638D) as in B with theoretical P(r) generated from GRLBD crystal structure (pdb 1M2Z).
D) SAXS scattering of sample buffer containing zwittergent 3-12, subtracted with sample buffer with out zwittergent 3-12.
E) P(r) of zwittergent 3-12 from (C). (Exp43)

Obtaining well behaved detergent free apo GRLBD for biophysical investigation

To enhance GRLBD expression, a codon optimized synthetic gene for bacterial expression of full length human GR (F602S) was purchased from GeneArt. Based on GeneArt's proprietary codon quality scoring algorithm, the gene for GR is enriched with rare codons and likely limiting expression in bacteria (Figure 3).

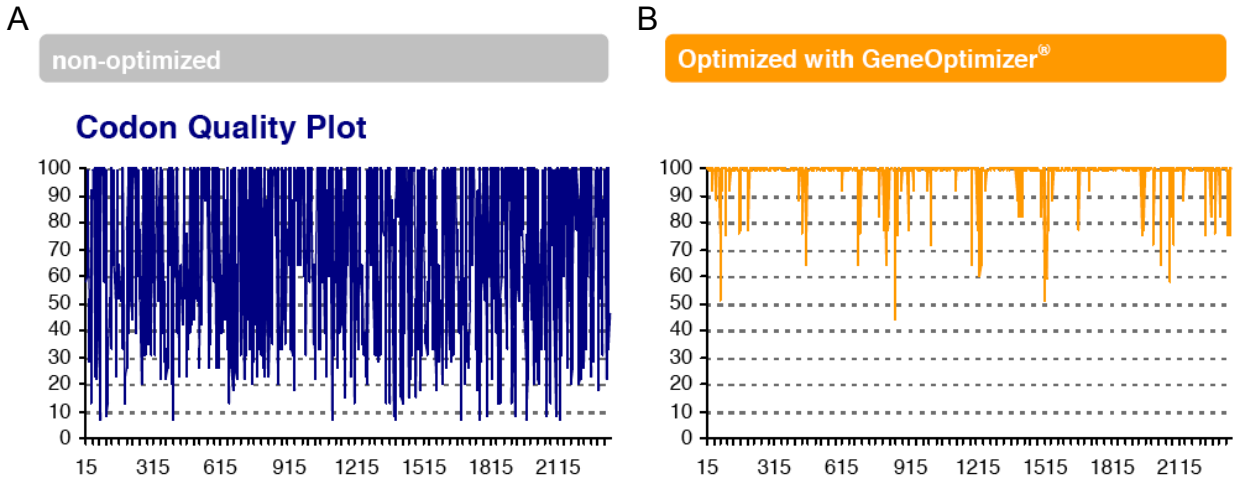

Figure 2. Codon quality plot for endogenous and synthetic GR.
Codon quality of codon used at indicated codon position for endogenous full length GR gene(A), and for GeneArt codon optimized GR gene for bacterial expression (B). Figure provided by GeneArt.

The sequence for the codon optimized GRLBD (F602S) (521-777) was cloned into two expression vectors, one with an N-terminal MBP tag and one free of a solubility tag. The monomeric MBP tag was preferable to the previous dimeric GST tag so that the state of GRLBD could be assessed without the complication of tag-induced dimerization. Attempts at purifying purely apo GRLBD proved extremely challenging with most of the GRLBD lost to degradation. For this reason, efforts were focused on purifying GRLBD expressed and purified in the presence of ligand, followed by extensive dialysis to remove the ligand. This strategy proved successful, allowing significant quantities (~10mg per liter of culture) of GRLBD to be obtained. GRLBD could be purified and obtained in the apo state without a solubility tag, however, the MBP tag was verified to not significantly interfere with shown experiments and was in many cases retained for enhanced stability over the long experimental time courses. Initial purifications were preformed with 0.04% CHAPS (a detergent with a high CMC), however, it was later found to be unnecessary and removed

from all experiments and purification buffers (except for the lysis buffer). Refer to the Protein Purification section of the Appendix for more details.

** From this point forward, GRLBD (F602S) is referred to simply as GRLBD, with the distinction between the F602S and WT protein indicated when relevant.*

Structural characterization of apo GRLBD

All experiments characterizing the apo GRLBD indicated that it is well folded and functional. Analytical size exclusion chromatography with an inline multi-angle light scatter detector (SEC-MALS) determined GRLBD to be mostly monomeric with trace amount of dimers (Figure 3). The amount of dimerization varied between purifications, depending on how rigorously the front shoulder on the S200 column was excluded from pooled fractions during the purification. Analysis by SAXS determined that apo GRLBD is a mostly folded globular protein. The P(r) profile fit between the theoretical P(r) of the monomer and dimereric GRLBD generated from the crystal structure (Figure 4A and B). Although it was not determined if the shift to longer distances was the result of dimers forming at the high concentrations used in SAXS or from a conformational expansion of the apo GRLBD monomer. Nevertheless, Kratky analysis clearly shows that the apo GRLBD is folded (Figure 4C), with a similar profile to that of the fully folded dex bound crystal structure (Figure 4D). Supporting this, hydrogen deuterium exchange coupled with mass spectrometry (HDX-MS) carried out by our collaborators (Devrishi Goswami in the Griffin Lab) also indicated that GRLBD is well structured (Figure 5). Surprisingly, neither the SEC-

MALS nor the HDX-MS revealed any detectable change upon ligand addition, suggesting that the apo GRLBD is in a very similar conformation to the ligand bound state.

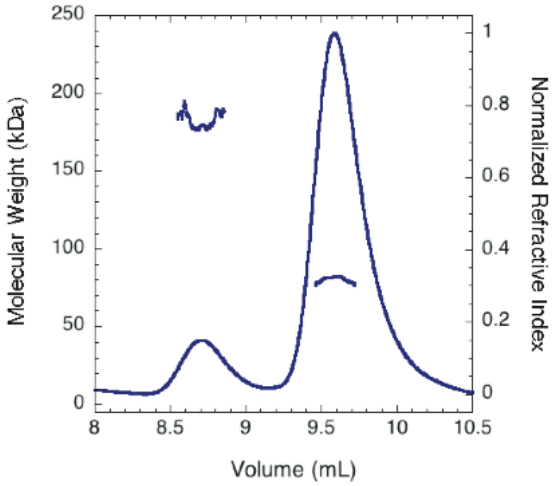

Figure 3. SEC-MALS of MBP-GRLBD shows GRLBD is mostly monomeric.
50µL of 6µM MBP-GRLBD (74kDa) was run on Showdex 803 column. Amount of dimer varied between purification from trace amounts as above, to non-detectable. (Exp645)

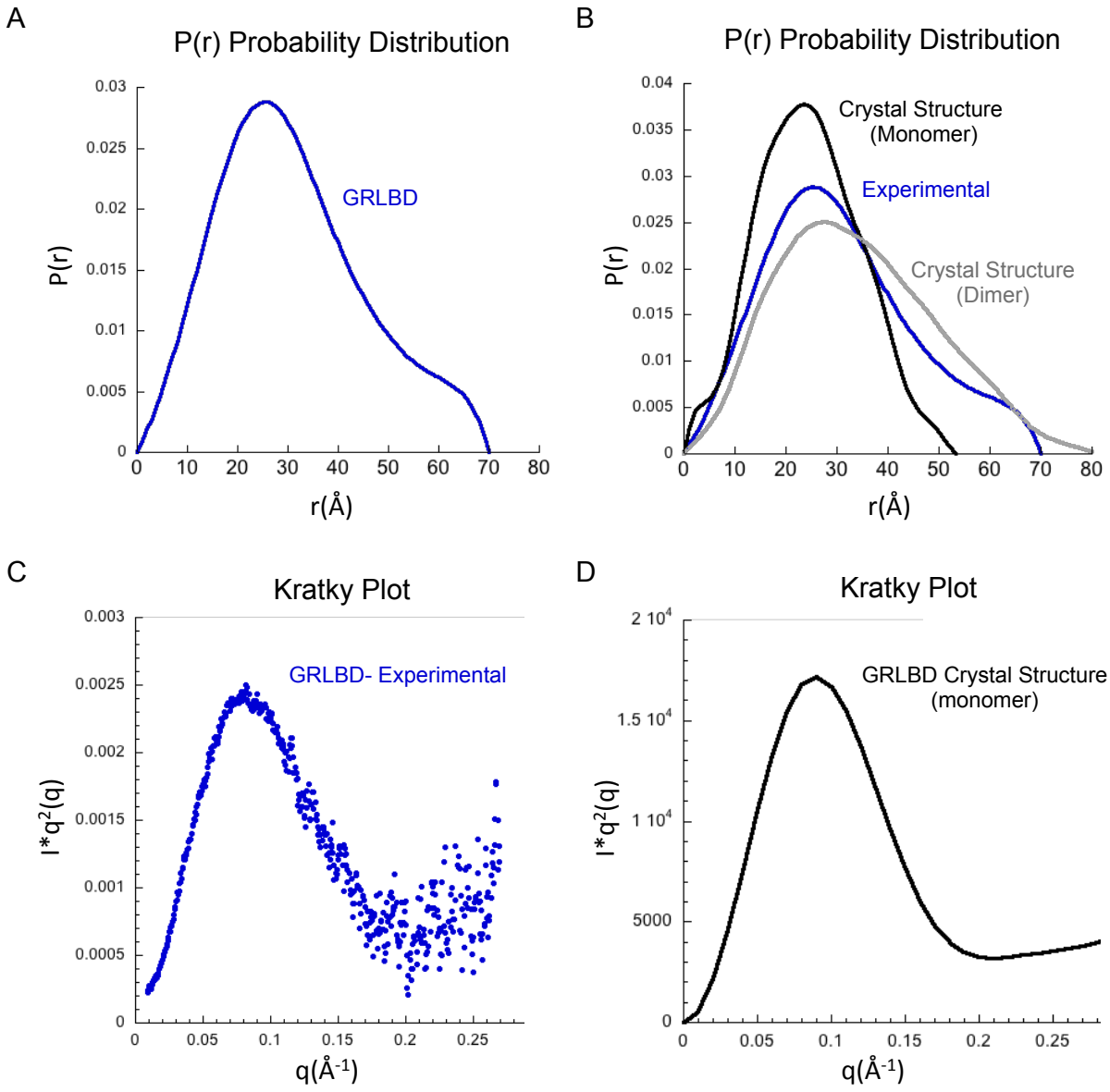

Figure 4. SAXS Anylysis of GRLBD
A) P(r) disribuition of apo GRLBD.
B) Comparison of P(r) of apo GRLBD as in A with theoretical P(r) generated from GRLBD crystal structure (pdb 1M2Z).
C) Kratky anaysis from apo GRLBD SAXS scattering indicates that apo GRLBD is well folded and comparable to the Katky plot obtained from the theoretical scattering of the GRLBD crystal structure (D). (Exp152)

A

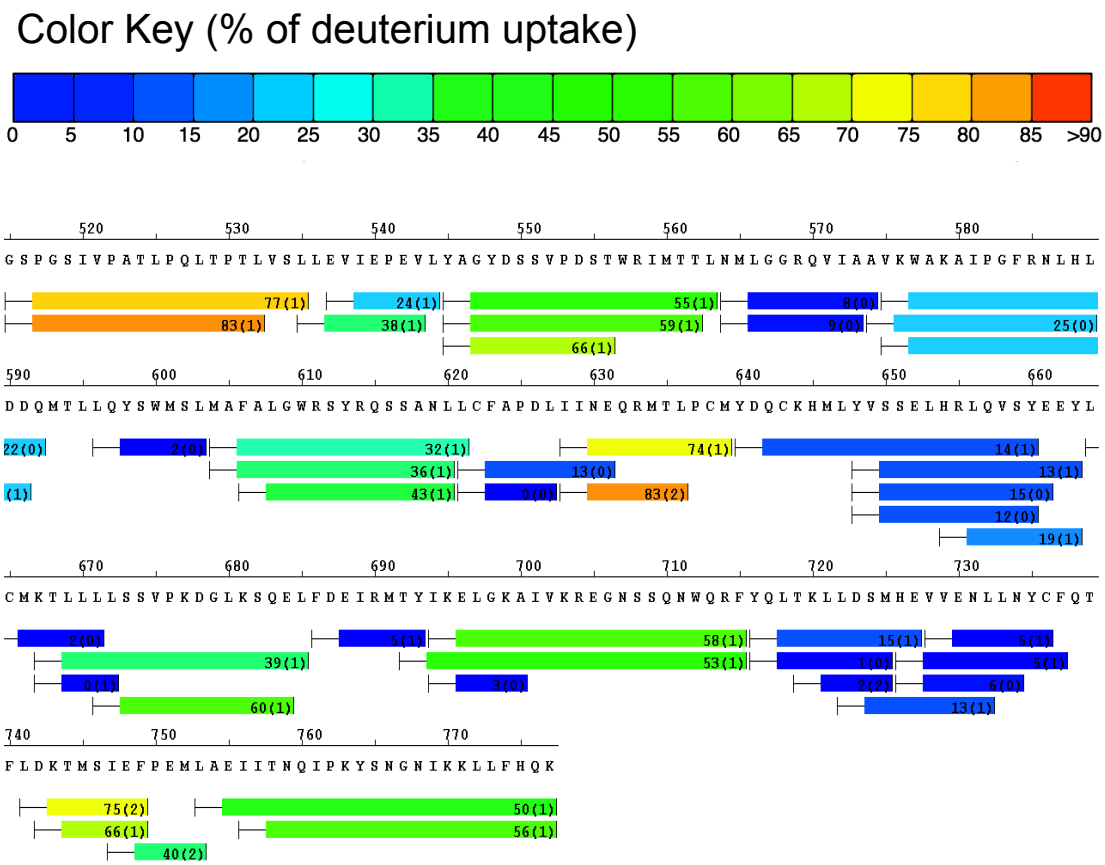

B

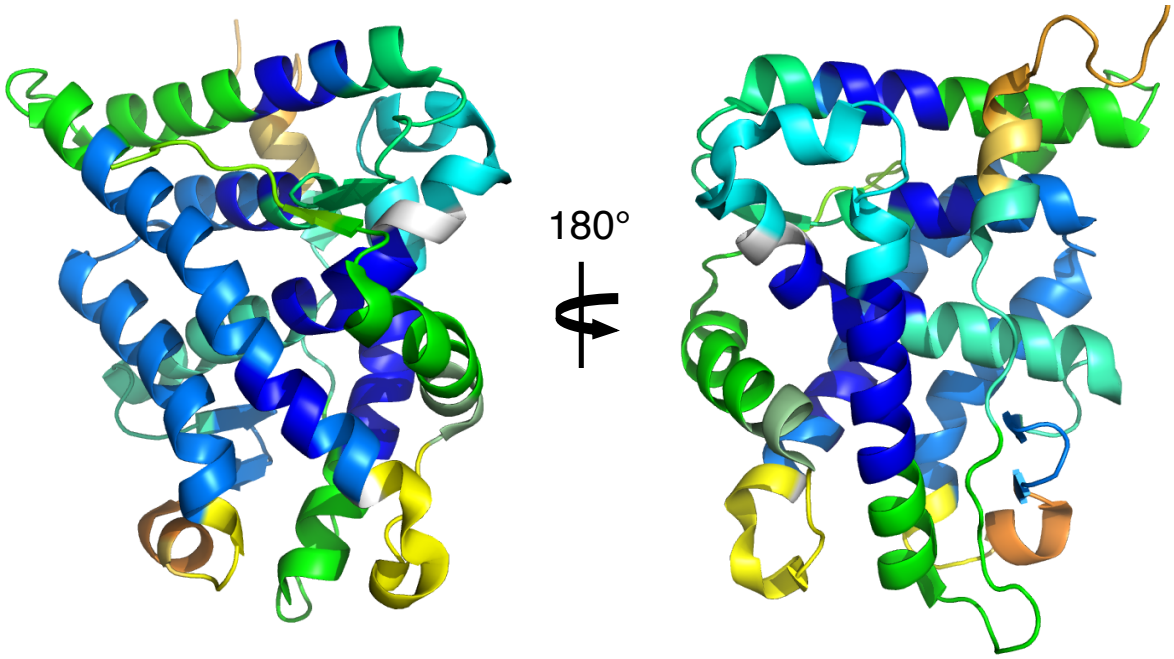

Figure 5. HDX-MX of apo GRLBD.

A) Sequence for GRLBD with detected peptide fragments color coded according to percent of deuterium uptake.
B) Percent of deuterium uptake for peptide fragments in (A) mapped onto the structure of GRLBD (pdb 1M2Z).

Functional characterization of apo GRLBD

For functional characterization, ligand binding was monitored by measuring the increase of fluorescence polarization of fluorescein labeled dexamethasone (F-dex) as it bound to GRLBD. As previously reported (Bledsoe et al., 2002; Pfaff and Fletterick, 2010; Simmons et al., 2008), but in contrast to *in vivo*, purified GRLBD binds ligand efficiently in the absence of chaperones (Figure 6). Under our experimental conditions, equilibrium measurements result in a dissociation constant (K_D) of 154±14 nM (Figure 6A). The kinetics of F-dex binding displayed standard single-phase association and dissociation kinetics (Figure 6C and D). While the surprising lack of difference between the apo and dex bound GRLBD as measured by HDX-MS raises the possibility that dex was not successfully removed, the ligand binding assays indicated that the GRLBD is in fact mostly ligand free, with the association much faster than dissociation. Additionally, the specific activity measurement indicated that GRLBD was about 50-70% active (depending on the purification) (Figure 6B), suggesting that least 50-70% was ligand free. Moreover, the specific activity did not change after an additional overnight dialysis (personal communication, Zygy Roe-Zurz).

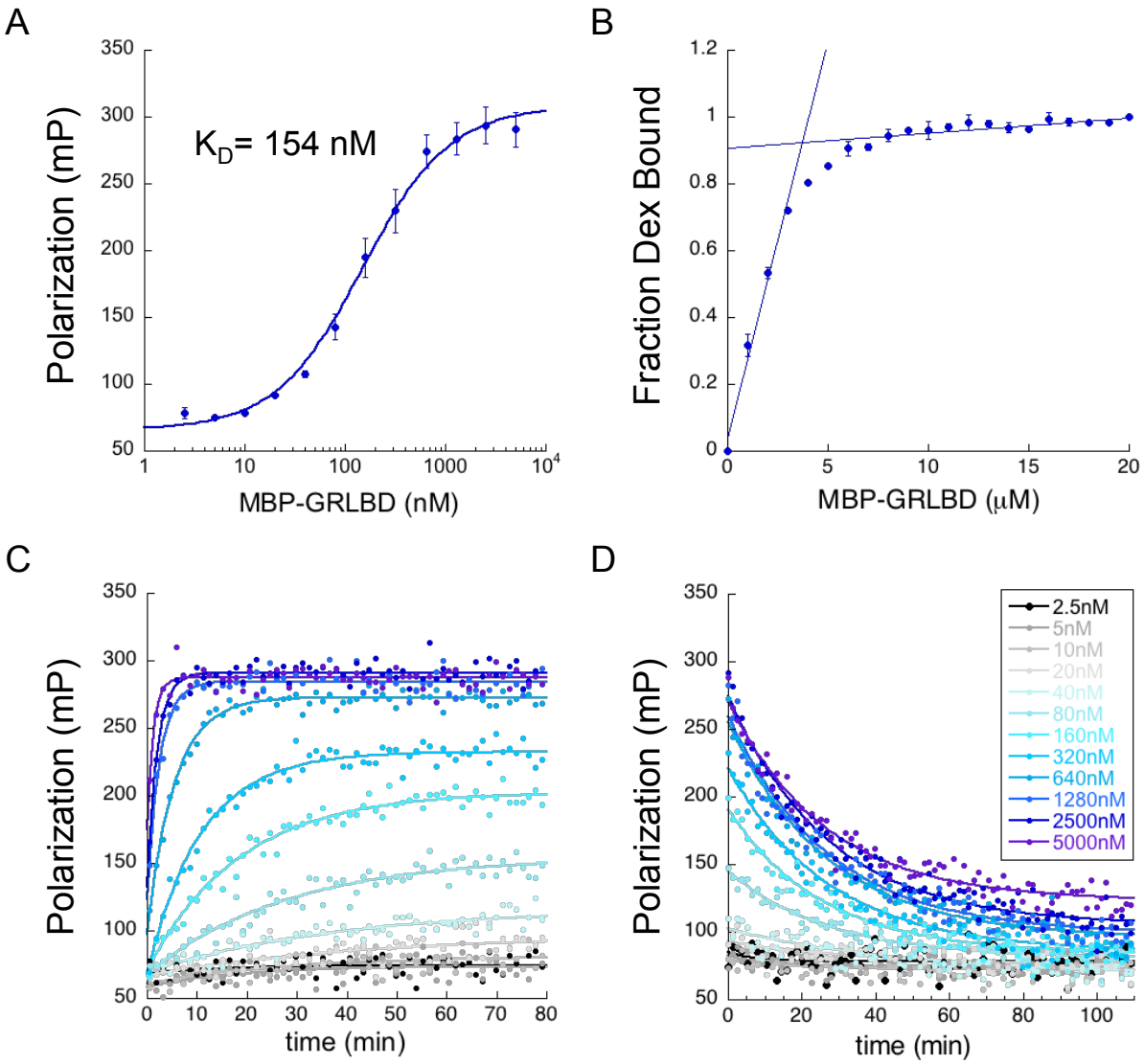

Figure 6. GRLBD ligand binding in the absence of chaperones.
A) Equilibrium ligand binding of 20 nM F-dex to varying concentrations of MBP-GRLBD fit with a single site binding model yields a K_D of 154±14 nM. (Exp585, 669, and 670)
B) Stoichiometric equilibrium binding of MBP-GRLBD with 2μM F-dex yields an approximate specific activity of 56±4%. (Exp846)
C) Association kinetics of 20nM F-dex (as in A) to varying concentration of MBP-GRLBD. (Exp585)
D) Dissociation kinetics of F-dex initiated with excess unlabeled dex. (Exp585)

Hsp90 does not enhance GRLBD ligand binding

Even more surprising than the fact that purified GRLBD binds ligand *in vitro* without Hsp90, was that I was unable to detect a significant enhancement in GRLBD ligand binding

upon the addition of Hsp90 (Figure 7). Additionally, I was unable to detect any indication of a stable high affinity interaction between just the two proteins by SEC-MALS (data not shown) or MBP-GRLBD pull-down (data not shown, Exp768). Detection of Hsp90 binding was attempted by fluorescence anisotropy of IADANS labeled GRLBD but results were unclear and complicated by the high baseline anisotropy of GRLBD alone (data not shown, Exp364-369 and 383). Additionally, I was unable to detect an effect of GRLBD on Hsp90's conformation cycle in the form of acceleration in Hsp90's ATP hydrolysis rate (discussed below) or Hsp90's closure rate measured by FRET with yeast Hsp90 (Hsc82) (data not shown, Exp446).

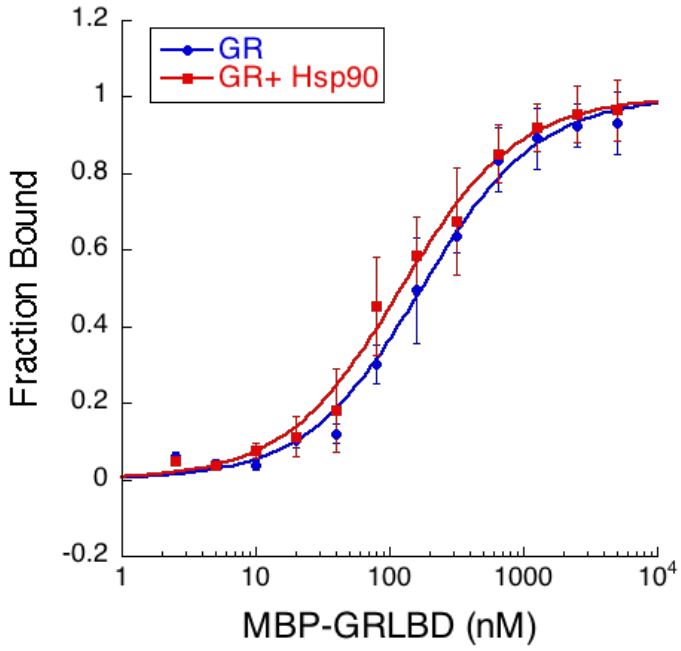

Figure 7. No significant enhancement in GRLBD ligand binding detected.
Equilibrium ligand binding of 20nM F-dex to varying concentrations of MBP-GRLBD alone or with 5μM Hsp90 (monomer). (Exp712 and 714)

F602S does not account for Hsp90 independent ligand binding *in vitro*

One caveat to the conclusions drawn above is that this work was with the GRLBD F602S mutant of Hsp90 that is less dependent on Hsp90 (discussed in Chapter1). Also, the previous report of the stimulation of Hsp90's ATP hydrolysis rate was with WT GRLBD. To validate our conclusion, WT GRLBD was purified. Purification yields were dramatically reduced for the WT protein, but co-expression with Hsp90 helped reduce the amount of GRLBD lost to degradation (data not shown, Exp430). GRLBD was also co-expressed with the co-chaperones p23 and FKBP52 (FKBP52 discussed in Chapter 6), although it was unclear to what extent the additional cochaperones helps with the solubility. Please see Appendix Section 1 for more details.

Remarkably, the WT GRLBD bound ligand better than the F602S mutants (Figure 8A), indicating that the lack of the Hsp90 dependence *in vitro* is not the result of the F602S mutation. SEC-MALS shows that like the F602S mutant, WT GRLBD is also monomeric (Figure 8B). Intriguingly, while both constructs are monomeric mono-dispersed peaks, the WT GRLBD elutes earlier on the size exclusion column, suggesting that the F602S mutation results in a conformational compaction compared to the WT. To test this further the F602S mutants was compared to WT by HDX-MS, but no significant difference in exchange rates could be detected (data not shown). While it is still unclear what the F602S mutation is doing to GRLBD and the exact mechanism by which it reduces the Hsp90 dependence *in vivo*, the F602S mutation is clearly not the reason behind the lack of Hsp90 dependence *in vitro*.

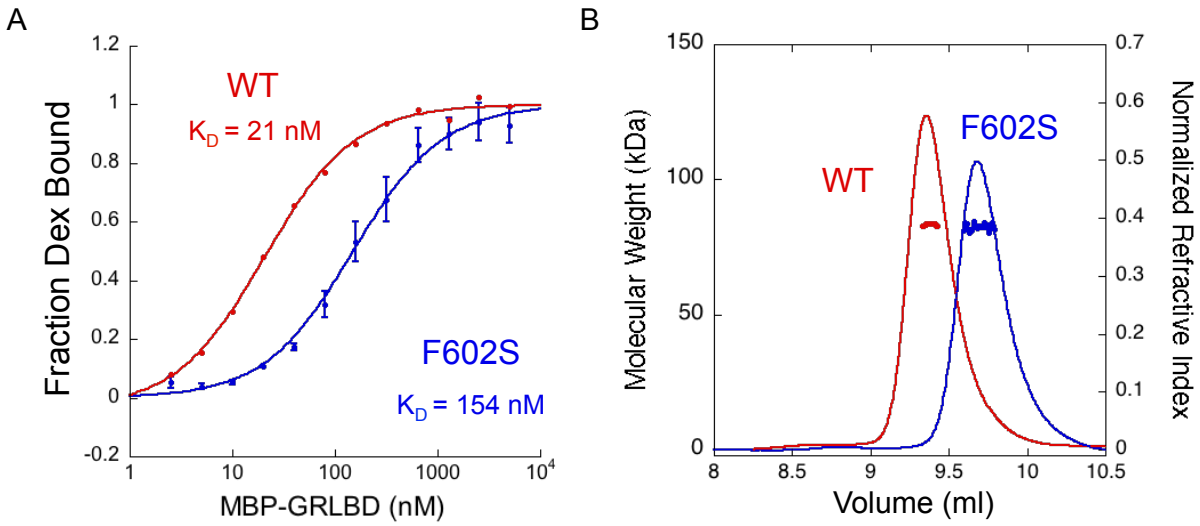

Figure 8. Comparison of GRLBD WT and F602S.
A) WT GRLBD binds ligand better than GRLBD F602S. Equilibrium ligand binding of 20nM F-dex to varying concentrations of MBP-GRLBD. (Exp648)
B) SEC-MALS of ~6μM MBP-GRLBD for WT in red (Exp647) and F602S in blue (Exp783).

Apo GRLBD inhibits Hsp90's ATPase activity

At the time the work covered in Chapters 3-5 was in press for publication, the Buchner lab published a manuscript reporting that GRLBD inhibits ATP hydrolysis on Hsp90 (Lorenz et al., 2014). This investigation was carried out with yeast Hsp90, which has a significantly enhanced ATP hydrolysis rate compared to human, and a variant of GRLBD containing five solubility enhancing mutation that were identified in a high-through put screen; F602S, A605V, V702A, E705G, and M752T referred to as GRLBDm (Seitz et al., 2010). While with slightly less potency (Ki of 7.1μM vs 8.7μM), the inhibition effect held true for the single F602S mutation, and was independent of the ligand state of the receptor. I was able to reproduce this effect with GRLBD F602S although with less potency (K_i on the order of ~12μM) (Figure 9A).

This inhibition effect on Hsp90 ATPase activity by GRLBD carried out with the F602S mutants is contradictory to the earlier report by the Jackson lab, which was performed with WT GRLBD (McLaughlin et al., 2002). To determine if the F602S mutation was responsible for this discrepancy, the effect of WT GRLBD on yeast Hsp90 ATPase rate was investigated. WT GRLBD was purified the same as GRLBD F602S with the exception that 0.04% CHAPS was added to all buffers to aid with solubility. Addition of the WT GRLBD at first seemed to accelerate the rate of ATP hydrolysis, however addition of equivalent GR storage buffer with 0.04% CHAPS alone was responsible for the observed stimulation. Rates normalized by buffer subtraction indicate that the WT GRLBD has no effect on Hsp90's ATPase rate (Figure 9B). This indicates that the F602S mutation does not account for the discrepancy between the reports.

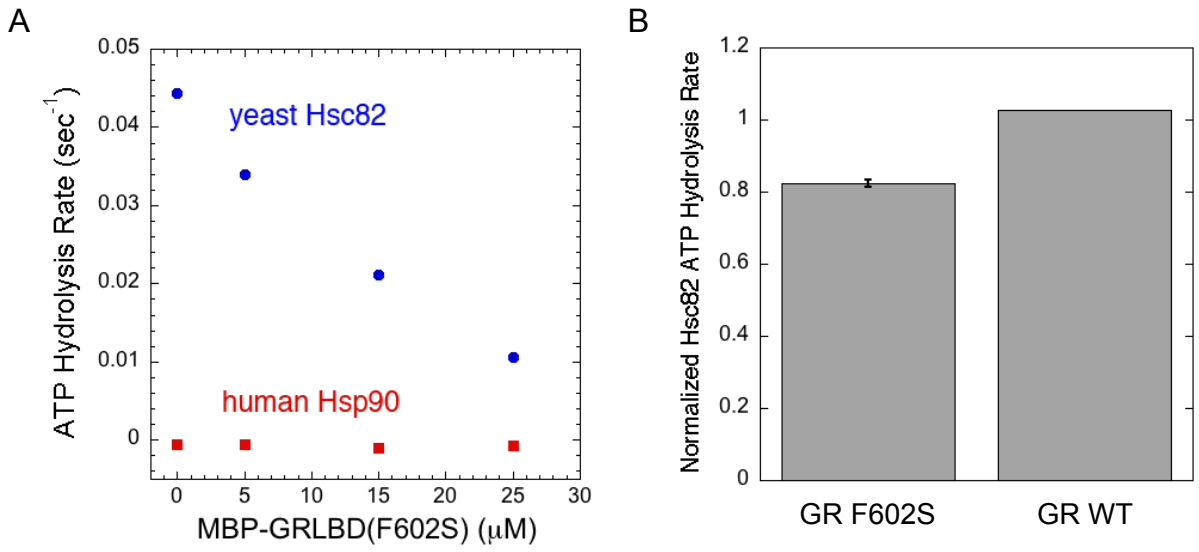

Figure 9. GRLBD Inhibits Hsp90 ATP Hydrolysis.
A) Inhibition of Hsp90's ATP hydrolysis is detected for yeast Hsp90. ATP hydrolysis rates measured for 5μM Hsp90 humanα (red square) and yeast Hsc82 (blue circle) with increasing amounts of MBP-GRLBD (F602S). Inhibition curve for yeast yields an IC50 on the order of 12μM. ATP hydrolysis rate measured by NADH coupled assay at 30°C. (Exp779)

B) Normalized ATP hydrolysis rates for yeast Hsc82 as in (A) for 5μM MBP-GRLBD F602S and WT. No detectable effect on Hsp90's ATP hydrolysis rate at 5μM MBP-GRLBD was detected for WT, indicating that the F602S mutation does not account for the discrepancy with previous reports in which stimulation was reported. (Exp851)

Discussion

Our results cannot rule out that the state of GRLBD obtained when purified with zwittergent was not contributing to some degree to the stimulation of ATP hydrolysis on Hsp90. Unfortunately, the detergent artifacts made it impossible to determine either way. The detergent free apo GRLBD that is more amenable to rigorous biophysical characterization used in this study is clearly in a different state than that of the zwittergent purified apo GRLBD from the Jackson lab, regardless of the F602S mutation. Because of this, the two reports should not necessarily be compared.

Even if there is some truth to the acceleration in Hsp90's ATPase activity by the zwittergent purified apo GLRBD, it is due to the state of GRLBD obtained from refolding the receptor from denatured protein in the presence of the zwittergent detergent and not due to a state favored by the WT GRLBD compared to the F602S mutant. Given that the WT GRLBD binds ligand with higher affinity than the F602S mutant, the exact reason as to why GRLBD F602S is less dependent on Hsp90 is still unclear. The source is likely due to either stability or some other cellular factors. Given that the WT protein can now be purified, the thermal stability of the WT compared to F602S GRLBD constructs can be directly measured to determine if in fact stability at physiological condition is the determining factor. If so, it would correlate with previous findings that showed that thermal stability was the only physical feature that correlated with the strength of the Hsp90 interaction (Taipale et al., 2012).

The inhibition of Hsp90's ATPase activity by GRLBD indicates that while weak, there is in fact a direct interaction between Hsp90 and GRLBD. However, this mode of interaction does not appear to have a significant functional consequence on GRLBD's ligand binding. We failed to detect the ATPase inhibition earlier in our work because this effect is not readily apparent with the human Hsp90 homologue, which was the focus of our efforts. In addition to the extremely low ATP hydrolysis rate of the human Hsp90, the interaction also appears weaker for the human homologue than the yeast homologue (Lorenz et al., 2014). This is likely due to the fact the GRLBD preferentially bound to a closed conformation of Hsp90, which is a conformational state that the human Hsp90 homologue rarely samples (Southworth and Agard, 2008).

In addition to the F602S mutation, GRLBDm used by the Buchner lab also contains a mutation on a residue corresponding to one of the GR mutants identified in the yeast genetics screen as being less dependent on Hsp90 (Ricketson et al., 2007). M752 has been characterized as being part of an allosteric network on GRLBD that regulates both ligand and co-activator binding, with M752I biasing GRLBD's conformation to the agonist state stabilized by co-activators (Pfaff and Fletterick, 2010; Ricketson et al., 2007). Intriguingly, based on the affinities derived from the ATPase inhibition assay, the GRLBDm has a slightly higher affinity to Hsp90 than GRLBD F602S (Lorenz et al., 2014). Given that the GRLBDm is likely in a more agonist like state than GRLBD F602S, the observation that GRLBDm has a higher affinity to Hsp90 correlates with the Darimont model (Chapter 1, Figure 3) in which Hsp90 preferentially binds to the agonist state of GRLBD.

While the functional relevance of the work by Lorenz and co-workers is still unclear, it seems to reflect the mode of interaction that Hsp90 has with the ligand bound state of

GRLBD that is likely involved in the translocation of GR to the nucleus (discussed in Chapter 6). Given the stringent requirement of Hsp90 *in vivo,* the lack of influence by Hsp90 on the ligand binding activity of GRLBD is surprising. However, the weak interaction and lack of an effect on ligand binding aligns with the work by Pratt and co-workers where prior interaction with Hsp70 was absolutely required for GR to bind Hsp90 and for the subsequent Hsp90 dependent ligand binding activation to take place.

Experimental Procedures

ATPase Activity

Earlier ATP hydrolysis assays with the apo purified GRLBD in zwittergent detergent were carried out by measuring radioactive ^{32}P phosphate release as previously described (Cunningham et al., 2008). 5μM Hsp90 (monomer) was used in each reaction with 5mM ATP and 0.8 pM [γ-32P]ATP (6000 Ci/mmol). Reactions were carried out at 37°C in 20mM Tris pH7.5, 20mM KCl, 10mM $MgCl_2$ and 1mM DTT, and time point were take at 10, 20, 40 and 60 minutes by quenching the reaction with 1% SDS and 25mM EDTA. Hydrolysis rates were determined by subtracting background rates determined for the equivalent reaction but in the presence of 20μM 17AAG.

Later ATP hydrolysis experiments such as for Figure 9, were preformed using NADH coupled ATP regenerating system consisting of 200μM NADH, 1mM PEP, 53 U/mL PK, 45 U/mL LDH, and 5mM ATP. Reactions were carried out in 30mM HEPES pH7.5, 150mM KCl, and 2mM DTT. 70μL reactions with 5μM Hsp90 (monomer) were performed at 30°C in quartz cuvettes with the reduction of NADH detected by the absorbance at 340nm using an Agilent 8453 UV-visible spectrophotometer.

SAXS Data Collection and Analysis

Scattering data was collected at the ALS SIBYLS beam line 12.3.1. Data was buffer subtracted using ogreNew, and the scattering data was transformed to P(r) using GNOM. Guinier analysis was preformed in PRIMUS. CRYSOL was used to generate theoretical scattering plots from GRLBD crystal structures.

SEC-MALS

50µL of the protein sample was injected and resolved on a Showdex 803 column attached to an Ettan LC (GE Healthcare). Molecular weights were determined by MALS with an in-line DAWN HELEOS MALS detector and Optilab rEX differential refractive index detector (Wyatt Technology Corporation). Data were analyzed by the ASTRA V software package (Wyatt Technology Corporation).

Hydrogen Deuterium Exchange Mass Spectrometry

Solution-phase amide HDX was carried out with a fully automated system (Goswami et al., 2013). For HDX, 5µl of 10µM GRLBD was diluted to 25µl with D_2O-containing HDX buffer and incubated at 4 °C for 10s, 30s, 60s, 900s or 3,600s. Following exchange, the protein was denatured by dilution to 50µl with 0.1% (v/v) TFA in 3 M urea and 50 mM TCEP and subjected to online pepsin digestion and electrospray ionization directly coupled to a high resolution (60,000 at m/z 400) Orbitrap mass spectrometer (LTQ Orbitrap XL with ETD, Thermo Fisher). In-house software was used for analysis (Pascal et al., 2012). For back exchange correction, an average of 70% recovery was estimated.

Fluorescence Polarization Assays

Fluorescence polarization of 20nM fluorescein-labeled dexamethasone (Molecular Probes, D1383) was measured on a SpectraMax M5 plate reader (Molecular Devices) with excitation/emission waves lengths of 485/538 nm, temperature control set at 25°C, and in 30mM HEPES pH7.5, 150mM KCl, and 2mM DTT.

Acknowledgements

I thank K. Krukenberg for help with the SAXS data collection and data analysis, S. Pfaff for all the helpful discussions related to GRLBD purification and for providing the apo GRLBD used in the SAXS analysis, and D. Southworth for help resolving the detergent effects on Hsp90.

References

Bledsoe, R.K., Montana, V.G., Stanley, T.B., Delves, C.J., Apolito, C.J., McKee, D.D., Consler, T.G., Parks, D.J., Stewart, E.L., and Willson, T.M. (2002). Crystal Structure of the Glucocorticoid Receptor Ligand Binding Domain Reveals a Novel Mode of Receptor Dimerization and Coactivator Recognition. Cell *110*, 93–105.

Cunningham, C.N., Krukenberg, K.A., and Agard, D.A. (2008). Intra- and Intermonomer Interactions Are Required to Synergistically Facilitate ATP Hydrolysis in Hsp90. J. Biol. Chem. *283*, 21170–21178.

Goswami, D., Devarakonda, S., Chalmers, M.J., Pascal, B.D., Spiegelman, B.M., and Griffin, P.R. (2013). Time window expansion for HDX analysis of an intrinsically disordered protein. J. Am. Soc. Mass Spectrom. *24*, 1584–1592.

Lorenz, O.R., Freiburger, L., Rutz, D.A., Krause, M., Zierer, B.K., Alvira, S., Cuellar, J., Valpuesta, J.M., Madl, T., Sattler, M., et al. (2014). Modulation of the Hsp90 Chaperone Cycle by a Stringent Client Protein. Mol. Cell *53*, 941–953.

McLaughlin, S.H., Smith, H.W., and Jackson, S.E. (2002). Stimulation of the weak ATPase

activity of human Hsp90 by a client protein. J. Mol. Biol. *315*, 787–798.

Pascal, B.D., Willis, S., Lauer, J.L., Landgraf, R.R., West, G.M., Marciano, D., Novick, S., Goswami, D., Chalmers, M.J., and Griffin, P.R. (2012). HDX Workbench: Software for the Analysis of H/D Exchange MS Data. J. Am. Soc. Mass Spectrom. *23*, 1512–1521.

Pfaff, S.J., and Fletterick, R.J. (2010). Hormone binding and co-regulator binding to the glucocorticoid receptor are allosterically coupled. Journal of Biological Chemistry *285*, 15256–15267.

Ricketson, D., Hostick, U., Fang, L., Yamamoto, K.R., and Darimont, B.D. (2007). A Conformational Switch in the Ligand-binding Domain Regulates the Dependence of the Glucocorticoid Receptor on Hsp90. J. Mol. Biol. *368*, 729–741.

Seitz, T., Thoma, R., Schoch, G.A., Stihle, M., Benz, J., D'Arcy, B., Wiget, A., Ruf, A., Hennig, M., and Sterner, R. (2010). Enhancing the stability and solubility of the glucocorticoid receptor ligand-binding domain by high-throughput library screening. J. Mol. Biol. *403*, 562–577.

Simmons, C.A., Bledsoe, R.K., Guex, N., and Pearce, K.H. (2008). Expression, purification, and characterization of multiple, multifunctional human glucocorticoid receptor proteins. Protein Expression and Purification *62*, 29–35.

Southworth, D.R., and Agard, D.A. (2008). Species-Dependent Ensembles of Conserved Conformational States Define the Hsp90 Chaperone ATPase Cycle. Mol. Cell *32*, 631–640.

Taipale, M., Krykbaeva, I., Koeva, M., Kayatekin, C., Westover, K.D., Karras, G.I., and Lindquist, S. (2012). Quantitative Analysis of Hsp90-Client Interactions Reveals Principles of Substrate Recognition. Cell *150*, 987–1001.

Chapter 3

Coordinated Actions of Hsp70 and Hsp90 Regulate GR Function

Contributing Authors: Devrishi Goswami, Patrick Griffin, and David Agard

Preface

Since Hsp70 can facilitate client delivery to Hsp90, we reasoned that Hsp70 might stabilize a state of GRLBD better capable of interacting with Hsp90; therefore enhancing any effect Hsp90 might have on GR ligand binding. This would be in line with the body of work by Pratt and co-workers in which Hsp70 was required for GR to interact with Hsp90 (discussed in Chapter 1).

Summary

Hsp70, with the aid of Hsp40, inactivates GR through partial unfolding, while Hsp90 reverses this inactivation, promoting ligand binding. Full recovery of ligand binding requires ATP hydrolysis on Hsp90 and the HOP and p23 cochaperones. Surprisingly, energy from Hsp90 ATP hydrolysis appears to regulate client transfer from Hsp70, suggesting a coupling of the two chaperone's ATP cycles. Incorporation of p23 into the receptor-chaperone complex requires ATP hydrolysis on Hsp90, indicating that p23 acts in a post hydrolysis state. Together, the entire Hsp70-Hsp90 chaperone system works cooperatively to enhance GR ligand binding.

Hsp70 Introduction

Hsp70 is an ATP dependent molecular chaperone, with the nucleotide state dictating substrate interactions and has been well reviewed (Mayer and Bukau, 2005; Mayer, 2013). Hsp70 has two main domains; a substrate binding domain (SBD) that binds substrates, and a nucleotide binding domain (NBD) which regulates the conformational state of the SBD in a nucleotide dependent. In the ATP state Hsp70 has weak and transient substrate binding allowing for substrate capture and release, and the ADP state has stable high affinity substrate binding (Figure 1A). Compared to Hsp90, Hsp70 is considered a more canonical chaperone in that it interacts with proteins in more unfolded states. This is in part based on the crystal structure of the SBD bound to a substrate peptide (Zhu et al., 1996). The SBD consists of two subdomains with substrates binding directly to the β-sheet subdomain that forms a deep hydrophobic groove to which completely extended stretches of about 5-7 mostly hydrophobic residues bind. At the top of the substrate binding groove, two loop residues from either side of the cleft form an arch over the substrate. The helical lid subdomain further stabilizes substrate binding by latching over the substrate binding site to form a secondary latch (Mayer et al., 2000).

In the ATP state, the NBD docks onto the SBD and makes extensive contacts with both the β-sheet and helical lid subdomains such that the lid is in an extended open state and the substrate binding groove becomes more shallow, together resulting in the transient and weak substrate binding required for capture and release (Figure 1B) (Kityk et al., 2012; Zhu et al., 1996). Upon ATP hydrolysis the NBD dissociates allowing the SBD to assume it high affinity client state (Figure 1C). Hsp70 by itself has a very slow rate of ATP hydrolysis with hydrolysis being an important point of regulation. While substrate binding alone will

stimulate hydrolysis, hydrolysis is largely regulated by J-domain containing proteins, such as Hsp40, which alone and synergistically with substrates promote ATP hydrolysis through a conserved J-domain (Kampinga and Craig, 2010). While the J-domain is sufficient for stimulating ATP hydrolysis, Hsp40 chaperones contains additional domains involved in client binding which allow for the coupling of client binding and stimulation of ATP hydrolysis on Hsp70 (Li et al., 2003). For the hormone receptors, Hsp40 clearly binds PR directly, with Hsp40 binding preceding Hsp70 (Hernández et al., 2002). While this suggests that Hsp40 is important for receptor loading on Hsp70, for GR it was argued that Hsp70 binds first in its ATP form and that Hsp40 functions solely to promote ATP hydrolysis on Hsp70 (Murphy et al., 2003).

Once in the ADP state, the substrate is securely bound until ADP/ATP exchange occurs resulting in the re-docking of the NBD, which in turn opens the substrate binding site so substrates can be released. In the presence of Hsp40, this becomes the rate-limiting step that is regulated by a class of proteins called nucleotide exchange factors (NEF), which facilitate this process (discussed in Chapter 5).

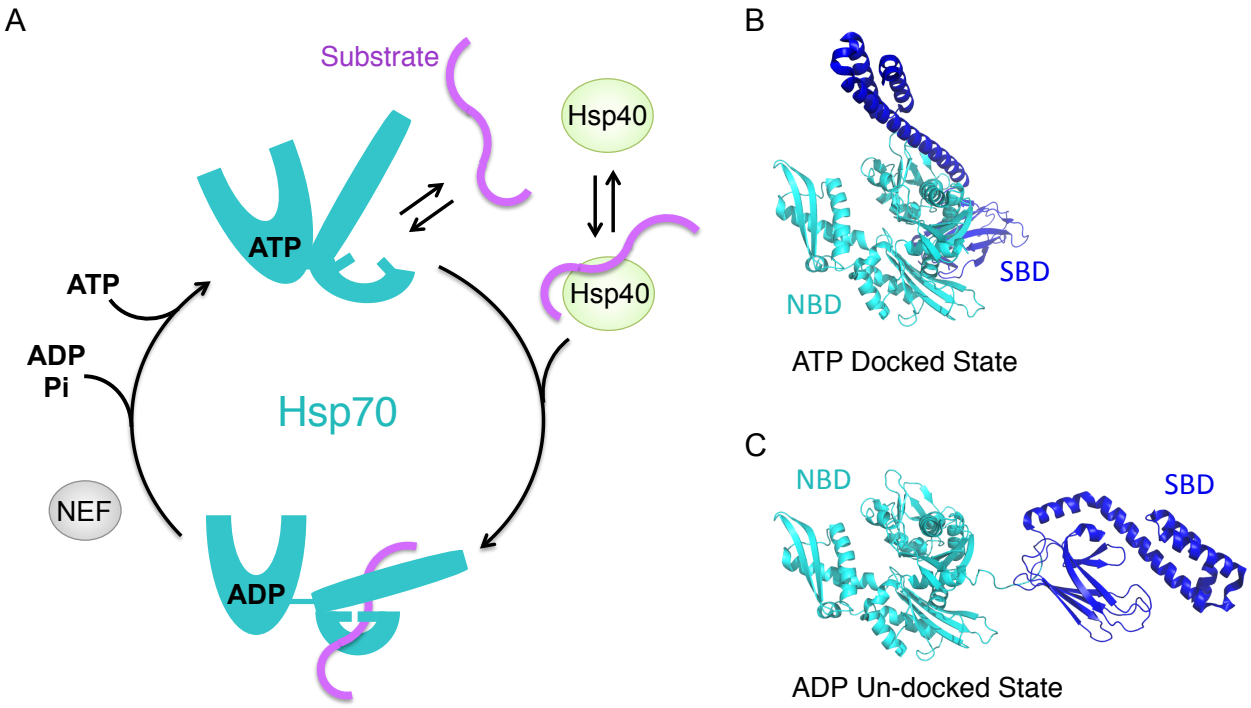

Figure 1. Hsp70's ATP driven chaperone cycle.
A) Chaperone cycle of Hsp70. In the ATP state, Hsp70 NBD induces an open conformation of the SBD such that substrate binding is highly dynamic and weak. Substrate and Hsp40 stimulate ATP hydrolysis, promoting the dissociation of the NBD from the SBD. This results in a high affinity substrate state in which the substrate is tightly bound in the substrate binding site with the lid latched down. Substrate release occurs upon ADP:ATP exchange which is promoted by nucleotide exchange factors (NEF).
B) Crystal structure of the ATP state of Hsp70 (pdb 4B9Q), with the NBD (cyan) docked onto the open state of the SBD (dark blue)
C) Crystal/NMR structure of the ADP state of Hsp70 (pdb 2KHO), with the NBD (cyan) dissociated from the SBD, resulting the a closed state of the SBD (dark blue).

Results

Hsp70 inhibits GR ligand binding

Remarkably, apo GRLBD preincubated with just the Hsp70 system resulted in complete inhibition of GRLBD ligand binding (Figure 2). Based on previous studies (Dittmar et al., 1998; Stancato et al., 1996), we used sub-stoichiometric amounts of yeast Hsp40 (Ydj1) to accelerate Hsp70 ATP hydrolysis. Hsp40 has no effect on its own, but is

required for GRLBD inhibition (Figure 2A) and to promote stable binding of Hsp70 to GRLBD (Figure 3B). Sub-stoichiometric amounts of Hsp40 was determined to be saturating in its effect (Figure S1). ATP hydrolysis is also essential, as no GRLBD inhibition is observed with AMPPNP or ADP (Figure 3A). Along these lines, almost no Hsp70 was bound in the presence of ADP. Weak binding is observed with AMPPNP, supporting the concept that Hsp70 first binds substrates in the ATP sate, but hydrolysis is required for inhibition. The concentration dependence of Hsp70 shows a cooperative mode of inhibition with an IC_{50} of 4.6±0.6μM and a Hill coefficient of 1.6±0.6 (Figure 2B).

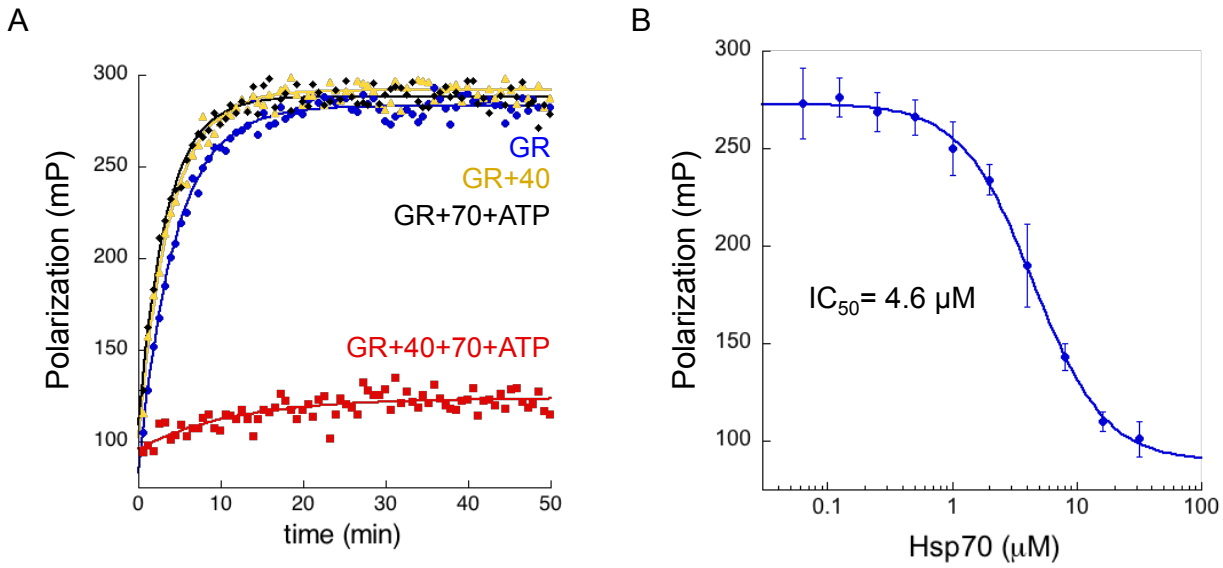

Figure 2. Hsp70 inhibits GRLBD ligand binding.
A) Association kinetics of F-dex to GRLBD alone (blue circle), with Hsp40 (yellow triangle), with Hsp70 and ATP (black diamond), and with Hsp40, Hsp70 and ATP (red square). Assay conditions: 5mM ATP/$MgCl_2$, 50nM F-dex, 1μM MBP-GRLBD, 2μM Hsp40 and 15μM Hsp70. (Exp638)
B) Hsp70 concentration dependence of equilibrium binding of 1μM MBP-GRLBD to 20nM F-dex (with 2μM Hsp40). Inhibition curve fit to a cooperative competitive binding model with an IC_{50} of 4.6±0.4 μM and a Hill coefficient of 1.6±0.4 μM (±SEM). (Exp672 and 619)

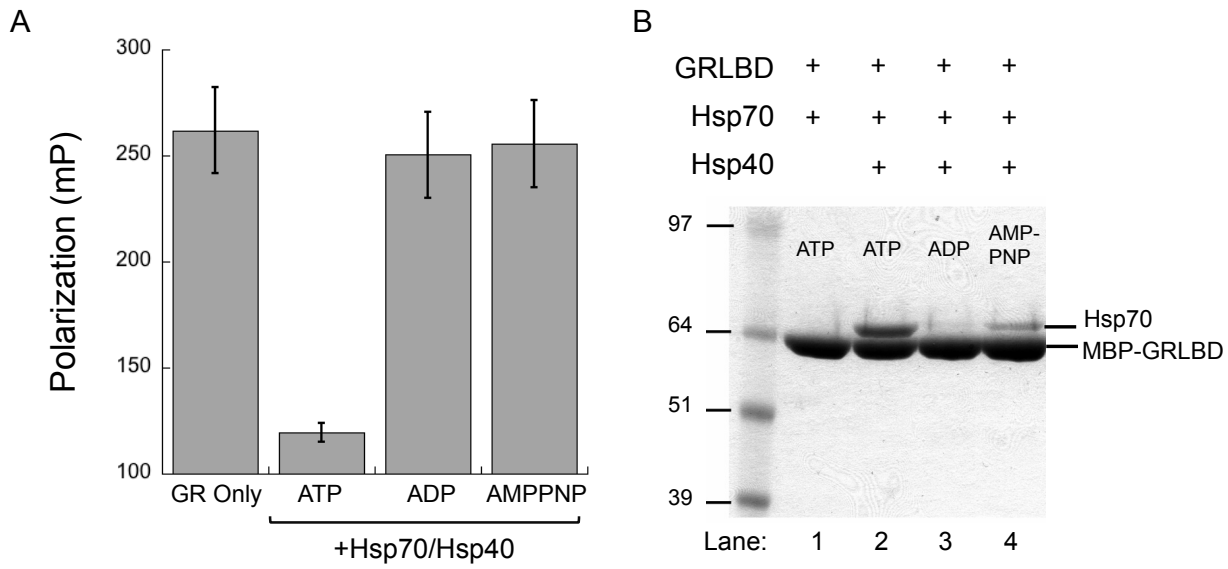

Figure 3. Hsp70 binding and inhibition of GRLBD requires Hsp40 and ATP hydrolysis.
A) Equilibrium binding of F-dex to GRLBD with and without Hsp40 and Hsp70 with indicated nucleotide (±SEM). Assay conditions: 20nM F-dex, 1μM MBP-GRLBD, 2μM Hsp40, 15μM Hsp70, and 5mM $MgCl_2$/nucleotide. (Exp805)
B) MBP pull down with MBP-GRLBD visualized by coomassie stained SDS-PAGE. Lane 1 and 2 shows no detectable interaction with Hsp70 without Hsp40. Lane 3 and 4 shows ATP hydrolysis is required for stable Hsp70 binding. Assay conditions: 5μM MBP-GRLBD, 2μM Hsp40, 15μM Hsp70, and 5mM corresponding nucleotide. (Exp806)

Hsp70 promotes GR ligand dissociation

While this data shows that Hsp70 can bind to apo GRLBD and prevent ligand binding, we wanted to know if Hsp70 actively displaces ligand from an already ligand bound GRLBD (Figure 4C). To investigate this, GRLBD was pre-equilibrated with Hsp40 and F-dex and ligand dissociation initiated by excess unlabeled dex with and without Hsp70 (Figure 4A). Hsp70 was found to accelerate F-dex dissociation more than 2-fold (Figure 4B), revealing that Hsp70 directly catalyzes ligand removal from GRLBD.

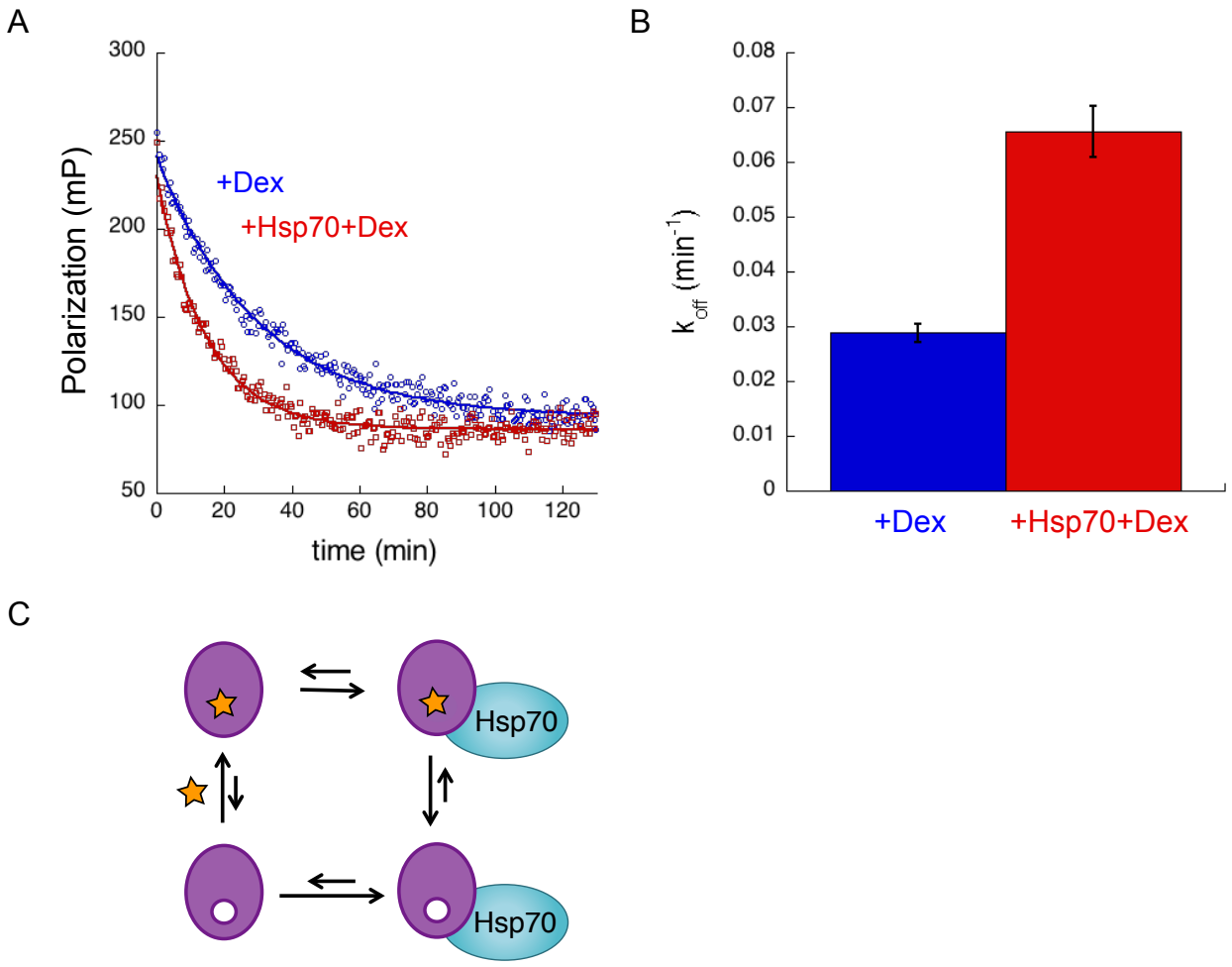

Figure 4. Hsp70 promotes GRLBD ligand dissociation.
A) Dissociation kinetics of 100nM F-dex from MBP-GRLBD (with 2μM Hsp40) initiated with excess (100μM) unlabeled dex (blue circle), or dex with 15μM Hsp70 (red square). Curves fit a single-phase exponential decay. (Exp680)
B) The average off rate; 0.029±0.002 min^{-1} for dex alone and 0.066±0.005 min^{-1} for dex with Hsp70 (±SEM). (Exp678-683)
C) Model for Hsp70 (teal) binding to both apo and holo GRLBD (purple).

Hsp70 induces partially unfolding of GRLBD

From the above, we hypothesized that Hsp70 is actively promoting GRLBD unfolding, thereby disrupting the conformation required for ligand recognition. Our expectation was that Hsp70 would significantly shift the equilibrium towards a completely unfolded GRLBD. However, limited proteolysis showed an increased sensitivity in only a

single region in helix 3 (Figure 5). Hsp70-induced unfolding was more quantitatively investigated by HDX-MS. While Hsp40 alone hand no effect (not shown), there was a significant increase in H/D exchange with both Hsp70 and Hsp40 in three limited GRLBD regions (Figure6). The most extensive increase was on helix 3 (residues 564-573) and then the β-sheet region (residues 621-631). This correlates with the limited proteolysis, confirming that Hsp70 induces only local unfolding. Interestingly, in addition to disrupting local structure and important hydrophobic contacts with the ligand, the region on helix 3 that was most effected contains residues N564 and Q570, which form three of the six hydrogen bonds between GRLBD and the ligand (Figure 6). This indicates that while the degree of overall unfolding is minimal, it is located for optimal disruption of ligand binding.

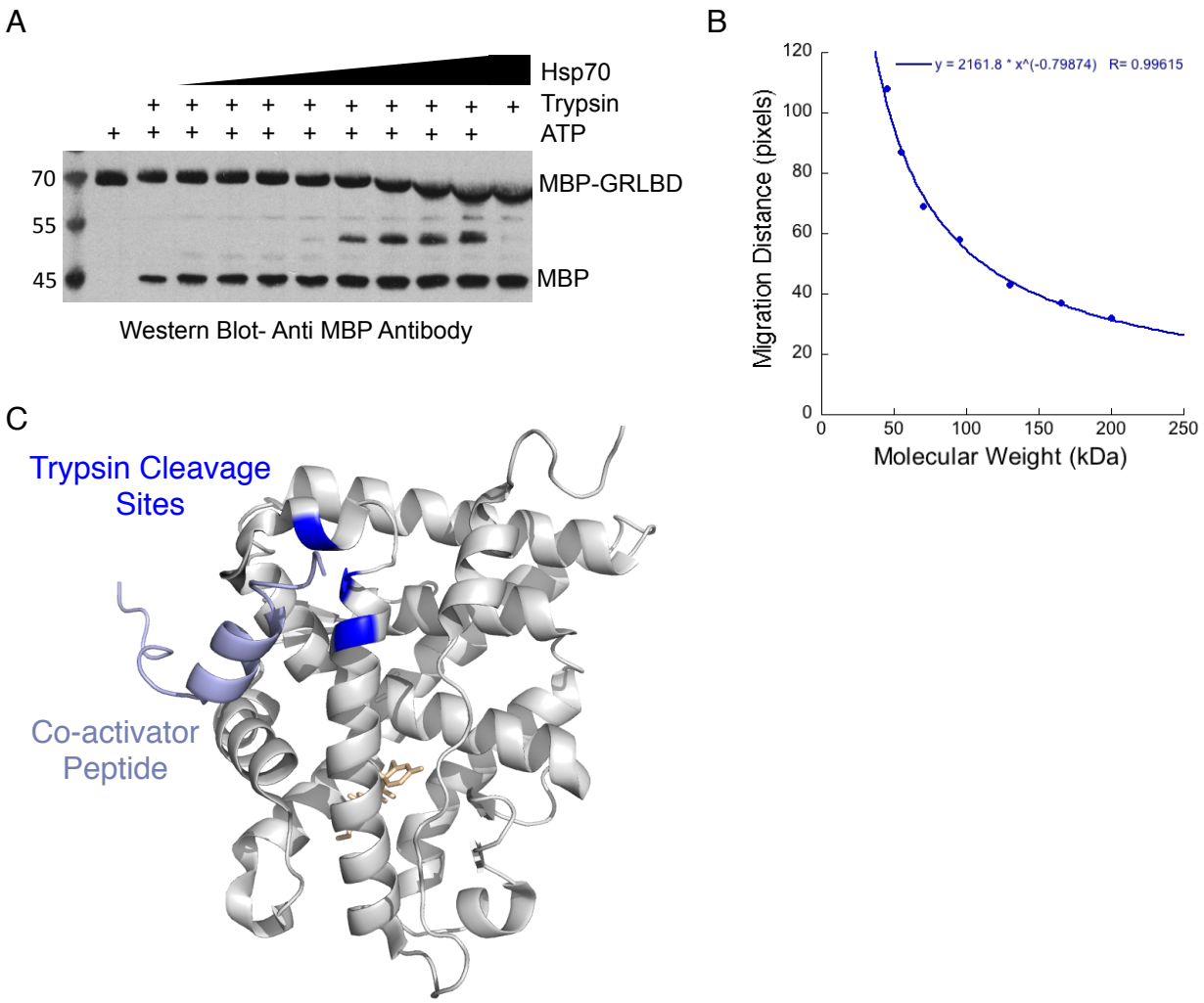

Figure 5. Partial unfolding of GRLBD by Hsp70 detected by limited proteolysis.
A) Limited proteolysis of GRLBD shows increased trypsin sensitivity with Hsp70. Western blot probed with MBP antibodies of reactions from trypsin digestion of 1μM MBP-GRLBD that were preincubated with 2μM Hsp40 and increasing concentrations of Hsp70 (0-32μM). (Exp618)
B) Migration distance measured in pixels of standards in marker according to molecular weight allows for…….fragment at 90-92 pixels would correspond to 52-54 kDa fragment – results from cleavage at either K576, K579, or R585 (blue).

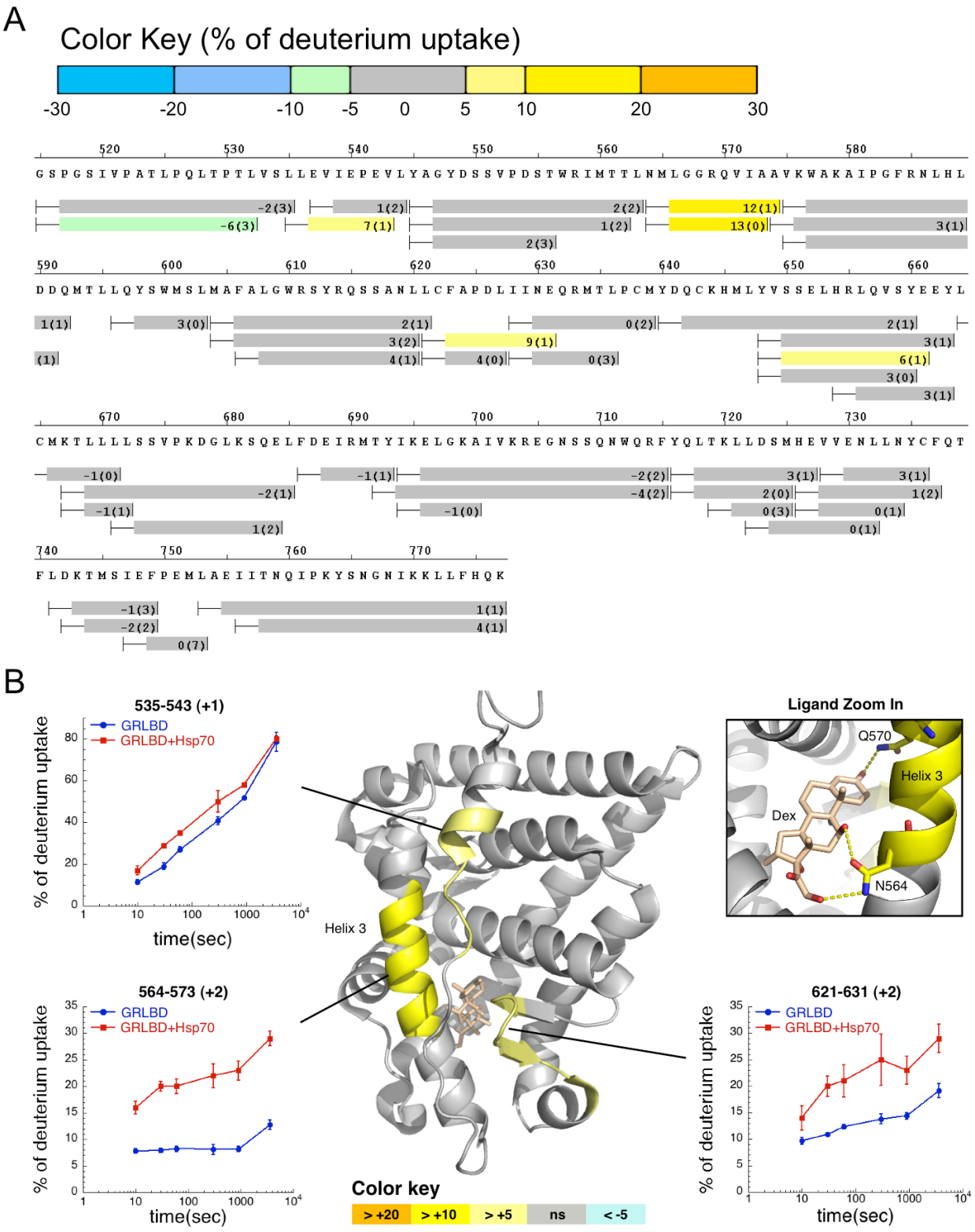

Figure 6. Partial unfolding of GRLBD by Hsp70 detected by HDX-MS.
A) Differential HDX-MS between 10μM GRLBD ± 12μM Hsp70 and 2μM Hsp40.

B) Differential HDX between GRLBD and Hsp70 bound GRLBD from (A) mapped onto the dex and coactivator peptide (not shown) bound crystal structure of GRLBD (pdb 1M2Z). Differences in the average HDX across six time points for Hsp70 bound and unbound LBD is represented as percentage change and colored according to the color key. Number within parentheses is the standard deviation between 3 replicates. Gray (ns), no significant changes between bound and unbound form; light yellow to orange is faster rates of HDX and light blue to dark blue is slower HDX in bound condition compare to unbound. Corresponding deuterium build-up curves for the regions that undergo the most significant conformational change are shown. Inset, top right, shows zoom in on dex, and the three hydrogen bonds it forms with helix 3.

Hsp90 recovers GR ligand binding

Given that Hsp90 is essential *in vivo* for ligand binding, and our finding that Hsp70 holds GRLBD in an inactive state, we explored Hsp90's ability to liberate GRLBD from Hsp70 inhibition. Including Hsp90 in the preincubation with Hsp70 and Hsp40 resulted in minimal recovery of ligand binding (Figure 7A). By contrast, significant recovery occurred with Hsp90 and either Hop or p23, the cochaperones that stabilize distinct states of Hsp90 (Figure 7A and B). Full recovery required both cochaperones. The concentrations used for Hop and p23 were saturating in their effect; thus partial recovery was not due to insufficient protein (Figure S2). Ligand binding recovery was entirely dependent on Hsp90, as no recovery was seen without Hsp90 or with the specific Hsp90 inhibitor, 17AAG. Thus, Hsp90 is the active component required for recovery of ligand binding, recapitulating the *in vivo* requirement. Interestingly, the Hsp90 concentration dependence of GRLBD recovery saturates at stoichiometric amounts of Hsp90 dimer and GRLBD (Figure 7C). This suggests a 1:1 interaction between monomeric GRLBD and dimeric Hsp90 and indicates tight binding of Hsp90 and cochaperones to the Hsp70:GRLBD complex, with an estimated K_D on the order of 200nM or less.

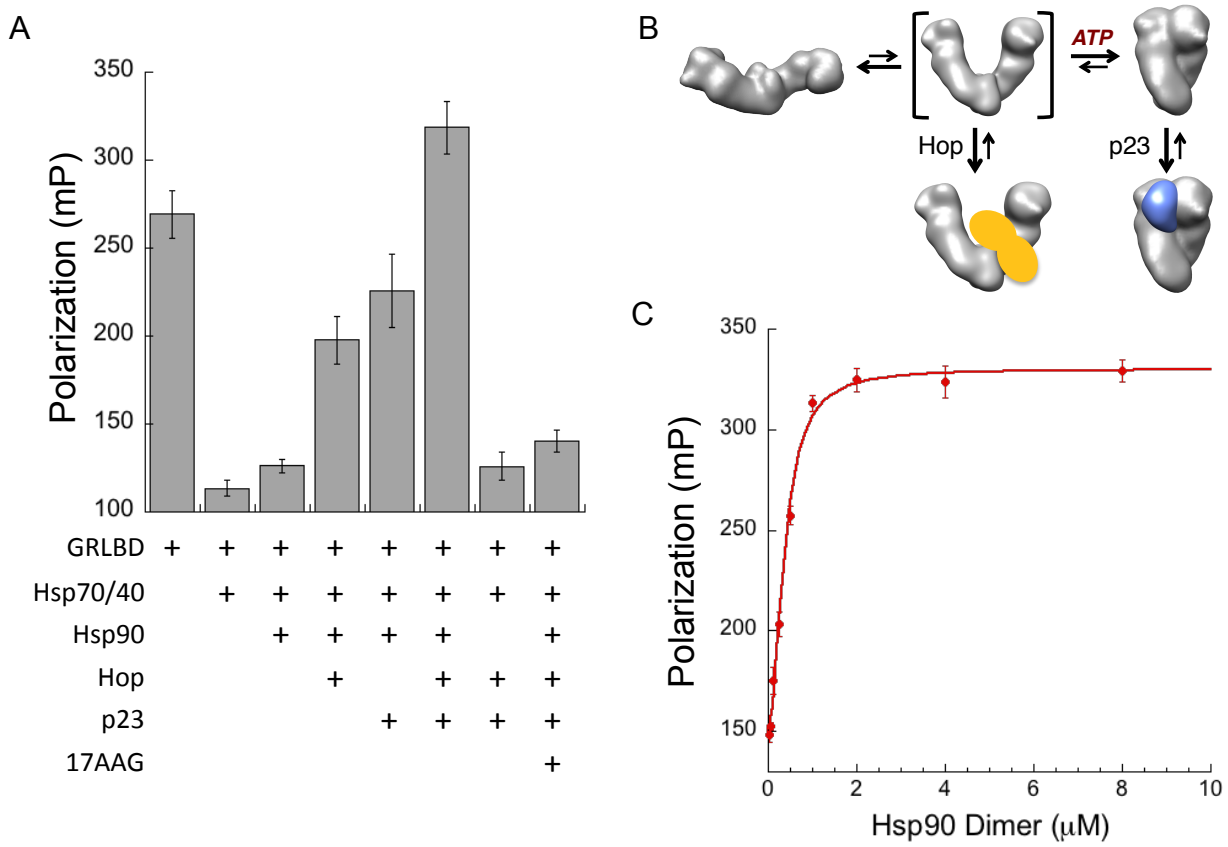

Figure 7. Hsp90 reverses the Hsp70 inhibition.
A) Equilibrium binding of 20nM F-dex to 1μM MBP-GRLBD with different chaperone components (±SE). Assay conditions; 50μM 17AAG, 2μM Hsp40, and 15μM Hsp70, Hsp90, Hop, and p23. (Exp674)
B) Schematic illustrating the different conformational states of Hsp90 and the distinct states stabilized by Hop and p23. Hop binds an intermediate state of Hsp90 that is on pathway to the closed state, to which p23 binds.
C) Stoichiometric equilibrium binding plot for 20nM F-dex binding to 1μM MBP-GRLBD with 2μM Hsp40, and 15μM Hsp70, Hop and p23, with increasing amounts of Hsp90. WT Hsp90 binding curve fit to a half maximal effective concentration equation. (Exp668)

As shown by MBP-GRLBD pull-down, the amount of GRLBD ligand binding activity correlates with the degree of Hsp90 incorporation into the receptor complex (Figure 8). Without Hop or p23, essentially no Hsp90 binding is detected. Partial binding is seen with p23 and Hop, with optimal binding detected with both. Binding of p23 and Hop appear weaker than the other components, and were additionally probed by western blot.

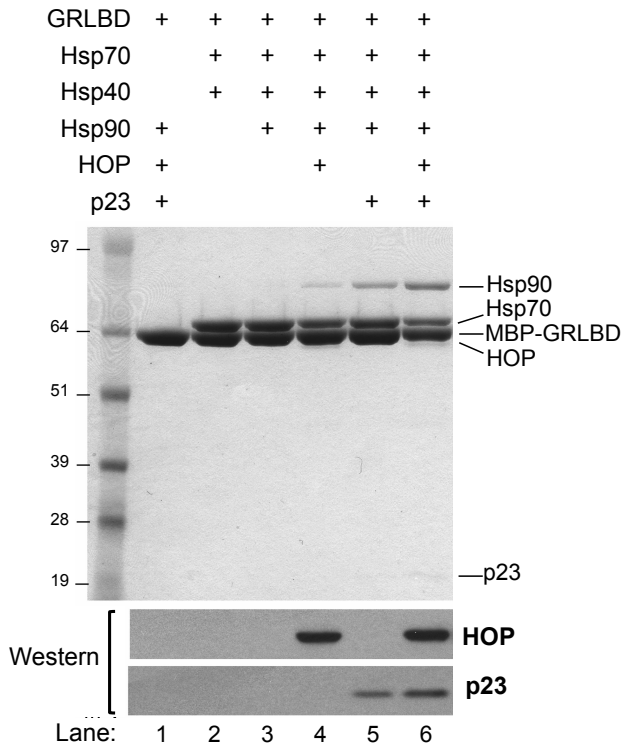

Figure 8. MBP-GRLBD pull-down with chaperones.
Coomassie stained SDS-PAGE (top), and western blot probing for HOP, p23, and Hsp40 (bottom). Lane 1 shows no/weak Hsp90 binding to GRLBD without Hsp70. Lane 2 shows Hsp70 binding with Hsp40. In addition to Hsp40 and Hsp70, lane 3 shows almost no detectable Hsp90 binding without Hop and p23. Lane 4 shows Hsp90 binding with just HOP, and lane 5 with just p23. Lane 6 shows more complete binding of Hsp90 with both Hop and p23. Assay conditions: 5μM MBP-GRLBD, 2μM Hsp40, and 15μM Hsp70, Hsp90, Hop, and p23. (Exp807)

Release of Hsp70 inhibition requires ATP hydrolysis by Hsp90

Inhibition by 17AAG, which binds to Hsp90's ATP binding pocket and prevents nucleotide binding, indicates the importance of ATP for recovery of GRLBD ligand binding. To explore further, we utilized two previously characterized hydrolysis dead mutations in Hsp90: D93N, which cannot bind nucleotide, and E47A, which can bind nucleotide and close but cannot hydrolyze ATP (Figure 9A) (Obermann et al., 1998). Neither mutant was

able to recover ligand binding (Figure 9B), indicating that both nucleotide binding and hydrolysis are required to reverse the Hsp70 inhibition.

Pull down studies show that in the presence of the chaperones an Hsp90:Hsp70:Hop:GRLBD complex forms and that neither 17AAG nor the Hsp90 mutations prevent formation of this large complex with Hsp90 (Figure 9C). By contrast, inhibition of ATP hydrolysis caused a loss in p23 association. Probing for Hop and p23 by western blot confirmed the presence of Hop and revealed no detectable incorporation of p23 with either Hsp90 mutant or 17AAG. For Hsp90 D93N, this is expected as this mutant cannot bind ATP which is required to stabilize the closed state to which p23 binds (Ali et al., 2006). By contrast, the significant loss in p23 binding to the GR complex with the Hsp90 E47A mutant was unexpected since E47A has been shown to support the binary interaction between p23 and Hsp90 (Johnson et al., 2007). The loss of p23 binding to the E47A mutant in the context of the full system indicates that p23 association is inhibited by some component of the Hsp90:GR complex prior to hydrolysis.

This, in combination with the inability to restore ligand binding, clearly illustrates that hydrolysis on Hsp90 facilitates an essential step in the pathway required for the release of Hsp70's inhibition, and that blocking hydrolysis results in a stalled inactive intermediate complex with Hsp70, Hsp90 and Hop but not p23. Consequently, p23's role in the receptor maturation pathway must occur on a post hydrolysis state of Hsp90.

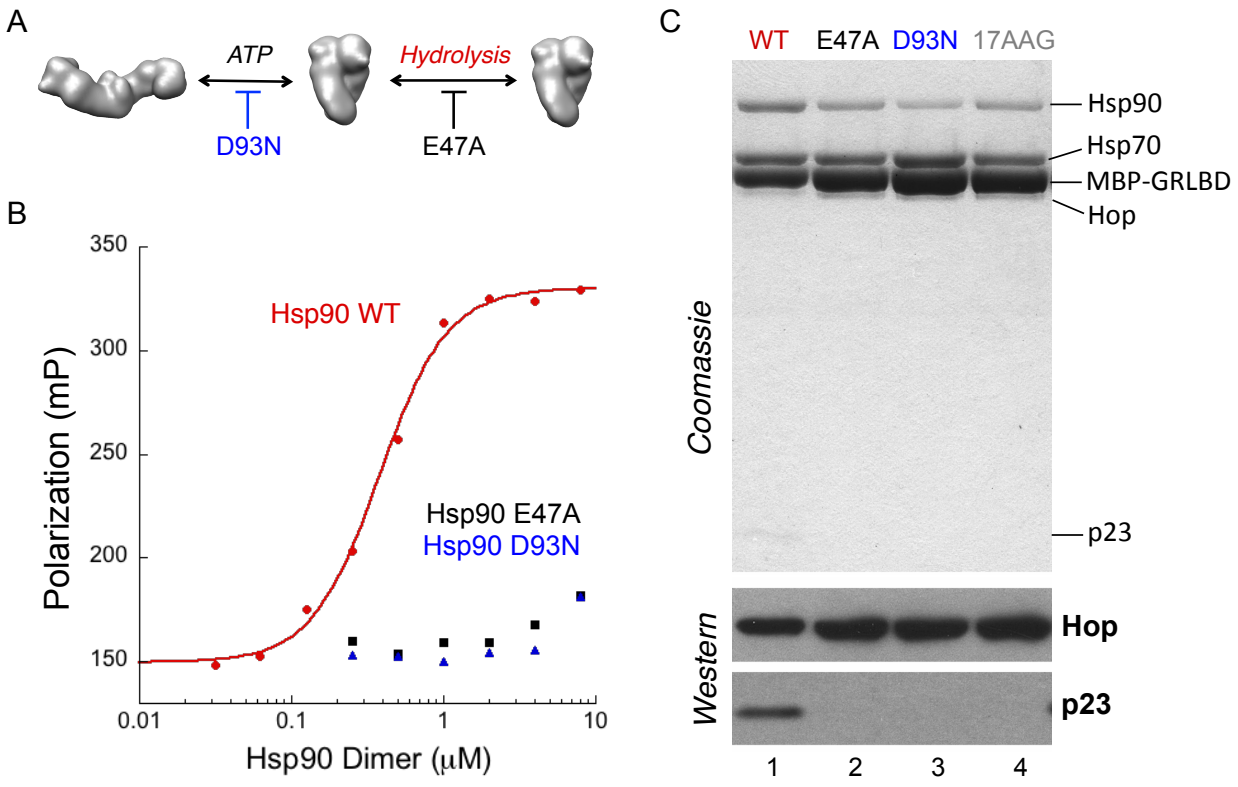

Figure 9. Reversal of Hsp70 inhibition requires ATP hydrolysis on Hsp90.
A) Schematic illustrating the effects of the two hydrolysis dead mutants of Hsp90. D93N prevents ATP binding, and thus inhibits closure. E47A can bind nucleotides and close, thus access the closed state, but cannot hydrolyze ATP once in the closed state.
B) Stoichiometric equilibrium binding plot as in Figure 7C with Hsp90 WT (red circle), hydrolysis dead Hsp90; E47A Hsp90 (black square) and D93N (blue triangle). WT Hsp90 binding curve fit to a half maximal effective concentration equation. (Exp615, 637, 668, 625, and 616)
C) MBP-GRLBD pulldown as Figure 8 with Hsp90 WT (lane 1), E47A (lane 2), D93N (lane 3) and WT with 50μM 17AAG (lane 4). (Exp807)

The coordinated action of Hsp70 and Hsp90 enhances GR ligand affinity

When investigating ligand binding recovery in response to the full chaperone system, an enhancement in the amount of GRLBD bound to ligand was noticed (Figure 7A). This enhancement is not due to activating a previously inactive portion of the GRLBD population, as the entire chaperone system did not change the specific activity of GRLBD (Figure 10A). Instead, the full chaperone system accelerates the ligand association rate in

an Hsp90 concentration-dependent manner (Figure10B). Comparing the ligand binding kinetics of F-dex to GRLBD alone or GRLBD pre-equilibrated with saturating amounts of the entire chaperone system (Figure 11A) revealed acceleration in both the association (Figure 11B) and dissociation rates (Figure 11C). The dissociation rate seen was about ~1.5 fold faster, similar to that measured with just the Hsp70 system (Figure 11F). On rates were determined from the slope of the linear fit of the k_{obs} measured at different GRLBD concentrations (Figure 11D), revealing ~2 fold faster on rate with chaperones (Figure 11E). Additionally, equilibrium measurements show ~3 fold enhancement in the K_D with the chaperones (Figures 12). These data indicate that within the full chaperone system, Hsp90 holds GRLBD in a higher ligand affinity conformation than GRLBD alone, and thus suggests that the chaperone-bound complex is directly capable of binding ligand.

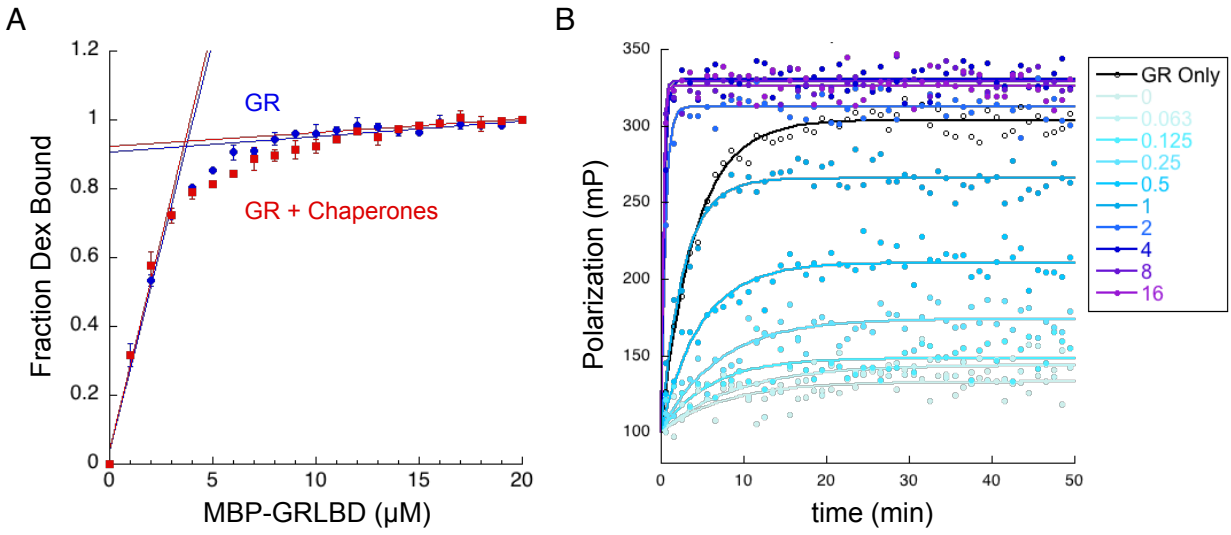

Figure 10. Hsp90 with the entire chaperones system enhance GRLBD ligand binding .
A) Specific ligand binding activity of GRLBD is unaffected by the chaperone system. 2μM F-dex, with increasing amounts of MBP-GRLBD alone (blue circle), and with 2μM Hsp40 and 10μM Hsp70, HOP, p23 and Hsp90 (red square). The specific activity for GRLBD was calculated to be 56±4% GR alone and 59±6% with the chaperone system (±SEM). (Exp844 and 846)
B) Hsp90 accelerates association kinetics. Shown is GRLBD ligand association kinetics of 20nM F-dex for 1μM MBP-GRLBD alone (black open circles), and with 2μM Hsp40, 15μM

Hsp70, HOP, and p23 with increasing concentration of Hsp90 (0-8μM dimer) (solid blue circles). (Exp637)

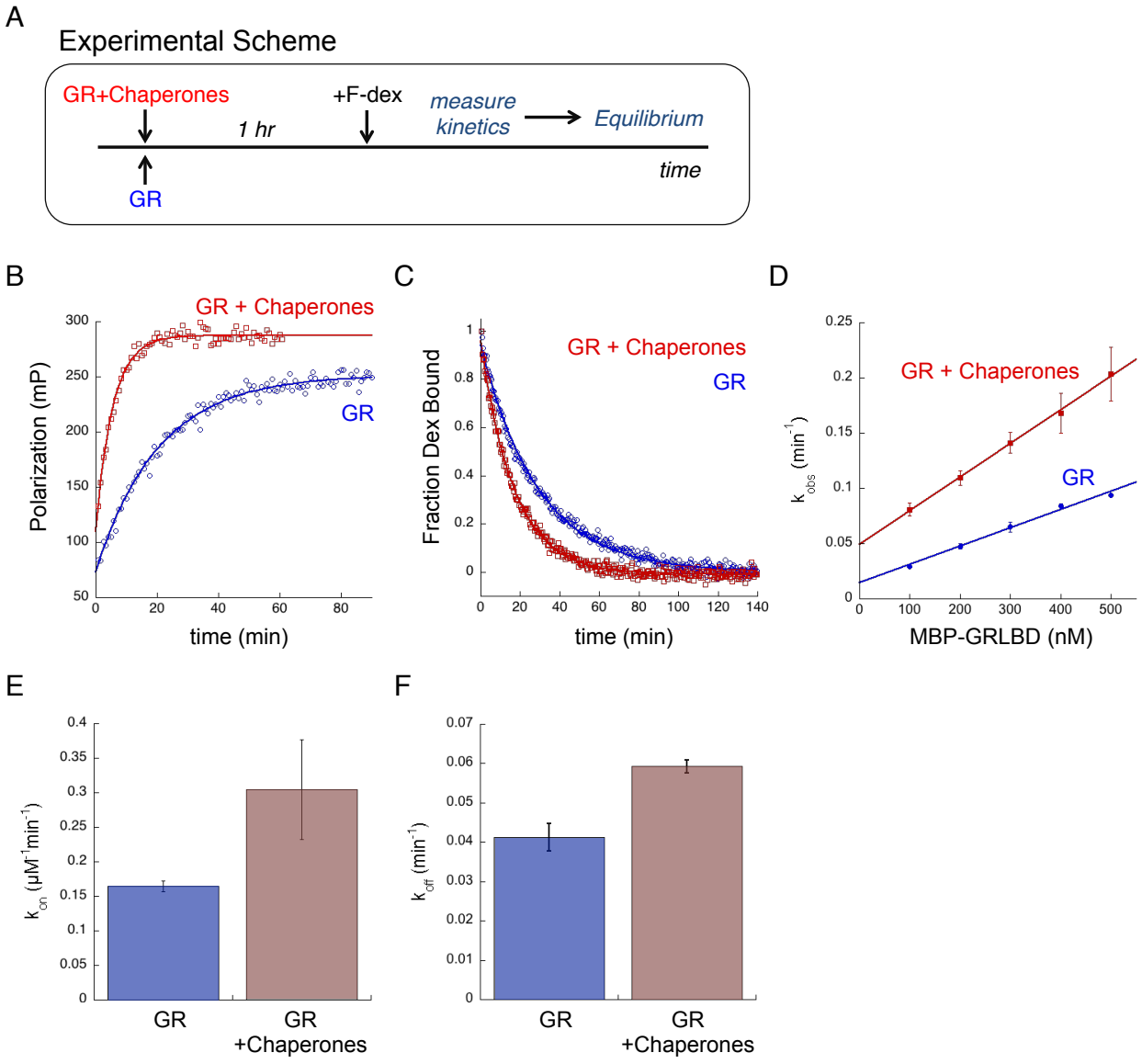

Figure 11. Chaperones enhance GRLBD ligand binding kinetics.
A) Experimental scheme for experiments in Figures 12 and 13.
B) Association kinetics of 20nM F-dex to 300nM MBP-GRLBD alone (blue circle) and with 2μM Hsp40, and 15μM Hsp70, Hsp90, HOP, and p23 (red square). Association binding curves fit to a single phase binding model. (Exp836)
C) Normalized dissociation kinetics of 100nM F-dex bound to 1μM MBP-GRLBD, for GLRBD alone (blue circle) or with 15μM Hsp70, 2μM Hsp40, and 10μM Hsp90, HOP, and p23 (red square). Dissociation was initiated with 100μM unlabeled dex. Off rates determined to be

0.041±0.004 min^{-1} for GRLBD alone and 0.059±0.002 min^{-1} with chaperones (±SEM). (Exp794)
D) Average k_{obs} measured at different GRLBD concentrations from 3-5 separate experiments for GRLBD alone (blue circle) or with 15μM Hsp70, 2μM Hsp40, and 10μM Hsp90, HOP, and p23 (red square) (±SEM). On rates determined from the slope of the linear fit to be 0.165±0.008 for GRLBD alone and 0.304±0.072 $\mu M^{-1}min^{-1}$ (± weighted error of slope). (Exp831)
E) Plotted on rates determined from (C).
F) Plotted dissociation rates from (B).

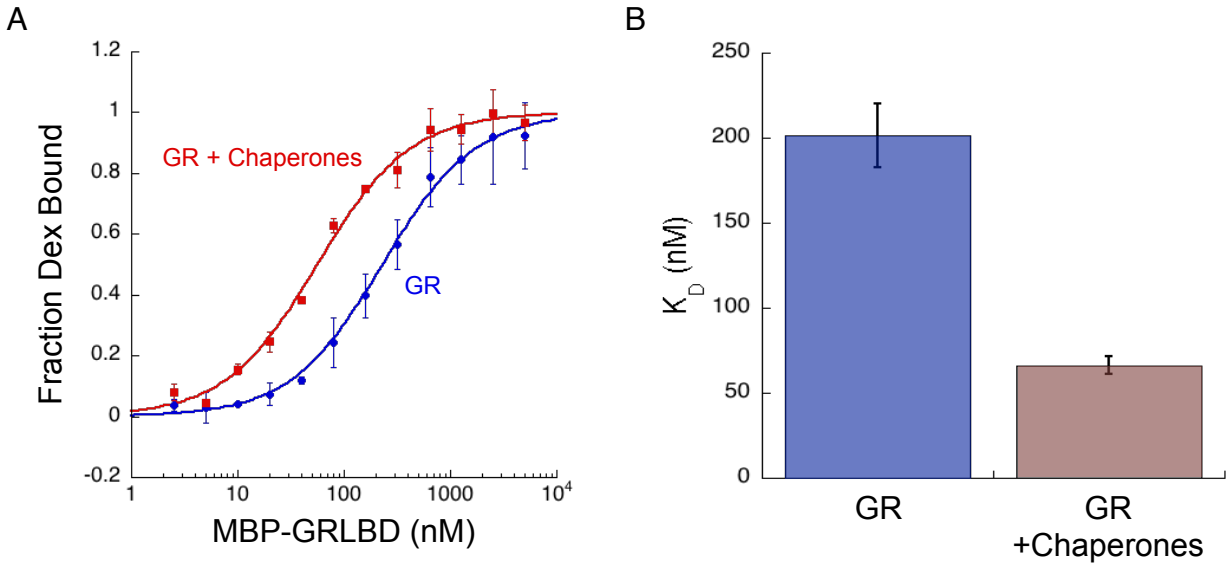

Figure 12. Chaperones enhance GRLBD ligand binding affinity.
A) Normalized equilibrium binding of 20nM F-dex to GRLBD alone (blue circle) and with 15μM Hsp70, 2μM Hsp40, and 10μM Hsp90, HOP, and p23 (red square) averaged from 2 separate experiments (±SE). (Exp715 and 716)
B) Average K_D for GRLBD with and without chaperones determined from 5 separate experiments as in Figure (A), shows a ~3 fold decrease in the ligand K_D from 201±42nM for GRLBD alone to 66±12nM in the presence of the chaperone system (±SEM). (Exp715, 716, 835, 842, and 843)

Discussion

Contrary to expectations, under conditions where recombinant GRLBD is stable, recapitulating the *in vivo* requirement of Hsp90 for activation entailed looking up stream in the pathway to the Hsp70 system. Here we showed that association with Hsp70 actively and locally unfolds GRLBD resulting in GRLBD inactivation. From this inhibited state, the

requirement for Hsp90 for GR activation is clearly seen in the complete recovery of ligand binding. This work provides the first direct evidence of functional enhancements provided by the Hsp90 system, and moreover explains the constitutive requirement for Hsp90 throughout the functional lifetime of GR and not just during initial folding.

ATP hydrolysis by Hsp90 is essential for the reversal of the Hsp70 inhibition, and thus provides new insight into how ATP hydrolysis promotes client activation. This is surprising given the general expectation that energy from hydrolysis is focused on driving client conformational rearrangements that promote activation. Instead, our results show that at least some of the energy from hydrolysis is utilized to regulate Hsp70 and possibly cochaperone release. Our work also provides new insight into how Hsp90 inhibitors can affect the chaperone system *in vivo*. As shown in previous work and here, Hsp90 inhibitors that block the ATP binding pocket do not prevent the association of Hsp90 to the intermediate complex with Hsp70, HOP, and GR (Whitesell and Cook, 1996). Our work demonstrates that it is the reversal of the Hsp70 inhibition that is being inhibited that prevents client activation. *In vivo*, inhibition of Hsp90's ATPase results in the proteolytic degradation of GR, as well as most other Hsp90 clients, revealing a direct link between failure of client hand off, and degradation that has been shown to proceed through Hsp70 pathways (Stankiewicz et al., 2010). Hand off from Hsp70 to Hsp90 is thus a crucial regulation point in which a client's fate is determined.

Hsp70 binds to and induces partial unfolding of GRLBD

Previous genetic studies have shown that deletion of Hsp40 *in vivo* leads to elevated GR signaling in both the absence and presence of hormone (Johnson et al., 2007; Kimura et

al., 1995). The Hsp40 dependent Hsp70 inhibition reported here helps explain this correlation. The elevated GR signaling in the absence of hormone suggests a further role of inactivation by Hsp70 beyond ligand binding inhibition, and points to Hsp70 as being a crucial component of the mechanism that holds GR in the inactive, non-DNA binding state in the absence of ligand.

The observation that Hsp70 facilitates ligand release is surprising because it implies that Hsp70 can bind a ligand bound form of GRLBD and actively promote ligand dissociation, presumably by inducing partial unfolding of the ligand binding pocket. This ability of Hsp70 to accelerate release of tightly bound GR ligand suggests an unappreciated mechanism whereby catalyzed unfolding can allow a more rapid response to sudden decreases in cellular ligand concentrations. The minimal degree of unfolding observed in GRLBD was also surprising as Hsp70 is known to mostly bind proteins in an unfolded state. (insight into this matter is provided by structural work and further discussed in Chapter 4). These findings parallel Hsp70 role in disassembly of clathrin coated vesicles, in which the current model is that Hsp70 promoting disassembly by inducing subtle but strategic structural perturbations that strain the lattice assembly (Xing et al., 2010). Together, this emphasizes Hsp70's disassembly property as general mechanism that is likely utilized in many other biological systems.

Modulation of GR's folded state by the Hsp70:Hsp90 system results in enhanced GR stability, function and regulation

While Hsp70's role in GR delivery to Hsp90 had been well studied by Pratt and coworkers, the inactivation function of Hsp70 and therefor the role of Hsp90 in the reversal

of the inhibition was not appreciated. This may be because the GR used in these studies was in an inactive state to begin with. It is worth noting that in related studies, purified PR while on ice, could bind ligand, and chaperones were only required to maintain ligand binding under elevated temperatures (Smith, 1993). Similarly, while our functional apo GRLBD could be maintained at 25°C, thermally induced aggregation of GRLBD without the solubility-enhancing MBP tag was detected at temperatures as low as 30°C (not shown). This indicates that under our experimental conditions, the apo receptor was only marginally stable. In addition, our attempts at purifying longer apo GR constructs containing the DNA binding domain proved much more challenging, suggesting that the full length wild type constructs used by Pratt and coworkers were likely more unstable. It seems likely that under their conditions GR was in a misfolded state or had already formed small aggregates such that both Hsp70 and Hsp90 were required to cooperatively unfold and then refold the receptor in order to gain ligand binding. This highlights the unstable nature of GR and the genuine need for chaperone interactions *in vivo* to maintain the integrity of the receptor under physiological conditions.

Pratt and coworkers previously proposed that Hsp90 is holding the ligand binding cleft open (Pratt et al., 2008). In their model, Hsp70 is required to "prime" the receptor, while Hsp90 opens the binding cleft in an ATP dependent manner. Our data shows that the "priming" by Hsp70 is opening of the binding pocket (discussed further in Chapter 5), and that the crucial event resulting from ATP hydrolysis on Hsp90 is the release of Hsp70. In either case, the end result is GRLBD bound to Hsp90 with an open binding pocket (hence our faster ligand on rate), for which Pratt and coworkers also provided evidence (Stancato et al., 1996).

With this in mind, the nuclear hormone receptors seem to have evolved a regulatory dependence on the Hsp90:Hsp70 chaperones because they represent a class of proteins where partial unfolding is potentially beneficial. As represented in our model (Figure #), we propose that the LBD has to sample a more unfolded state to allow for ligand entry and release. Evidence for this model has been reported for ER (Carlson et al., 1997). Unfolding by Hsp70 is thus a crucial step in opening the binding pocket. The mechanism by which Hsp70 achieves this is still unclear. The cooperativity in the equilibrium inhibition curve could be the result of two Hsp70 binding events acting simultaneously, however with a multi state equilibrium of GRLBD conformations, it could also be the result of different binding affinities between one Hsp70 and the different GRLBD folded states, manifesting as an apparent cooperativity. Kinetic modeling could not rule out either model. Along these lines, a previous report suggested that either one Hsp70 interactively cycles on GR or two Hsp70s act sequentially in the Hsp70 priming step (Ali et al., 2006; Morishima et al., 2001). While the exact mechanism is still unknown, it is clear that while bound to Hsp70, GRLBD lacks the essential structural determinants of high affinity ligand binding, which can only be gained once folding completes after Hsp70 release by the Hsp90 system.

While the unfolding/inactivation by Hsp70 and the refolding/reactivation by Hsp90 might seem wastefully contradictory, our data suggest how their combined actions can be complementary. The constant rounds of Hsp70-mediated unfolding/ligand release and Hsp90-mediated refolding/ligand binding that we observe facilitates GR's ability to provide both rapid and subtle responses to changing hormone levels while also maintaining apo GR in a non-aggregating, high affinity state. Moreover this provides additional opportunities for regulatory control and to even coordinate signaling with protein homeostasis.

Additionally, the reliance of both chaperones on cochaperones and numerous post-translational modifications enables additional levels of fine-tuning. Repeated cycles of unfolding and refolding have the additional benefit of allowing the chaperones to ensure a functional protein population by preventing the buildup of nonfunctional misfolded states and by constantly utilizing refoldability as a metric for targeting damaged proteins for degradation. These results provide clear benefits for the evolution of this complex chaperone system and helps explain reasons beyond enhanced stability for why many signaling proteins have evolved a dependence on the Hsp70:Hsp90 chaperone system.

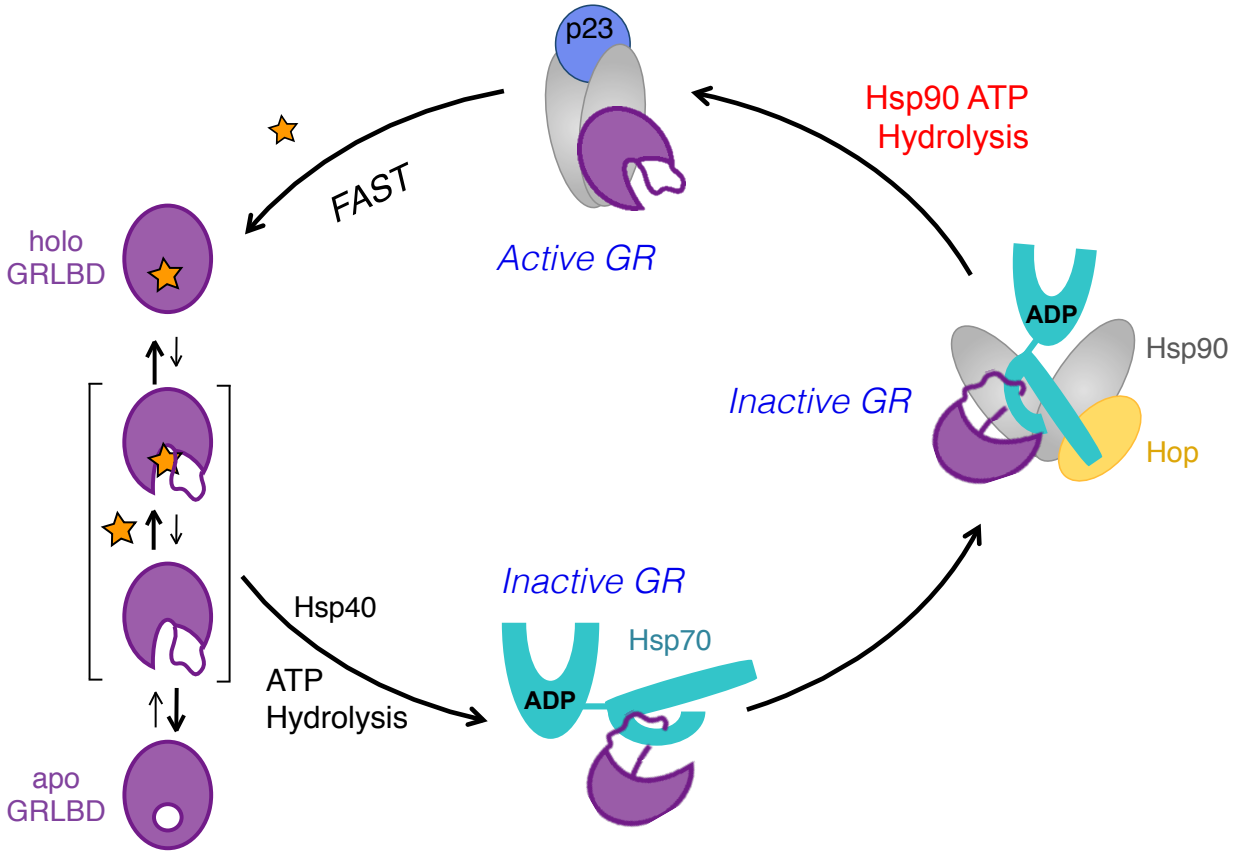

Figure 13. Model for GR ligand binding.
Apo GRLBD on its own (left) is mostly folded and transiently samples a more unstructured state where the binding pocket at the core of the protein is accessible and thus allows ligand association and dissociation. Ligand binding stabilizes the more folded GRLBD state.

In a process that requires ATP hydrolysis and Hsp40, Hsp70 binds to GRLBD and promotes ligand release by stabilizes a partially unfolded inactive state. In the presence of the Hsp90 system, GRLBD bound Hsp70 is brought together with Hsp90 by Hop, to form an inactive complex. Subsequent ATP hydrolysis on Hsp90 is required to release Hsp70 (and Hop), which in turn allow for progression to the closed state, and p23 binding.

Experimental Procedures

Fluorescence Polarization Assays

GRLBD ligand binding to fluorescein labeled dexamethasone was measured as described in Chapter 2 with experiment specific details described below.

GRLBD Ligand Binding Experiments with Hsp70

For association kinetics (Figure 2A), 1μM MBP-GRLBD was pre-equilibrated together with 2μM Hsp40, 15μM Hsp70 and 5mM ATP/$MgCl_2$ for 60-70 minutes at room temperature. Reactions were equilibrated to 25°C before the kinetics was initiated with 50nM F-Dex. Association curves were fit to a single exponential binding equation were k_{obs} is the observed association rate:

$$Y(mP) = Y_{max} * \left(1 - e^{(-1-t*k_{obs})}\right) + NS$$

For the Hsp70 inhibition curve (Figure2B) samples were prepared as in Figure # with varying concentration of Hsp70. Association kinetics was measured until binding reached equilibrium. Plotted equilibrium values are the average of 3 independent experiments with error bars representing the standard deviation. The IC_{50} curve was fit to cooperative inhibition model were n is the Hill coefficient:

$$Y(mP) = \frac{Y_{max} - NS}{1 + (\frac{[Hsp70]}{IC_{50}})^n} + NS$$

The reported IC_{50} and n were determined by averaging the parameters obtained from the fitting of the three separate experiments, and the error for the parameters represents the standard error of the mean.

For dissociation kinetics (Figure 4), the concentration of F-dex was increased to improve the signal to noise to most accurately determine the off rates. 100nM F-dex was pre-bound to 1μM MBP-GRLBD in the presence of 2μM Hsp40 and 5mM ATP/$MgCl_2$. Association was monitored to ensure the binding had reached equilibrium. Dissociation was then initiated with 100μM unlabeled dex ± 15μM Hsp70. Dissociation curves were fit to a single-phase exponential decay:

$$Y(mP) = (Y_{max} - NS)e^{-t*k_{off}} + NS$$

The reported off rates (k_{off}) were determined by averaging the rates obtained from six independent experiments, and the errors represents the standard error of the mean (inset).

GRLBD Ligand Binding Experiments with Entire Chaperone System

For equilibrium ligand binding in Figure 7A, proteins were pre-equilibrated together with 5mM ATP/$MgCl_2$ for 60 to 70 minutes at room temperature. Proteins and reagents were added at the following concentration: 1μM MBP-GRLBD, 2μM Hsp40, 15μM Hsp70, 15μM Hsp90, 15μM HOP, 15μM p23, and 50μM 17AAG. Ligand binding was initiated with 20nM F-dex, and association measured until saturation reached. Plotted

equilibrium values represent the mean of 3 independent experiments, with error bars representing the standard deviation.

For Hsp90 concentration dependence of GRLBD ligand binding recovery (Figure 7C and 9B), experiment was carried out as in Figure 7A with varying concentrations of Hsp90 WT, E47A, and D93N. For Hsp90 WT, values are the mean of 3 independent experiments with error bars representing the standard deviation. Data was fit to a half maximal effective concentration equation (EC_{50}):

$$Y(mP) = \frac{Y_{max} - NS}{1 + (\frac{[Hsp90]}{EC_{50}})^n} + NS$$

For GRLBD ligand association kinetics with the entire chaperone system (Figure 10B and 11B) was carried out as shown in Figure 7A. MBP-GRLBD was pre-incubated with 2μM Hsp40, 15μM Hsp70, 10μM Hsp90, 10μM HOP, 10μM p23 with 5mM ATP/$MgCl_2$ for 60 minutes at room temperature. MBP-GRLBD alone was prepared with matching volumes of chaperone storage buffer. Reactions were equilibrated to 25°C for several minutes before the kinetics was initiated with 20nM F-Dex. Association curves were fit to a single exponential to determine the observed association rate, k_{obs}:

$$Y(mP) = Y_{max} * \left(1 - e^{(-1-t*k_{obs})}\right) + NS$$

For Figure 11D, the k_{obs} obtained at varying MBP-GRLBD concentration was determine as in Figure 11B. Each point represents the average k_{obs} from 3-5 separate experiments with error bars representing the standard error of the mean. The on rate

(Figure 11E) was determined from the slope of the linear fit in Figure 11D, with the error determined by the weighted errors of the individual points.

For GRLBD ligand dissociation kinetics with the entire chaperone system (Figure 11C), proteins were pre-incubated at 1μM MBP-GRLBD with 2μM Hsp40, 15μM Hsp70, 10μM Hsp90, 10μM HOP, 10μM p23 with 5mM ATP/$MgCl_2$ or equivalent volume of chaperone buffer for 60-70 minutes at room temperature, followed by equilibration with 100nM F-dex for about 50 minutes. Ligand dissociation was initiated with 100μM unlabeled dex. Off rates were determined from the average of 3 separate experiments (Figure 11F), with the reported error corresponding to the standard error of the mean.

For determination of ligand binding affinity with and without chaperones (Figure 12), samples were prepared as described for the ligand association kinetics in Figure 11, with varying concentrations of MBP-GRLBD. Ligand binding was measured and fit as described for GRLBD alone in Chapter 2. The K_D was determined from the average of 5 separate experiments (Figure 12B), with error bars representing the standard error of the mean. While investigating GRLBD ligand binding, it was noted that GRLBD ligand binding behavior was affected by buffer conditions. For this reason when comparing GR with and without chaperones, reactions were always normalized such that without chaperones, equivalent amounts of chaperones storage buffer was added to normalize for any changes. The difference in K_D for GRLBD alone between Figure 12 and Chapter 2, Figure 6 is therefore attributed to the difference in buffer conditions after normalizing for the significant volume of chaperone storage buffer.

Limited Proteolysis

Proteins were mixed at 1μM MBP-GRLBD, 2μM Hsp40, and 0.5, 1, 2, 4, 8, 16, and 32μM Hsp70 in 30mM HEPES pH7.5, 150mM KCl, 2mM DTT, and 5mM $MgCl_2$, supplemented with 5mM ATP. Proteins were equilibrated at room temperature for one hour. Trypsin (Sigma) was added at 4ng/μL and incubated on ice for 30 minutes. Reactions were quenched by addition of 4X SDS loading buffer. 250ng of digested MBP-GRLBD was separated by SDS-PAGE, followed by western transfer to nitrocellulose and probed with an antibody against MBP (Rockland antibodies and assays, 200-401-385). Primary antibody was incubated at 1:1,000 at room temperature for 1 hour in 4% milk/TBST.

Hydrogen Deuterium Exchange Mass Spectrometry

GRLBD and Hsp70 was mixed at 1:1.2 molar ratio with 2μM Hsp40 and 5mM ATP/ $MgCl_2$ and incubated for 1h at room temperature before HDX as described in Chapter 2.

MBP-GRLBD Pull Down

Proteins were incubated at 5μM MBP-GRLBD, 2μM Hsp40, 15μM His-Hsp70/Hsp90/HOP/p23 for 45 min at room temperature in a buffer containing 30mM HEPES pH7.5, 150mM KCl, 2mM DTT, 0.05% Tween20, 5mM ATP/$MgCl_2$. The 6xhis tag along with a V5 epitope tag was left on Hsp70 for this assay to allow for separation between Hsp70 and MBP-GRLBD. Following room temp incubation, 10μL amylose magnetics beads (New England BioLabs- E8035S) was added per 20μL reaction and were further incubated on ice for one hour. Beads were then washed 3 times with the incubation buffer, before eluting proteins with 50mM maltose. Samples were than separated by SDS-

PAGE and visualized with Coomassie blue stain. For enhanced detection of HOP, p23, and Hsp40 a separate SDS-PAGE was transferred to nitrocellulose and separately probed with antibodies against p23 (Santa Cruz Biotechnology, sc-68399), Hop (Santa Cruz Biotechnology, sc-136082), and Ydj1 (sigma, SAB5200011). Primary antibodies were incubated at 1:5,000 for p23 and 1:10,000 for Hop and Ydj1 at room temperature for 1 hour in PBST with 3% BSA.

Acknowledgements

I thank D. Southworth for providing both helpful scientific discussions and the protein that lead to trying the first GRLBD ligand binding assay with Hsp70.

References

Ali, M.M.U., Roe, S.M., Vaughan, C.K., Meyer, P., Panaretou, B., Piper, P.W., Prodromou, C., and Pearl, L.H. (2006). Crystal structure of an Hsp90–nucleotide–p23/Sba1 closed chaperone complex. Nature *440*, 1013–1017.

Carlson, K.E., Choi, I., Gee, A., Katzenellenbogen, B.S., and Katzenellenbogen, J.A. (1997). Altered ligand binding properties and enhanced stability of a constitutively active estrogen receptor: evidence that an open pocket conformation is required for ligand interaction. Biochemistry *36*, 14897–14905.

Dittmar, K.D., Banach, M., Galigniana, M.D., and Pratt, W.B. (1998). The role of DnaJ-like proteins in glucocorticoid receptor.hsp90 heterocomplex assembly by the reconstituted hsp90.p60.hsp70 foldosome complex. J. Biol. Chem. *273*, 7358–7366.

Hernández, P.M., Chadli, A., and Toft, D.O. (2002). HSP40 binding is the first step in the HSP90 chaperoning pathway for the progesterone receptor. Journal of Biological Chemistry *277*, 11873–11881.

Johnson, J.L., Halas, A., and Flom, G. (2007). Nucleotide-Dependent Interaction of Saccharomyces cerevisiae Hsp90 with the Cochaperone Proteins Sti1, Cpr6, and Sba1. Mol. Cell. Biol. *27*, 768–776.

Kampinga, H.H., and Craig, E.A. (2010). The HSP70 chaperone machinery: J proteins as

drivers of functional specificity. Nat Rev Mol Cell Biol *11*, 579–592.

Kimura, Y., Ichiro, Y., and Lindquist, S. (1995). Role of the Protein Chaperone YDJ1 in Establishing Hsp90-Mediated Signal Transduction Pathways. Science *268*, 1362–1365.

Kityk, R., Kopp, J., Sinning, I., and Mayer, M.P. (2012). Structure and Dynamics of the ATP-Bound Open Conformation of Hsp70 Chaperones. Mol. Cell *48*, 863–874.

Li, J., Qian, X., and Sha, B. (2003). The Crystal Structure of the Yeast Hsp40 Ydj1 Complexed with Its Peptide Substrate. Structure.

Mayer, M.P., and Bukau, B. (2005). Hsp70 chaperones: Cellular functions and molecular mechanism. CMLS, Cell. Mol. Life Sci. *62*, 670–684.

Mayer, M.P., Schröder, H., Rüdiger, S., Paal, K., Laufen, T., and Bukau, B. (2000). Multistep mechanism of substrate binding determines chaperone activity of Hsp70. Nat. Struct. Biol. *7*, 586–593.

Mayer, M.P. (2013). Hsp70 chaperone dynamics and molecular mechanism. Trends in Biochemical Sciences *38*, 507–514.

Morishima, Y., Kanelakis, K.C., Murphy, P.J., Shewach, D.S., and Pratt, W.B. (2001). Evidence for iterative ratcheting of receptor-bound hsp70 between its ATP and ADP conformations during assembly of glucocorticoid receptor.hsp90 heterocomplexes. Biochemistry *40*, 1109–1116.

Murphy, P.J.M., Morishima, Y., Chen, H., Galigniana, M.D., Mansfield, J.F., Simons, S.S., and Pratt, W.B. (2003). Visualization and mechanism of assembly of a glucocorticoid receptor.Hsp70 complex that is primed for subsequent Hsp90-dependent opening of the steroid binding cleft. J. Biol. Chem. *278*, 34764–34773.

Obermann, W.M.J., Sondermann, H., Russo, A., Pavletich, N., and Hartl, F.U. (1998). In vivo function of Hsp90 is dependent on ATP binding and ATP hydrolysis. The Journal of Cell Biology *143*, 901–910.

Pratt, W.B., Morishima, Y., and Osawa, Y. (2008). The Hsp90 Chaperone Machinery Regulates Signaling by Modulating Ligand Binding Clefts. Journal of Biological Chemistry *283*, 22885–22889.

Smith, D.F. (1993). Dynamics of heat shock protein 90-progesterone receptor binding and the disactivation loop model for steroid receptor complexes. Mol. Endocrinol. *7*, 1418–1429.

Stancato, L.F., Silverstein, A.M., Gitler, C., Groner, B., and Pratt, W.B. (1996). Use of the thiol-specific derivatizing agent N-iodoacetyl-3-[125I]iodotyrosine to demonstrate conformational differences between the unbound and hsp90-bound glucocorticoid receptor hormone binding domain. J. Biol. Chem. *271*, 8831–8836.

Stankiewicz, M., Nikolay, R., Rybin, V., and Mayer, M.P. (2010). CHIP participates in protein triage decisions by preferentially ubiquitinating Hsp70-bound substrates. FEBS Journal *277*, 3353–3367.

Whitesell, L., and Cook, P. (1996). Stable and specific binding of heat shock protein 90 by geldanamycin disrupts glucocorticoid receptor function in intact cells. Molecular Endocrinology *10*, 705–712.

Xing, Y., Böcking, T., Wolf, M., Grigorieff, N., Kirchhausen, T., and Harrison, S.C. (2010). Structure of clathrin coat with bound Hsc70 and auxilin: mechanism of Hsc70-facilitated disassembly. Embo J. *29*, 655–665.

Zhu, X., Zhao, X., Burkholder, W.F., Gragerov, A., Ogata, C.M., Gottesman, M.E., and Hendrickson, W.A. (1996). Structural Analysis of Substrate Binding by the Molecular Chaperone DnaK. Science, New Series *272*, 1606–1614.

Supplemental Information

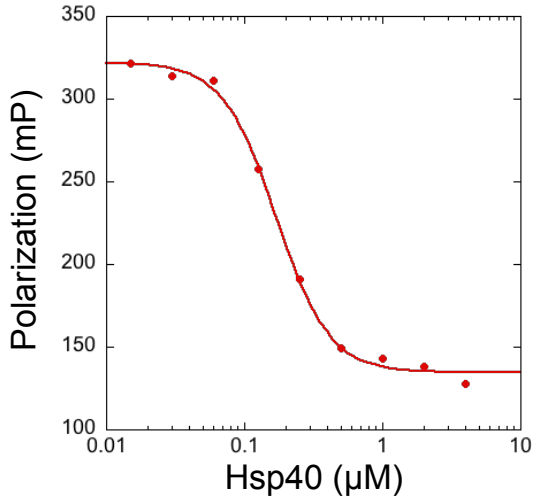

Figure S1. Hsp40 dependence for Hsp70 inhibition of GRLBD ligand binding.
A) GRLBD ligand binding assay with 20nM F-dex, 1μM MBP-GRLBD, 15μM Hsp70 and varying concentrations of Hsp40. Curve fit to the IC_{50} equation used for Hsp70, yielding a IC_{50} of 170nM and an n of 2.3. (Exp591)

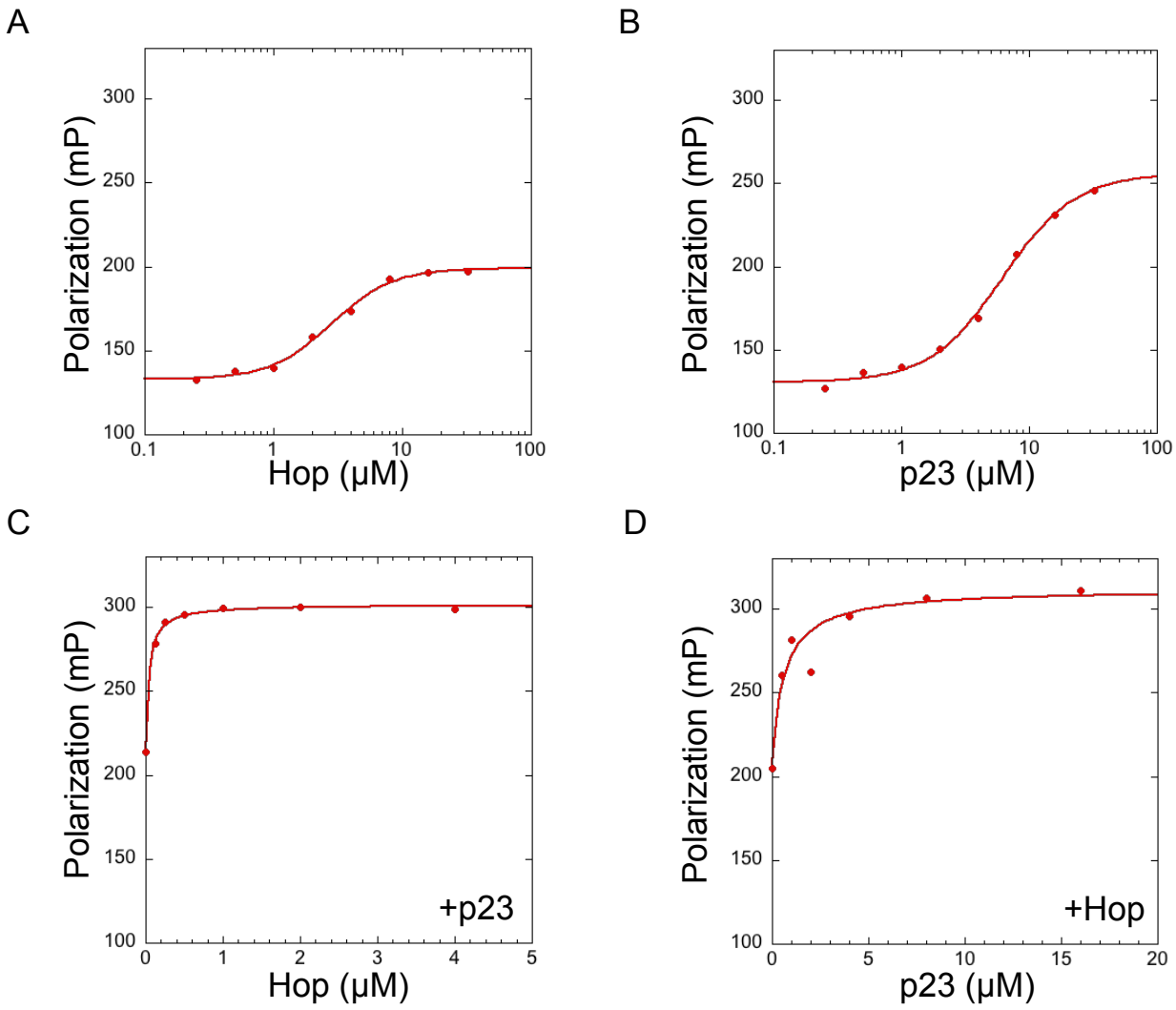

Figure S2. Hop and p23 titrations in GRLBD ligand binding assay.
A) Hop titration without p23. Equilibrium ligand binding for 1μM MBP-GRLBD to 20nM F-dex with 2μM Hsp40, 15μM Hsp70, and 10μM Hsp90 (monomer). Curve fit with EC_{50} equation used for Hsp90 with an EC_{50} of 2.8μM and an n of 1.8. (Exp626)
B) p23 titration without Hop. Equilibrium ligand binding for 1μM MBP-GRLBD to 20nM F-dex as in (A) but withp23. EC_{50}=6.2μM and n=1.5. (Exp629)
C) Hop titration with p23. Equilibrium ligand binding for 1μM MBP-GRLBD to 20nM F-dex with 2μM Hsp40, 15μM Hsp70, 10μM Hsp90 (monomer), and 20μM p23. EC_{50}=41nM. (Exp663)
D) p23 titration with Hop. Equilibrium ligand binding for 1μM MBP-GRLBD to 20nM F-dex with 2μM Hsp40, 15μM Hsp70, 10μM Hsp90 (monomer), and 15μM Hop. EC_{50}=0.6μM. (Exp661)

Chapter 4

Structure of Hsp70:Hsp90:Hop:GRLBD Complex by Cryo-EM

Contributing Authors: Daniel Southworth and David Agard

Preface

Given the clear importance of client hand off from Hsp70 to Hsp90 as the critical event controlling GR activation, a structure of the intermediate complex with Hsp90, Hop, Hsp70 and GR would provide valuable mechanistic information into how hand off is coordinated and would provide a structural frame work for understanding how Hsp90 reverses the Hsp70 inhibition. For this reason, efforts were directed towards obtaining a cryo-EM reconstruction of the GR bound Hsp90:Hop:Hsp70 complex by building upon previous structural work with Hsp90 and Hop, as well as preliminary work attempting to obtain an EM reconstruction of the Hsp70:Hop:Hsp90 complex.

Summary

A cryo-EM reconstruction of the Hsp90:Hop:Hsp70:GRLBD complex reveals a highly interconnected structure in which Hop makes extensive contacts with Hsp90 that allows for precise delivery of GRLBD on Hsp70 to the client binding region on Hsp90. Additionally, Hop induces specific conformational changes in Hsp90 necessary for a direct interaction between Hsp90's and Hsp70's ATPase domains. This direct contact is likely the key interaction governing client hand off and supports the coupling of the two ATP

hydrolysis cycles suggested by the reversal of Hsp70's inhibition by Hsp90 in the ligand binding assay.

In this complex, Hsp90 is in the previously observed Hop induced state with a more compact V-shape and the NTD's rotated upward. Hop binds to Hsp90 with the three domains necessary and sufficient for GR activation *in vivo*: TPR2A, TPR2B and DP2. TPR2B binds near the cleft on Hsp90's MD-CTD interface in a way that recruits and orients Hsp70's SBD towards Hsp90's client binding site. The electron density for Hsp70 SDB suggests that the SBD helical lid is in a partially open conformation that could accommodate a partially folded GRLBD. The direct contact of the ATPase domains requires the Hop induced conformation of Hsp90, which appears to result from the binding of Hop's DP2 domain into Hsp90's MD-NTD interface.

Introduction

Hop structure and function

Hop, short for Hsc70/Hsp90-organizing protein, facilitates the transfer of client proteins from Hsp70 to Hsp90. This cochaperone is a modular protein with three TPR (tetratricopeptide repeat) domains: TPR1, TPR2A and TPR2B; and two DP domains (rich in aspartate and proline residues): DP1 and DP2 (Figure 1A). Hop provides a physical link between Hsp70 and Hsp90 by simultaneously binding the two chaperones through its TPR domains. Of the three TPR domains, TPR2A selectively binds to the MEEVD motif at the C-terminal tail of Hsp90 with high affinity, and both the TPR1 and TPR2B bind to the EEVD motif at the C-terminal tail of Hsp70 with moderate affinities (Scheufler et al., 2000; Schmid et al., 2012). Crystal structures of the TPR1 and TPR2A bound to their respective EEVD

peptides show that the TPR domains form concave helical bundles, with the peptide binding within the concave groove and forming an important charge clamp interaction between the C-terminal Asp of the peptide and conserved residues on the TPR domain (Figure 1C) (Scheufler et al., 2000).

The crystal structure of the TPR1 domain bound to the Hsp70 peptide led to the premature conclusion that Hsp70 preferentially binds to TPR1. Although, genetic studies questioned this by showing that mutations in both TPR1 and TPR2B are required to disrupt Hsp70 binding *in vivo,* therefor suggesting that TPR1 and TPR2B carry out redundant functions (Flom et al., 2007; 2006). However, this was found to not always hold true. In the case of the synthetically lethal interaction between Ydj1 (Hsp40) and Sti1 (Hop) (Flom et al., 2005), the Hop TPR2A-TPR2B-DP2 construct was the minimal and sufficient fragment required for viability of the Ydj1 knockout strain, demonstrating that in some cases the TPR1 domain cannot fulfill the same function as the TPR2B domain (Flom et al., 2006). This was confirmed to be the case for GR, in which the minimal and sufficient fragment of Hop required for GR activation *in vivo* is the equivalent TPR2A-TPR2B-DP2. This indicates that in the context of GR, Hsp70 recruitment to Hsp90 is likely mediated by TPR2B (Schmid et al., 2012).

While TPR2A initiates binding to Hsp90 by binding the MEEVD motif, TPR2B also interacts directly with Hsp90. In fact, both the TPR2A and TPR2B domains are required for Hsp90 interaction *in vivo* (Flom et al., 2007) and for ATPase inhibition of Hsp90 (Lee et al., 2012; Schmid et al., 2012). A crystal structure of the TPR2A-TPR2B fragment (Figure 1D) revealed that the domains are connected by a structured linker, with a defined orientation of the linker with respect to the TPR2B required for Hop function *in vivo* (Schmid et al.,

2012). Further investigation by NMR revealed that the TPR2A makes additional contacts with Hsp90 other than the C-terminal MEEVD tail. Extensive contacts between the TPR2A-TPR2B fragment and Hsp90 are centered on the middle domain (MD) of Hsp90, with both TPR domains binding the MD independently, although with significantly reduced affinity. Comparable findings were also found by HDX-MS (Lee et al., 2012).

In contrast, the NMR and HD-XMS studies were preceded by an EM reconstruction of a Hop-Hsp90 complex that suggested that Hop's interaction with Hsp90 is mediated by TPR2A and TPR1 (Figure 1B) (Southworth and Agard, 2011). While Hop preferentially binds with a stoichiometry of one Hop per Hsp90 dimer, two Hops can occupy one Hsp90 dimer but with the second Hop binding with significantly lower affinity. For the cryo-EM complex, the stoichiometry was artificially biased to two Hops per Hsp90 dimer by an engineered disulfide cross-link. The binding of the second Hop results in a symmetrical complex, allowing two-fold symmetry to be imposed during the EM refinement and was extremely helpful for obtaining an EM reconstruction of such a small complex. While the complex was formed with full length Hop, there was only extra density that could accommodate two TPR domains per Hsp90 monomer. The extra density begins near the MD-CTD interface on the left monomer and stretched across the cleft to the MD-NTD interface of the opposing monomer. Given the proximity to the CTD, the lower density was attributed to TPR2A, and gold labeling indicated that the upper density corresponded to TPR1.

In is still unclear if the origin for the two different models is due to the second Hop, and/or issues associated the assignment of the Hop domains in the EM map. Nonetheless, the most interesting aspect of the EM reconstruction is that it revealed that Hop stabilizes a

distinct open conformation of Hsp90 in which the MD-CTD is more compact and the NTD's are pre-organized for closure in an upward rotated orientation matching that seen in the ATP closed state. Simultaneously, in this state the hydrophobic regions along Hsp90's cleft are aligned in a way that could facilitate client binding.

The function of the DP domains is entirely unknown. Based on structures determined by NMR (Figures 1E and F), they were proposed to make direct contact with client proteins (Schmid et al., 2012). While the DP1 domain is dispensable for GR activation, deletion of the DP2 domain completely negates Hop's effect on GR activation *in vivo.* This indicates that DP2 is carrying out a very important and yet unidentified function (Flom et al., 2006; Schmid et al., 2012).

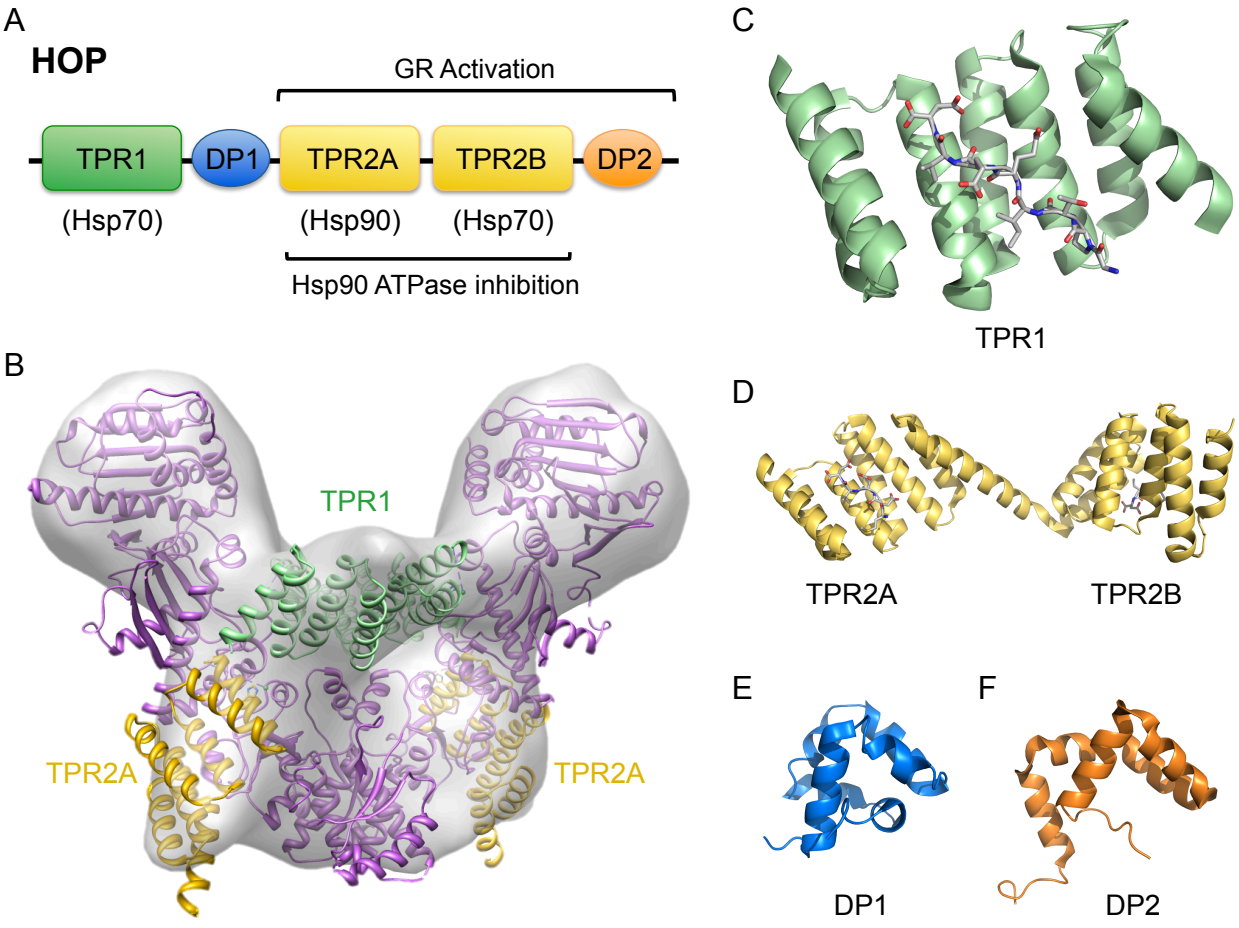

Figure 1. Domain architecture and structure of Hop.
A) Domain architecture of Hop.
B) Cryo-EM reconstruction of symmetric $Hsp90_2$:Hop_2 complex (Southworth and Agard, 2011) fit with model of Hsp90 (magenta) in the Hop induced conformation with NTDs rotated to match the closed state, and two Hop TOR domains. TPR2A was predicted to occupy the lower density centered around the Hsp90 MD-CTD interface, and gold labeling indicated that the TPR1 domain occupied the upper density centered at the Hsp90 dimer cleft (Southworth and Agard, 2011).
C) Crystal structure of Hop TPR1 bound to Hsp70 EEVD containing peptide (pdb 1ELW) (Scheufler et al., 2000).
D) Crystal structure of peptide bound Hop TPR2A-B fragment (pdb 3UQ3) (Schmid et al., 2012).
E) NMR solution structure of Hop DP1 domain (pdb 2LLV) (Schmid et al., 2012).
F) NMR structure of Hop DP2 domain (pdb 2LLW) (Schmid et al., 2012).

Refinement of the HOP-Hsp90-Hsp70 complex hindered by heterogeneity

Building upon the Hsp90:Hop EM complex, incorporation of Hsp70 onto the complex required Hsp70 be in its ADP state, which was accomplished by addition of catalytic ratios of Hsp40 to the assembly reaction (Southworth and Agard, 2011). By SEC-MALS, it was determined that only one Hsp70 could be loaded per Hsp90:Hop complex, independent of the number of Hops. This indicated that the asymmetric arrangement including one Hop is likely relevant for loading of Hsp70 client complexes. In light of this, Hsp90:Hop:Hsp70 complexes were formed with the wild type components that preferentially contain one Hop per Hsp90 dimer. A $Hsp90_2$:Hop_1:$Hsp70_1$ complex was formed and appeared homogenous by SEC-MALS. However, after acquiring a relatively large cryo-EM data set, the data failed to refine to a reliable reconstruction (Figure 2A).

It was later determined that the likely source of the refinement related issues was heterogeneity, with at least three distinct cross-linked complexes resolved by SDS-PAGE (Figure 2B). Utilizing crosslinking and SDS-PAGE as a strategy to identify homogenous complexes for EM, the GRLBD bound Hsp90:Hop:Hsp70 complex was obtained and a low

resolution cryo-EM reconstruction acquired. This complex reveals extensive interactions between all the components, with GRLBD appearing to be simultaneously bound to both Hsp70 and Hsp90. Hop facilitates both the precise delivery of GRLBD to the client binding region on Hsp90 and coordinates a direct interaction between Hsp90's and Hsp70's ATPase domains that likely allows ATP hydrolysis on Hsp90 to promote client release from Hsp70.

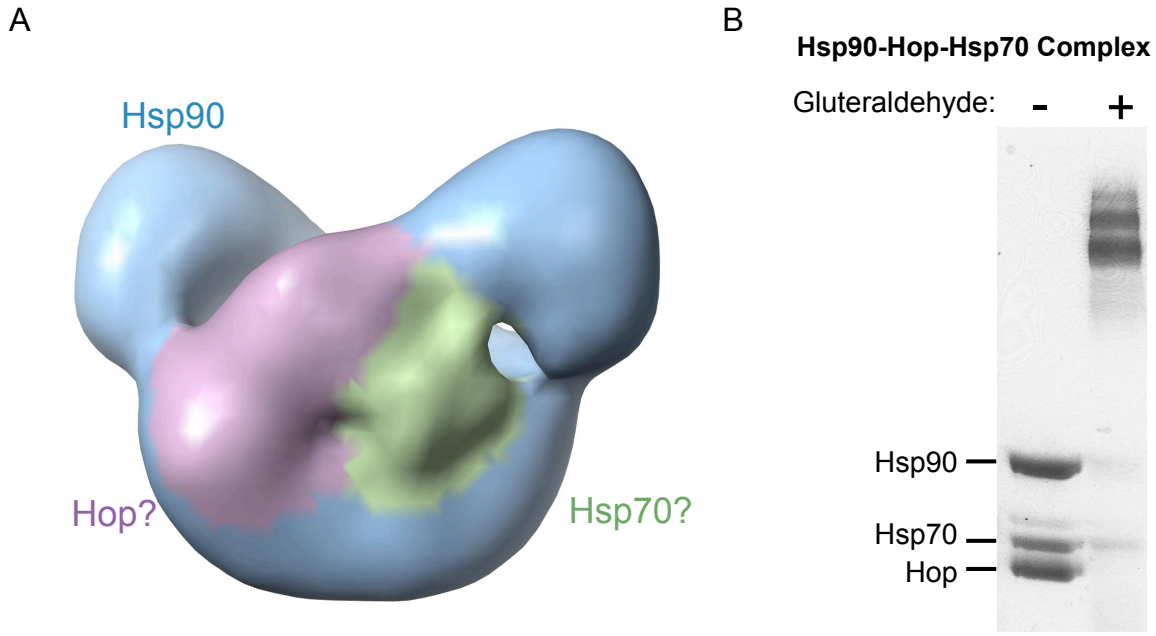

Figure 2. Sample heterogeneity prevents refinement of the Hsp90:Hop:Hsp70 cryo-EM complex
A) Cryo-EM data of Hsp90:Hsp70:Hop complex failed to refine to reliable high resolution structure. Shown is the best reconstruction obtain by imposing 2 fold symmetry with density attributed to Hsp90 in blue, Hop in purple, and Hsp70 in green. Figure provided by Daniel Southworth.
B) SDS-PAGE gel of Hsp90:Hsp70:Hop complex reveals heterogeneity in the cross-linked sample. The sample was obtained from a single gel filtration peak and used for cyro-EM reconstruction in (A).

Results

Obtaining the Hsp90:Hop:Hsp70:GR complex for cryo-EM

The intermediate complex consisting of Hsp90, Hsp70, Hop and GRLBD was pre-assembled and purified by SEC. The assembly reactions and running buffers were used with the intention of capturing the GRLBD bound ADP state of Hsp70 and the apo Hop bound state of Hsp90. To this end, the complex was formed with limiting amounts of ATP, and then run over the size exclusion column with 200μM ADP. While the major elution peak corresponded to the peak from the $Hsp90_2$:Hop_1:$Hsp70_1$ complex, there was a distinct shoulder to the front of the peak only seen with MBP-GRLBD (Figure 3A). Fractions were cross-linked with gluteralderhyde immediately after eluting off the column and were resolved by SDS-PAGE to determine the homogeneity of each fraction. With MBP-GRLBD, two distinct cross-linked species were resolved, with the front of the shoulder more enriched in the larger of the two species (Figure 3B). The smaller species was interpreted as the $Hsp90_2$:Hop_1:$Hsp70_1$ complex, and the larger species as the corresponding complex with GRLB bound. Optimal build up of the GRLBD containing shoulder was obtained with Hsp70 expressed from sf9 cells as compared to bacterial expressed Hsp70 (Figure S1A), and with the MBP-GRLBD as compared with the tag free GRLBD (Figure S1B). Using the sf9 expressed Hsp70 and MBP-GRLBD, the complex assembly was further optimized such that fractions from the shoulder consisting of a single cross-linked species could be obtained. In order to minimize issues associated with sample heterogeneity during the EM reconstruction, only fractions consisting predominately of a single species were utilized for cryo-EM data collections (Figure 4).

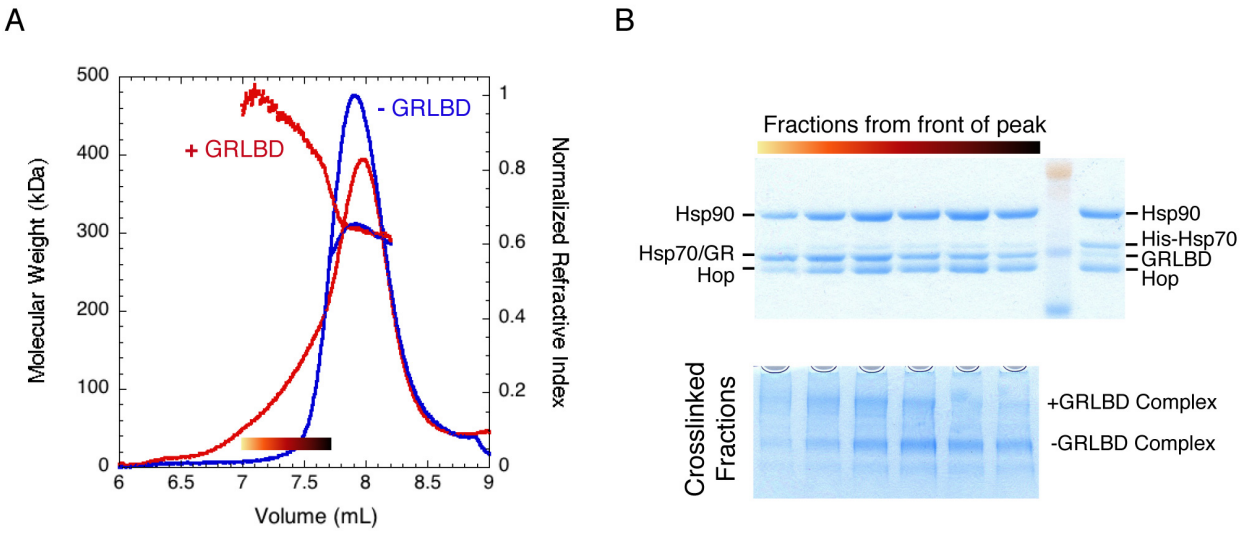

Figure 3. Incorporation of GRLBD onto the Hsp90:Hop:Hsp70 complex
A) SEC-MALS of Hsp90:Hsp70:Hop complex (blue) and with GRLBD (red). Without GRLBD, a 300kDa complex of one HOP, one Hsp70 bound to a Hsp90 dimer is obtained. With GRLBD, there is a shoulder on the front of the peak with an increase in mass indicating the incorporation of MBP-GRLBD (74kDa) into the complex. Complexes were formed with 10µM Hsp90, 15µM Hsp70 (sf9), 15µ Hop, 2µM Hsp40, and 20µM MBP-GRLBD.
B) SDS-PAGE of fractions from front shoulder in the SEC run with GRLBD in (A). Top gel shows incorporation of Hsp70, GRLBD, and Hop. MBP-GRLBD and Hsp70 cannot be resolved by SDS-PAGE due to their comparable size. The sample to the right of ladder was from an equivalent run with a his-tagged bacterial expressed Hsp70, which allows the separation of Hsp70 from MBP-GRLBD and therefore shows the incorporation of both proteins. Bottom gel contains the same fractions from top gel, but cross-linked with 0.02% gluteraldehyde. Two major cross-linked complexes are resolved and interpreted as the $Hsp90_2$:Hop_1:$Hsp70_1$ complex (lower band) and with GRLBD (upper band).
(Exp516)

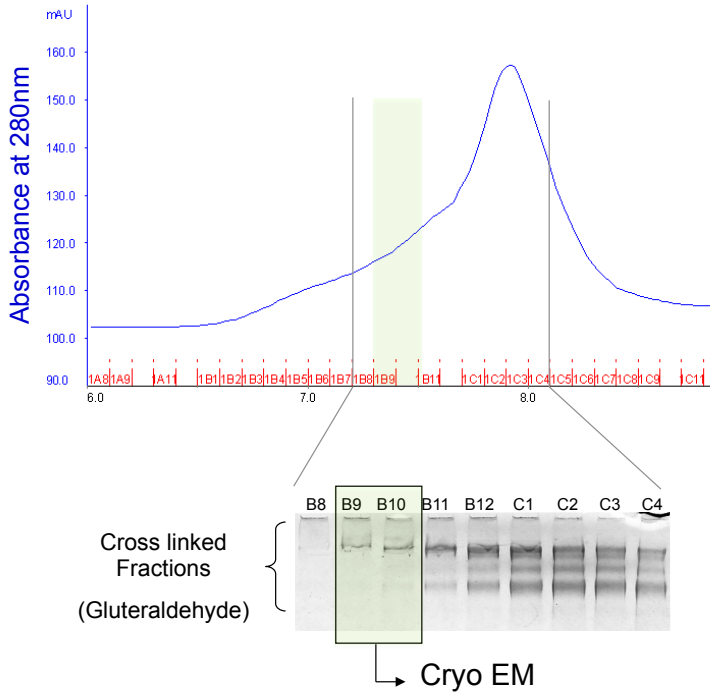

Figure 4. Purifying the GR:Hsp70:Hop:Hsp90 complex for cryo-EM.
SEC of Hsp70:Hop:Hsp90:GR complex showing the UV absorbance at 280m. Below shows the corresponding cross-linked fractions run on coomassie stained SDS-PAGE gel. Only the homogenous fractions B9 and 10 highlighted in green were used for cryo-EM. (Exp518)

Fitting of Hsp90:Hop:Hsp70:GR cryo-EM map

A single particle cryo-EM data set consisting of 10,149 particles was acquired (Figure 5), and from these a 3D reconstruction obtained (Figure 6). While resolution of the reconstruction is estimated to be 38Å (Figure 5B), the size and distinct shape of the individual Hsp90 and Hsp70 domains allowed the general organization of these components in the complex to be determined with high confidence. To verify the fitting for Hsp90 and Hsp70 at the given resolution, low-resolution density maps matching the resolution of the reconstruction (38Å) were generated from the crystal structures of Hsp90 and Hsp70. Because of the distinct size and shape of the chaperones, the low-resolution maps generated from the crystal structures could be uniquely fit into the EM map with the

specific orientations matching that of the fitting provided. This indicates that the placement and orientation of these domains could be determined at 38Å resolution.

Hsp90 is in a V-shaped state similar to the previous Hsp90-Hop EM structure (Southworth and Agard, 2011), however the overall Hsp90 organization is distinctly asymmetric with only one monomer having the fully rotated N-terminal domain (NTD) orientation seen in the Hop complex and originally in the Hsp90 closed ATP state crystal structure (Ali et al., 2006). To fit our density, the other Hsp90 NTD needs to be rotated ~23° outwards about the NTD-middle domain (MD) interface (Figure 6). Without this outward rotation, Hsp90 NTD would clash with density attributed to Hsp70 NBD, suggesting that Hsp70 NBD prevents Hsp90 NTD from attaining the fully rotated position. The opposing Hsp90 monomer that fits the Hop induced conformation has two regions of extra density centered on the MD, which likely corresponds to Hop domains shown to be necessary and sufficient for GR-activation (TPR2A, TPR2B and the C-terminal DP2 domain) (Schmid et al., 2012).

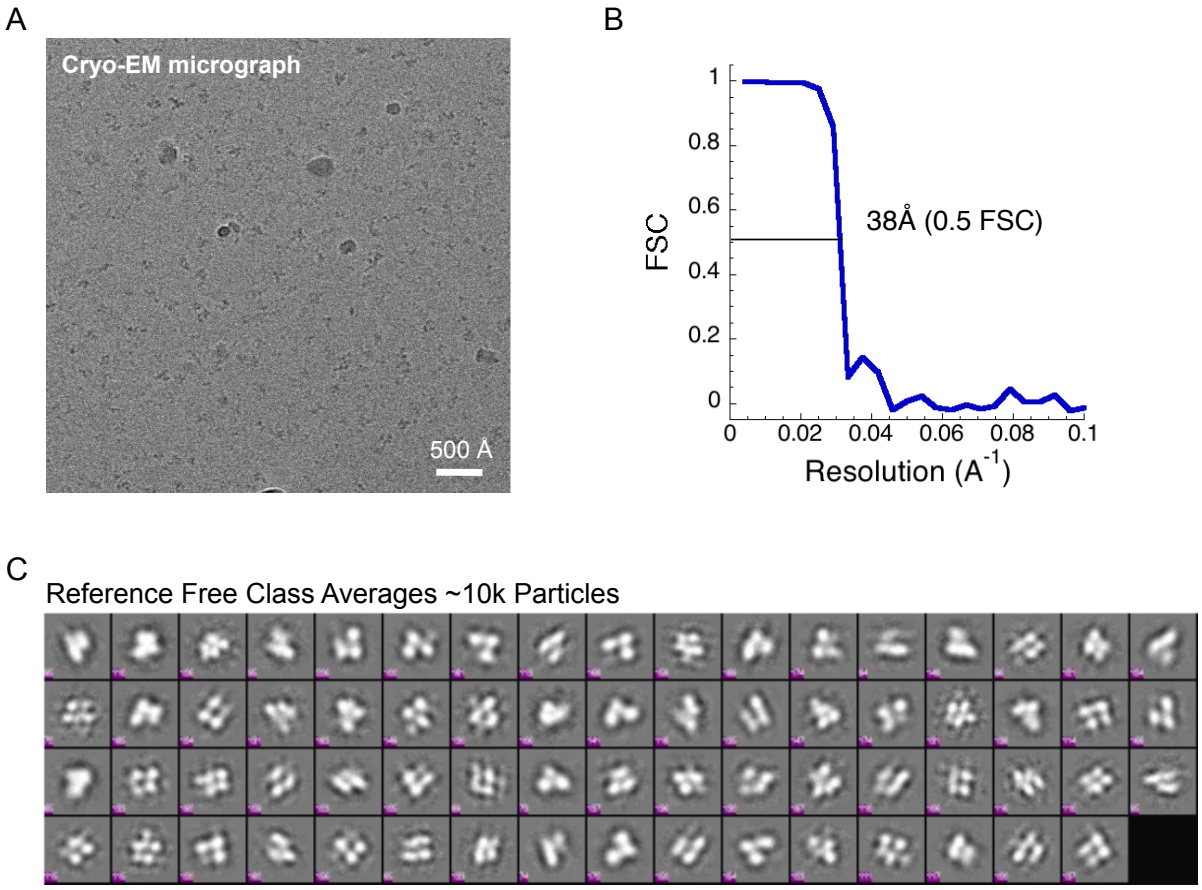

Figure 5. Cryo-EM of GR:Hsp70:Hop:Hsp90 complex.
A) Example of raw micrograph from Cryo-EM data set.
B) Resolution of the cryo EM reconstruction is estimated to be 38Å by the fourier shell correlation method (FSC).
C) Reference free class averages of 10,149 particles from cryo-EM data

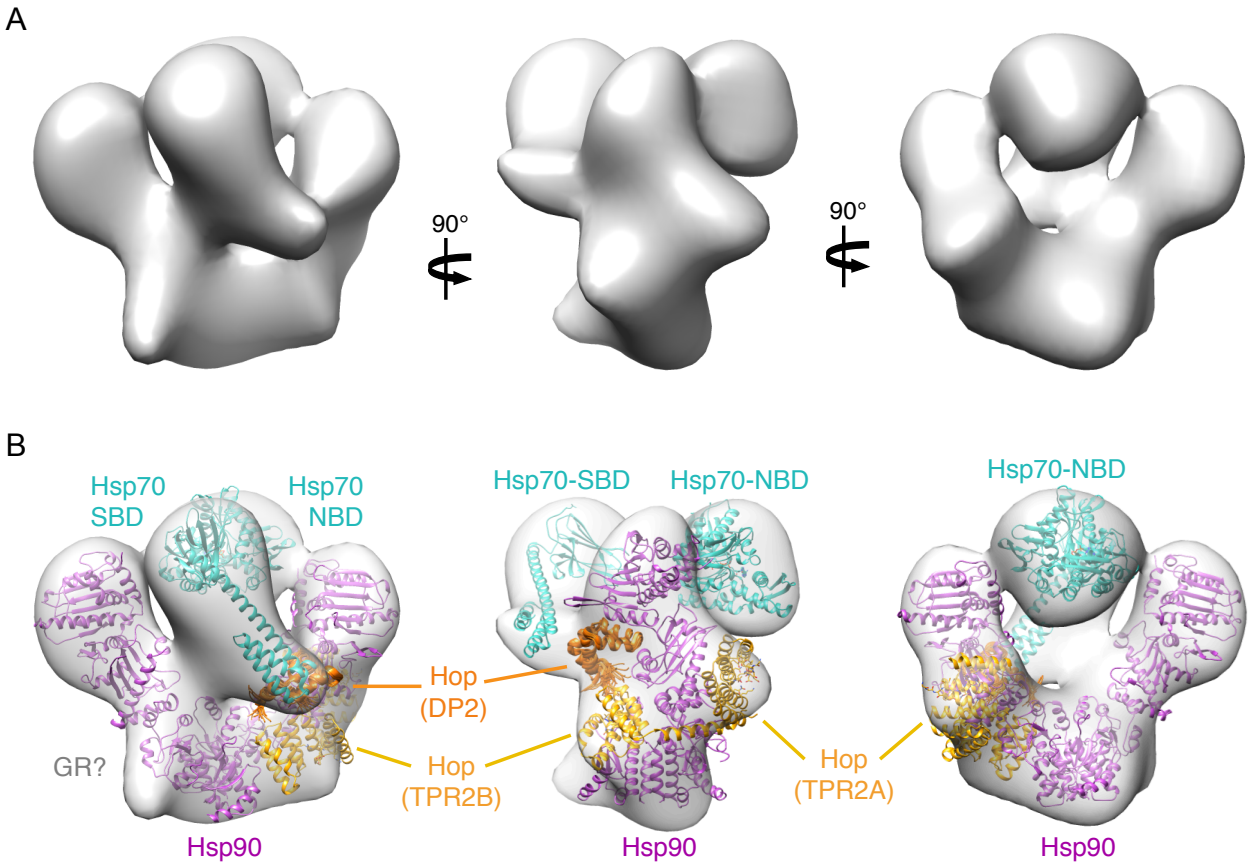

Figure 6. Cryo-EM Reconstruction of GR:Hsp70:Hop:Hsp90 complex.
A) Cryo-EM reconstruction of Hsp90:Hsp70:Hop:GRLBD complex.
B) Cryo-EM reconstruction as in A with placement of Hsp70 NTD (pdb 3ATU) and SBD (pdb modeled from 1DKX and 4B9Q, see Figure 7) in cyan, Hsp90 modeled from the Hop induced conformation in magenta (see Figure 6), Hop TPR2A-2B (modeled from pdb 3UQ3, see Figure 10) in yellow, and Hop DP2 (pdb 2LLW) in orange (see Figure 11).

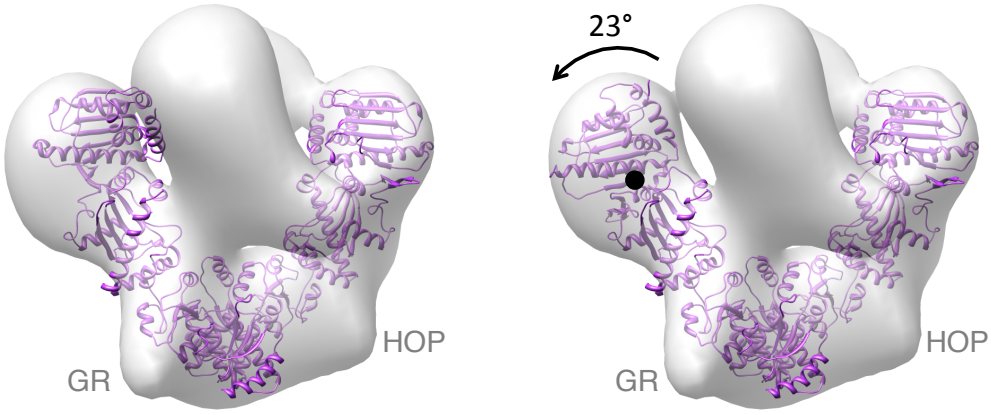

Figure 7. Hsp90 is in a slightly asymmetric conformation similar to the Hop induced state
Fitting of Hsp90 Hop structure into the density requires a rotation in the NTD of the client bound arm. View on left shows that the reconstruction fit with the symmetric Hsp90 structure with the Hop induced NM rotation does not fit into the EM density (left). A 23° rotation away from the center about the NM pivot point (black dot) allows for the NTD to fit into the density (right).

The most distinguishable feature of the complex is the Hsp70 substrate binding domain (SBD). While the corresponding density has the distinct shape of Hsp70 SBD, the substrate peptide bound crystal structure of the SBD could not accommodate the entire length of the density (Figure 8B). The length of the density best fit a conformation of the SBD in which the lid is in a straight conformation (Figure 8). This conformation of Hsp70 was proposed previously based on experimental results indicating that the lid was more extended when bound to a partially folded full length client protein (Schlecht et al., 2011).

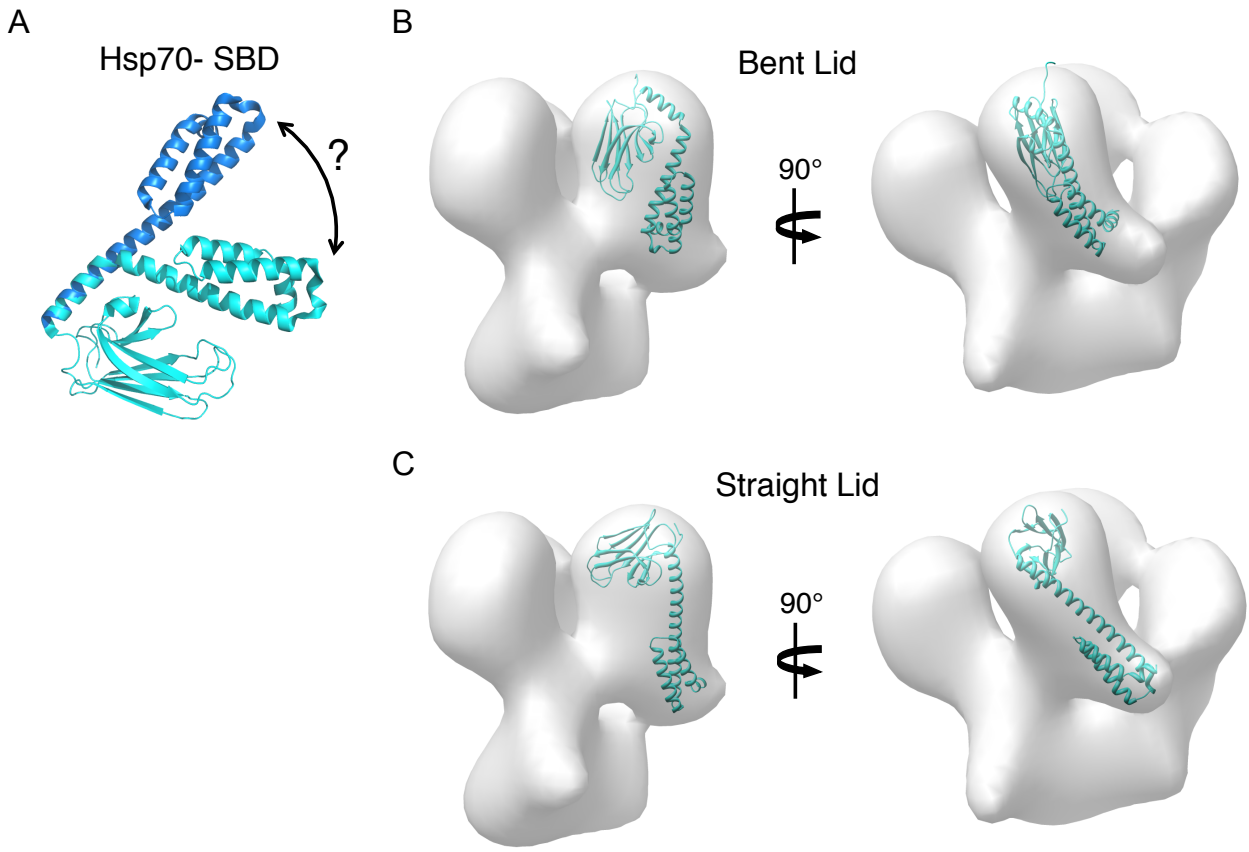

Figure 8. Hsp70's SBD lid is in open conformation in Hsp70:Hsp90:Hop:GRLBD complex
A) Crystal structure of bacterial Hsp70 bound to substrate peptide in cyan (pdb1DKX) with the lid in the fully closed conformation, and model structure of Hsp70 SBD with the lid in an open conformation in marine blue as previously proposed (Schlecht et al., 2011). Open lid was modeled with the lid from the ATP state crystal structure (pdb 4B9Q).
B) EM complex fit with peptide bound structure of Hsp70 SBD (pdb 1DKX) with the α-helical lid in a bent conformation.
C) EM complex fit with a model of the SDB with the α-helical lid in a straight conformation accommodates the density better than the bent conformation in (B). The extra density between the substrate binding site and the lid is likely GRLBD.

Extra density from the substrate-binding site on Hsp70 extends to the MD and CTD interface of Hsp90, suggesting that GRLBD is simultaneously bound to both Hsp90 and Hsp70. Additionally, Hsp70 appears to be delivering GRLBD directly to the client binding site originally identified on the *E. coli* Hsp90 (Genest et al., 2013) (Figure 9). When tested

in yeast, mutations in this region had a significant impact on GR signaling *in vivo*. Indeed, the portion of the binding site mapped to the CTD amphipathic helix had been suggested to make direct contact with apo GRLBD (Fang et al., 2006).

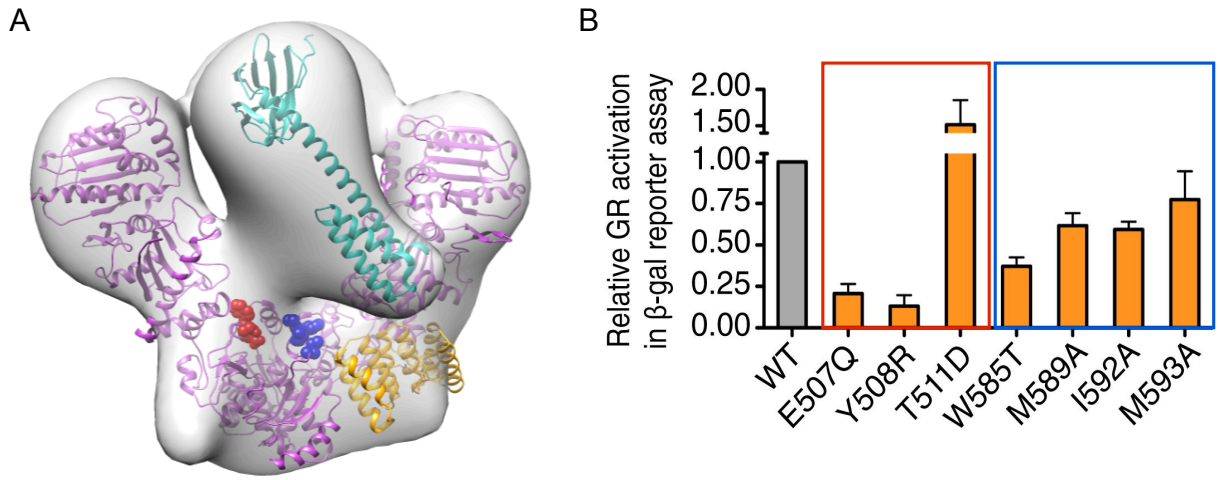

Figure 9. Hsp70 delivers GRLBD to client binding sites on Hsp90
A) Complex as in Figure 5 with Hsp90 client binding site residues for *E. coli* Hsp90 displayed as spheres; E466, W467, N470 shown in red and M546, M550, L553, F554 in blue (Genest et al., 2013).
B) Hsp90 client binding residues identified in the bacterial system were tested in yeast with the GR reporter assay illustrating the significant effect the client binding site residues have on GR signaling *in vivo*. Figure adapted from Genest et al, 2013, with highlighted residues color-coded to match coloring in (A).

As expected for Hsp70 in the ADP state, the Hsp70 SBD is separated from its nucleotide binding domain (NBD). Not only is there a distinct orientation between the two domains, but also the connecting density is readily visible (Figure 10A). The most surprising aspect of the reconstruction is the location of the Hsp70 NBD nestled between the two Hsp90 NTDs. Such a direct contact between Hsp90 and Hsp70 was unexpected, as *in vitro* binding between just Hsp90 and Hsp70 is only detected in the presence of Hop, which binds both independently through separate TPR domains. This led to the conclusion that HOP was a passive linker, and that the Hsp70:Hsp90 interaction was purely through

the physical connection to Hop. While the Hsp70 NBD seems to contact both Hsp90 NTDs, it makes a stronger connection with the ATPase domain of the Hop bound Hsp90 monomer. Formation of this connection requires the Hsp90 conformation induced by Hop (Figure 10C), indicating that not only does Hop pre-organize Hsp90 for receiving clients, but also for interaction with Hsp70.

Utilizing the Hsp70 domain linker as a restraint, Hsp70 NTD best fits into the EM density such that the IB lobe is in proximity to the HOP arm of Hsp90, and the base of the IIA lobe is in proximity to the opposing Hsp90 NTD (Figure 10B). Intriguingly, this orientation suggests that the lid of the Hsp90 nucleotide binding pocket is in the region making these contacts with Hsp70 NBD. The functional implications of this potential interaction are significant, as the direct contact between the ATPase domains of Hsp70 and Hsp90 provides a direct structural basis for the coupling of the two ATP hydrolysis cycles suggested by the ligand binding studies.

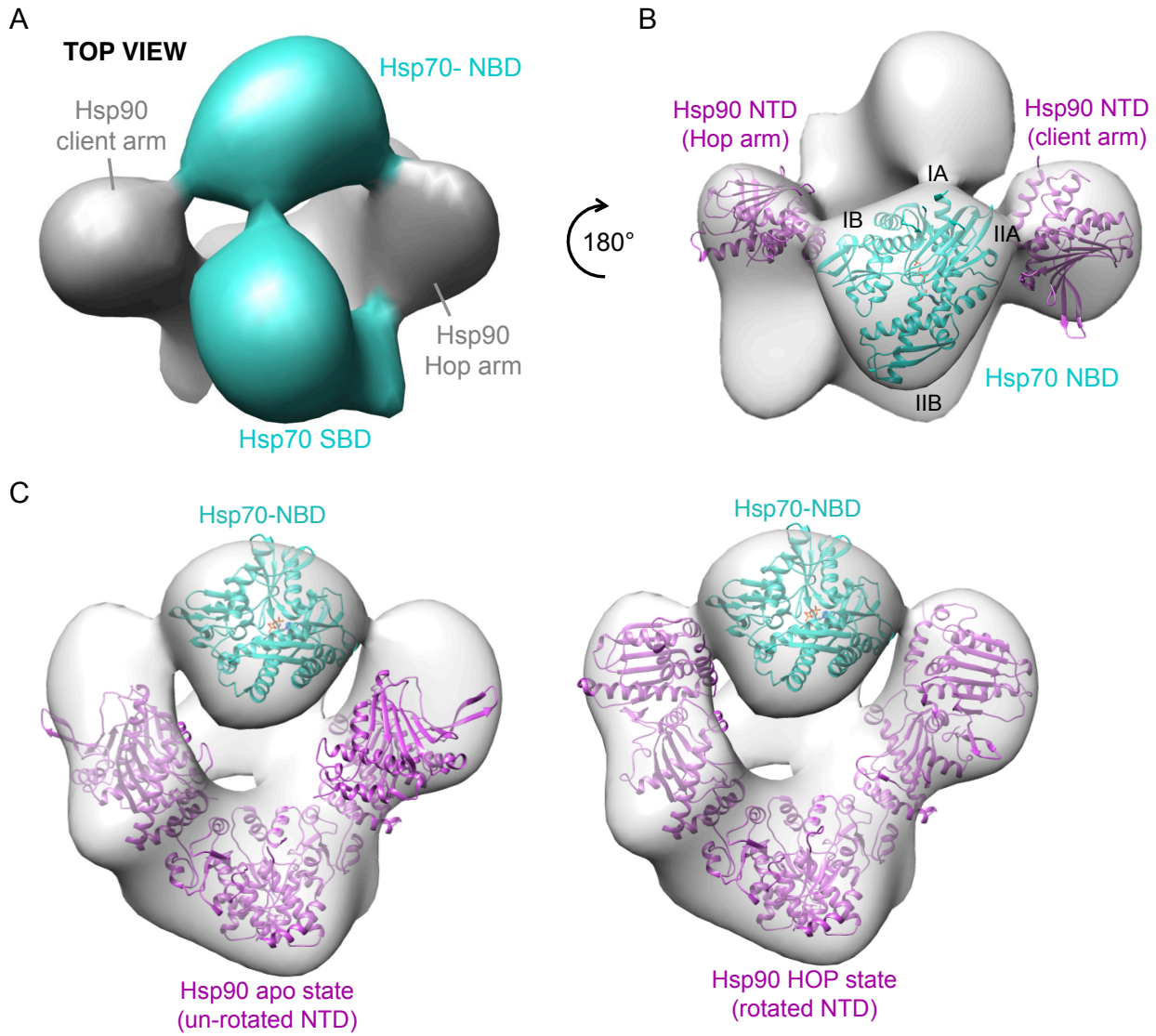

Figure 10. Hsp90 and Hsp70 ATPase domains make direct contact in Hsp90:Hsp70:Hop:GRLBD complex

A) Top view of complex showing density for the linker between the two Hsp70 domains (cyan).

B) Top view showing positioning of Hsp70's NTD between the NTDs of Hsp90. Hsp90's Hop arm NTD is in proximity to Hsp70 NBD lobe IB and Hsp90's client arm NTD is in proximity to Hsp70 NBD lobe IIA.

C) Direct contact between Hsp70 and Hsp90 ATPase domains requires the Hop induced conformation of Hsp90. Shown is the Cryo-EM density fit with Hsp70 NDB (pdb 3ATU) in cyan, and Hsp90 in magenta with apo state crystal structure (pdb 2IOQ) (left) and model structure of Hsp90 the NTDs in the HOP induced NTD rotated state (right).

Fitting of Hop into cryo-EM map

Due to the structural similarity shared between the Hop domains, docking of Hop was mostly guided by the combination of previous structural, biochemical and functional findings. Only three of the five Hop domains are required for enhancement of GR function *in vivo*; two TPR domains, TPR2A and TPR2B, and the C-terminal DP2 domain (Schmid et al., 2012) (Figure 1A). TPR2A has a high affinity to Hsp90's C-terminal MEEVD tail (Scheufler et al., 2000), and TPR2B can bind to Hsp70's EEVD C-terminal tail (Schmid et al., 2012). Together, TPR2A and TPR2B are expected to make extensive contacts with Hsp90 that are sufficient for Hsp90's ATPase inhibition (Lee et al., 2012; Schmid et al., 2012). Placement of TPR2B into the lower Hop density near Hsp90 M-C interface agrees with both NMR (Schmid et al., 2012), and crystallographic data (Philippe Meyer, personal communications). This places the TPR2B in close proximity to the end of Hsp70's SBD to allow for binding to the EEVD tail located at the end of Hsp70's helical lid (Figure11A).

With TPR2B in this position, the rigid helical linker between the TPR2B and TPR2A domains wraps around the outside of Hsp90 MD. However, for the TPR2A to fit into the EM density the TPR2A six helix bundle must rotate up around the rigid linker helix, breaking contacts between the linker helix and the first helix in the helix bundle (Figure 11B). In turn, the TPR2A seems to pack against the middle domain of Hsp90 (Figure 11C). This rotation of the TPR2A does not perturb the orientation at the TPR2B side of the linker that was shown to be functionally important and is supported by the observation that at high concentrations, the isolated TPR2A domain made direct contact with a middle domain fragment of Hsp90 (Schmid et al., 2012). This location of the TPR2A places the MEEVD of

Hsp90 about 78Å distance from the last resolved residue in the Hsp90 CTD, making this distance acceptable.

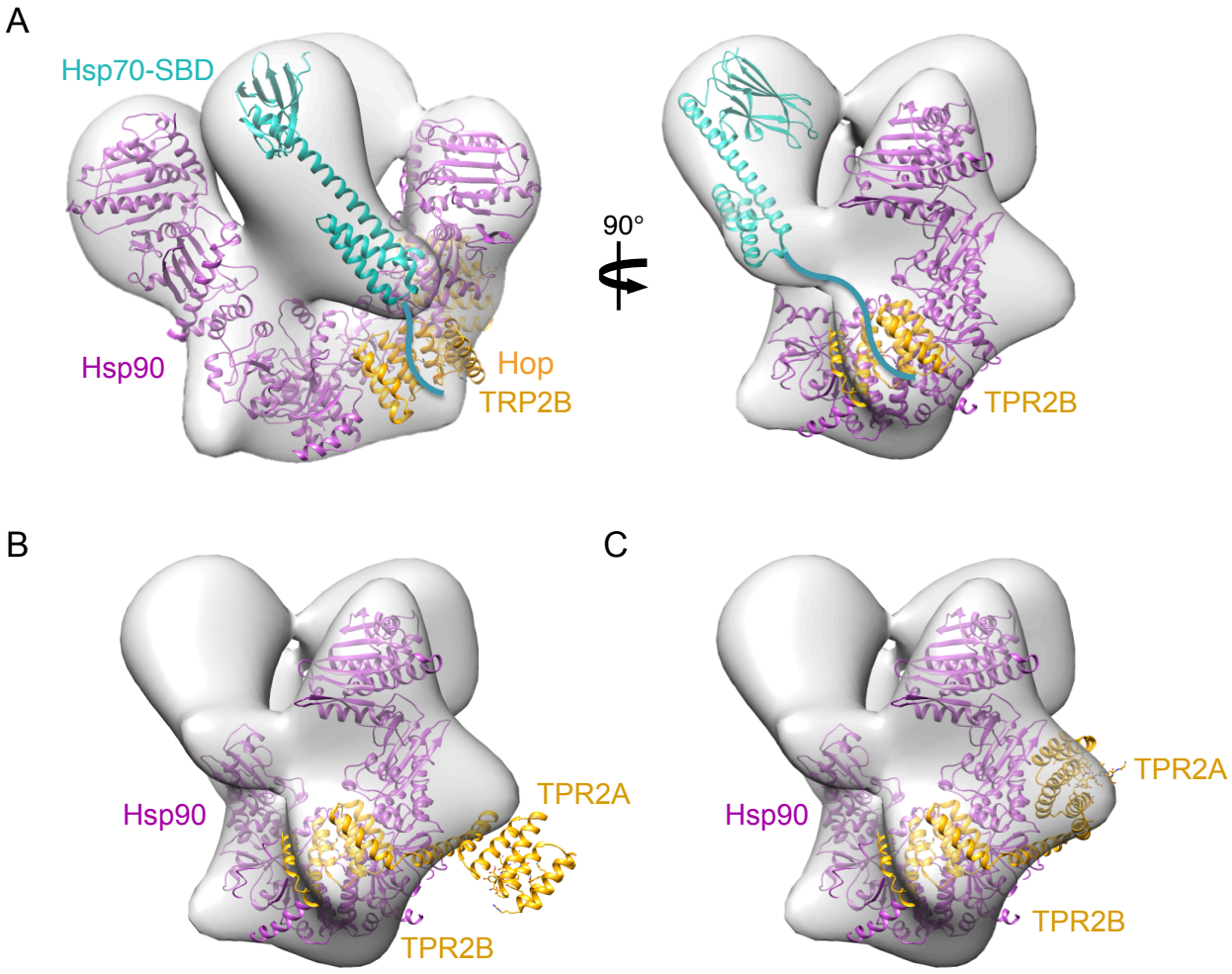

Figure 11. Positioning of Hop TPR2A and 2B in complex
A) Hop facilitates the recruitment and positioning of Hsp70 SBD. Hop TPR2B (pdb 3UQ3) bound at Hsp90's MD-CTD interface places it in close proximity to the EEVD tail motif at the C-terminus of Hsp70's lid to which it binds.
B) Docking of TPR2A-2B fragment (pdb 3UQ3) based on the fitting of the TPR2B in (A).
C) An upward rotation of TPR2A's helical bundle domain around the linker helix fit TPR2A into the EM density.

The most interesting aspect of this positioning of TPR2B is that it positions the DP2 domain into an unoccupied region of density in the NTD-MD interface of Hsp90. The DP2 domain fits into the density in a way that clashes with an un-rotated NTD-MD conformation

(Figure 12), thus suggesting that the DP2 domain of Hop maybe responsible for promoting the MD-NTD rotation. This structure reveals how Hop plays an important role in mediating client transfer: TPR2B recruits and positions Hsp70 SBD in proximity to the client binding site on the opposing Hsp90 monomer, and DP2 stabilizes the orientation of Hsp90's NTD required for the direct interaction between the ATPase domains allowing for release of client from Hsp70 mediated through the coupling of the chaperone cycles.

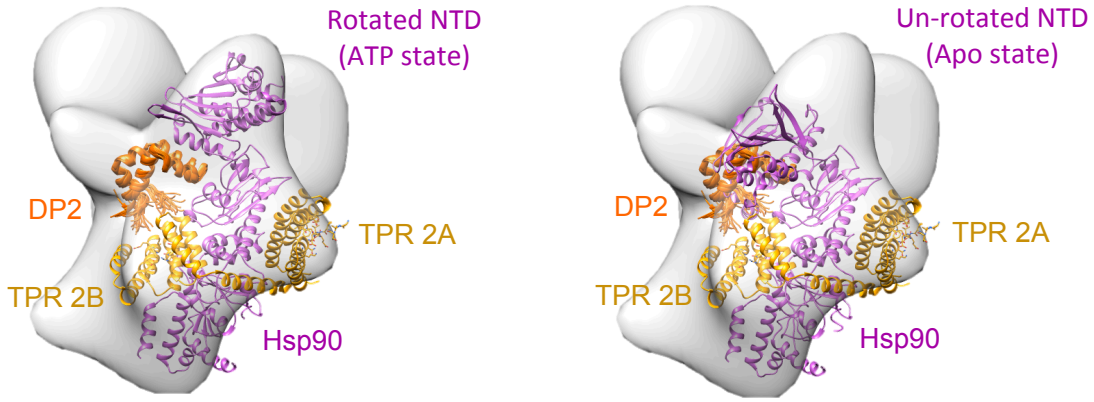

Figure 12. Structural evidence that Hop DP2 domain promotes Hsp90's N-M rotation. Hop DP2 (pdb 2LLW) domain fits into the empty density located at that the C-terminus of the TPR2B domain (left). In this position, the DP2 domain clashes with the un-rotated NTD conformation from the apo Hsp90 crystal structure (right). Once bound, the DP2 domain would thus prevent the Hsp90 NTD from falling back into the un-rotated state.

Discussion

The intricate connectivity between all the components in the Hsp90:Hop:Hsp70:GRLBD complex reveals that instead of tenuous interactions in a brief handoff, there is tightly coordinated activity of an entire set of cochaperones and the biochemical coordination is matched by an integral physical coordination. In this complex, the interconnection between Hsp90 and Hsp70 manifests in the positioning of Hsp70

substrate binding region near the MD:CTD client binding site on Hsp90 and the direct interaction between the two ATPase domains. This provides a structural explanation for the coupling of the two hydrolysis cycles suggested by the recovery of GRLBD ligand binding. More explicitly, Hsp90 reverses the Hsp70 inhibition, most likely by promoting GR release from Hsp70. This requires ATP hydrolysis on Hsp90, and client release from Hsp70 requires ADP/ATP exchange. Given the direct contact between ATPase domains of Hsp90 and Hsp70 observed in the EM complex, the most likely explanation is that ATP hydrolysis on Hsp90 promotes ADP/ATP exchange on Hsp70, and thus induces GR release. While direct evidence for this is still required, based on our current understanding, it is the most likely explanation. Future biochemical studies directly investigating nucleotide release on Hsp70 in the presence of the Hsp90 system will likely shed more light on to the validity of this model.

Hop coordinates the interaction between Hsp70 and Hsp90

In the presence of the Hsp90 system, Hop recruits the GRLBD:Hsp70 complex such that GRLBD is delivered in close proximity to Hsp90's client binding site. The EM density suggests that GRLBD makes direct contact with Hsp90 while still bound to Hsp70. Progression from this inhibited state involving Hsp70 release requires hydrolysis on Hsp90. Hop mediates this interaction by promoting the NM rotation required to make contact between Hsp70 and Hsp90's ATPase domain. The most likely location of DP2 domain suggests DP2 is responsible for inducing the NM rotation and thus explaining the importance of the DP2 domain for Hop function *in vivo*. In the absence of Hop, Hsp90 can likely access this conformation, although with lower efficiency, thus explaining the partial

ligand binding recovery seen without Hop (Chapter 3). These results are consistent with previous findings that also showed ~50% GR activation without Hop (Morishima et al., 2000a), and that Hop facilitated an Hsp70-Hsp90 interaction that could take place without HOP, but only with low efficiency (Morishima et al., 2000b).

The functional consequence of the strategic locations of the TPR2B and DP2 domain are quite apparent in the EM structure, but the functional significance of TPR2A's contact with Hsp90's MD is still very unclear. The TPR2A has the well-established function of initiating the interaction with Hsp90 by binding to the MEEVD motif, but the contact with the MD suggests a secondary function that is not yet clear. The crystal structure of the TPR2A-TPR2B fragment in the extended conformations suggests that the extended state is the low energy state, and that binding energy from Hsp90 provides the energy to access the flipped alternative state seen in the EM map. Perhaps this is a way for Hop to sense a conformational change on Hsp90, or it could be an allosteric site on Hsp90, with Hop regulating another aspect of Hsp90, such as the conformational state of the nucleotide lid on Hsp90.

The EM map is best explained by the Hop interaction being mediated with the TPR2A, TPR2B and DP2 domains and with Hsp70 recruitment occurring through the TPR2B domain. This aligns with both the structural studies by the Buchner lab and genetic studies by the Johnson lab. However, this raises the question as to what the first Hsp90:Hop EM reconstruction represents and in what context the TPR1 and DP1 domains function. It is possible that the TPR1 and DP1 are involved in setting up a preloading conformation on Hsp90, and/or maybe differentially utilized in a client dependent fashion. The original EM map may represents a state that is normally less populated, but becomes

the preferred state when two Hops are bound. However, the question remains as to what context of Hsp90 function this complex would be functionally relevant.

Implications for Hsp70's lid in the straight conformation

Based on the peptide bound Hsp70 SBD crystal structure in which Hsp70's lid fully latches down over the stretch of unfolded polypeptide (Zhu et al., 1996), substrate binding would require at least a 10 Å separation between the bound segment and any other folded region. In most cases, this would require significant domain unfolding. However, there is evidence that Hsp70 can bind to some bacterial proteins while in their native state (Wawrzynow et al., 1995). Of these, the Hsp70 substrate σ^{32} was similarly shown to have only limited unfolding upon Hsp70 binding (Rodriguez et al., 2008). In this case, recent evidence revealed that the Hsp70 lid was not in a fully locked down position (Schlecht et al., 2011), suggesting that Hsp70 could accommodate protein substrates with varying degrees of tertiary structure, such as the partially folded state of GRLBD. The extended lid conformation suggested by the EM map further supports this model and provides an explanation as to how only a limited degree of unfolding was observed on GRLBD when bound to Hsp70. Since most of the gain in substrate affinity in the ADP state comes from conformational changes within the substrate binding site originating from the deepening of the hydrophobic groove and the arch residues that form the primary latch over the substrate (Mayer et al., 2000), it is plausible that GRLBD is still securely bound with the lid in this conformation.

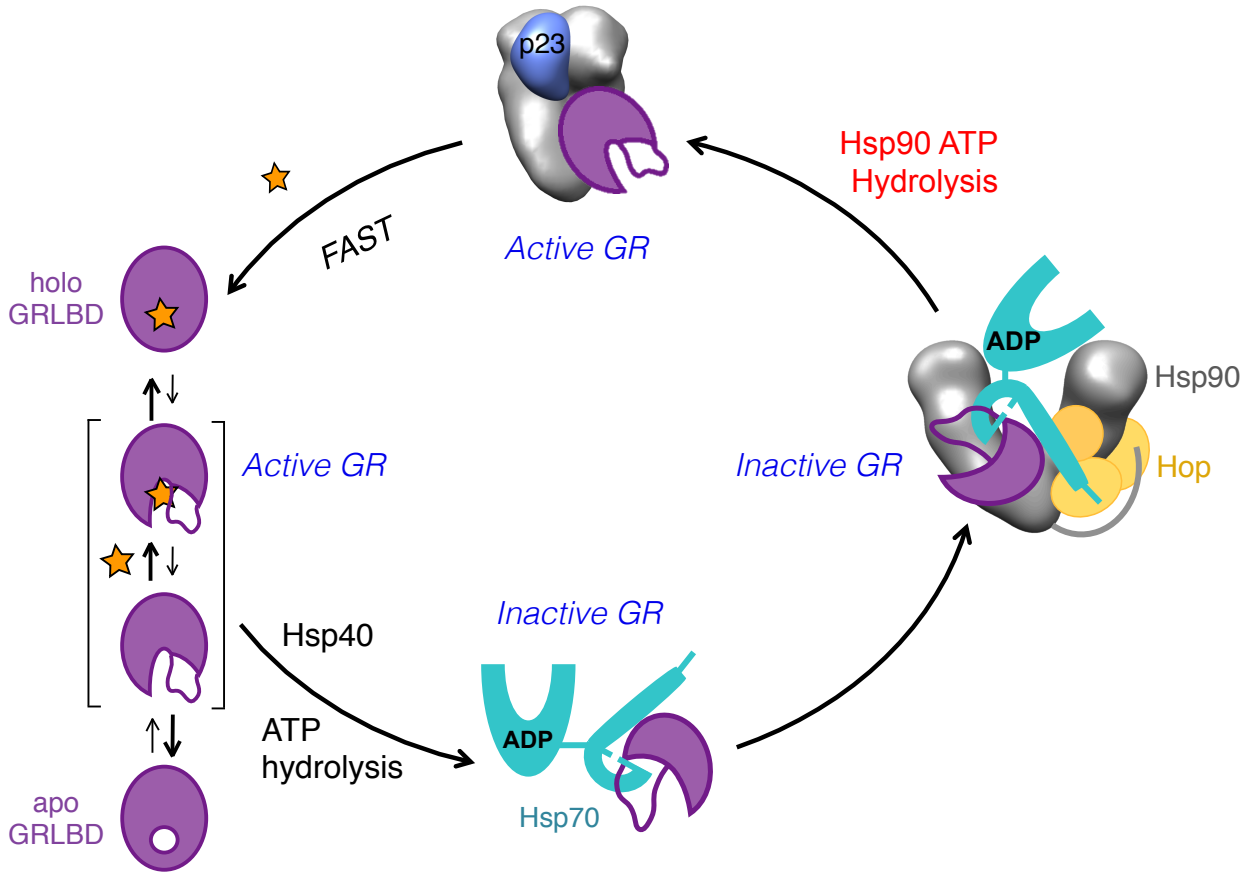

Figure 13. Model for GR ligand binding incorporating structural data form cryo-EM. Hsp70 can accommodate a partially folded GRLBD bound in the substrate binding site with the lid in a straight and partially open conformation. For the Hsp70:Hop:Hsp90:GRLBD complex, Hop recruits and positions Hsp70 SBD in a way that delivers GRLBD to Hsp90's client binding site, and makes extensive interaction with Hsp90, inducing a specific conformation in Hsp90 that is required to coordinate the direct interaction with Hsp70's NBD to facilitate GR release.

Experimental Procedures

Assembly of Hsp90:Hop:Hsp70:GR Complex

10μM Hsp90 dimer, 15μM Hop, 15μM Hsp70, 20μM MBP-GRLBD, and 3μM Hsp40 were incubated with 400μM ATP for 1 hour at room temperature in 30mM HEPES pH7.5, 50mM KCl, 5mM $MgCl_2$, 2mM DTT, 10% Glycerol, and 0.05% n-Octyl-β-D-Glucopyranoside (β-OG). 50μL of the complex was purified by SEC on a Wyatt 050S5 column on an Ettan LC

(GE Healthcare) equilibrated with 50mM HEPES pH7.5, 50mM KCl, 5mM $MgCl_2$, 2mM DTT, 0.01% β-OG and 200μM ADP. Fractions were cross-linked with 0.02% gluteraldehyde for 20 minutes at room temperature and quenched with 20mM Tris HCl pH 7.5. Cross-linked fractions were analyzed by SDS-PAGE. Only fractions containing the single, GR bound complex were used for cryo-EM data collections.

Electron Microscopy and Three Dimensional Reconstructions

Given the expectation that the Hsp90:Hop:Hsp70:GRLBD complex would consist of the Hsp90:Hop complex with extra density for Hsp70 and GRLBD, other than a preliminary screen, negative stain data was not collected. Instead, efforts were immediately focus on cryo-EM, anticipating that the Hsp90:Hop cryo-EM reconstruction would suffice as an initial model. Cryo-EM data was collected as previously described (Southworth and Agard, 2011). 10,149 particles were picked from 214 images with a 2.2-4 μm defocus range. Defocus values were determined using CTFFIND (Mindell and Grigorieff, 2003) and corrected using a Weiner filter. Surprisingly, reconstructions using the Hsp90:Hop structure as an initial model failed to refine to a reliable reconstruction. In turn, an initial model was built from a featureless sphere with 2D class averages by projection matching in SPIDER (Frank et al., 1996). The 3D reconstruction was preformed using EMAN with ten rounds of refinement with 15° angular increments (Ludtke et al., 1999). The resolution was determined by the even-odd test in EMAN. The handedness of the map was determined by the distinct curvature of the Hsp70 SBD, and is consistent with the NMR data for Hop TPR2A-TPR2B bound to Hsp90 MD-CTD (Schmid et al., 2012).

Acknowledgements

I thank J. Kollman, M. Liao, and Y. Cheng for help with the initial model for EM refinement.

References

Ali, M.M.U., Roe, S.M., Vaughan, C.K., Meyer, P., Panaretou, B., Piper, P.W., Prodromou, C., and Pearl, L.H. (2006). Crystal structure of an Hsp90–nucleotide–p23/Sba1 closed chaperone complex. Nature *440*, 1013–1017.

Fang, L., Ricketson, D., Getubig, L., and Darimont, B.D. (2006). Unliganded and hormone-bound glucocorticoid receptors interact with distinct hydrophobic sites in the Hsp90 C-terminal domain. Proc. Natl. Acad. Sci. U.S.a. *103*, 1847–18492.

Flom, G., Behal, R.H., Rosen, L., Cole, D.G., and Johnson, J.L. (2007). Definition of the minimal fragments of Sti1 required for dimerization, interaction with Hsp70 and Hsp90 and in vivo functions. Biochem. J. *404*, 159.

Flom, G., Weekes, J., Williams, J.J., and Johnson, J.L. (2006). Effect of mutation of the tetratricopeptide repeat and asparatate-proline 2 domains of Sti1 on Hsp90 signaling and interaction in Saccharomyces cerevisiae. Genetics *172*, 41–51.

Flom, G., Weekes, J., and Johnson, J.L. (2005). Novel interaction of the Hsp90 chaperone machine with Ssl2, an essential DNA helicase in Saccharomyces cerevisiae. Curr. Genet. *47*, 368–380.

Frank, J., Radermacher, M., Penczek, P., Zhu, J., Li, Y., Ladjimi, M., and Leith, A. (1996). SPIDER and WEB: Processing and Visualization of Images in 3D Electron Microscopy and Related Fields. J. Struct. Biol. *116*, 190–199.

Genest, O., Reidy, M., Street, T.O., Hoskins, J.R., Camberg, J.L., Agard, D.A., Masison, D.C., and Wickner, S. (2013). Uncovering a region of heat shock protein 90 important for client binding in E. coli and chaperone function in yeast. Mol. Cell *49*, 464–473.

Lee, C.-T., Graf, C., Mayer, F.J., Richter, S.M., and Mayer, M.P. (2012). Dynamics of the regulation of Hsp90 by the co-chaperone Sti1. Embo J. *31*, 1518–1528.

Ludtke, S.J., Baldwin, P.R., and Chiu, W. (1999). EMAN: semiautomated software for high-resolution single-particle reconstructions. J. Struct. Biol. *128*, 82–97.

Mayer, M.P., Schröder, H., Rüdiger, S., Paal, K., Laufen, T., and Bukau, B. (2000). Multistep mechanism of substrate binding determines chaperone activity of Hsp70. Nat. Struct. Biol. *7*, 586–593.

Mindell, J.A., and Grigorieff, N. (2003). Accurate determination of local defocus and specimen tilt in electron microscopy. J. Struct. Biol. *142*, 334–347.

Morishima, Y., Kanelakis, K.C., Silverstein, A.M., Dittmar, K.D., Estrada, L., and Pratt, W.B. (2000a). The Hsp organizer protein hop enhances the rate of but is not essential for glucocorticoid receptor folding by the multiprotein Hsp90-based chaperone system. J. Biol. Chem. *275*, 6894–6900.

Morishima, Y., Murphy, P.J., Li, D.P., Sanchez, E.R., and Pratt, W.B. (2000b). Stepwise assembly of a glucocorticoid receptor.hsp90 heterocomplex resolves two sequential ATP-dependent events involving first hsp70 and then hsp90 in opening of the steroid binding pocket. J. Biol. Chem. *275*, 18054–18060.

Rodriguez, F., Arsène-Ploetze, F., Rist, W., Rudiger, S., Schneider-Mergener, J., Mayer, M.P., and Bukau, B. (2008). Molecular basis for regulation of the heat shock transcription factor sigma32 by the DnaK and DnaJ chaperones. Mol. Cell *32*, 347–358.

Scheufler, C., Brinker, A., Bourenkov, G., and Pegoraro, S. (2000). Structure of TPR Domain–Peptide Complexes: Critical Elements in the Assembly of the Hsp70–Hsp90 Multichaperone Machine. Cell.

Schlecht, R., Erbse, A.H., Bukau, B., and Mayer, M.P. (2011). Mechanics of Hsp70 chaperones enables differential interaction with client proteins. Nat. Struct. Mol. Biol. *18*, 345–351.

Schmid, A.B., Lagleder, S., Gräwert, M.A., Röhl, A., Hagn, F., Wandinger, S.K., Cox, M.B., Demmer, O., Richter, K., Groll, M., et al. (2012). The architecture of functional modules in the Hsp90 co-chaperone Sti1/Hop. Embo J. *31*, 1506–1517.

Southworth, D.R., and Agard, D.A. (2011). Client-Loading Conformation of the Hsp90 Molecular Chaperone Revealed in the Cryo-EM Structure of the Human Hsp90:Hop Complex. Mol. Cell *42*, 771–781.

Wawrzynow, A., Banecki, B., Wall, D., Liberek, K., Georgopoulos, C., and Zylicz, M. (1995). ATP hydrolysis is required for the DnaJ-dependent activation of DnaK chaperone for binding to both native and denatured protein substrates. J. Biol. Chem. *270*, 19307–19311.

Zhu, X., Zhao, X., Burkholder, W.F., Gragerov, A., Ogata, C.M., Gottesman, M.E., and Hendrickson, W.A. (1996). Structural Analysis of Substrate Binding by the Molecular Chaperone DnaK. Science, New Series *272*, 1606–1614.

Supplemental

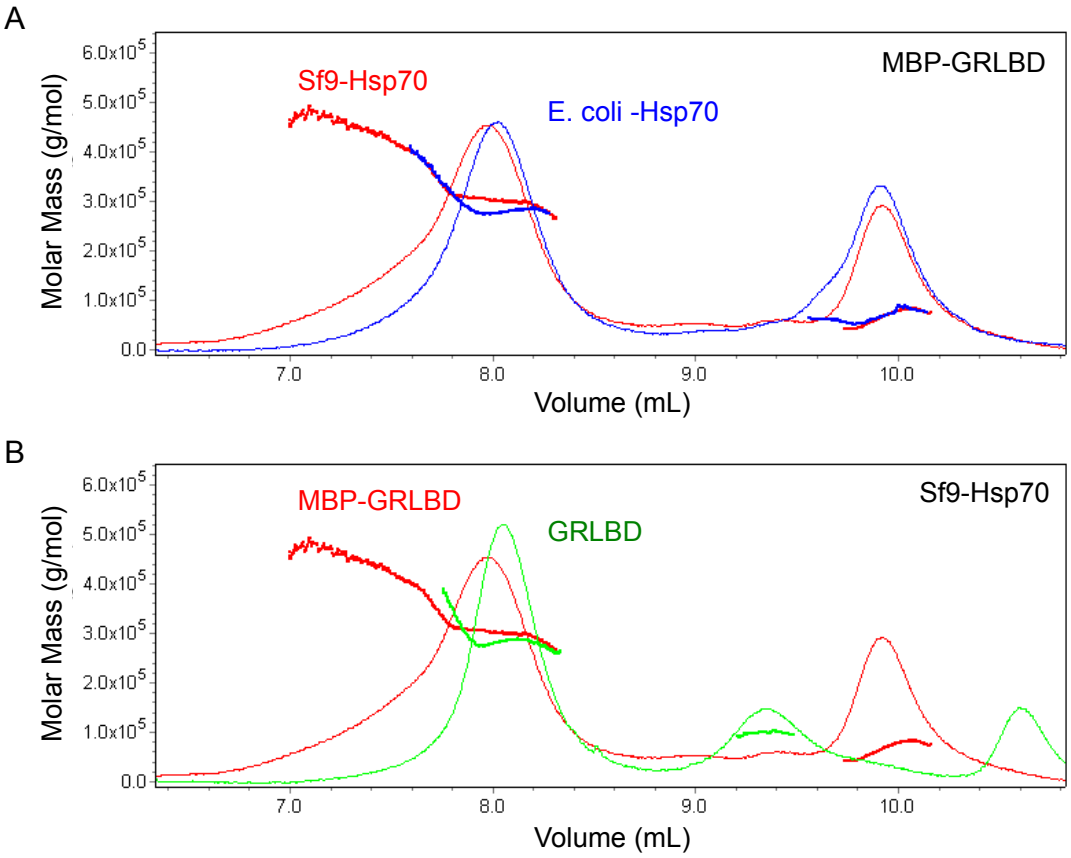

Figure S1. Optimal GRLBD incorporation onto Hsp90:Hop:Hsp70 complex is obtained with Sf9 expressed Hsp70 and MBP-GRLBD
SEC-MALS of preformed Hsp90:Hop:Hsp70:GRLBD complex for 5μM Hsp90 dimer, 15μM Hsp70, 15μM Hop, 10μM MBP-GRLBD and 3.6μM Hsp40.
A) Hsp90:Hop:Hsp70:MBP-GRLBD complex formed with either Sf9 expressed Hsp70 (red) or bacterial expressed Hsp70 (blue).
B) Hsp90:Hop:Hsp70:GRLBD MBP-GRLBD formed with sf9 expressed Hsp70 with either MBP-GRLBD (red) or tag free GRLBD (green).
(Exp516)

Chapter 5

Comparison of Hsp90 to the Hsp70 Nucleotide Exchange Factor, Bag-1

Preface

The experiments described in the previous chapters indicate that Hsp90's reversal of the Hsp70 inhibition requires ATP hydrolysis by Hsp90, likely by promoting Hsp70 release from GRLBD. In the absence of other factors, client release from Hsp70 is slow, but is facilitated by nucleotide exchange factors (NEF) that accelerate ADP release, allowing ATP rebinding, and the consequent opening of the lid and substrate binding site. We sought to directly contrast Hsp90 with a traditional Hsp70 NEF in the GR ligand binding assay. The well characterized human NEF, Bag-1, was chosen due to its well characterized ability to stimulate Hsp70 ADP and client release (Gässler et al., 2001; Sondermann et al., 2001). Additionally, there is evidence that Bag-1 acts in the GR pathway (Demand et al., 2001; Kullmann et al., 1998).

Summary

Direct binding studies confirm that the NEF, Bag-1, promotes the release of GRLBD from Hsp70. Functional investigations show that Bag-1 also reverses the Hsp70 ligand binding inhibition of GRLBD, clearly correlating Hsp70 release with GRLBD reactivation. However, Bag-1 can only reverse the Hsp70 inhibition at non-physiological near stoichiometric levels. Comparison of Bag-1 to the Hsp90 system (with Hop and p23)

reveals that GRLBD ligand binding recovery by Bag-1 is rapid, whereas the Hsp90 system displays a lag phase followed by a more gradual recovery. The lag phase with the Hsp90 system can be accelerated by physiological concentrations of Bag-1, indicating that in the cellular context, Bag-1 likely functions in collaboration with Hsp90. While the Hsp90 system can maintain the GRLBD ligand binding activity during a long experimental time course, the rapid recovery by Bag-1 is immediately followed by an unexpected gradual and complete loss of function. This loss of GRLBD function correlates with aggregation, demonstrating that GRLBD released directly from Hsp70, but not from Hsp90, is in an aggregation prone state, and that Hsp90 carries out an important chaperone function in addition to promoting Hsp70 release. While ATP hydrolysis on Hsp90 is essential for reversing the Hsp70 inhibition, the chaperone function is independent of hydrolysis, but is enhanced by nucleotide binding. Detailed GRLBD ligand binding kinetics show that the acceleration in the association kinetics seen with the entire chaperone system is also seen with Bag-1, revealing that it is the release from Hsp70 that accounts for the enhanced ligand binding activity. However, this high affinity state only persists in the presence of Hsp90 and not with Bag-1.

Introduction

Bag-1, the first characterized human NEF

In the bacterial system, GrpE is the archetypical NEF that regulates client release from Hsp70 by promoting ADP release (Mayer and Bukau, 2005). The significance of the NEF function is seen in substantial enhancement in Hsp70 mediated protein refolding with GrpE (H Schröder, 1993; Packschies et al., 1997). Optimal refolding is seen with both GrpE

and the J-protein (DnaJ), which together constitute the minimal bacterial Hsp70 system (Szabo et al., 1994). While eukaryotic J-proteins has been well documented, the eukaryotic equivalent of GrpE for sometime remained elusive, with the genome-sequencing projects failing to reveal a GrpE homolog in eukaryotes. This raised the question of what protein component regulates client release form Hsp70 in the eukaryotic cytosol.

Bag-1 was the first identified human NEF. It was first identified for its ability to bind to Bcl-2 and promote Bcl-2's anti-apoptotic activity (Takayama et al., 1995). Following investigations revealed Bag-1 binds to Hsp70's ATPase domain through its conserved bag domain and accelerate ADP release (Gässler et al., 2001; Höhfeld and Jentsch, 1997). Bag-1's status as a bona fide NEF was solidified by the crystal structure of Bag-1's Bag domain bound to Hsp70 NBD (Figure 1A) (Sondermann et al., 2001). Although the Bag domain is structurally unrelated to GrpE and utilizes a distinct mode of interaction, both NEFs stabilize the same "open" state of Hsp70 NBD. In this open state, Hsp70 NBD lobe IIB is rotated outward by 14° and results in significant destabilization of nucleotide binding (Figure 1B).

Unlike GrpE which has a clear positive effect on protein refolding, early reports with Bag-1 indicated a negative impact on Hsp70 mediated protein refolding (Bimston et al., 1998; Nollen et al., 2000; Takayama, 1997). More rigorous investigations have since revealed that under physiological phosphate levels, which slow nucleotide release of human Hsp70, low concentrations of Bag-1 positively effect protein refolding (Gässler et al., 2001; Rauch and Gestwicki, 2014). This positive effect is modest compared to GrpE and higher Bag-1 concentrations revert to a negative effect. Notably, the optimal enhancement correlated with the *in vivo* concentration range of Bag-1 which ranges between 0.1 to 2μM

(Nollen et al., 2000). While Bag-1 is clearly a NEF, there appears to be subtle mechanistic differences between GrpE and Bag-1, likely arising from fundamental differences in human and bacterial Hsp70s (Brehmer et al., 2001).

Since Bag-1's discovery, five other Bag-1 like proteins have been identified and together are classified as the Bag family of proteins (Kabbage and Dickman, 2008). All Bag proteins contain a conserved Bag domain that is necessary and sufficient for binding to Hsp70's NDB and stimulation of ADP release (Gässler et al., 2001; Sondermann et al., 2001). In addition to the shared Bag domain, Bag proteins contain additional domains specific to individual functions. The variety of these additional interaction and functional domains suggests that Bag proteins likely play a more complex role in targeting the release of clients than simply tuning of the chaperone cycle.

There are four Bag-1 isoforms in the cell resulting from alternative translation initiation start sites, with the Bag-1 isoform being the most abundant (Figure 1C) (Simon Alberti, 2003; Yang et al., 1998). All isoforms contain the conserved C-terminal Bag domain required for NEF function. The specific functions for the other domains are less understood. Bag-1 isoforms are mostly cytoplasmic, except for the full length Bag-1L that has an N-terminal nuclear localization sequence resulting in nuclear localization. Both the cytoplasmic Bag-1M, and nuclear Bag-1L contain a non-specific DNA binding region involved in inhibiting GR transactivation (discussed below). The N-terminal TRSEEX repeats in Bag-1M, not in Bag-1, accounts for variations in modulation of Hsp70 chaperone function. Compared to Bag-1, Bag-1M is 4-fold less effective at stimulating Hsp70 ADP release, and has been proposed to negatively impact protein refolding through a direct and transient interaction with clients (Gässler et al., 2001; Luders, 2000).

All isoforms contain a non-cleavable ubiquitin like domain whose function has been connected to the coupling of the Hsp70 chaperone system to the proteasome degradation system. Bag-1 provides a direct link between Hsp70 and the proteasome (Luders et al., 2000). Association with the 26S proteasome requires the amino region that contains the TRSEEX repeat motif and the ubiquitin like domain. Furthermore, Bag-1 interacts directly with CHIP, an ubiquitin ligase associated with the Hsp70 and Hsp90 chaperone machinery, and was shown to promote CHIP induced degradation of GR (Demand et al., 2001). Bag-1's role in client degradation sets up an interesting parallel between Hsp90 and Bag-1, with client release from Hsp70 by Hsp90 associated with folding, and release by Bag-1 associated with degradation.

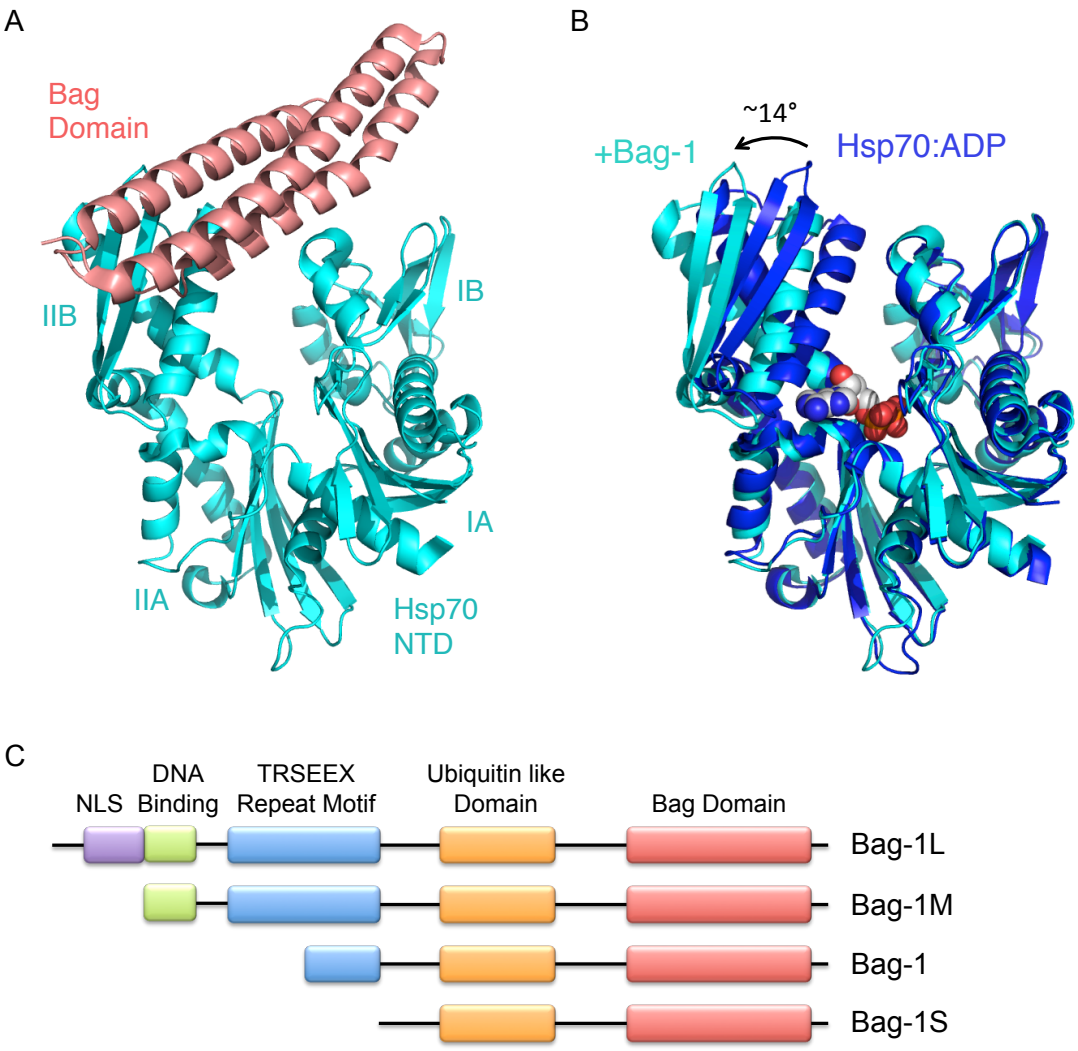

Figure 1. Bag-1 promotes Hsp70 ADP release by stabilizing a more open state of Hsp70 NBD.
A) Crystal structure (pbd 1HX1) of Hsp70 NBD (cyan) bound to the bag domain of Bag-1 (salmon).
B) Bag-1 induces an 14° outward rotation of Hsp70 NBD lobe IIB to promote nucleotide release. Shown is Hsp70 NBD from the Bag-1 structure in A (cyan), superimposed on the ADP bound Hsp70 NBD (pbd 3ATU) in dark blue.
C) Domain architecture of the four human Bag-1 isoforms from varying translation initiation start sites.

Role of Bag-1 in nuclear receptor regulation

Beyond degradation, Bag-1 is involved in other aspects of GR regulation. Around the time of Bag-1's initial discovery, Bag-1 turned up in a separate study related to GR. In

searching for proteins that interact with ligand activated GR, Bag-1 was identified and confirmed to interact with GR and several other steroid receptors independent of their ligand state (Zeiner and Gehring, 1995). In light of this, Bag-1 was investigated by Pratt and co-workers in the GR reconstitution system (Kanelakis et al., 1999). Bag-1 was indeed present at ~0.03 ratios of Bag-1:Hsp70 in the reticulocyte lysate capable of reactivation GR, with low levels of Bag-1 immunoprecipitating with the GR chaperone components. However, depletion of Bag-1 from the lysate had no effect on GR activation. In the reconstituted system, low concentrations of Bag-1 reflecting the physiological ratios was found to modulate the chaperone cycle by promoting Hop release without inhibiting GR activation. Conversely, stoichiometric concentrations of Bag-1 were inhibitory, preventing GR assembly with the chaperones. Equivalently, overexpression of Bag-1 inhibited GR activity *in vivo.*

While this suggest a minor role in modulating GR ligand binding cycle in the cytoplasm, some isoforms of Bag-1 carry out a distinct role in regulating GR in the nucleus. The cytosolic Bag-1M isoform gets recruited to the nucleus with ligand bound GR (Schneikert et al., 1999). Once in the nucleus, Bag-1L and Bag-1M inhibit GR transactivation function by disrupting GR DNA binding (Kullmann et al., 1998). This effect is specific to transactivation since no effect was observed for AP-1 transrespression (Schneikert et al., 1999). Inhibition of transactivation requires the Bag domain, with Hsp70 required for binding of Bag-1 to GR (Schneikert et al., 2000). Additionally, inhibition of transactivation also requires the non-specific DNA binding region, making this function unique to the Bag-1L and Bag-1M isoforms (Schmidt et al., 2003). Together, there is substantial evident that Bag-1 is involved in GR regulation, and in light of the new

discovery that Hsp70 inhibits GR ligand binding, the functional consequences of Bag-1 on the *in vitro* GR chaperone system are worth investigating.

Results

Hsp90 is an Hsp70 release factor with chaperone function

The most abundant Bag-1 isoform, Bag-1, was chosen for this investigation. Bag-1 induced GRLBD release from Hsp70 was confirmed by pull-down (Figure 2). Bag-1's ability to reverse the Hsp70 inhibition was investigated in the fluorescent GRLBD ligand binding assay. Like Hsp90, Bag-1 reverses the Hsp70 inhibition, thus correlating Hsp70 release with GRLBD reactivation (Figure 2B). However, catalytic ratios of Bag-1 to Hsp70 were not very effective, and full ligand binding recovery required near stoichiometric amounts of Bag-1 compared to Hsp70 (Figure 2C).

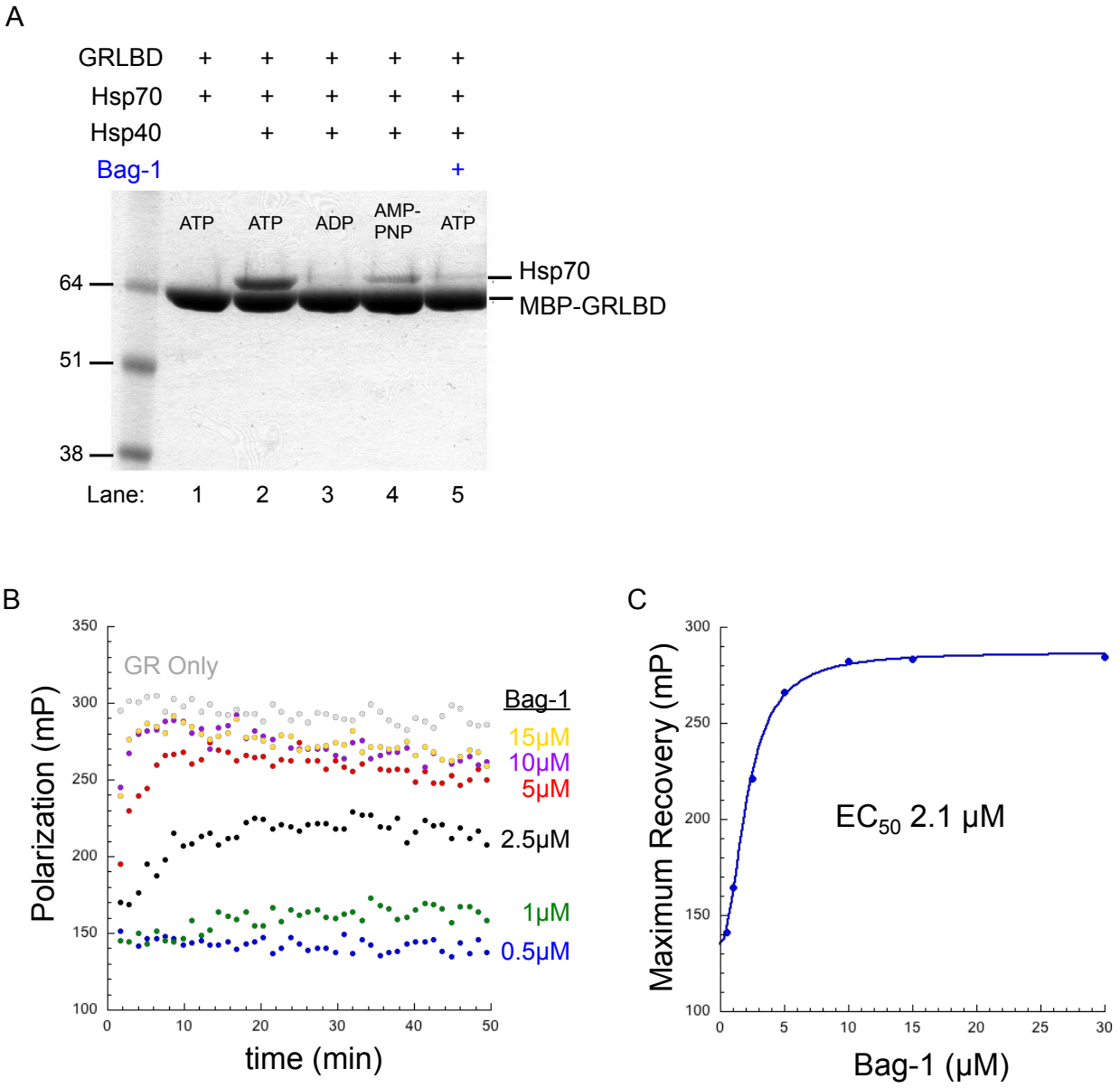

Figure 2. Bag-1 promotes GRLBD dissociation from Hsp70 and GRLBD reactivation.
A) MBP pull down with MBP-GRLBD visualized by coomassie stained SDS-PAGE as in Chapter 3, Figure 3, but also with Bag-1 (lane 5). Assay conditions: 5μM MBP-GRLBD, 2μM Hsp40, 15μM Hsp70, and 5mM corresponding nucleotide. (Exp806)
B) Ligand binding recovery kinetics of pre-inhibited GRLBD with Hsp70/40 carried out as described in Figure 3A, with varying concentrations of Bag-1. Grey data points are for GRLBD and F-dex without Hsp70/40, and thus represent full binding activity. Assay conditions: 50nM F-dex, 1μM MBP-GRLBD, 2μM Hsp40, 15μM Hsp70, and indicated concentration of Bag-1. (Exp863)
C) Maximal recovery observed in (A) plotted against Bag-1 concentration fit to an EC_{50} of 2.1μM.

For comparison to Hsp90, inhibited Hsp70-GRLBD complexes were preformed, and then the kinetics of F-dex binding resulting from Hsp70 release stimulated by either saturating amounts of Bag-1, or Hsp90 (with Hop and p23) was monitored (Figure 3A). Under these conditions, the Hsp90 system showed a lag phase for 5-10 minutes followed by ligand binding recovery, with full ligand binding restored by 30 minutes (Figure 3B). Full ligand binding is then maintained for the duration of the experiment. Remarkably, Bag-1 functions very quickly with a fast recovery of ligand binding (<10min). The ligand association rate observed by release with Bag-1 is ~2-fold faster than the basal association of F-dex to GRLBD on its own, however this is followed by an unexpected steady decrease in ligand binding (Figure 3C). This decrease is relatively slow and occurs linearly with time until almost all ligand binding is lost by 3 hours. Increase in light scattering demonstrated that this loss of function correlates with aggregation (Figure 4B). It should be noted that the GRLBD alone, without any chaperones, was able to maintain full ligand binding during the course of the experiment and shows no aggregation at this temperature by light scattering (Figure 4). This shows that GRLBD directly released from Hsp70, but not from the Hsp90 system, is in an aggregation prone state, and implies that an additional GRLBD folding event likely occurs while on Hsp90. This indicates two distinct functions of Hsp90, one being the release of GRLBD from Hsp70, and the other being a chaperone function.

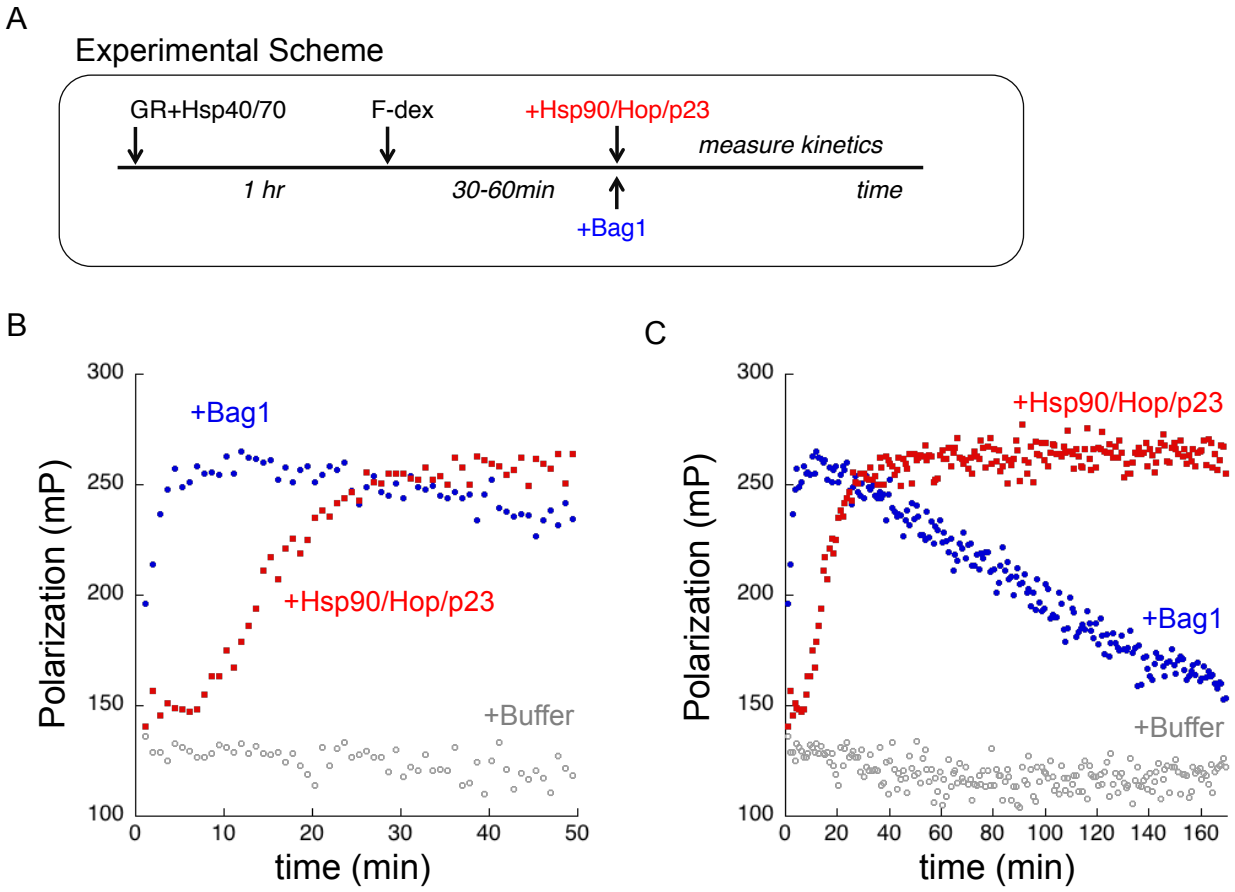

Figure 3. Release of GRLBD from Hsp70 by Bag-1 reactivates GR but results in the gradual loss of ligand binding over time.

A) Experimental scheme for (A), (B), Figure 4 and Figure 5. GRLBD was pre-inhibited by Hsp70 and Hsp40, followed by equilibration with F-dex. Ligand binding is initiated with either Bag-1 or the Hsp90 system.

B) Ligand binding kinetics for first 50 minutes of MBP-GRLBD as described in (A). Kinetics initiated with, buffer (grey circle), Bag-1 (blue circles), or Hsp90 with HOP and p23 (red square). Assay conditions: 50nM F-dex, 1μM MBP-GRLBD, 2μM Hsp40, 15μM Hsp70, Hsp90, HOP, p23 and Bag-1. (Exp700)

C) Same experiment as B, with time scale extended to 170 minutes.

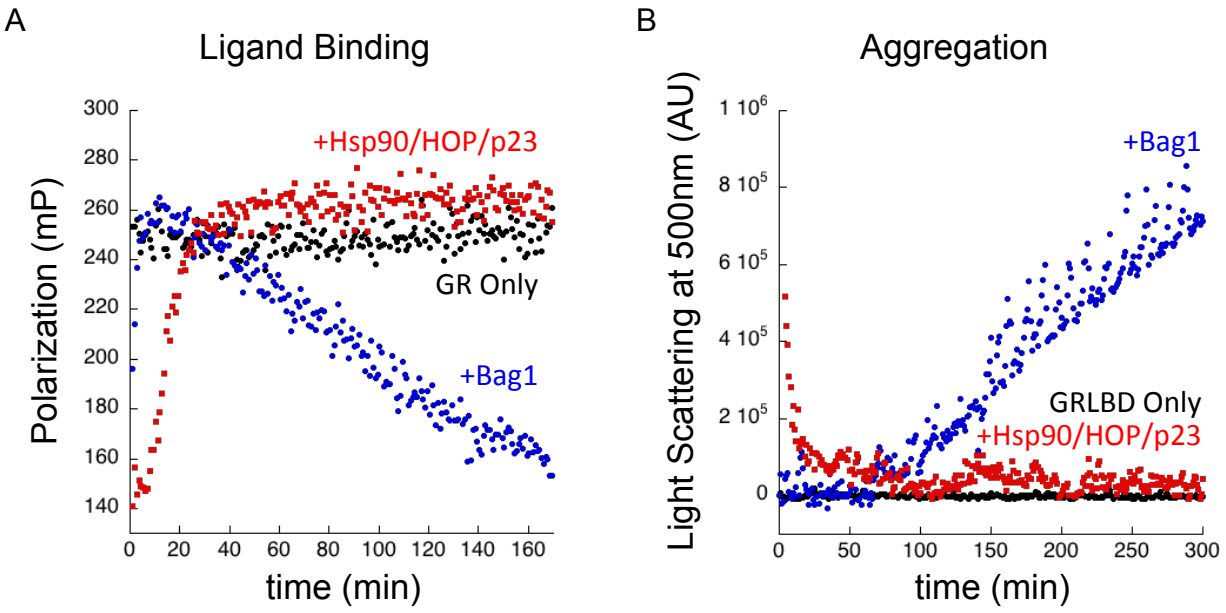

Figure 4. Loss of ligand binding by release from Hsp70 by Bag-1 correlates with aggregation.
A) GRLBD alone is stable during the experimental time course. Shown is the same experiment as in Figure 3C with trace of GRLBD alone also included (black). (Exp700)
B) Release of GRLBD from Hsp70 by Bag-1 results in GR loss of function due to aggregation. Time course of light scattering for GRLBD (black), and for GRLBD pre-incubated with Hsp40 and Hsp70 as for A, with time course initiated with Bag-1 (blue). Same conditions as (A) but without F-dex. (Exp698 and 699)

Hsp90's chaperone function does not require ATP hydrolysis

Hsp90's ability to reverse the Hsp70 inhibition is dependent on ATP hydrolysis. However, we wanted to determine if the chaperone function related to the maintained function over time is as well. To this end, we investigated the combined effects of Bag-1 and Hsp90 (with Hop and p23). When added together, a fast Bag-1 like recovery is seen, but then the full activity is maintained by the Hsp90 system. This indicates that in the context of Hsp70 release by Bag-1, Hsp90 with Hop and p23 can function to prevent GRLBD loss of function. To truly decouple Hsp70 release from the chaperone function, Bag-1 was added with hydrolysis dead Hsp90 E47A (with HOP and p23). Remarkably, with Bag-1, the

hydrolysis dead Hsp90 is just as capable as the wild type Hsp90 at preventing GRLBD loss of function (Figure 5), clearly showing that the chaperone function is independent of ATP hydrolysis.

Further investigation into the combined effect with Bag-1 and Hsp90 revealed that the absence of Hop and p23 resulted in only partial suppression of the loss of function, indicating that both cochaperones are required to fully maintain GRLBD function (Figure S1B). Equivalent loss of function was seen without p23 as with the D93N mutant of Hsp90 with p23. This indicates that accessing the closed state with p23 is beneficial for Hsp90's chaperone function (Figure S1A).

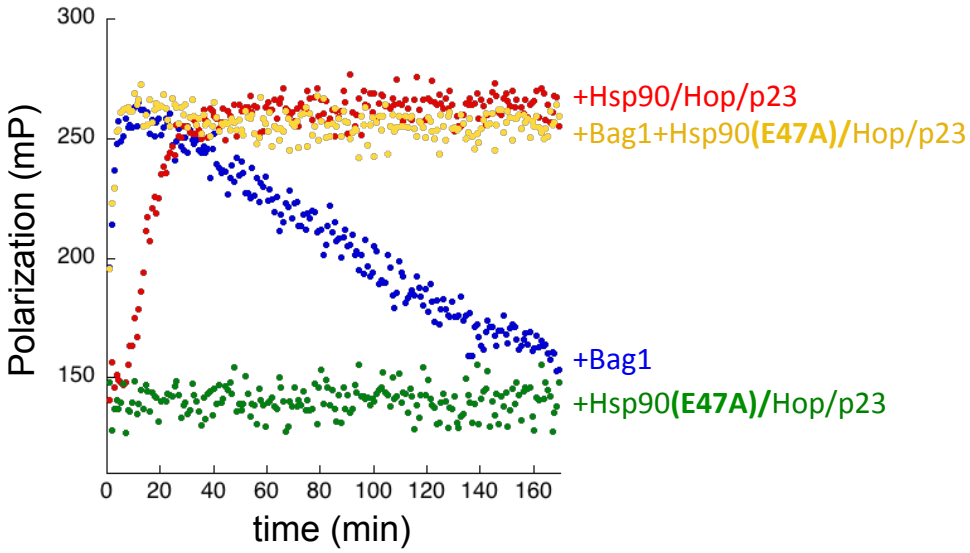

Figure 5. Hsp90 chaperone function does not require ATP hydrolysis.
Same experiment as in Figure 3, but also showing the hydrolysis dead Hsp90(E47A) with Hop, and p23 (green), and in combination with Bag-1 (yellow). (Exp700 and 819)

Bag-1 functions in cooperation with the Hsp90 system

Based on the affinity of Bag-1 for Hsp70 NBD (K_D of 1-3μM (Sondermann et al., 2001)), compared to the affinity of Hsp90:Hop for the Hsp70:GRLBD complex (estimated to

be 200nM or less (Chapter 3, Figure 7C)), the Hsp90 system would preferentially form over the Bag-1 complex. In the EM structure, the Bag-1 binding site on Hsp70 is accessible in the complex (Figure 6A), suggesting that Bag-1 can act within the pathway to promote nucleotide exchange on Hsp70. In the case of the hydrolysis dead mutant of Hsp90 (E47A), the inactive Hsp90:Hop:Hsp70 complex would stall, and Bag-1 could promote Hsp70 release on the stalled complex. Further evidence for Bag-1 promoting the same process as ATP hydrolysis on Hsp90 which results in the progression of the inactive Hsp70:Hop:Hsp90 complex to the active Hsp90:p23 complex is seen when Bag-1 is added to the GRLBD pull-down assay with the Hsp90 system. Addition of Bag-1 results in reduced levels of Hsp70 and Hop, and significantly enhanced incorporation of p23 (Figure 7A).

Given that Bag-1 on its own is ineffective at promoting GRLBD release at biological concentrations (0.1 to 2μM) (Figure 7B), in the cellular context, Bag-1 most likely acts within the Hsp90 pathway. In support of this, Bag-1's effective concentration range for accelerating GRLBD ligand binding recovery in the presence of Hsp90 is 0.1-2μM (Figure 7B and 7C), exactly matching Bag-1's physiological concentration range. Notably, in this experiment the concentration of Hsp90 (10μM) and Hsp70 (15μM) are also within physiological regimes.

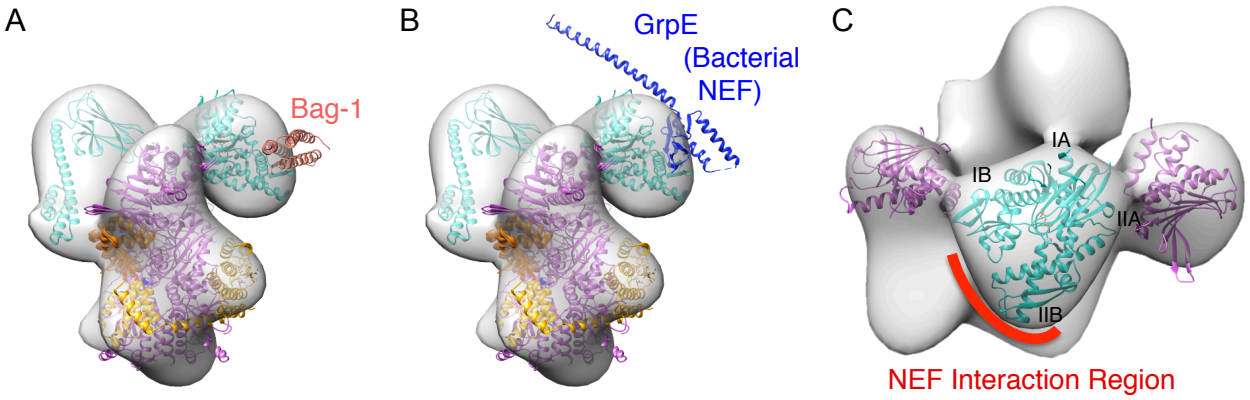

Figure 6. NEF:Hsp70 interaction compatible with Hsp70:Hsp90:HOP:GR complex.
A) Bag-1 bound Hsp70 NDB crystal structure (pdb 1HX1) aligned onto Hsp70 NBD in the Hsp70:Hop:Hsp90:GR EM complex with Bag-1 in salmon.
B) GrpE:Hsp70 NDB crystal structure (pbd 1DKG) aligned onto Hsp70 NBD in the Hsp70:Hop:Hsp90:GR EM complex with GrpE in blue.
C) Top view of Hsp70:Hop:Hsp90:GR EM complex showing Hsp90 NTDs (magenta) and Hsp70 NBD (teal) with the general region utilized in NEF interactions indicated (Liu et al., 2010).

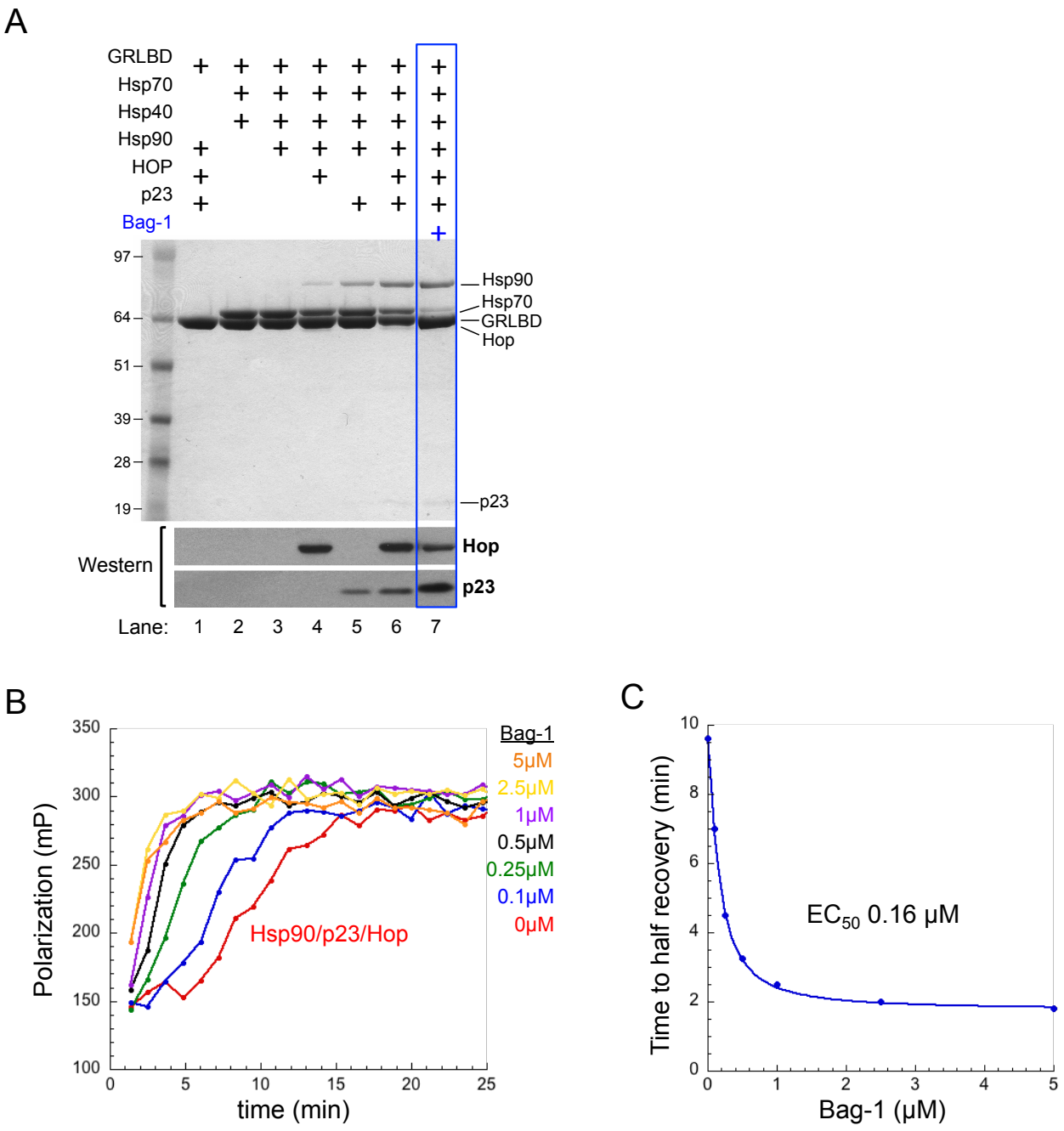

Figure 7. Bag-1 promotes progression of GR from the inactive Hsp70:Hsp90:Hop complex to the active Hsp90:p23 complex.

A) Same MBP-GRLBD pull-down in Chapter 3, Figure 8, but additionally with 15μM Bag-1 in the context of the full chaperone system (lane 7). Assay conditions: 5μM MBP-GRLBD, 2μM Hsp40, and 15μM Hsp70, Hsp90, Hop, p23, and Bag-1. (Exp807)

B) The effective concentration range of Bag-1 with the Hsp90 system. GRLBD ligand binding recovery, as in Figure 6, with 1μM GRLBD inhibited with 15μM Hsp70 and 2μM hsp40. Recovery initiated with 10μM Hsp90, Hop and p23 (red) and with varying concentrations of Bag-1 as indicated. In the context of the Hsp90 system, Bag-1 is effective

at lower concentration ranges (0.1-2μM) compared to without the Hsp90 system (1-10μM) (Figure 2B). (Exp904)
C) Approximate time to half recovery in (B) for varying concentrations of Bag-1. Data fit an EC_{50} of 0.16μM.

Release from Hsp70 accounts for the acceleration in GRLBD ligand binding

Since the rate of ligand binding recovery from saturating amounts of Bag-1 is about 2-fold faster than the basal GR association rate, Bag-1 must also work with Hsp70 to enhance GRLBD ligand binding, as does the Hsp90 system. This suggests that the enhancement seen with the Hsp90 system likely results from Hsp70 release and not necessarily the direct actions of Hsp90. To investigate this more carefully, association experiments similar to those in Chapter 3 were carried out under conditions that minimize aggregation, such as lower MBP-GRLBD concentrations. Also, based on the above experiment, Bag-1 acts very rapidly, and therefor only needs a short time to equilibrate with Hsp70. Bag-1 was therefor added only for the last 10 minutes of the incubation with Hsp70 (Figure 8A).

GRLBD ligand association in the presence of Bag-1 is indeed much faster than GRLBD alone, with the initial ligand association rates comparable to those from the Hsp90 system (Figure 8B). As shown in Chapter 3, in the presence of the Hsp90 system, the binding plateaus to the higher equilibrium level than GRLBD alone, reflecting the lower K_D (Chapter 3, Figure 12). However, while the initial association rate for Bag-1 match that of the Hsp90 system, it equilibrates to the same level as GRLBD alone, without any enhancement in the equilibrium binding. Similar results were observed for the three GRLBD concentrations tested. All the k_{obs} determined for Bag-1 matched those of the Hsp90 system, indicating that the ligand k_{on} with Bag-1 and the Hsp90 system are

equivalent (Figure 8C). This proves that the acceleration in the ligand on rate indeed results from Hsp70 release. However, the equilibration to the GRLBD alone levels suggests that with saturating Bag-1, either the ligand off rate is faster, or that Bag-1 bound Hsp70 does not rebind GRLBD.

To differentiate between the two possibilities, ligand dissociation rates where investigated. Firstly, the ligand dissociation rate after reaching equilibrium, as in Figure 8B, is the same for GRLBD alone as with Hsp70 and Bag-1 (data not shown). This indicates that at the equilibration stage of the experiment, Hsp70 is no longer interacting with GRLBD and promoting ligand release. This was further investigated in the dissociation experiment where GRLBD alone is fully equilibrated with ligand and Hsp70 is added with the excess unlabeled ligand. In this case, addition of Bag-1 was also found to inhibit the Hsp70 induced acceleration in the ligand dissociation (data not shown). Together, this indicates that in addition to promoting GRLBD release, the concentrations of Bag-1 required to build up a significant amount of active GRLBD also prevents Hsp70 from productively rebinding GRLBD. Thus, unlike a traditional NEF, Hsp90 has a unique ability to promote GRLBD release without interfering with Hsp70's ability to reengage GRLBD, and thus allows for the continuous cycling and the high affinity GR state to persist.

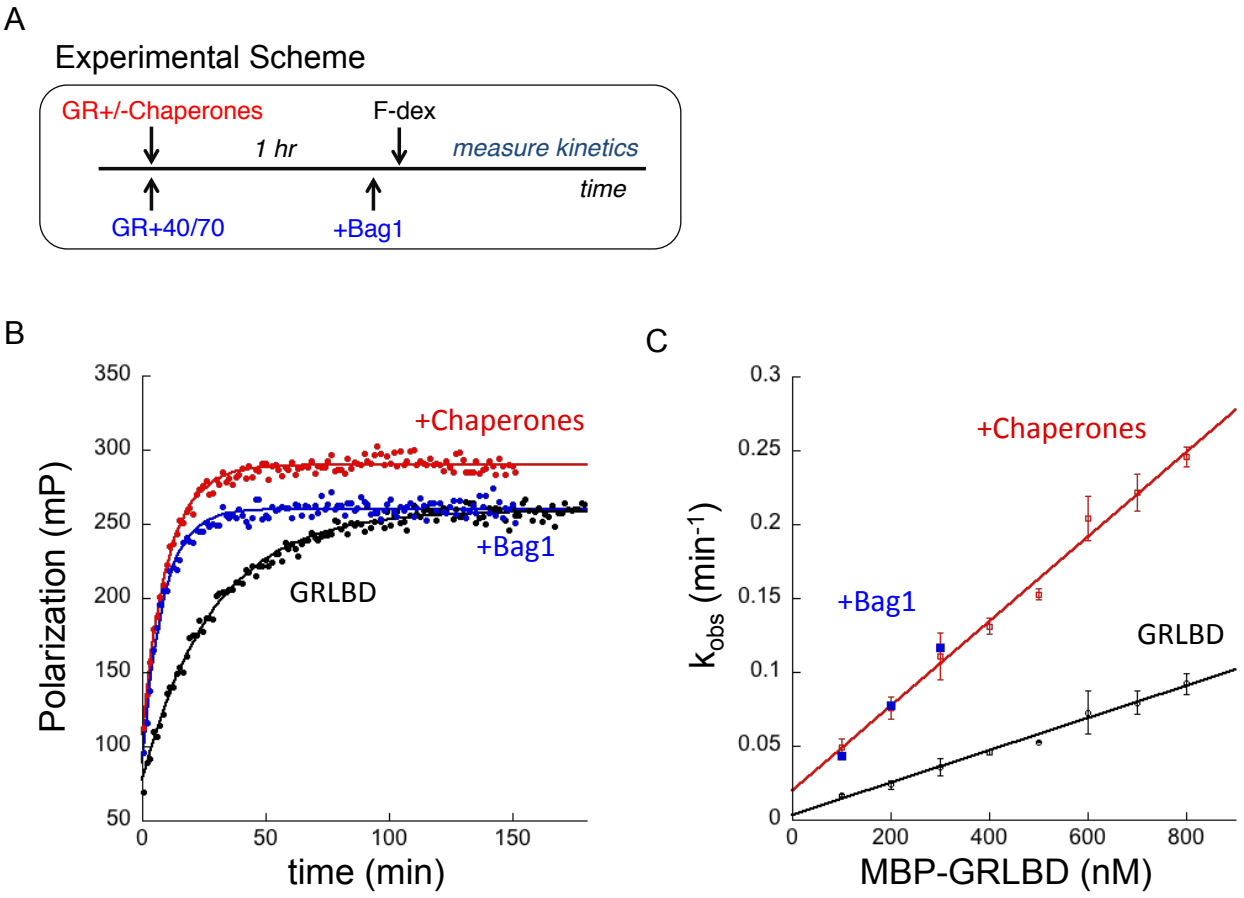

Figure 8. Release from Hsp70 accounts for acceleration in GRLBD ligand association.
A) Experimental scheme for experiments shown in (A) and (B). "Chaperones" refers to the complete Hsp70/Hsp90 system: Hsp40, Hsp70, Hop, Hsp90, and p23.
B) Ligand association kinetics for 300nM MBP-GRLBD alone (black), or pre-incubated with the entire chaperone system (Hsp40, Hsp70, Hop, Hsp90, and p23) (red), or pre-incubated with Hsp70/Hsp40 for 50 minutes before addition of Bag-1 for 10 minutes (blue). Assay condition: 2uM Hsp40, 15uM Hsp70, 10uM Hsp90, Hop, p23, 15uM Bag-1, and 20nM F-dex. (Exp763)
C) Plot of the observed association rate determined as in (B) for varying concentrations of GRLBD. The ligand on rate in the presence of Bag-1 matches that from the Hsp90 system. (Exp763 and 793)

Discussion

The recovery of GRLBD ligand binding by the NEF, Bag-1 indicates that Hsp70 release is sufficient for GRLBD reactivation, and therefore reinforces the conclusion that Hsp90 reactivates GR by directly inducing Hsp70 release. More specifically, it suggests that

Hsp90 likely does so by acts as a NEF, and through an ATP hydrolysis dependent process, Hsp90 promotes ADP/ATP exchange on Hsp70 to drive client release. GRLBD released from Hsp70 is in a partially folded state that has a high affinity for ligand, suggesting that the ligand binding pocket is accessible and that Hsp70, not Hsp90, is responsible for opening of the binding pocket. However, while populating this high affinity partially folded state is beneficial for ligand binding, this state is also prone to aggregation and results in the loss of function seen upon sudden release by Bag-1. In contrast, Hsp90 prevents this loss of function, indicating a distinct chaperone function in addition to Hsp70 release. Given the loss of function that can occur with just a NEF, it is logical that Hsp70 release would be coupled with a chaperone function. The requirement for further chaperone assistance upon Hsp70 release may likely be client specific. In some cases, a NEF may be sufficient, with more stable proteins folding efficiently on their own without risk of aggregation. However, other more complex and less stable proteins may more stringently require Hsp90's assistance to stabilize the final stages of folding that occurs after Hsp70 release.

The equilibration of the ligand binding with Hsp70 and Bag-1 to the level of GRLBD alone suggests that Hsp70 does not continue to cycle with GRLBD under stoichiometric amounts of Bag-1. This is likely the result of Bag-1 constantly holding Hsp70 in the ATP docked state that has very weak affinity for clients, and therefore prevents rebinding of GRLBD. This correlates with the observed loss of GRLBD binding to Hsp70 in the presence of stoichiometric Bag-1 under equilibrium conditions, and aligns with the results from Pratt and co-workers where stoichiometric amounts of Bag-1 prevented GR association with chaperones and thus activation (Kanelakis et al., 1999). NEFs generally function

catalytically, however we find that Bag-1 does not recover GRLBD ligand binding at catalytic amounts. Together, these results highlight distinct limitations of the traditional NEF. The NEF interaction with Hsp70 is driven almost entirely by binding to Hsp70's NBD, act relatively independent of where Hsp70 is in the cycle. On the other hand, Hsp90's actions are specific to a distinct point in the Hsp70 cycle. Assuming that Hsp90 does in fact promote nucleotide exchange, it is only doing so to the client bound ADP state of Hsp70, and therefor Hsp90 does not interfere with Hsp70's ability to reengage the client. This continual cycling is functionally important because it allows for the persistence of enhanced function and regulation of GR by the chaperones.

Cooperation between Hsp90 and NEFs

As shown in our model (Figure 10), at physiological concentrations, Bag-1 cannot effectively promote GRLBD reactivation, but can act within the Hsp90 system to facilitate the progression from the inactive Hop complex to the active p23 complex. This aligns with the work by Pratt and coworkers, who showed that while Bag-1 was not required for GR activation, catalytic amounts of Bag-1 resulted in the loss of Hop (Kanelakis et al., 1999). For the Hsp90 system, the slow recovery associated with the transition to the active p23 complex is likely due to the dependence on the slow Hsp90 hydrolysis rate. Indeed, previous results indicated that the Hsp90 ATP hydrolysis dependent step is the rate limiting step in the cycle (Morishima et al., 2001). The fact that a NEF facilitates this same process further supports ATP hydrolysis on Hsp90 as promoting nucleotide exchange on Hsp70. In the case of the catalytically dead Hsp90 where the inactive Hsp70:Hop:Hsp90 complex is stalled, Bag-1 can completely compensate by providing the necessary nucleotide

exchange function required for release of Hsp70 and the subsequent progression to the active p23 complex. Together, this demonstrates how Hsp90 and nucleotide exchange factors can work cooperatively to promote Hsp70 release and client refolding. This also provides an explanation for how in the bacterial system, GrpE was shown to work synergistically with Hsp90 and Hsp70 to refold denatured proteins (Genest et al., 2011). Moreover, this implies that our findings are not necessarily specific to GR, but likely extend to the Hsp70:Hsp90 system at a fundamental level.

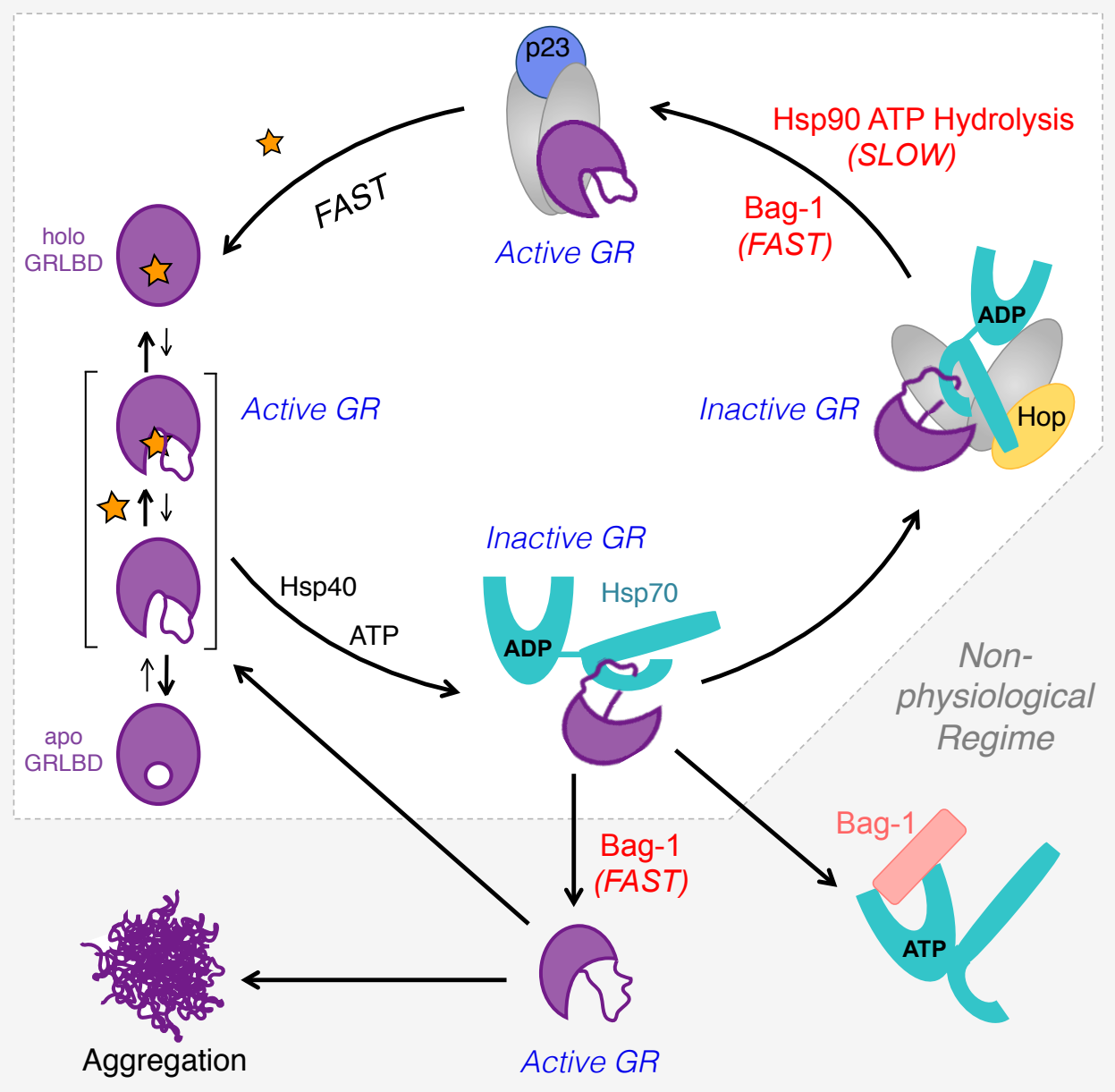

Figure 9. Model for GRLBD ligand binding with chaperones and Bag-1
Starting from the Hsp70 inhibited state of GRLBD, physiological (low) concentrations of Bag-1 are ineffective, but near stoichiometric amounts of Bag-1 cause the release of GRLBD from Hsp70 by promoting the ATP docked state of Hsp70. GRLBD released from Hsp70 in a partially unfolded state that has a high affinity for ligand but is also aggregation prone. In the context of the Hsp90 system, Bag-1 can act within the pathway at physiological concentrations to facilitate the progression from the inactive Hsp70:Hop:Hsp90:GR complex to the active Hsp90:p23:GR complex, where GRLBD is held in the high affinity ligand state and is protected from aggregation by Hps90. In the case that ATP hydrolysis on Hsp90 is prevented and the inactive Hsp70:Hop:Hsp90:GR complex is stalled, the NEF, Bag-1 can compensate for the loss of ATP hydrolysis on Hsp90 and allow for GRLBD reactivation.

Hsp90's hydrolysis independent chaperone function

There is previous evidence throughout the literature for the two distinct functions of Hsp90. In the luciferase reactivation assay the Hsp90 inhibitor, geldanamycin can only partially inhibit reactivation (Grenert et al., 1999). This implies that Hsp90 functions in two separate ways, one being ATP-dependent and the other ATP-independent. Our data demonstrates that the Hsp70 release is the ATP hydrolysis dependent process, and a more passive holdase like chaperone functions independently of ATP hydrolysis. However, the passive chaperone function can be modulated by nucleotide binding, likely in a client specific manner. This correlates with some of the first *in vitro* characterization of Hsp90 which showed that Hsp90's ability to interact with unfolded intermediates and prevent aggregation is ATP independent (Jakob et al., 1995).

The two distinct functions of Hsp90 also surfaced during investigations with Hsp90's client, p53, and provides an interesting parallel to the GR system. This well-known Hsp90 client is also a DNA binding transcription factor. At 4°C, p53 can bind DNA without the aid of chaperones. However, under physiological conditions (37°C), p53 starts to unfold and loose DNA binding activity. Under these conditions, Hsp90 can independently protect p53 and prevent loss of DNA binding (Müller et al., 2004). In this case, this function was specific to Hsp90, with Hsp90 significantly out performing other chaperones. This has been referred to as Hsp90's "direct" mode of interaction with p53. At elevated heat shock temperatures (42°) both Hsp90 and Hsp70 are required to maintain p53 function, with Hsp90 acting through a "cooperative" mode of interaction (Walerych et al., 2009). In line with our data, the direct mode of interaction with Hsp90 that carries out the chaperone function at 37°C is independent of ATP hydrolysis, although ATP binding is required

(Walerych et al., 2010). In this case, the nucleotide binding deficient D mutant was non-functional and the hydrolysis dead E mutant out performed wild type Hsp90. This all points to Hsp90 being able to directly interact with specific states of clients that are early in the unfolding pathway and provide protection from aggregation. These interactions can be modulated by nucleotide induced conformational changes on Hsp90, however, ATP hydrolysis so far seems to have no role in this aspect of Hsp90's function, with hydrolysis being specifically utilized when acting in cooperation with other chaperones for regulating client hand off from Hsp70.

Experimental Procedures

GRLBD Ligand Binding Recovery

For the GRLBD ligand binding recovery, experiment was carried out as shown in Figure 3A. 1μM MBP-GRLBD was pre-incubated with 2μM Hsp40, 15μM Hsp70 and 5mM ATP/$MgCl_2$ for 50-60 minutes at room temperature, followed by incubation with 50nM F-dex for 45-60 minutes. Ligand binding recovery was initiated with 15μM Bag-1 and/or 15μM Hsp90, Hop and p23.

Fluorescence Polarization Assays

GRLBD ligand binding to fluorescein labeled dexamethasone was measured as described in Chapter 2 with experiment specific details described below.

GRLBD Ligand Binding Recovery

For Figures 2-5 and 7, experiments were carried out as depicted in Figure 3A. 1μM MBP-GRLBD was pre-inhibted by 15μM Hsp70 and 2μM Hsp40 for 1 hour at room temperature with 5mM ATP and $MgCl_2$. Then 50nM F-dex was added and allowed to equilibrate for 30-60 minutes. Recovery was initiated with indicated concentrations of Bag-1 and/or the varying chaperone components.

GRLBD Ligand Association Rates

For the GRLBD ligand binding recovery, experiment was carried out as shown in Figure 8A, similarly to association experiment shown in Chapter 3, Figure 11, with the exception that Bag-1 was added only for the last 10 minuets of the pre-incubation.

Aggregation Assay

Aggregation was monitored with a Jobin Yvon FluoroMax-3 fluorescence spectrophotomer with a temperature controlled jacket set to 25°C. Right angle light scattering was measured with excitation and emission wavelengths set to 500 nm with 1.4 nm slit widths.

MBP-GRLBD Pulldown

Pulldown experiment carried out as described in Chapter 3.

References

Bimston, D., Song, J., Winchester, D., Takayama, S., Reed, J.C., and Morimoto, R.I. (1998). BAG-1, a negative regulator of Hsp70 chaperone activity, uncouples nucleotide hydrolysis

from substrate release. Embo J. *17*, 6871–6878.

Brehmer, D., Rüdiger, S., Gässler, C.S., Klostermeier, D., Packschies, L., Reinstein, J., Mayer, M.P., and Bukau, B. (2001). Tuning of chaperone activity of Hsp70 proteins by modulation of nucleotide exchange. Nat. Struct. Biol. *8*, 427–432.

Demand, J., Alberti, S., Patterson, C., and Höhfeld, J. (2001). Cooperation of a ubiquitin domain protein and an E3 ubiquitin ligase during chaperone/proteasome coupling. Curr. Biol. *11*, 1569–1577.

Gässler, C.S., Wiederkehr, T., Brehmer, D., Bukau, B., and Mayer, M.P. (2001). Bag-1M accelerates nucleotide release for human Hsc70 and Hsp70 and can act concentration-dependent as positive and negative cofactor. J. Biol. Chem. *276*, 32538–32544.

Genest, O., Hoskins, J.R., Camberg, J.L., Doyle, S.M., and Wickner, S. (2011). Heat shock protein 90 from Escherichia coli collaborates with the DnaK chaperone system in client protein remodeling. Proceedings of the National Academy of Sciences *108*, 8206–8211.

Grenert, J.P., Johnson, B.D., and Toft, D.O. (1999). The importance of ATP binding and hydrolysis by hsp90 in formation and function of protein heterocomplexes. J. Biol. Chem. *274*, 17525–17533.

H Schröder, T.L.F.U.H.B.B. (1993). DnaK, DnaJ and GrpE form a cellular chaperone machinery capable of repairing heat-induced protein damage. Embo J. *12*, 4137.

Höhfeld, J., and Jentsch, S. (1997). GrpE-like regulation of the hsc70 chaperone by the anti-apoptotic protein BAG-1. Embo J. *16*, 6209–6216.

Jakob, U., Lilie, H., Meyer, I., and Buchner, J. (1995). Transient Interaction of Hsp90 with Early Unfolding Intermediates of Citrate Synthase. Journal of Biological Chemistry *270*, 7288–7294.

Kabbage, M., and Dickman, M.B. (2008). The BAG proteins: a ubiquitous family of chaperone regulators. Cell. Mol. Life Sci. *65*, 1390–1402.

Kanelakis, K.C., Morishima, Y., Dittmar, K.D., Galigniana, M.D., Takayama, S., Reed, J.C., and Pratt, W.B. (1999). Differential effects of the hsp70-binding protein BAG-1 on glucocorticoid receptor folding by the hsp90-based chaperone machinery. J. Biol. Chem. *274*, 34134–34140.

Kullmann, M., Schneikert, J., Moll, J., Heck, S., Zeiner, M., Gehring, U., and Cato, A.C. (1998). RAP46 is a negative regulator of glucocorticoid receptor action and hormone-induced apoptosis. J. Biol. Chem. *273*, 14620–14625.

Liu, Y., Gierasch, L.M., and Bahar, I. (2010). Role of Hsp70 ATPase domain intrinsic dynamics and sequence evolution in enabling its functional interactions with NEFs. PLoS Comput. Biol. *6*.

Luders, J. (2000). Distinct Isoforms of the Cofactor BAG-1 Differentially Affect Hsc70 Chaperone Function. Journal of Biological Chemistry *275*, 14817–14823.

Luders, J., Demand, J., and Höhfeld, J. (2000). The Ubiquitin-related BAG-1 Provides a Link between the Molecular Chaperones Hsc70/Hsp70 and the Proteasome. J. Biol. Chem. *275*, 4613–4617.

Mayer, M.P., and Bukau, B. (2005). Hsp70 chaperones: Cellular functions and molecular mechanism. CMLS, Cell. Mol. Life Sci. *62*, 670–684.

Morishima, Y., Kanelakis, K.C., Murphy, P.J., Shewach, D.S., and Pratt, W.B. (2001). Evidence for iterative ratcheting of receptor-bound hsp70 between its ATP and ADP conformations during assembly of glucocorticoid receptor.hsp90 heterocomplexes. Biochemistry *40*, 1109–1116.

Müller, L., Schaupp, A., Walerych, D., Wegele, H., and Buchner, J. (2004). Hsp90 regulates the activity of wild type p53 under physiological and elevated temperatures. J. Biol. Chem. *279*, 48846–48854.

Nollen, E.A., Brunsting, J.F., Song, J., Kampinga, H.H., and Morimoto, R.I. (2000). Bag1 functions in vivo as a negative regulator of Hsp70 chaperone activity. Mol. Cell. Biol. *20*, 1083–1088.

Packschies, L., Theyssen, H., Buchberger, A., Bukau, B., Goody, R.S., and Reinstein, J. (1997). GrpE accelerates nucleotide exchange of the molecular chaperone DnaK with an associative displacement mechanism. Biochemistry *36*, 3417–3422.

Rauch, J.N., and Gestwicki, J.E. (2014). Binding of Human Nucleotide Exchange Factors to Heat Shock Protein 70 (Hsp70) Generates Functionally Distinct Complexes in Vitro. Journal of Biological Chemistry *289*, 1402–1414.

Schmidt, U., Wochnik, G.M., Rosenhagen, M.C., Young, J.C., Hartl, F.U., Holsboer, F., and Rein, T. (2003). Essential Role of the Unusual DNA-binding Motif of BAG-1 for Inhibition of the Glucocorticoid Receptor. Journal of Biological Chemistry *278*, 4926–4931.

Schneikert, J., Hübner, S., Langer, G., Petri, T., Jaattela, M., Reed, J., and Cato, A.C.B. (2000). Hsp70-RAP46 interaction in downregulation of DNA binding by glucocorticoid receptor. Embo J. *19*, 6508–6516.

Schneikert, J., Hübner, S., Martin, E., and Cato, A.C. (1999). A nuclear action of the eukaryotic cochaperone RAP46 in downregulation of glucocorticoid receptor activity. The Journal of Cell Biology *146*, 929–940.

Simon Alberti, C.E.J.H. (2003). BAG-1—a nucleotide exchange factor of Hsc70 with multiple cellular functions. Cell Stress Chaperones *8*, 225.

Sondermann, H., Scheufler, C., Schneider, C., Höhfeld, J., Hartl, F.U., and Moarefi, I. (2001).

Structure of a Bag/Hsc70 Complex: Convergent Functional Evolution of Hsp70 Nucleotide Exchange Factors. Science *291*, 1553–1557.

Szabo, A., Langer, T., Schröder, H., Flanagan, J., Bukau, B., and Hartl, F.U. (1994). The ATP hydrolysis-dependent reaction cycle of the Escherichia coli Hsp70 system DnaK, DnaJ, and GrpE. Proceedings of the National Academy of Sciences *91*, 10345–10349.

Takayama, S. (1997). BAG-1 modulates the chaperone activity of Hsp70/Hsc70. Embo J. *16*, 4887–4896.

Takayama, S., Sato, T., Krajewski, S., Kochel, K., Irie, S., Milian, J.A., and Reed, J.C. (1995). Cloning and functional analysis of BAG-1: A novel Bcl-2-binding protein with anti-cell death activity. Cell *80*, 279–284.

Walerych, D., Olszewski, M.B., Gutkowska, M., Helwak, A., Zylicz, M., and Zylicz, A. (2009). Hsp70 molecular chaperones are required to support p53 tumor suppressor activity under stress conditions. Oncogene *28*, 4284–4294.

Walerych, D., Gutkowska, M., Klejman, M.P., Wawrzynow, B., Tracz, Z., Wiech, M., Zylicz, M., and Zylicz, A. (2010). ATP binding to Hsp90 is sufficient for effective chaperoning of p53 protein. J. Biol. Chem. *285*, 32020–32028.

Yang, X., Chernenko, G., Hao, Y., Ding, Z., Pater, M.M., Pater, A., and Tang, S.C. (1998). Human BAG-1/RAP46 protein is generated as four isoforms by alternative translation initiation and overexpressed in cancer cells. Oncogene *17*, 981–989.

Zeiner, M., and Gehring, U. (1995). A protein that interacts with members of the nuclear hormone receptor family: identification and cDNA cloning. Proc. Natl. Acad. Sci. U.S.a. *92*, 11465–11469.

Supplemental

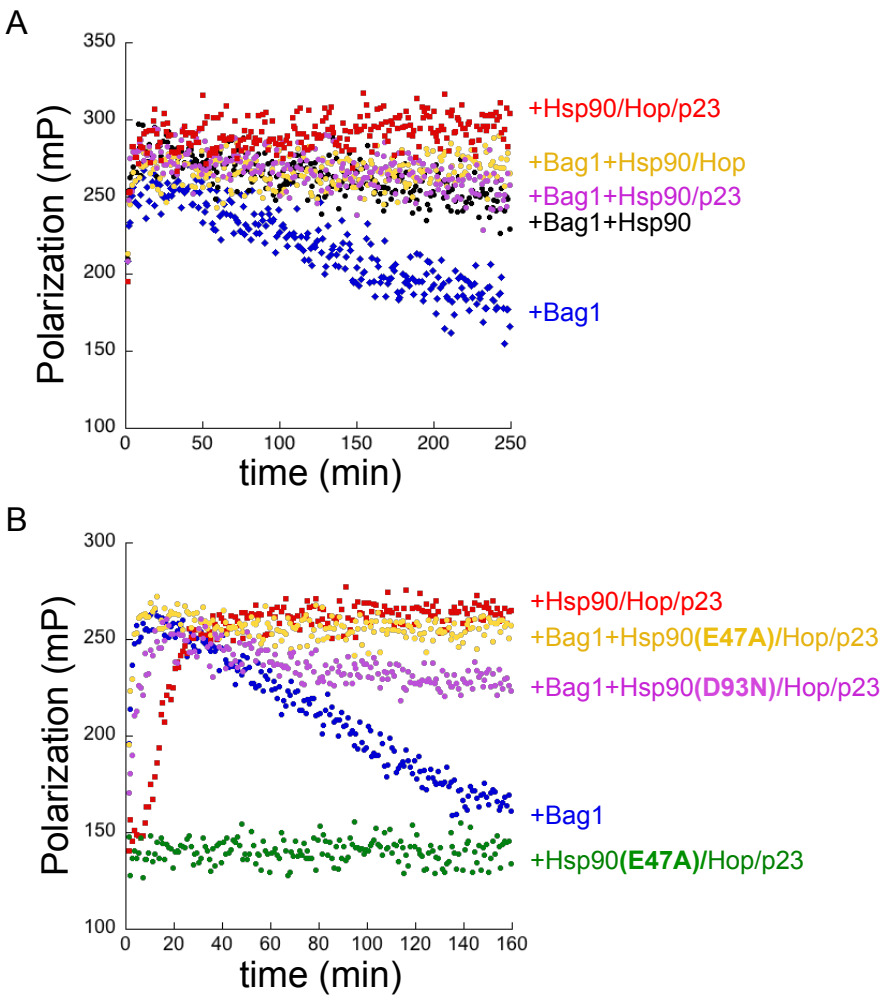

Figure S1. Hsp90 closure facilitates chaperone function.
A) Ligand binding recovery kinetics from Figure 5, additionally showing the combined effect of Bag-1 and the nucleotide binding deficient mutant of Hsp90 (D93N) with p23 and HOP (magenta). (Exp700)
B) Ligand binding recovery kinetics of 1μM MBP-GRLBD pre-inhibited with 15μM Hsp70 and 2μM Hsp40, as in Figure 3. Kinetics initiated with Bag-1 alone (blue), Hsp90 alone (black), Hsp90 with HOP (yellow), Hsp90 with p23 (blue), and Hsp90 with HOP and p23 (red). (Exp697)

Chapter 6

Structural Analysis of the Hsp90-FKBP52 Complex

Preface

FKBP52 is a specific Hsp90 co-chaperone that plays a significant role in steroid hormone signaling. This large immunophillin gets incorporated into the later Hsp90 complex associated with the activated, ligand bound receptors and has been implicated as playing an essential role in the active translocation of the ligand bound receptors to the nucleus. For GR, it has been shown to potentiate GR signaling with a least part of its actions due to enhanced ligand binding. The biological significance for its actions is apparent due to its implication in many diseases that includes specific cancers and psychiatric disorders.

A preliminary EM reconstruction by Daniel Southworth of the FKBP52 bound Hsp90 complex indicated a compact structure with Hsp90 in a closed AMPPNP stabilized state, making this structure an attractive target for crystallography. At the time, there was very little high resolution structural information for the human Hsp90 and even now, a full length human Hsp90 crystal structure is still lacking. A crystal structure of this complex would be extremely valuable since it would provide both mechanistic insight into the actions of FKBP52 and basic structural information on human Hsp90.

Summary

Hsp90 and FKBP52 form a stable (2:1) complex *in vitro*. The purified complex was extensively screened in crystallography trials (both in the absence and presence of

AMPPNP), yet no reproducible hits were obtained. Subsequent SAXS analysis followed up with a DAMMIN ab initio reconstruction indicate that FKBP52 bound Hsp90 is in an extended conformation, with no detectible difference upon the addition of AMPPNP. This suggests that flexibility of Hsp90 in the complex may likely be hindering crystallization. Preliminary investigations reveal that Hop and FKBP52 are not compatible on the Hsp90 complex, with Hop outcompeting binding of FKBP52.

Introduction

FKBP51 and FKBP52 are Hsp90 binding, TPR containing large immunophilin proteins that carry out important roles in regulating steroid hormone signaling at the levels of receptor maturation, ligand binding and nuclear translocation (Storer et al., 2011). FKBP51 and FKBP52 were first identified as proteins that co-immunoprecipitated with GR and PR chaperone complexes (Sanchez, 1990; Smith et al., 1990). While structurally are very similar (70% sequence similarity), FKBP51 and FKBP52 are functionally divergent. FKBP51 attenuates GR signaling (Denny et al., 2000; Reynolds et al., 1999). Opposing, FKBP52 potentiates hormone receptor transcription activation, however just for GR (Riggs et al., 2003), PR (Tranguch et al., 2005), and AR (Cheung-Flynn et al., 2005), but not ER or MR (Riggs et al., 2003). Interestingly, FKBP52 is under GR regulation, with FKBP51 transcription unregulated upon GR ligand activation (Yoshida et al., 2002), indicating that FKBP51 functions as a negative feedback mechanism for GR signaling.

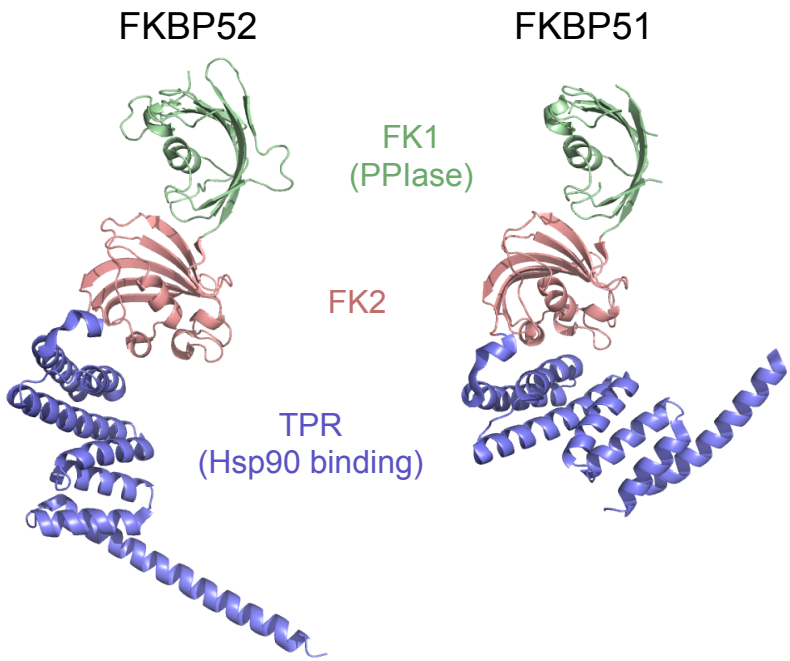

Figure 1. Structure of FKBP51 and FKBP52.
Composite crystal structure of FKBP52 (pdb 1Q1C and 1P5Q) and crystal structure of FKBP51 (pdb 1KT0). The N-terminal FK1, PPIase domain is rendered in green, the FKBP like domain (salmon), and the C-terminal Hsp90 binding TPR domain (blue).

Structurally, in addition to the Hsp90 binding C-terminal TPR domain, both FKBP51 and FKBP52 poses peptidylprolyl isomerase (PPIase) activity in their N-terminal FK1 domain, which also binds the immunosupressent drug FK506 (Figure 1). Both proteins also contain a second, less understood FK2 domain that is structurally similar to FK1, but does not possess PPIase activity or FK506 binding. FKBP51 preferentially gets incorporated into the ligand free matured receptor complex and hormone binding is then accompanied by a switch between FKBP51 and FKBP52 (Davies et al., 2002) (Figure 2). FKBP52 preferentially gets incorporated into the ligand bound chaperone complex, binding with a stoichiometry of one FKBP52 per Hsp90 complex (Silverstein et al., 1999). FKBP52 then carries out an crucial role in the translocation of the chaperone bound receptor complex to the nucleus (Galigniana et al., 2001; Wochnik et al., 2005).

In the active retrograde translocation process, FKBP52 coordinates the association of the receptor chaperone complex to microtubules (Czar et al., 1994), by forming a direct contact between dynein and the KF1 PPIase domain (Galigniana et al., 2002; Silverstein et al., 1999). FKBP52's actions are coordinated with Hsp90, with active translocation requiring Hsp90 since is inhibited by the specific Hsp90 inhibitor geldanacycin (Czar et al., 1997). Pulled down experiments by the Pratt lab indicate that the FK2 domain directly binds GR, with the interaction mostly with the LBD and some contribution from the hinge region (Silverstein et al., 1999). The direct contact between FKBP52 and the steroid receptor provides a physical basis for the specificity of the FKBP's actions to a very select subset of Hsp90 clients.

For GR, FKBP52 has a unique ability to enhance GR ligand affinity. This was demonstrated using the *in vivo* yeast reporter assay. Since yeast does not possess FKBP51 or FKBP52 homologues, their affects were determined by co-expression of FKBP51 and FKBP52 alone and in combination. Co-expression of FKBP51 alone essentially had no effect, but co-expression of FKBP52 displayed up to 10-fold enhancement in GR transactivation. Intriguingly, dual expression of both FKBP51 and FKBP52 revert to the basal levels of GR signaling, indicating that FKBP51 acts to outcompete FKBP52, and inhibit the FKBP52 potentiation. The transcription activation enhancement correlated with an enhanced ligand affinity *in vivo*, indicating that the potentiation by FKBP52 is at least in part due to enhanced ligand binding. Further investigation determined that the functional difference between FKBP51 and FKBP52 resides in the FK1 domains, however the IPPase function is not required (Riggs et al., 2007). The enhancement in ligand binding was found to be specific to the GRLBD with no enhancement occurring with AR, PR or ER LBD's (Riggs

et al., 2003). The ability of FKBP51 to negate FKBP52's enhancement in ligand binding provides an explanation for the cortisol resistance found in new world primates that constitutive expression high levels of FKBP51 (Denny et al., 2000; Reynolds et al., 1999).

Given the potent potentiation effect of FKBP52 specific to GR signaling, it was somewhat surprising that the biological phenotypes from knock out mice have striking reproductive phenotypes that are instead attributed to PR and AR function. Female FKBP52 knockout mice are sterile (Tranguch et al., 2005), originating from defects with PR-A signaling. The loss of FKBP52 did not disrupt Hsp90 interaction nor hormone binding function (Yang et al., 2006). Male FKBP52 knock out mice display the equivalent phenotype as partial androgen insensitivity, and similar to the female knockout mice with PR, there was no effect on AR hormone binding or on nuclear translocation (Yong et al., 2007). Together, this indicates that FKBP52's primary role in steroid receptor regulation occurs down stream of hormone binding and that the regulation of GR ligand binding is secondary and specific to GR. While the exact mechanism of FKBP51/FKBP52's actions in steroid signaling regulation is still unclear, they have gained increasing interested due to their pharmacological potential for endocrine related diseases that includes breast cancer, prostate cancer and stress related psychological disorders. In this case, targeting FKBP52/FKBP51 is a more specific way of modulating Hsp90 steroid hormone interactions without disrupting Hsp90's interaction with other critical Hsp90 clients. For this, structural information regarding the Hsp90 and FKBP52 interaction would be highly valuable.

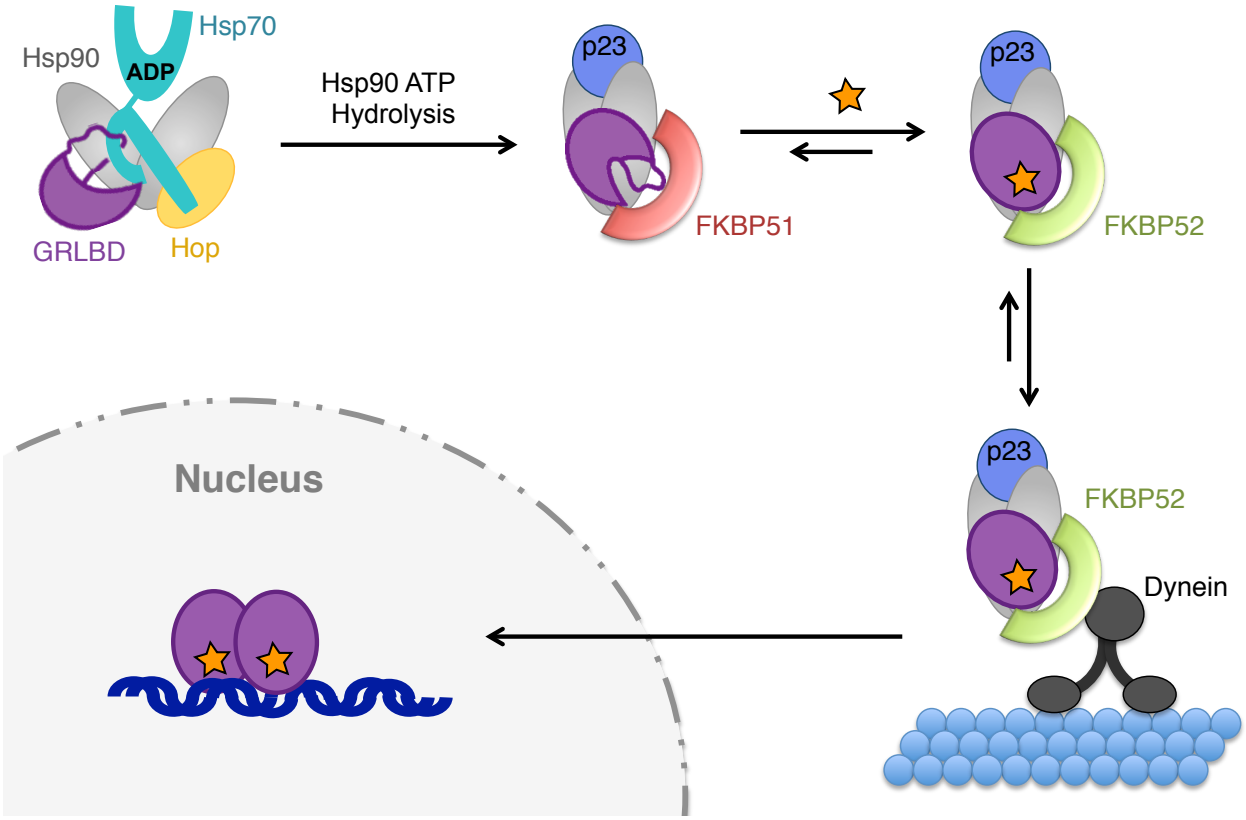

Figure 2. Model for actions of FKBP51 and FKBP52 in steroid hormone signaling. FKBP51 preferentially associates with mature apo GR complex with Hsp90 and p23. Hormone binding to GR results in a switching of the two immunophilins, with FKBP52 preferentially binding to the ligand bound complex. By mediating the interaction with dynein, FKBP52 promotes the retrotranslocation of the Hsp90 and ligand bound GR complex to the nucleus.

Preliminary EM map of Hsp90-FKBP52 in a compact complex by Dr. Southworth

The Hsp90:FKBP52 complex with engineered disulfide crosslinks between FKBP52's TPR domain and Hsp90's MEEVD motif was preassembled and purified by SEC-MALS. The light scattering measured a mass of 300kDa for the complex formed, indicating 2 FKBP52s bound per Hsp90 dimer (Figure 3A). By negative stain EM, addition of AMPPNP was found to stabilize a compact complex (Figure 3B). This was supported by a negative stain reconstruction of the AMPPNP stabilized complex which produced a compact

structure that clearly fit the closed state of Hsp90 with extra density extending along the length of the Hsp90 dimer from the CTD all the way to the NTD (Figure 3C). The highly coordinated nature of this compact complex suggested that this complex might be readily crystallized. My objective was to attempt to obtain a high resolution crystal structure of the FKBP52:Hsp90 complex.

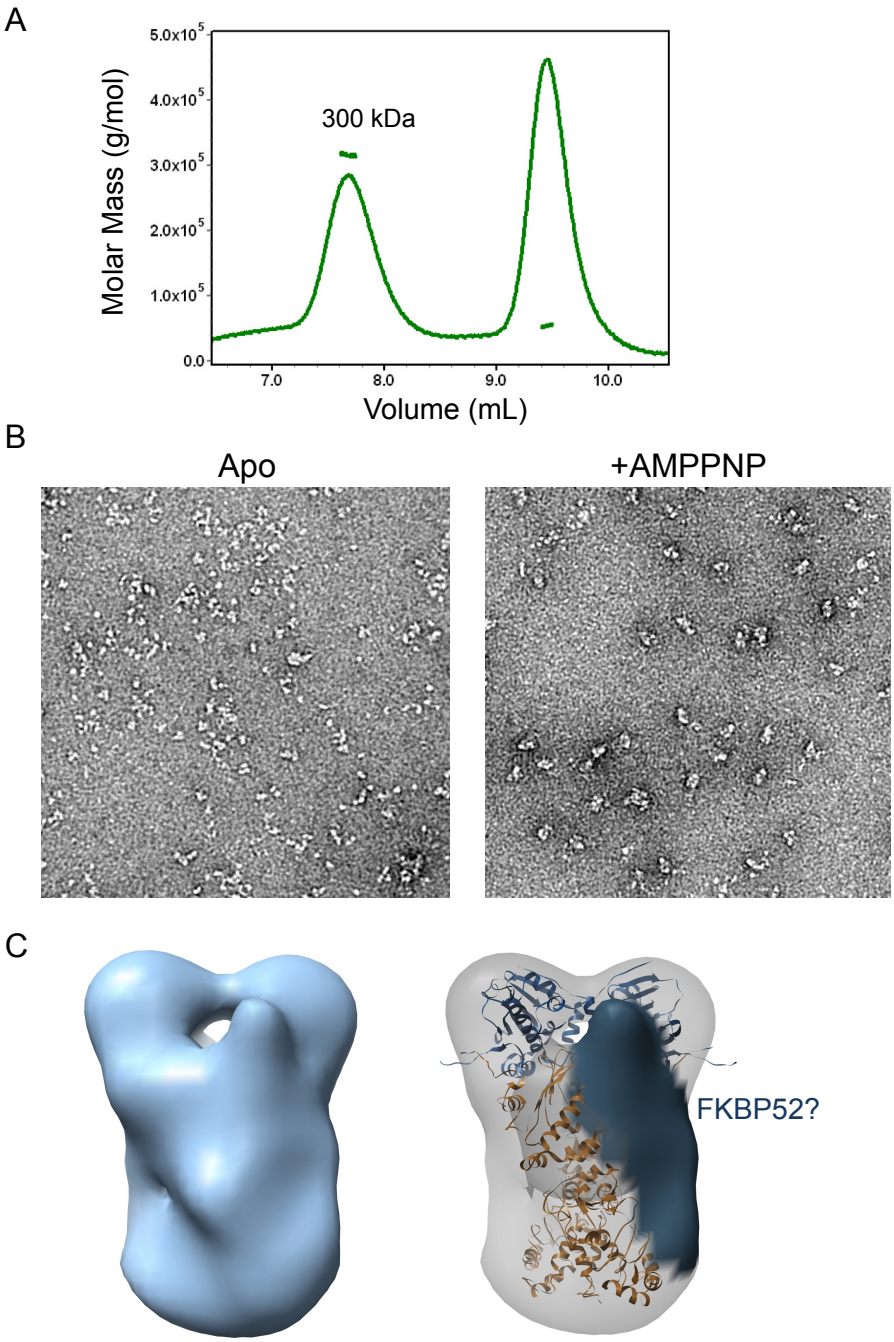

Figure 3. Preliminary EM reconstruction indicates FKBP52 stabilizes a compact state of Hsp90.
A) SEC-MALS of disulfide cross-linked Hsp90:FKBP52 complex. The mass of about 300kDa indicates a stoichiometry of two FKBP52s bound to an Hsp90 dimer.
B) Negative stain EM images of purified disulfide cross-linked Hsp90:FKBP52 complex without nucleotide (left) and with AMPPNP (right).
C) Negative statin EM reconstruction of Hsp90:FKBP52 complex (left). EM density with Hsp90 closed state crystal structure docked into density (right).
Data and figures provided by Daniel Southworth.

Results

FKBP52 forms stable asymmetric complex with Hsp90

The FKBP52 bound Hsp90 complex could be formed and purified without the aid of disulfide crosslinks (Figure 4). The complex was very stable, however, like Hop, without the disulfide cross-links, by SEC-MALS only one FKBP52 was found to bind per Hsp90 dimer (Figure 4C). Large-scale purification of the complex (Figure 4A) was then extensively screened in crystal trials, both with and without AMPPNP (see Experimental Procedures). While there were a few potential hits, none could be reproduced suggesting that the hits from the mosquito screen were either false hits or failed to scale up in larger crystal trays.

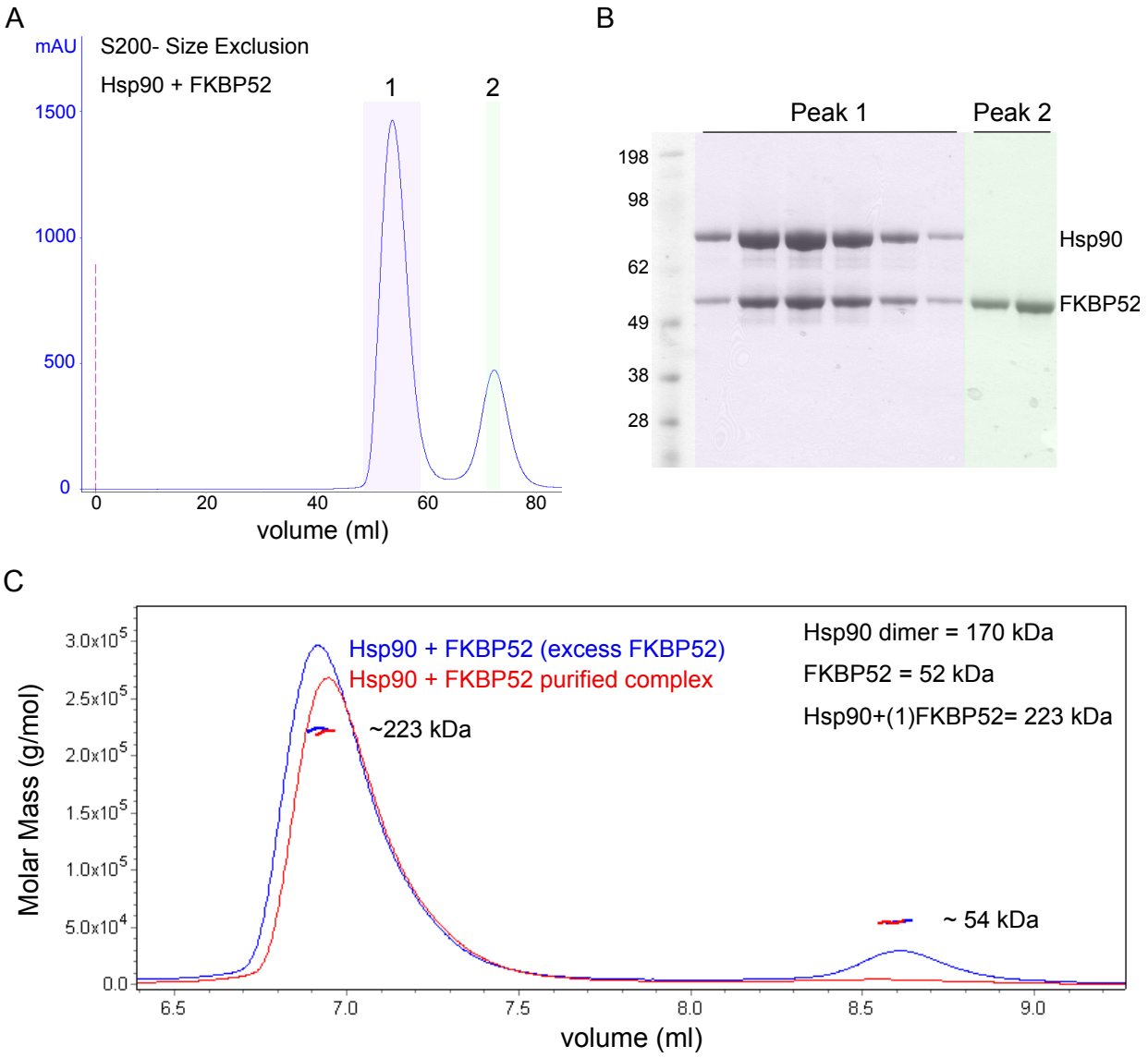

Figure 4. Purification of a stable asymmetric Hsp90 and FKBP52 complex.
A) Gel filtration of Hsp90 incubated with FKBP52 run on an S200 16/60 size exclusion column. Injected was 2.5 mL of 44µM Hsp90 (monomer) with 88µM FKBP52 incubated overnight at 4°C in 20mM Tris 7.5, 50mM KCl, 1mM DTT, and 10% glycerol. (Exp247)
B) SDS-PAGE gel of fraction from indicated peaks in (A) according to color code.
C) The Hsp90:FKBP52 complex is very stable and resistant to dissociation on gel filtration as shown by SEC-MALS of purified Hsp90:FKBP52 complex in Figure 2 (red) compared to a complex before the size exclusion column as in (A) (blue). (Exp248)

FKBP52 bound Hsp90 is extended

Given how unsuccessful the crystallization trials of the purified complex was, biophysical characterization of the complex was carried out to obtain a better understanding for the nature of the wild type complex. The purified complex was analyzed by SAXS (Figure 5). Addition of FKBP52 indeed led to the formation of a larger Hsp90 complex with a shift in the interatomic probability distribution to longer distances. Surprisingly, unlike with the negative stain EM, there was no significant detectable difference upon the addition of AMPPNP. Furthermore, an *ab initio* reconstruction using DAMMIN (Svergun, 1999) suggested that the complex is extended with Hsp90 very much in the open conformation (Figure 5B). In the open state, Hsp90 is generally flexible, resulting from variable orientations of the MD in respect to the CTD (Shiau et al., 2006). Without FKBP52 stabilizing a defined conformation of Hsp90, the flexibility of Hps90 in the extended state would greatly hindering crystallization of the complex and could be the reason for the lack of success in the crystal trials.

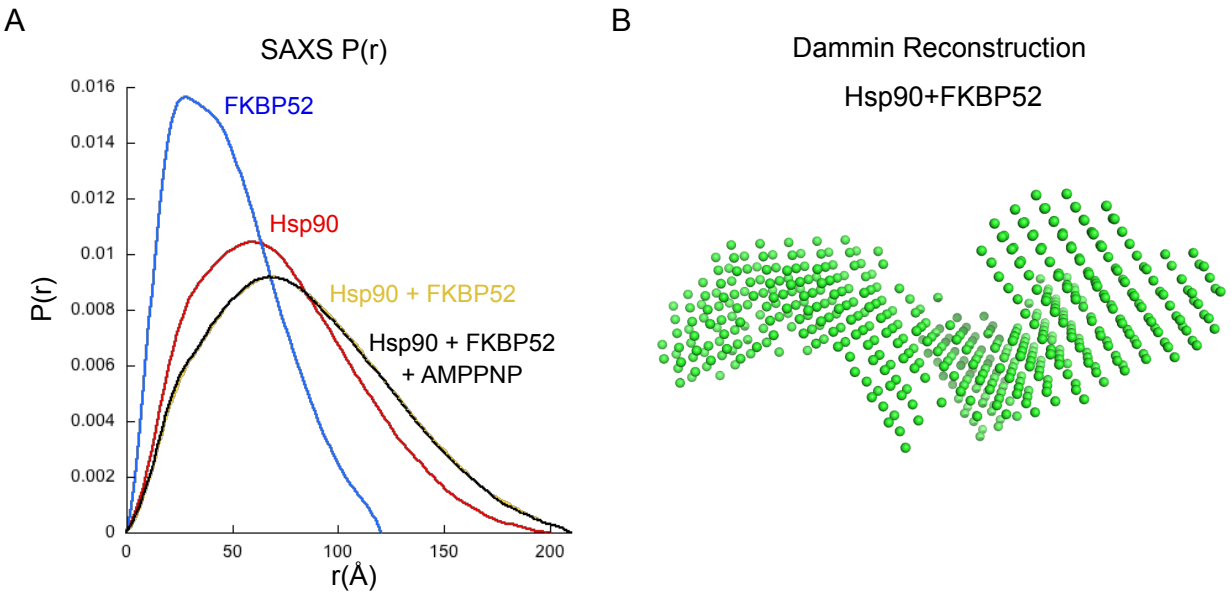

Figure 5. Hsp90 and FKBP52 form an extended complex.
A) Hsp90:FKBP52 complex does not undergo a significant conformation change with nucleotide as shown by the SAXS distance probability distributions for the Hsp90:FKPB52 complex in the absence of nucleotide (yellow) and with AMMPPNP (black) compared to Hsp90 alone (red) and FKBP52 alone (blue). (Exp258)
B) DAMMIN reconstruction of Hsp90:FKBP52 complex suggesting Hsp90 is in an extended conformation.

FKBP52 forms a distinct complex with Hsp90 that is not compatible with Hop

The extended conformation seen even with AMPPNP suggests FKBP52 might prefer interacting with an open state of Hsp90. In support of this, around the time of this investigation, the Buchner lab published a study indicating that Hop forms a complex with Hsp90 that is compatible with the binding of FKBP51 (Li et al., 2010). To determine if this was also true for FKBP52, the compatibility between Hop and FKBP52 binding to Hsp90 was investigated by analyzing preformed complexes by SEC-MALS. In contrast, to the previous results with FKBP51, I found that Hop is not compatible with FKBP52 (Figure 6). Addition of FKBP52 to Hsp90 and Hop, has essentially the same gel filtration profile for the

complex of Hsp90 and Hop alone, with the mass of the Hsp90 containing peak very close to that of the expected weight of the $Hsp90_2$:Hop_1 complex (Figure 6A). SDS-PAGE of the Hsp90 containing peak indicate that there is some FKBP52 incorporation but it is predominately just Hop. This indicates that under apo conditions Hsp90 preferential forms a complex with one Hop, which occludes the binding of either a second Hop or FKBP52.

In line with the SAXS results, AMPPNP had no effect on the interaction of FKBP52 with Hsp90. Addition of AMPPNP to the assembly reaction resulted in no significant difference (Figure 6B). Interestingly, comparing the gel filtration profiles of the FKBP52:Hsp90 complex to that of the Hop:Hsp90 complex, the Hop:Hsp90 complex elutes later, indicating that it is more compact than the FKBP52:Hsp90 complex. This aligns with the previous cryo-EM reconstruction of the Hsp90:Hop complex in which Hop stabilized a more compact open state of Hsp90. Furthermore, the fact that the FKBP52:Hsp90 complex appears more extended by gel filtration is supported by the extended structure observed in the DAMMIN reconstruction.

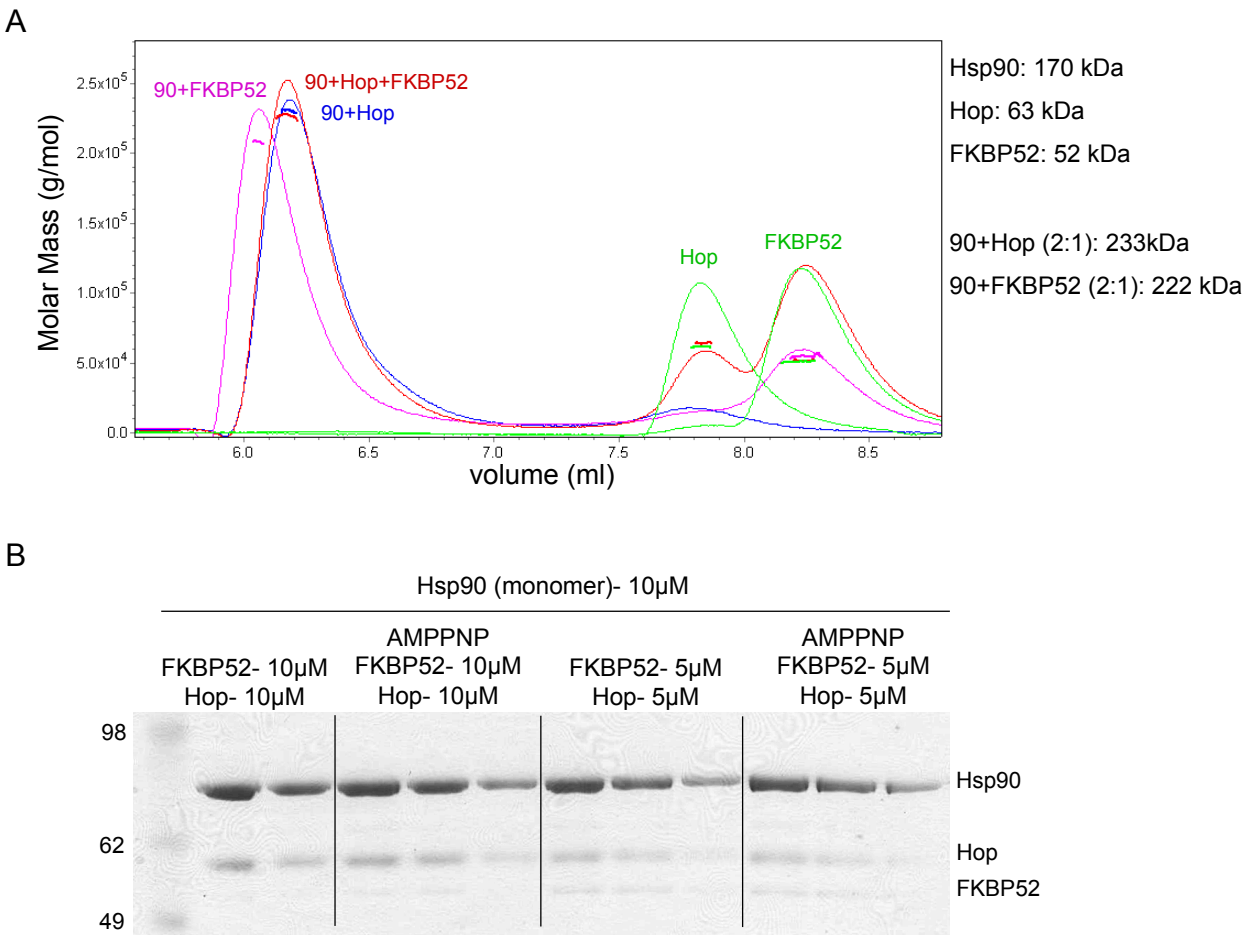

Figure 6. Hop out competes FKBP52 to form a more compact complex.
A) SEC-MALS of Hsp90 with 10μM Hop (blue), FKBP52 (magenta), and both (red) compared with Hop and FKBP52 alone (green). All proteins run at 10μM monomer concentration. (Exp390)
B) SDS-PAGE of Hsp90 containing peaks as in (A), with indicated amounts of FKBP52 and Hop, with and without AMPPNP.

Discussion

The extended state of Hsp90 observed with the wild type Hsp90:FKBP52 complex seems non-biological given the evidence that FKBP52 and FKBP51 get incorporated with the mature steroid hormone complexes associated with the p23. However the stoichiometry of one FKBP52 per Hsp90 dimer while in the extended state indicates that

the binding of the first somehow hinders binding of the second, suggesting more extensive contacts are being made between FKBP52 and an Hsp90, even in an extended state, and excludes the possibility that FKBP52 is simply bound to the MEEVD tail on Hsp90. At this point, the nature of these contacts and their biological significance is still very unclear.

Since the closed complex was observed upon AMPPNP addition in the preliminary negative stain EM experiment, it was surprising that I was unable to detect a difference in the SAXS profiles with AMPPNP. However, it should be noted that at some point during his investigation, Daniel Southworth was unable to reproduce the closure of the complex, indicating that some yet unidentified component or condition was promoting the closed state in the preliminary experiments. Given the biological evidence that FKBP52 should prefer the closed state, it seems logical that FKBP52 would be able to shift Hsp90's equilibrium towards the closed state. One possibility to consider for future investigations is that AMPPNP may not be a good nucleotide analogue for the FKBP52 closed state, and it might be worth trying to form the complex with the E47A Hsp90 mutant with ATP. This might better stabilize the ATP bound closed state and would also be beneficial since inclusion of ATP in the SEC running buffers is not cost prohibited, as is AMPPNP. Also, FKBP52 combined with p23 may synergistically stabilize a closed state of Hsp90 that might be more stable for structural investigations.

At the functional level, Riggs and co-workers provided compelling evidence that FKBP52 enhance GRLBD ligand affinity (Riggs et al., 2003). However, the caveat to the *in vivo* work is that FKBP51 and FKBP52 are likely disrupting interactions with other endogenous TPR containing cochaperones such as Cpr6 and Cpr7, complicating the interpretation of the results. The enhanced ligand affinity induced by FKBP52 could be

directly validate in the *in vitro* ligand binding assay that is now developed with the reconstituted system. Preliminary ligand binding experiments were attempted but did not reveal a noticeable difference with either FKBP51 or FKBP52. However, these experiments were not preformed under the correct concentration regimes where enhancement in ligand affinity would have been most apparent. To investigate this correctly would require the determination of GLRBD ligand K_D with the chaperone system additionally with FKBP52 as was performed in Chapter 3, Figure 12. Given the biological implications, this would be worth doing.

Experimental Procedures

Assembly and Purification of Hsp90:FKBP52 Complex

For the large scale purification of the Hsp90:FKBP52 complex for crystallography, Hsp90 and FKBP52 were mixed at high concentrations with excess FKBP52 (44μM Hsp90 and 88μM FKBP52). The assembly reaction was dialyzed overnight against 20mM Tris pH 7.5, 50mM KCl, 1mM DTT, and 10% glycerol. The complex was purified by SEC on Superdex S200 16/60 (GE Healthcare) column equilibrated with 20mM Tris pH 7.5, 50mM KCl, 1mM DTT, and 10% glycerol.

SEC-MALS

SEC-MALS was carried out as described in Chapter 2.

SAXS Data Collection and Analysis

SAXS data collection and analysis were carried out as described in Chapter 2.

Crystallization Trials

The purified Hsp90:FKBP52 complex was screened at 16 and 19mg/mL with and without 5mM AMPPNP/$MgCl_2$. The following QIAGEN screens were setup using the mosquito: ComPAS Suite, CLASSICS Suite, CLASSICS II Suite, JCSG+ Suite, PACT Suite, and MPD suite. 100nL of the protein at indicated concentration was mixed 1:1 with the mother liquor and trays stored at room temperature. The complex was also screened at 9.5 and 16mg/ml with trays stored at 4°C. Exp249, 341, and 344

References

Cheung-Flynn, J., Prapapanich, V., Cox, M.B., Riggs, D.L., Suarez-Quian, C., and Smith, D.F. (2005). Physiological role for the cochaperone FKBP52 in androgen receptor signaling. Mol. Endocrinol. *19*, 1654–1666.

Czar, M.J., Galigniana, M.D., Silverstein, A.M., and Pratt, W.B. (1997). Geldanamycin, a heat shock protein 90-binding benzoquinone ansamycin, inhibits steroid-dependent translocation of the glucocorticoid receptor from the cytoplasm to the nucleus. Biochemistry *36*, 7776–7785.

Czar, M.J., Owens-Grillo, J.K., Yem, A.W., Leach, K.L., Deibel, M.R., Welsh, M.J., and Pratt, W.B. (1994). The hsp56 immunophilin component of untransformed steroid receptor complexes is localized both to microtubules in the cytoplasm and to the same nonrandom regions within the nucleus as the steroid receptor. Mol. Endocrinol. *8*, 1731–1741.

Davies, T.H., Ning, Y.-M., and Sánchez, E.R. (2002). A new first step in activation of steroid receptors: hormone-induced switching of FKBP51 and FKBP52 immunophilins. J. Biol. Chem. *277*, 4597–4600.

Denny, W.B., Valentine, D.L., Reynolds, P.D., Smith, D.F., and Scammell, J.G. (2000). Squirrel monkey immunophilin FKBP51 is a potent inhibitor of glucocorticoid receptor binding. Endocrinology *141*, 4107–4113.

Galigniana, M.D., Radanyi, C., Renoir, J.M., Housley, P.R., and Pratt, W.B. (2001). Evidence that the peptidylprolyl isomerase domain of the hsp90-binding immunophilin FKBP52 is involved in both dynein interaction and glucocorticoid receptor movement to the nucleus. J.

Biol. Chem. *276*, 14884–14889.

Galigniana, M.D., Harrell, J.M., Murphy, P.J.M., Chinkers, M., Radanyi, C., Renoir, J.-M., Zhang, M., and Pratt, W.B. (2002). Binding of hsp90-associated immunophilins to cytoplasmic dynein: direct binding and in vivo evidence that the peptidylprolyl isomerase domain is a dynein interaction domain. Biochemistry *41*, 13602–13610.

Li, J., Richter, K., and Buchner, J. (2010). Mixed Hsp90–cochaperone complexes are important for the progression of the reaction cycle. Nat. Struct. Mol. Biol. *18*, 61–66.

Reynolds, P.D., Ruan, Y., Smith, D.F., and Scammell, J.G. (1999). Glucocorticoid resistance in the squirrel monkey is associated with overexpression of the immunophilin FKBP51. J. Clin. Endocrinol. Metab. *84*, 663–669.

Riggs, D.L., Cox, M.B., Tardif, H.L., Hessling, M., Buchner, J., and Smith, D.F. (2007). Noncatalytic Role of the FKBP52 Peptidyl-Prolyl Isomerase Domain in the Regulation of Steroid Hormone Signaling. … And Cellular Biology.

Riggs, D.L., Roberts, P.J., Chirillo, S.C., Cheung-Flynn, J., Prapapanich, V., Ratajczak, T., Gaber, R., Picard, D., and Smith, D.F. (2003). The Hsp90-binding peptidylprolyl isomerase FKBP52 potentiates glucocorticoid signaling in vivo. Embo J. *22*, 1158–1167.

Sanchez, E.R. (1990). Hsp56: a novel heat shock protein associated with untransformed steroid receptor complexes. J. Biol. Chem. *265*, 22067–22070.

Shiau, A.K., Harris, S.F., Southworth, D.R., and Agard, D.A. (2006). Structural Analysis of E. coli hsp90 Reveals Dramatic Nucleotide-Dependent Conformational Rearrangements. Cell *127*, 329–340.

Silverstein, A.M., Galigniana, M.D., Kanelakis, K.C., Radanyi, C., Renoir, J.M., and Pratt, W.B. (1999). Different regions of the immunophilin FKBP52 determine its association with the glucocorticoid receptor, hsp90, and cytoplasmic dynein. J. Biol. Chem. *274*, 36980–36986.

Smith, D.F., Faber, L.E., and Toft, D.O. (1990). Purification of unactivated progesterone receptor and identification of novel receptor-associated proteins. J. Biol. Chem. *265*, 3996–4003.

Storer, C.L., Dickey, C.A., Galigniana, M.D., Rein, T., and Cox, M.B. (2011). FKBP51 and FKBP52 in signaling and disease. Trends in Endocrinology & Metabolism *22*, 481–490.

Svergun, D.I. (1999). Restoring low resolution structure of biological macromolecules from solution scattering using simulated annealing. Biophys. J. *76*, 2879–2886.

Tranguch, S., Cheung-Flynn, J., Daikoku, T., Prapapanich, V., Cox, M.B., Xie, H., Wang, H., Das, S.K., Smith, D.F., and Dey, S.K. (2005). Cochaperone immunophilin FKBP52 is critical to uterine receptivity for embryo implantation. Proc. Natl. Acad. Sci. U.S.a. *102*, 14326–14331.

Wochnik, G.M., Rüegg, J., Abel, G.A., Schmidt, U., Holsboer, F., and Rein, T. (2005). FK506-binding proteins 51 and 52 differentially regulate dynein interaction and nuclear translocation of the glucocorticoid receptor in mammalian cells. J. Biol. Chem. *280*, 4609–4616.

Yang, Z., Wolf, I.M., Chen, H., Periyasamy, S., Chen, Z., Yong, W., Shi, S., Zhao, W., Xu, J., Srivastava, A., et al. (2006). FK506-binding protein 52 is essential to uterine reproductive physiology controlled by the progesterone receptor A isoform. Mol. Endocrinol. *20*, 2682–2694.

Yong, W., Yang, Z., Periyasamy, S., Chen, H., Yucel, S., Li, W., Lin, L.Y., Wolf, I.M., Cohn, M.J., Baskin, L.S., et al. (2007). Essential Role for Co-chaperone Fkbp52 but Not Fkbp51 in Androgen Receptor-mediated Signaling and Physiology. Journal of Biological Chemistry *282*, 5026–5036.

Yoshida, N.L., Miyashita, T., U, M., Yamada, M., Reed, J.C., Sugita, Y., and Oshida, T. (2002). Analysis of gene expression patterns during glucocorticoid-induced apoptosis using oligonucleotide arrays. Biochem. Biophys. Res. Commun. *293*, 1254–1261.

Chapter 7

Investigation of the Smyd2 Methylase as a Potential Hsp90 Cochaperone

Preface

This side project was a collaboration initiated by Laura Donlin in the Tarakhovsky lab. Laura's objective was to find a cytoplasmic methylase and characterize a lysine methylation dependent protein network in the cytoplasm. Her screen identified the lysine methylase Smyd2 as being localized predominantly to the cytoplasm. Hsp90 was then identified as the most abundant Smyd2-methylated protein, with mono-methylation occurring on lysine 616, located on Hsp90's CTD amphipathic helix. This methylation was found to be specifically due to Smyd2, as none of the other four closely related methylases, Smyd1, 3, 4 or 5, were able to methylate K616, nor was methylation detected upon Smyd2 shRNA knockdown. Further details about the identification of Smyd2 and K616 methylation of Hsp90 can be found in the paper that was later published by Laura (Donlin et al., 2012). At the time, very little was known about Smyd2, or its close family members. Laura reached out to the Agard lab for help characterizing the effect the K616 methylation as a potential mechanism for modulating Hsp90 function at a molecular level.

This project was of particular interest to me because Laura's early preliminary results suggested that Smyd2 is involved in the steroid hormone receptor pathway. Based on co-immunoprecipitation with Smyd2, GR and MR bound to Smyd2 but not the kinases protein kinase B (Akt) or glycogen synthase kinase 3 (Gsk) (Figure 1A). Furthermore,

Smyd2 association with MR and GR depends on Smyd2 methylation activity, as shown by the loss of MR and GR association with the enzyme dead (ED) Smyd2 (Figure 1B). In contrast, Hsp90 was still bound to the methylase dead Smyd2 along with p23 (Figure 1B). However, Laura discontinued investigating Smyd2's interaction with the steroid hormone receptors after tissue specific expression of Smyd2 and Hsp90 K616 methylation revealed that, with the exception of low levels of expression in heart and lung, Smyd2 is almost exclusively expressed in skeletal muscles. In line with this, K616 methylated Hsp90 was only detected in the skeletal muscles and heart (Donlin et al., 2012). In light of this, Laura focused her efforts on muscle cell specific biology. This led her to discover that Smyd2 and Hsp90 form a complex with titan and together promote titin stability and proper muscle function, with this function dependent on the specific methylation of Hsp90 K616 (Donlin et al., 2012).

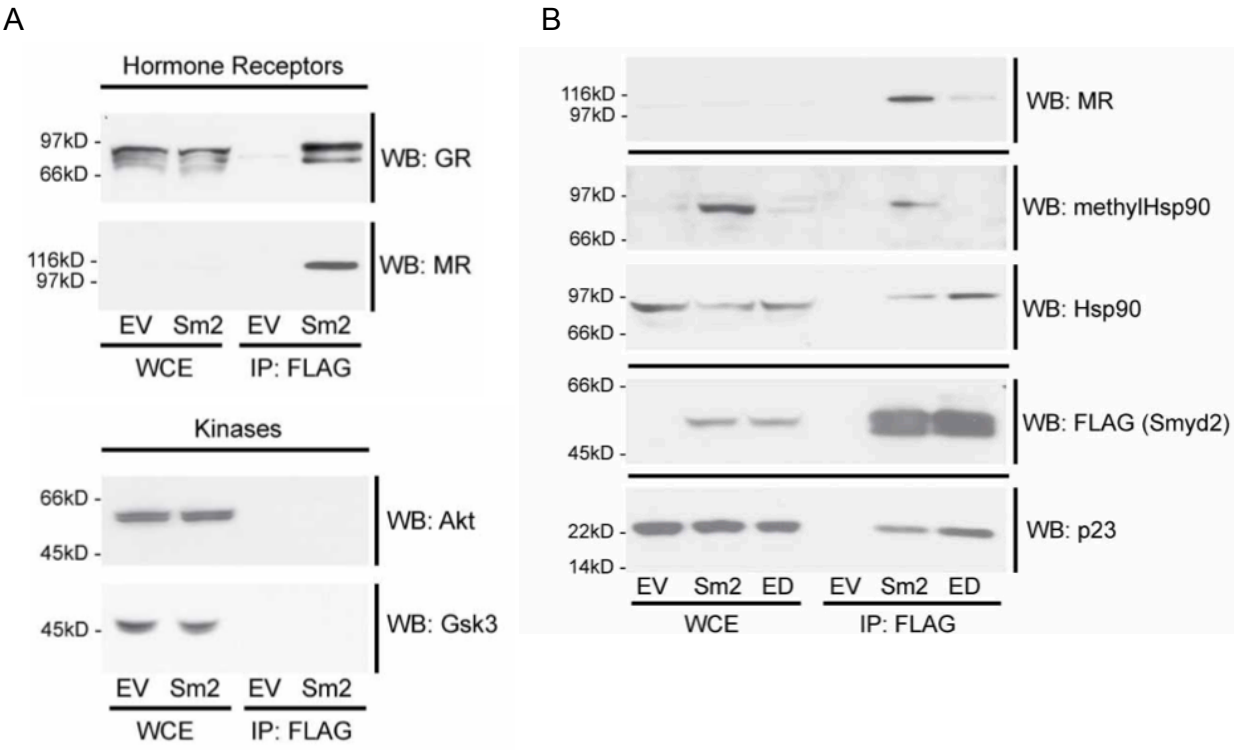

Figure 1. Smyd2 association with GR and MR depends on methylation activity.
A) West blot (WB) analysis for representative members of two Hsp90 client families, hormone receptors and kinases, in FLAG-tagged-Smyd2 (Sm2) protein purification in HEK 293 cells. WCE, whole cell extracts. IP, immunoprecipitation. Akt, or protein kinase B (PKB). Gsk, glycogen synthase kinase 3.
B) Western blot analysis of proteins associated with FLAG-tagged-Smyd2 from HEK 293 cells expressing WT Smyd2 (Sm2), or enzymatic dead (ED) Smy2 or cells containing an empty vector (EV). These data are a representation of three (MR) and two (GR) independent experiments assaying for Smyd2 association. Unpublished results provided by Laura Donlin while in the Tarakhovsky lab.

Summary

Hsp90 K616 methylation by Smyd2 can be reconstituted *in vitro* with purified components. While SAXS could not detect a significant conformational change in Hsp90 after Smyd2 methylation, preliminary biochemical experiments suggest Smyd2 methylation inhibits ATP hydrolysis on human Hsp90α, although further validation is required. Association between Hsp90 and Smyd2 is very weak. Preliminary attempts at

stabilizing a complex through engineered cysteine crosslinks between Smyd2's TPR domain and Hsp90 MEEVD motif, as was done for Hop, were unsuccessful, and could be due to the unusual architecture of Smyd2's TPR domain. In screening for conditions that enhance Smdy2 association to Hsp90, it was found that Smyd2 binding is inhibited by p23, suggesting that Smyd2 preferentially interacts with an open conformation of Hsp90.

Introduction

While little was known about Smyd2 at the time of this work (2009 - early 2011), this introduction reflects the current state of the field and incorporates many significant advances that occurred in the recent years.

Smyd proteins are crucial for cardiac and skeletal muscle development and function

Smyd2 belongs to a family of five related lysine methyl transferases (Smyd1-5) that play critical roles in myofibril assembly of skeletal and cardiac muscle during development (Du et al., 2014). Smyd1, 2 and 3 are currently the best studied of the family, with more sparse information available on Smyd4 and Smyd5. Smyd proteins are verified as having histone methylation activity, but are also found to methylate nonhistone protein substrates. The Smyd proteins have very tissue specific expression profiles (Donlin et al., 2012; Hamamoto et al., 2004; Tan et al., 2006) and each possess unique substrate specificity (Abu-Farha et al., 2007; Brown et al., 2006; Hamamoto et al., 2004; Xu et al., 2011b).

Smyd1 is crucial in cardiac development (Gottlieb et al., 2002), and plays a key role in cardiac and skeletal muscle function (Li et al., 2013; Tan et al., 2006). As described

above, Smyd2 is also important for skeletal muscle stability, with lowered Smyd2 levels manifesting as severely impaired mobility in zebrafish (Donlin et al., 2012). The reduced Smyd2 expression in zebrafish also had a moderate impact on cardiac muscles (Donlin et al., 2012). However, in an independent mouse study, cardiomyocyte-specific deletion of Smyd2 revealed Smyd2 to be dispensable for cardiac development, suggesting a compensatory mechanism for Smyd2 in higher-vertebrate heart development (Diehl et al., 2010). In zebrafish, Smyd3 is required for both cardiac and skeletal muscle development (Fujii et al., 2011), and has been implicated in skeletal muscle atrophy in mammals (Proserpio et al., 2013).

Smyd2 and Smyd3's association with cancer progression

Interest in the Smyd proteins intensified when Smyd3 up regulation was discovered to be associated with several cancers that includes colorectal, hepatocellular and breast cancer, with Smyd3 expression levels correlating with rates of cancer cell growth (Hamamoto et al., 2004; 2006). A possible mechanism for Smyd3's link to breast cancer has been suggested by the fact the Smyd3 was found to directly bind ER LBD and potentiate ER signaling (Kim et al., 2009). This Smyd3 mediated enhancement in ER signaling correlated with Smyd3 recruitment with ER to the promoter and with H3-K4 methylation at the ER target genes.

Smyd2 is also an emerging cancer target. Two of Smyd2's nonhistone protein substrates, p53 and tetinoblastoma tumor suppressor (Rb), are tumor suppressor proteins that carry out important roles in gene transcription, apoptosis and cell cycle regulation. Rb's function is regulated by Smyd2 mono-mehtylation at lysine 860 (Saddic et al., 2010),

and Smyd2 methylation of p53 K370 impairs p53 DNA binding ability (Huang et al., 2006). Furthermore, there is a strong reverse correlation between Smyd2's overexpression in esophageal cell carcinoma and patient out come, with following cell line studies revealing a correlation between Smyd2 expression and tumor cell proliferation (Komatsu et al., 2009). Together, this highlights Smyd2 and Smyd3 as a promising prognostic markers and therapeutic targets.

Structural insight into Smyd autoinhibition and potential mechanism for Hsp90 activation

Currently, several crystal structures of Smdy1, 2 and 3 have been solved (Figure 2). The methylation activity resides entirely in catalytic SET domains (including the post-SET domain), which consist of an evolutionarily conserved catalytic motif that utilizes S-adenosylmethionine (SAM) as a donor substrate to add methyl groups to acceptor lysine residues. The Smyd family of proteins are distinguished from other classes of histone lysine methyltransferases (HKMT) by the insertion of a MYND domain into the catalytic SET domain, resulting in the split SET domain architecture (Figure 2A). While dispensable for methylation activity (Abu-Farha et al., 2007), the MYND domain contains a zinc finger motif that functions as a protein interaction domain that mediates interaction with proline-rich sequences (Liu et al., 2007), with Smyd2's MYND domain preferentially binding PXLXP motifs (Abu-Farha et al., 2007). Additionally, some data from Smyd3 suggest this region binds DNA (Hamamoto et al., 2004), with DNA binding up regulating HKMT activity (Xu et al., 2011a).

Smyd1-3 all contain a C-terminal TPR domain. For Smyd1 and Smyd3, the TPR domain has been shown to be auto-inhibitory for HKMT activity *in vitro* (Sirinupong et al., 2010; 2011). However, for Smyd1, deletion of the TPR domain abolishes its function *in vivo* (Just et al., 2011). Intriguingly, Hsp90 interacts with Smyd1, Smyd2 and Smyd3 through their TPR domains and has been shown to enhance HKMT activity (Abu-Farha et al., 2007; Hamamoto et al., 2004; Tan et al., 2006). For Smyd2, the enhancement in activity is substrate specific, with Hsp90 regulating both Smyd2's HKMT activity and specificity (Abu-Farha et al., 2007).

Insight gained from differences between the crystal structures of Smyd1 and Smyd3 have produced some theories as to the nature of the auto-inhibition and the Hsp90 activation. The TPR domain is located near the substrate binding site and forms a deep and narrow groove for the substrate (Figure 2B). Smyd1 crystalized in a more 'open' conformation (Figure 2C) compared to the 'closed' conformation seen in the Smyd3 crystal structure (Figure 2D). This conformation change results from a clamshell, hinge like motion of the TPR domain about its connection to the catalytic SET domains. In the 'closed' conformation of Smyd3, the TPR domain is rotated upward such that the TPR domain partially blocks the substrate binding site and thus was proposed to represent the auto-inhibited state, and that the Smyd1 'open' state captures a more active state stabilized by crystal packing (Sirinupong et al., 2011). Based on this observation, it has been proposed that the Hsp90 activation results from the release of the auto-inhibition, with Hsp90 binding to the TPR domain and removing the TPR domain from the substrate binding site.

Soon after, three independent studies released crystal structures of Smyd2 (Ferguson et al., 2011; Jiang et al., 2011; Xu et al., 2011b). Compared to Smyd1 and Smyd3,

Smyd2 is in an intermediate state that is slightly closer to the Smyd1 'open' state than the Smdy3 'closed' state. More specifically, for Smyd2, the TPR domain is rotated outward by ~16° degree with respect to Smyd3's TPR domain, this is compared to the ~23° degree outward rotation seen with Smyd1 (Xu et al., 2011b). There are several different crystal structure of Smyd2 with different cofactors and substrates bound (Ferguson et al., 2011; Jiang et al., 2011). While co-factors can affect more subtle conformation changes within the TPR domain (Jiang et al., 2011), generally, all are in the same 'intermediate' state. This suggests that the angle is not necessarily a result of crystal packing, but more likely determined by intrinsic property of the individual protein, with differences in the substrate binding sites formed with the TPR domain accounting for the divergence in substrate specificity (Xu et al., 2011b). Thus, the mechanism for the Hsp90 activation is still very unclear and more thoughts are provided in the discussion.

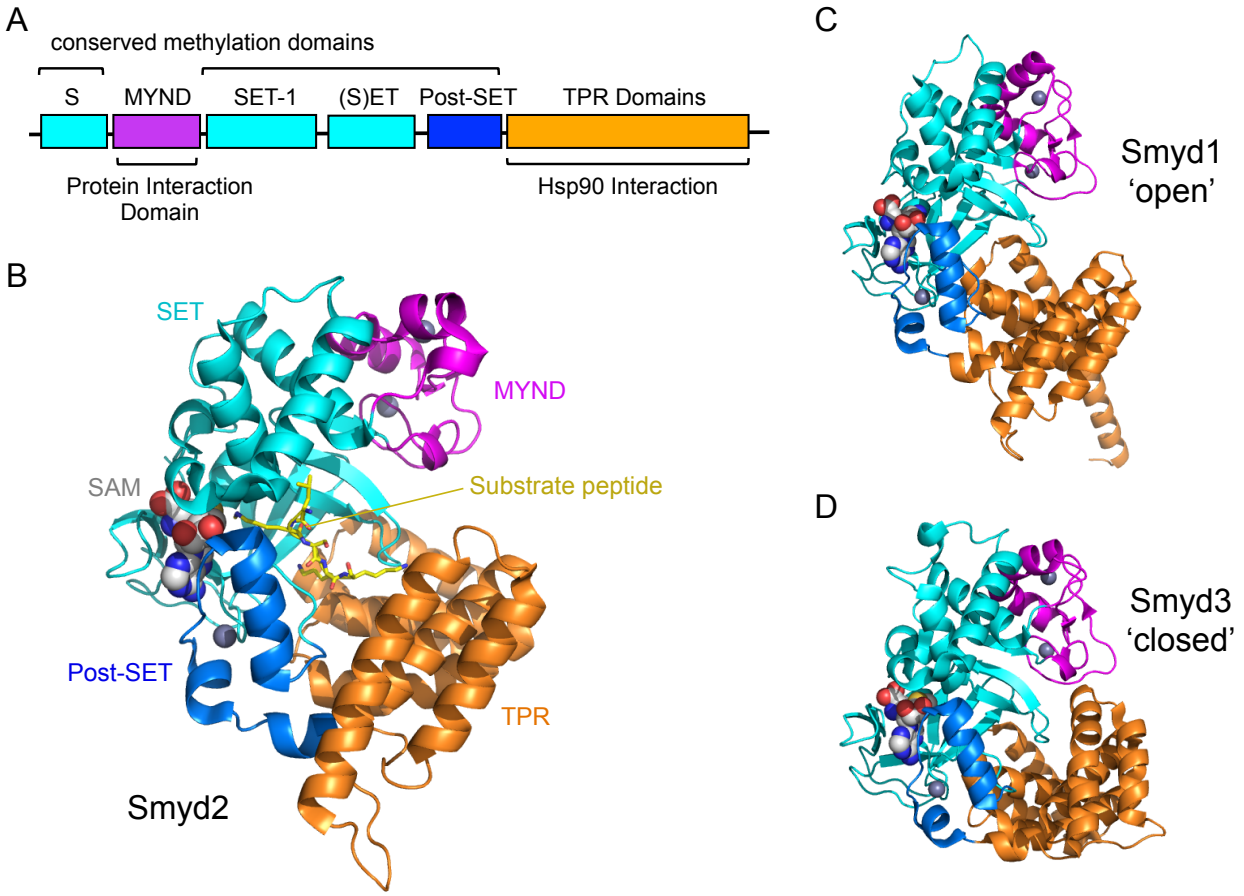

Figure 2. Domain architecture and structure of Smyd2.
A) Domain architecture of Smyd2 (Same for Smyd1 and Smyd3)
B) Crystal structure of Smyd2 bound to SAM and p53 substrate peptide (pdb 3S7D). Domains colored as indicated in (A). The electron density indicates that the methyl group from SAM has transferred to the substrate peptide.
C) Crystal structure of SAM bound Smyd1 (pdb 3N71) in a 'open' conformation in which the TPR domain (orange) is the most removed from the substrate binding site.
D) Crystal structure of SAM bound Smyd3 (pdb 3QWP) in a 'closed' conformation in which the TPR domain (orange) is rotated inward to partially occlude the substrate binding site.

Results

Smyd2 methylation of Hsp90 *in vitro*

Utilizing the Hsp90 K616 monomethylation specific antibody as a probe, I was able to show Smyd2 specific methylation of Hsp90 *in vitro* (Figure 3A). Surprisingly, the substrate S-adensylmethionine (SAM) was not required for Hsp90 methylation. However,

this was with stoichiometric levels of Hsp90 and Smyd2, indicating that Smyd2 likely purifies with SAM still bound. This was also found to be the case in another investigation involving Smyd2 (Ferguson et al., 2011). Importantly, methylation rates were shown to be dependent on Smyd2 concentration (Figure 3B), time (Figure 3C), and temperature (Figure 3B and C). Of notice was that Smyd2 methylation of Hsp90 is relatively slow. However, this aligns with later biochemical characterization of Smyd2, which determined that Smyd2's activity is very pH sensitive, with maximal activity achieved at pH 9.5 (Wu et al., 2011). This is consentient with the notion that lysine methyltransferase utilize the basicity of their active site to facilitate the deprotonation-methylation reaction (Zhang and Bruice, 2008). Under the conditions the reactions were carried out (pH 7.5), Smyd2 has approximately 20% of its maximal activity.

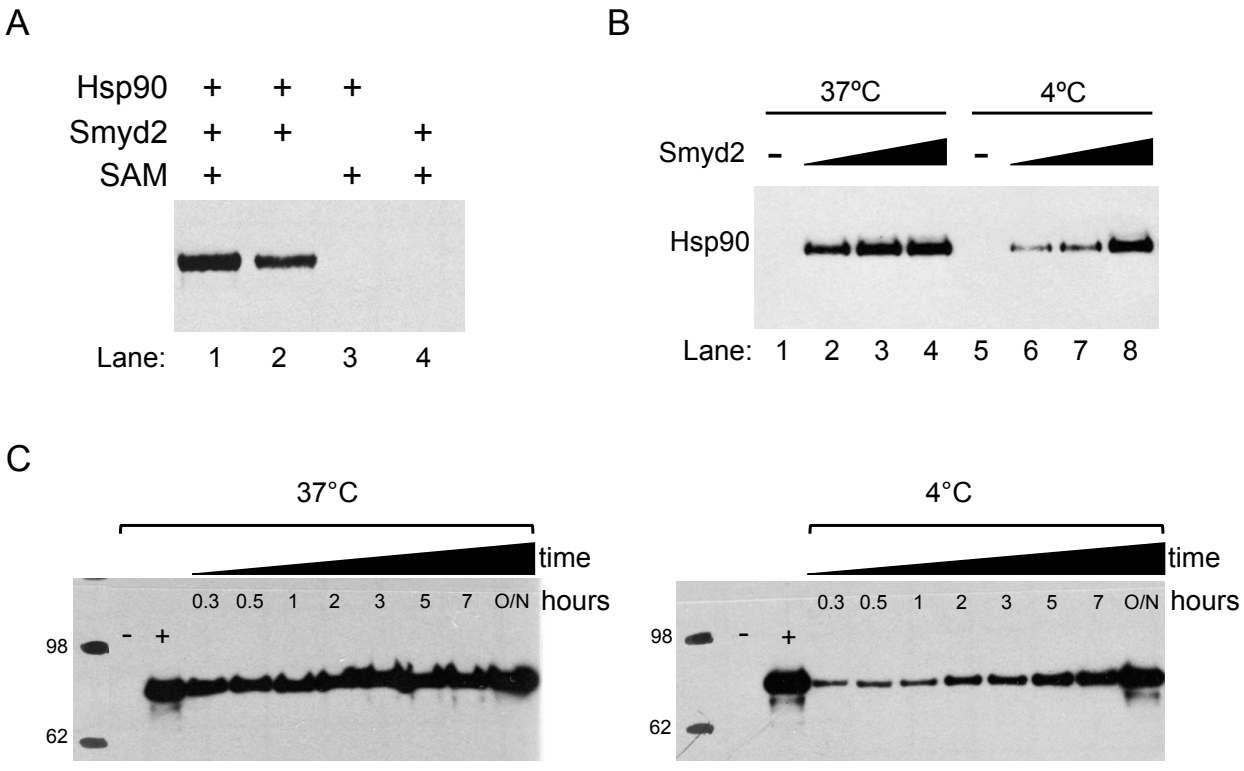

Figure 3. Smyd2 methylation of Hsp90 K616 *in vitro*.
A) Western blot measuring K616 methylation shows that Smyd2 dependent methylation (lanes 1 vs 3) at stoichiometric levels of Hsp90 and Smyd2 does not require SAM (lanes 1 vs 2), indicating that SAM co-purifies with Smyd2. (Exp236)
B) Western blot measuring K616 methylation of 5μM Hsp90 with 0 (lanes 1 and 5), 0.5 (lanes 2 and 6), 1μM (lanes 3 and 7) and 5μM (lanes 4 and 8) of Smyd2 at 37°C (lanes 1-4), and 4°C (lanes 5-6) overnight. (Exp214)
C) Western blot measuring K616 methylation shows rate of methylation at 37°C (left) and 4°C (right). Reactions carried out at 10μM Hsp90 and Smyd2. Control reactions were carried out at 37°C overnight either without Smyd2 (-) or with excess (50μM) Smyd2 (+). (Exp216)

Characterization of Smyd2 methylated Hsp90

The primary objective after establishing the Hsp90 K616 methylation *in vitro* was to determine the effect methylation has on Hsp90 function. Preliminary investigation of ATP hydrolysis rates of the entire methylation reactions with Smyd2 were problematic due to high background originating from Smyd2 (data not shown). To pursue the effects of just

the methylation on Hsp90, without complications of Smyd2, large-scale methylation reactions were carried and purified to remove Smyd2 (Figure 4). The initial attempt as separating Smyd2 from Hsp90 after the methylation reaction indicated that under low salt conditions (50mM KCl), sub-stoichiometric amounts of Smyd2 were detected in the second half of the Hsp90 peak. This indicates that Hsp90 and Smyd2 from a relatively weak complex, that partially dissociates during the gel filtration. Complete dissociation of Smyd2 was accomplished by rerunning the samples in high salt (500mM KCl), allowing for pure methylated Hsp90 to be obtained and transferred back into low salt conditions by dialysis (Figure 4B).

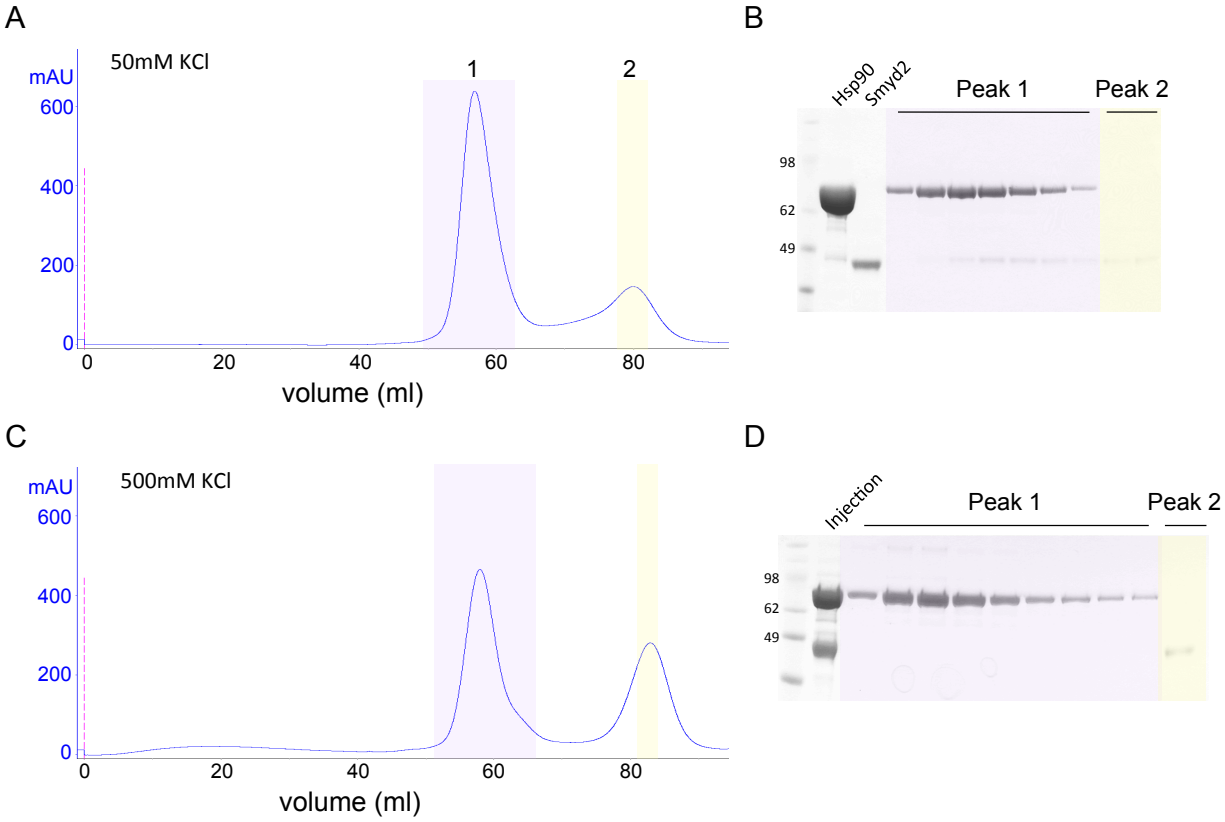

Figure 4. Large-scale purification of Smyd2 methylated Hsp90.
A) A 2mL Hsp90 methylation reactions was carried out with 31μM Hsp90α and 29μM Smyd2 overnight and was then purified on a S200 16/60 size exclusion buffer (left).

Elution fractions were then run on a coomassie stained SDS PAGE gel. Under the low salt (50mM KCl), Smyd2 was detected in the Hsp90 peak, indicating Hsp90-Smyd2 complex. B) Fractions from (A) were pooled and rerun over the S200 column in 500mM KCl (left), with the gel indicating clean separation of Smyd2 from Hspp90 (right). (Exp254)

Purified methylated Hsp90 was investigated for structural changes by SAXS, and functional changes reflected in the ATP hydrolysis rates. In both the absence and presence of AMPPNP, methylated and un-methylated Hsp90 were indistinguishable by SAXS (Figure 5A). However, there was a noticeable difference in the ATP hydrolysis rates, with the methylated Hsp90 having a significantly lower ATP hydrolysis rate than the unmethylated Hps90 (Figure 5B and D). This is in contrast with a separate report from another group that individual discovered Smyd2 methylation of Hsp90 (Abu-Farha et al., 2011). In this report, methylation was reported to have no effect on Hsp90's ATP hydrolysis rate, however their rates were not rigorously calculated using background subtraction with a specific Hsp90 inhibitor. Give the low ATP hydrolysis rate of human Hsp90 compared to the background; this is important factor for accurate determination of the hydrolysis rate. In light of this discrepancy and the challenges associated with accurately measuring human Hsp90's ATPase rate, this result should be validated using a more active Hsp90 homologue, or with the NTD chimera of Hsp90 containing the NTD of yeast and MD and CTD of human Hsp90 (see Appendix Section 4, Figure 3C). This mutant has the high ATPase activity of yeast, and contains the human CTD that can be methylated by Smyd2 and detected using the mono-methylation specific Hsp90 antibody (Figure 6). Investigations with this construct would provide better signal to noise and thus making any inhibition effect more readily detected.

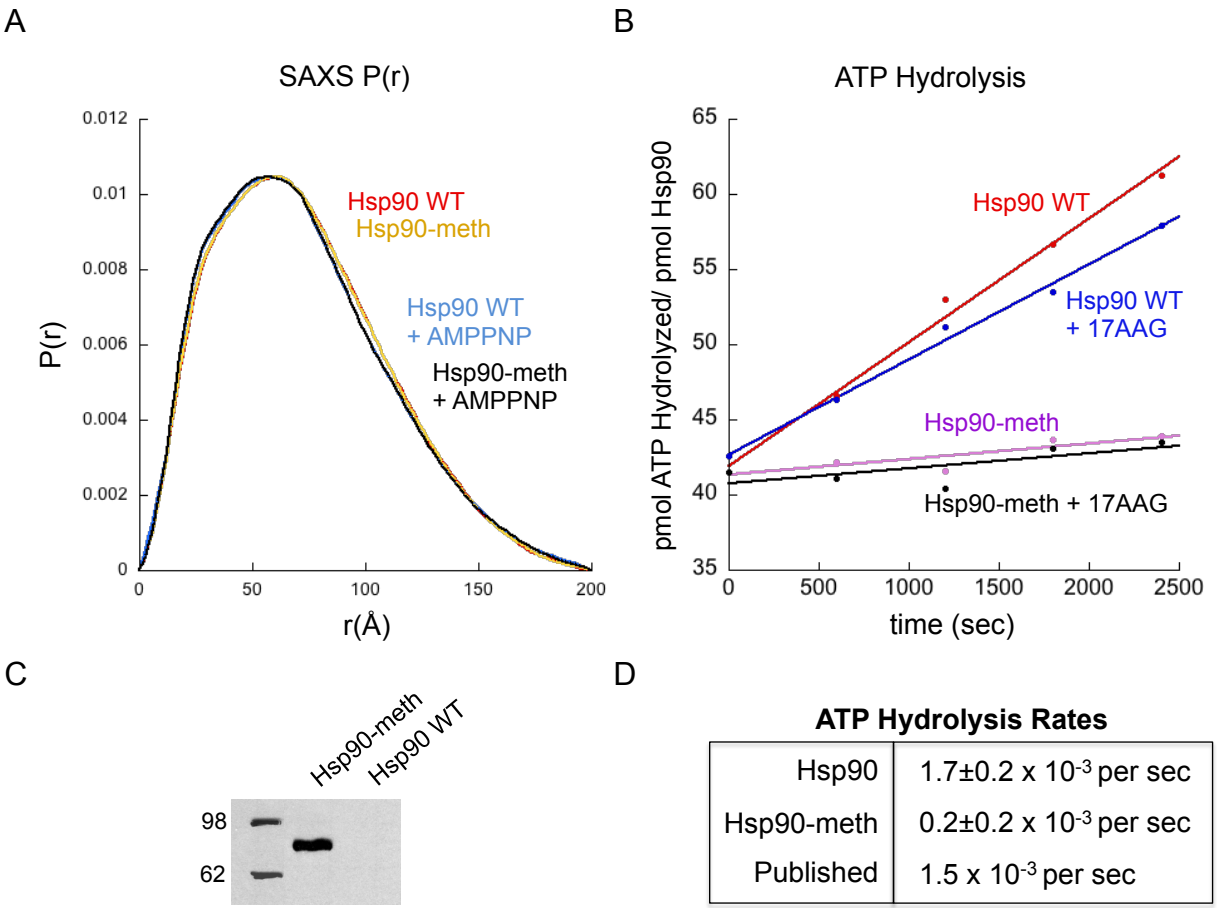

ATP Hydrolysis Rates

Hsp90	1.7±0.2 x 10^{-3} per sec
Hsp90-meth	0.2±0.2 x 10^{-3} per sec
Published	1.5 x 10^{-3} per sec

Figure 5. Smyd2 methylation of Hsp90 has little effect on Hsp90's conformation, but inhibits ATP hydrolysis.

A) SAXS analysis show no detectable conformation change upon Smyd2 methylation for apo Hsp90 WT (red) and Smyd2 methylated and re-purified Hsp90 (yellow). No difference was noticed in the presence of AMPPNP for Hsp90 WT (blue) or methylated Hsp90 (black). (Exp258)

B) Representative ATP hydrolysis measured by radioactive ^{32}P phosphate release at 37°C for untreated Hsp90 WT (red) and Smyd2 methylated and re-purified Hsp90 (purple). Hydrolysis rates were calculated by subtracting the background rates determined with the specific Hsp90 inhibitor, 17AAG for WT (blue) and for methylated Hsp90 (black). The lower background in the methylated Hsp90 is likely due to the extra purification step. (Exp265)

C) Western blot analysis probing for Hsp90 K616 methylation from protein obtained from purification in Figure 4B and used in experiments shown in A and B, showing that the methylated Hsp90 is indeed methylated, as compared to the untreated WT Hsp90.

D) Average background subtracted ATP hydrolysis rates determined from 2 independent experiments (Exp257 and 265) as in B, compared to the published rates for human Hsp90 (McLaughlin et al., 2002). Errors represent the standard deviation.

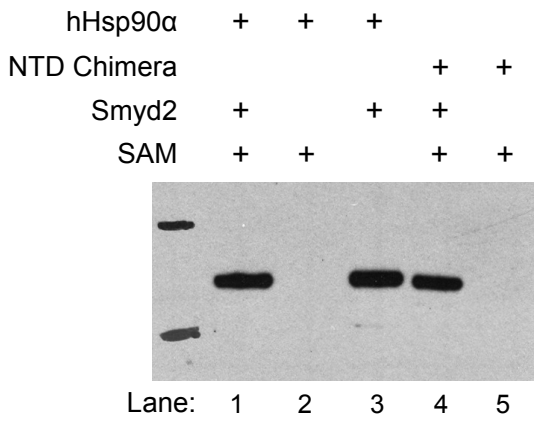

Figure 6. Smyd2 methylates the Hsp90 yeast/human NTD Chimera.
West blot analysis probing for K616 methylation of Hsp90 from Smyd2 methylation reaction for human Hsp90 WT (lanes 1-3) and for the yeast/human NTD chimera (lanes 4 and 5). (Exp312)

Attempts at crosslinking Smyd2 to Hsp90 for structural characterization

As shown in Figure 4, while association between Smyd2 and Hsp90 was detected at low salt, it was not strong enough to form a stable complex resistant to dissociation during gel filtration. Additionally at lower protein concentrations (~10-20μM) no complex formation was detected (not shown- Exp357). This suggests that the complex is not stable enough to investigate by EM. To this end, I attempted to engineer cysteine crosslinks between the TPR domain of Smyd2 and the MEEVD motif on Hsp90 (Hsp90 733C), as was done for Hop (Southworth and Agard, 2011).

At the beginning of this investigation, there was no structural information for any of the Smyd proteins. So at first, Smyd2 H341C, the equivalent residue to Hop's T260 which was successful for crosslinking of Hop, was tested (Figure 7A). Partway through this endeavor the structures of the closely related Smyd1 and Smyd3 were determined (Sirinupong et al., 2010; 2011). Based on structural alignment between Smyd3's TPR domain and Hop's TPR domain, the helix containing H341 is father away from the MEEVD

binding site due to the less concave structure of Smyd3's TPR domain compared to Hop's (Figure 7B). The structure of Smyd3 was used to guild the design of a second potential cysteine crosslinks site. Smyd2 S383C was chosen because of its better alignment to Hop and remains close to the MEEVD peptide binding site (Figure 7B). However, for both Smyd2 H341C and S383C, only a very small fraction of cross-linked complex was detected, and both were significantly worse compared to Hop T260C (Figure 7C).

Given that there was some small fraction that formed the cross-linked complex, a possible explanation for the weak affinity is that only a small fraction of the Hsp90 population access a specific state required for Smyd2 binding. In this case, binding could be improved by stabilizing the state of Hsp90 required for Smyd2 interaction. In a preliminary attempt to identify preferred conditions three variables were explored: SAM, AMPPNP, and p23 (Figure 7D). The degree of complex formation was compared for ±SAM, with SAM ± AMPPNP, and with SAM and AMPPNP ± p23. While varying SAM or AMPPNP had little effect, the addition p23 with AMPPNP completely prevented the formation of the cross-linked complex. This suggests that Smyd2 binding is incompatible with the closed state. The reason just AMMPNP was not inhibitory is likely because AMPPNP on its own is not effective at shifting Hsp90's equilibrium to the closed state (Southworth and Agard, 2008).

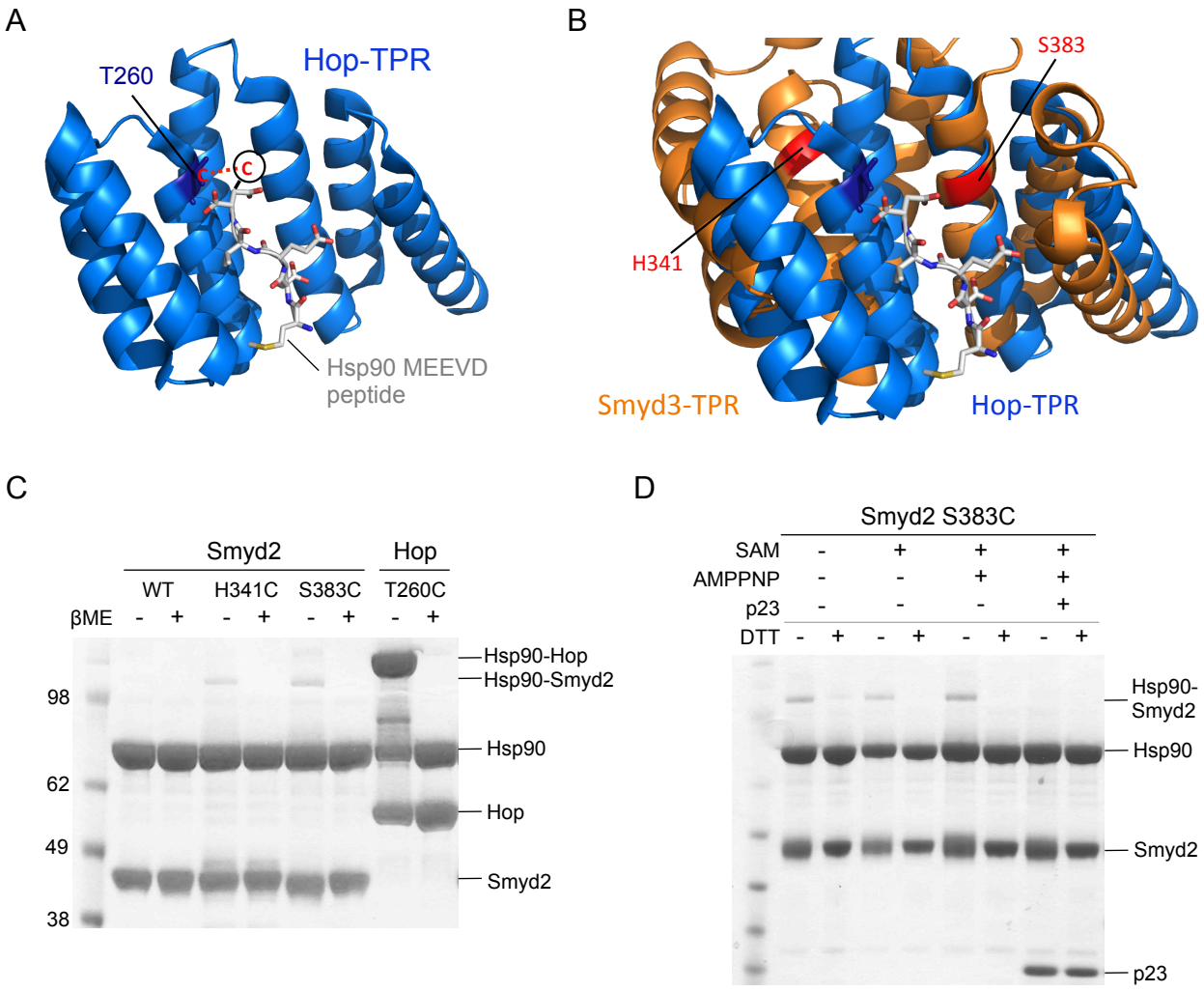

Figure 7. Engineered cysteine in Smyd2 TPR domain designed to crosslink to Hsp90 773C.

A) Crystal structure of Hop TPR2A (blue) bound to Hsp90 MEEVD peptide (grey) (pdb 1ELR). The cysteine crosslinks used to crosslink Hsp90 to Hop for EM structural determination are shown in red, with Hop T260 mutated to cysteine, and an extra cysteine added onto the C-terminus of Hsp90's MEEVD motif (Southworth and Agard, 2011).

B) The crystal structure of Smyd3 TPR domain (pdb 3MEK) in orange, aligned to Hop TPR2A (blue) as in A. Residues in red, H341 and S383, on Smyd3 indicate locations of cysteine mutation on Smyd2 tested for crosslinking to Hsp90 733C. Smyd2 H341 corresponds to Hop residue T260.

C) Smyd2 cysteine mutants H341C and S383C were tested for their ability to crosslink to Hsp90 733C as compared to Hop T260C. Disulfide crosslinks are only stable under non-reducing conditions (- βME). Only weak crosslinking between Smyd2 and Hsp90 are detected for both Smyd2 mutants. Complexes were formed in the presence of SAM. (Exp389)

D) Smyd2 S383C was tested for is ability to crosslink to Hsp90 733C as in (A) under different conditions: ±SAM, with SAM ± AMPPNP, and with SAM and AMPPNP ± p23. No

significant difference was observed for ±SAM, or SAM ± AMPPNP. However, complex formation was inhibited by the addition of p23 with AMPPNP. (Exp384)

Discussion

Based on the preliminary results, the fact that Smyd2 seems to preferentially binding to an open state of Hsp90, and that methylation of Hsp90 also seems to stabilize the open state, as reflected in the inhibition on the ATP hydrolysis rate, suggests that Smyd2 may acts earlier in the Hsp90 pathway. These results are somewhat surprising given Laura's preliminary results that p23 gets incorporated into the Smyd2 chaperone complexes. However, it is interesting that in Laura's pull-down, there seems to be less p23 incorporation with the wild type complexes compared to the catalytically dead Smyd2 complexes (Figure 1B). This correlates with the methylation of Hps90 inhibiting access to the closed state. Unfortunately, these results are still too preliminary to make any conclusive remarks.

It is still unclear why the *in vitro* binary association between Hsp90 and Smyd2 is so weak. Smyd2 may specifically act in the context of other specific cochaperones and/or clients, which could be required to observe the formation of a more stable complex. In this case, a better understanding of biological context would greatly help. It is also possible that Smyd2 is acting purely enzymatically to methylate Hsp90 and not necessary acting as a cochaperone in the structural sense. In this case a more transient association would be expected, and the focus should be on the functional effect of methylation on Hsp90.

It is unclear if the weak crosslinking reflects a small amount of complex formation, or low crosslinking efficiency resulting from non-optimal placement of cysteine in Smyd2's TPR domain. While there is now a structure of Smyd2, a structure of Smyd2's TPR domain

bound to a MEEVD peptide is still lacking. Based on the alignment of Smyd2 TPR domain with Hop, the residues chosen seem reasonable, with Y344 being a candidate still worth test. Intriguingly, the Smyd protein's TPR domains are different from the TPR domains of other Hsp90 cochaperones such as Hop, FKBP52/51 and CHIP, in that the Smyd TPR domains have a different superhelical twist that results in a less concave peptide binding surface (Figure 8A). Smyd2's flat TPR domain makes it unclear exactly how the MEEVD peptide would bind, and thus harder to predict which residues would best form a cysteine crosslink. It is possible that the TPR domain undergoes a conformational change upon binding the MEEVD motif that involves adopting a more concave like structure similar to Hop. However, in order to do so without forming a steric clash with the rest of the protein, the TPR domain would have to rotate outward, away from the substrate binding site and thus would provide an explanation for how Hsp90 activated HKMT activity (Figure 9).

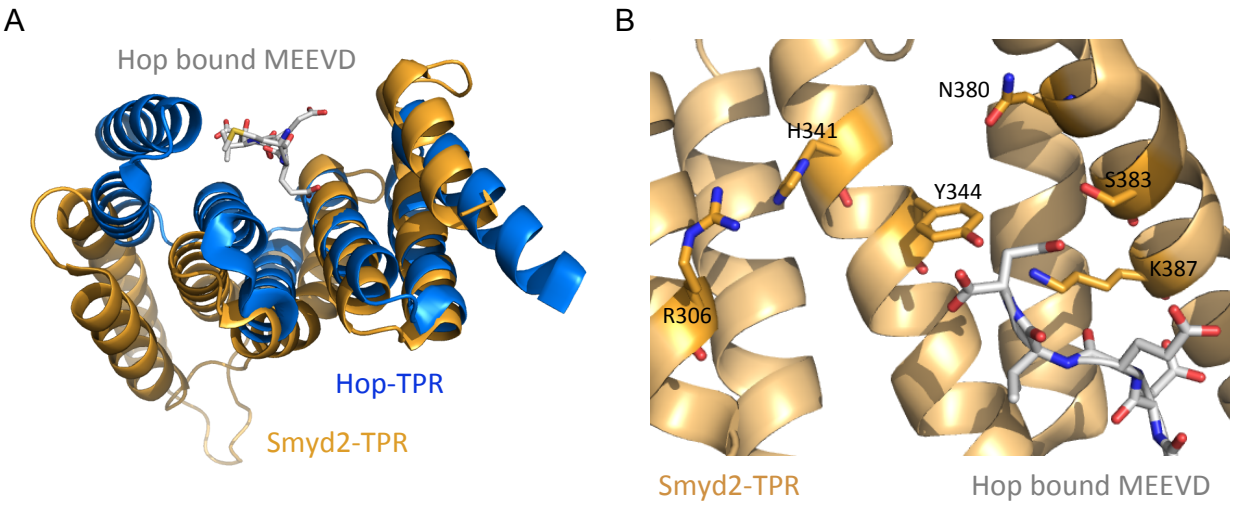

Figure 8. Crystal structure of Smyd2 TPR domain.
A) Crystal structure of Smyd2 TPR (pdb 3TG4) in orange aligned to the MEEVD (grey) bound Hop TPR2A domain (pdb 1ELR) in blue show
B) Zoom in on potential peptide binding region on Smyd2 TPR (orange) with aligned Hop bound MEEVD peptide (grey) as in (A).

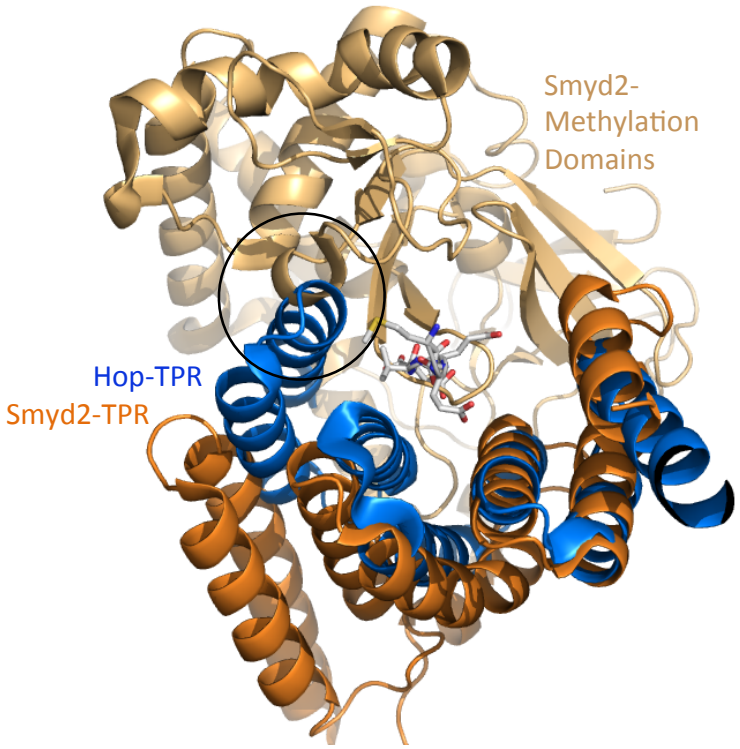

Figure 9. The typical concave TPR domain conformation is not compatible with the Smyd2 structure.
Shown is the crystal structure of Smyd2 (pdb 3TG4) in yellow with its TPR domain highlighted in orange. The MEEVD (grey) bound Hop TPR2A domain (pdb 1ELR) in blue is aligned to Smyd2's TPR domain. Based on the alignment, the concave conformation of Hop's TPR domain results in a steric clash with the Smyd2 methylation domains.

Recently, Smyd2 was found to methylate ER K266 which resulted in the attenuation of chromatin recruitment of ER, implicating Smyd2 in fine tuning of ER signaling (Zhang et al., 2013). This, together, with the evidence indicating that Smyd3 interacts directly with ER LBD to enhance ER signaling (discussed above) (Kim et al., 2009), suggests that there may be some merit to Laura Dolin's initial finding that Smyd2 gets incorporation into GR and MR chaperone complexes. However, it is still unclear what role Smyd2 could be carrying in the GR pathway. Preliminary investigations with methylated Hsp90 in the GR ligand binding assay indicates that under equilibrium conditions, the Smyd2 methylation

on Hsp90 does not have a significant effect on Hsp90's ability to reverse the Hsp70 inhibition (not shown, Exp510).

Nonetheless, there is clearly a three-way interaction between the Smyd proteins, Hsp90, and specific Hsp90 clients, such as the hormone receptors and p53, but at this moment it is not entirely clear who is regulating whom and under what biological or pathological context. In regards to the TPR autoinhibition and the Hsp90 activation of the Smyd proteins, while the substrate binding groove can accommodate a substrate peptide with the TPR domain in the intermediate position seen in the p53 peptide bound crystal structure of Smyd2 (Ferguson et al., 2011), even in the more open conformation the TPR domain would still induce significant restrictions for the access of a target region on a folded full length protein. An interesting possibility is that Hsp90 is regulating Smyd2 specificity by acting (potentially with Hsp70) to unfold specific target regions in the Smyd substrates to allow the Smyd methylases to be able to access the target methylation sites on folded substrates.

Experimental Procedures

Smyd2 Expression and Purification

The gene for full length human Smyd2 was codon optimized for E. coli expression by GeneArt and subcloned into pET-151-D Topo vector expressed with a N-terminal 6xHis tag. Smyd2 was expressed and purified using the standard purification scheme as described for Hsp90. While Zn was entirely excluded from earlier purifications, in later Smyd2 purifications, 50μM $ZnCl_2$ was added to the growth medium and purification buffers to help with the stability of the zinc finger containing MYND domain.

Lysine Methyltranseferase (KMTase) Assay

All methylation reactions were carried out with 128μM S-adensylmethionine (SAM) (NEB B9003S) in 30mM HEPES pH 7.5, 50mM KCl, 5mM $MgCl_2$, and 2-4mM DTT. Methylation was measured by western blot probed with a custom antibody specific for monomethylated K616 Hsp90 provided by the Tarakhovsky lab (Donlin et al., 2012). For the western blot, about 100ng Hsp90 was resolved on 4-12% SDS-PAGE, followed by western transfer. The membrane was blocked for 30 minutes in 4% milk/TBST at room temperature, before incubation with primary rabbit anti-methyl Hsp90 antibody in 4% milk/TBST for 1 hour at room temperature at 1:200 for purified antibody, or 1:500 for serum. After 3, 10 minute washes with TBST, the secondary anti-rabbit antibody was incubated at 1:5000 for 1 hour at room temperature. The membrane was then washed 3 times, for 10 minutes in TBST before exposure with chemiluminescent substrate (SuperSignal West Pico, Thermo Scientific).

Small Angle X-ray Scattering

SAXS was carried at as described in Chapter 2.

ATPase Assay

ATP hydrolysis was measured by radioactive ^{32}P phosphate release at 37°C as described in Chapter 1.

Assembly of cysteine cross-linked complexes

10μM of Hsp90 733C (monomer) was mixed with 20μM Smyd2 cystein mutants or Hop T260C, with or without 53μM SAM, and with or without 3.7mM AMPPNP in 30mM HEPES pH 7.5, 50mM KCl, 5mM $MgCl_2$, 0.05% β-O-G, and 20μM $ZnCl_2$. Reactions were incubated at 30°C for 1 hour and then incubated on ice over night.

References

Abu-Farha, M., Lambert, J.P., Al-Madhoun, A.S., Elisma, F., Skerjanc, I.S., and Figeys, D. (2007). The Tale of Two Domains: Proteomics and Genomics Analysis of SMYD2, A New Histone Methyltransferase. Molecular & Cellular Proteomics *7*, 560–572.

Abu-Farha, M., Lanouette, S., Elisma, F., Tremblay, V., Butson, J., Figeys, D., and Couture, J.F. (2011). Proteomic analyses of the SMYD family interactomes identify HSP90 as a novel target for SMYD2. Journal of Molecular Cell Biology *3*, 301–308.

Brown, M.A., Sims, R.J., Gottlieb, P.D., and Tucker, P.W. (2006). Identification and characterization of Smyd2: a split SET/MYND domain-containing histone H3 lysine 36-specific methyltransferase that interacts with the Sin3 histone deacetylase complex. Mol. Cancer *5*, 26.

Diehl, F., Brown, M.A., van Amerongen, M.J., Novoyatleva, T., Wietelmann, A., Harriss, J., Ferrazzi, F., Böttger, T., Harvey, R.P., Tucker, P.W., et al. (2010). Cardiac deletion of Smyd2 is dispensable for mouse heart development. PLoS ONE *5*, e9748.

Donlin, L.T., Andresen, C., Just, S., Rudensky, E., Pappas, C.T., Kruger, M., Jacobs, E.Y., Unger, A., Zieseniss, A., Dobenecker, M.W., et al. (2012). Smyd2 controls cytoplasmic lysine methylation of Hsp90 and myofilament organization. Genes Dev. *26*, 114–119.

Du, S.J., Tan, X., and Zhang, J. (2014). SMYD Proteins: Key Regulators in Skeletal and Cardiac Muscle Development and Function. Anat. Rec. *297*, 1650–1662.

Ferguson, A.D., Larsen, N.A., Howard, T., Pollard, H., Green, I., Grande, C., Cheung, T., Garcia-Arenas, R., Cowen, S., Wu, J., et al. (2011). Structural Basis of Substrate Methylation and Inhibition of SMYD2. Structure *19*, 1262–1273.

Fujii, T., Tsunesumi, S.-I., Yamaguchi, K., Watanabe, S., and Furukawa, Y. (2011). Smyd3 is required for the development of cardiac and skeletal muscle in zebrafish. PLoS ONE *6*, e23491.

Gottlieb, P.D., Pierce, S.A., Sims, R.J., Yamagishi, H., Weihe, E.K., Harriss, J.V., Maika, S.D., Kuziel, W.A., King, H.L., Olson, E.N., et al. (2002). Bop encodes a muscle-restricted protein containing MYND and SET domains and is essential for cardiac differentiation and

morphogenesis. Nat. Genet. *31*, 25–32.

Hamamoto, R., Furukawa, Y., Morita, M., Iimura, Y., Silva, F.P., Li, M., Yagyu, R., and Nakamura, Y. (2004). SMYD3 encodes a histone methyltransferase involved in the proliferation of cancer cells. Nat. Cell Biol. *6*, 731–740.

Hamamoto, R., Silva, F.P., Tsuge, M., Nishidate, T., Katagiri, T., Nakamura, Y., and Furukawa, Y. (2006). Enhanced SMYD3 expression is essential for the growth of breast cancer cells. Cancer Sci. *97*, 113–118.

Huang, J., Perez-Burgos, L., Placek, B.J., Sengupta, R., Richter, M., Dorsey, J.A., Kubicek, S., Opravil, S., Jenuwein, T., and Berger, S.L. (2006). Repression of p53 activity by Smyd2-mediated methylation. Nature *444*, 629–632.

Jiang, Y., Sirinupong, N., Brunzelle, J., and Yang, Z. (2011). Crystal Structures of Histone and p53 Methyltransferase SmyD2 Reveal a Conformational Flexibility of the Autoinhibitory C-Terminal Domain. PLoS ONE *6*, e21640.

Just, S., Meder, B., Berger, I.M., Etard, C., Trano, N., Patzel, E., Hassel, D., Marquart, S., Dahme, T., Vogel, B., et al. (2011). The myosin-interacting protein SMYD1 is essential for sarcomere organization. The Journal of Cell Science *124*, 3127–3136.

Kim, H., Heo, K., Kim, J.H., Kim, K., Choi, J., and An, W. (2009). Requirement of Histone Methyltransferase SMYD3 for Estrogen Receptor-mediated Transcription. Journal of Biological Chemistry *284*, 19867–19877.

Komatsu, S., Imoto, I., Tsuda, H., Kozaki, K.-I., Muramatsu, T., Shimada, Y., Aiko, S., Yoshizumi, Y., Ichikawa, D., Otsuji, E., et al. (2009). Overexpression of SMYD2 relates to tumor cell proliferation and malignant outcome of esophageal squamous cell carcinoma. Carcinogenesis *30*, 1139–1146.

Li, H., Zhong, Y., Wang, Z., Gao, J., Xu, J., Chu, W., Zhang, J., Fang, S., and Du, S.J. (2013). Smyd1b is required for skeletal and cardiac muscle function in zebrafish. Molecular Biology of the Cell *24*, 3511–3521.

Liu, Y., Chen, W., Gaudet, J., Cheney, M.D., and Roudaia, L. (2007). Structural Basis for Recognition of SMRT/N-CoR by the MYND Domain and Its Contribution to AML1/ETO's Activity. Cancer Cell *11*, 483–497.

McLaughlin, S.H., Smith, H.W., and Jackson, S.E. (2002). Stimulation of the weak ATPase activity of human Hsp90 by a client protein. J. Mol. Biol. *315*, 787–798.

Proserpio, V., Fittipaldi, R., Ryall, J.G., Sartorelli, V., and Caretti, G. (2013). The methyltransferase SMYD3 mediates the recruitment of transcriptional cofactors at the myostatin and c-Met genes and regulates skeletal muscle atrophy. Genes Dev. *27*, 1299–1312.

Saddic, L.A., West, L.E., Aslanian, A., Yates, J.R., Rubin, S.M., Gozani, O., and Sage, J. (2010). Methylation of the retinoblastoma tumor suppressor by SMYD2. Journal of Biological Chemistry *285*, 37733–37740.

Sirinupong, N., Brunzelle, J., Ye, J., Pirzada, A., Nico, L., and Yang, Z. (2010). Crystal Structure of Cardiac-specific Histone Methyltransferase SmyD1 Reveals Unusual Active Site Architecture. J. Biol. Chem. *285*, 40635–40644.

Sirinupong, N., Brunzelle, J., Doko, E., and Yang, Z. (2011). Structural Insights into the Autoinhibition and Posttranslational Activation of Histone Methyltransferase SmyD3. J. Mol. Biol. *406*, 149–159.

Southworth, D.R., and Agard, D.A. (2008). Species-Dependent Ensembles of Conserved Conformational States Define the Hsp90 Chaperone ATPase Cycle. Mol. Cell *32*, 631–640.

Southworth, D.R., and Agard, D.A. (2011). Client-Loading Conformation of the Hsp90 Molecular Chaperone Revealed in the Cryo-EM Structure of the Human Hsp90:Hop Complex. Mol. Cell *42*, 771–781.

Tan, X., Rotllant, J., Li, H., De Deyne, P., DeDeyne, P., and Du, S.J. (2006). SmyD1, a histone methyltransferase, is required for myofibril organization and muscle contraction in zebrafish embryos. Proc. Natl. Acad. Sci. U.S.a. *103*, 2713–2718.

Wu, J., Cheung, T., Grande, C., Ferguson, A.D., Zhu, X., Theriault, K., Code, E., Birr, C., Keen, N., and Chen, H. (2011). Biochemical Characterization of Human SET and MYND Domain-Containing Protein 2 Methyltransferase. Biochemistry *50*, 6488–6497.

Xu, S., Wu, J., Sun, B., Zhong, C., and Ding, J. (2011a). Structural and biochemical studies of human lysine methyltransferase Smyd3 reveal the important functional roles of its post-SET and TPR domains and the regulation of its activity by DNA binding. Nucleic Acids Res. *39*, 4438–4449.

Xu, S., Zhong, C., Zhang, T., and Ding, J. (2011b). Structure of human lysine methyltransferase Smyd2 reveals insights into the substrate divergence in Smyd proteins. Journal of Molecular Cell Biology *3*, 293–300.

Zhang, X., Tanaka, K., Yan, J., Li, J., Peng, D., Jiang, Y., Yang, Z., Barton, M.C., Wen, H., and Shi, X. (2013). Regulation of estrogen receptor α by histone methyltransferase SMYD2-mediated protein methylation. Proceedings of the National Academy of Sciences *110*, 17284–17289.

Zhang, X., and Bruice, T.C. (2008). Enzymatic mechanism and product specificity of SET-domain protein lysine methyltransferases. Proceedings of the National Academy of Sciences *105*, 5728–5732.

Chapter 8

Future Directions

Mechanism for GRLBD inactivation by Hsp70

Many of the mechanistic details of how Hsp70 inhibits GRLBD are still unknown. One of the most basic questions still remaining is: where on GRLBD is Hsp70 binding? Surprisingly, there were no regions that under went a significant degree of protection upon Hsp70 binding as monitored by HDX-MS that would have suggested a binding site. It is not entirely clear why this is the case. One possible explanation is that Hsp70 binds a region that in the unbound state is well structured and/or buried, resulting in a slow exchange rate. Hsp70 binding would then results in the unstructuring of the binding region. However, this loss of structure would be masked by the protection associated with burring of the binding site in the GRLBD-Hsp70 interface, which would result in an overall neutral change. If this is the case, there is potentially an important region where Hsp70 is binding that is not being revealed in the HDX-MS experiment.

I attempted to find the Hsp70 binding sites using an Hsp70 binding site prediction algorithm. However, when these predicted sites were mutated and experimentally tested, none of the sites showed a significant change in the IC_{50} for GRLBD ligand binding inhibition by Hsp70 (see Appendix Section 3). Other approaches will be required to identify the Hsp70 binding sites. One such approach

would be to screening a peptide array of the GRLBD sequence to find new candidate binding sites that can be experimentally validated by mutational studies.

The nature of the cooperative behavior seen in the IC_{50} curves is also a currently unexplained observation, and has important implications into the stoichiometry and mechanism for inhibition. Hsp70 dimers have been extensively documented, however, the function of these dimers has remained elusive, with client binding shifting the equilibrium towards Hsp70 monomers (Aprile et al., 2013; Thompson et al., 2011). Consistent with this; native mass spectrometry data indicates that only one Hsp70 binds per GRLBD monomer (Carol Robinson's lab, personal communications), suggesting that Hsp70 dimers are not involved in the GRLBD inhibition.

The cooperativity may instead reflect a sequential mechanism of inhibition in which multiple rounds of ATP hydrolysis on more than one Hsp70 are required for GRLBD to reach the inhibited state. In this case, it could take two or more Hsp70s to partially unfold GRLBD, and then one to hold it in the final inhibited state. A key concept that may shed light on this topic is the determination of the number of cycles of ATP hydrolysis on Hsp70 that are required for GRLBD to reach the inhibited state. Supporting this model, it was found to require five cycles of ATP hydrolysis for Hsp70 to refold a misfolded firefly luciferase (Sharma et al., 2010). Similarly, for the disassembly of clathrin coated vesicles, data suggests that three separate sequential ATP hydrolysis events are required (Rothnie et al., 2011). Together, this suggests that a mechanism involving multiple, sequential ATP

hydrolysis events is a universal mechanism being utilized by Hsp70 to partially or fully unfold its client proteins, and is likely also the case for GRLBD inhibition.

Many of the in depth mechanistic questions regarding the inhibition of GRLBD by Hsp70 would perhaps be more efficiently worked out with the well-characterized bacterial Hsp70 system. Like the human Hsp70, DnaK, the canonical bacterial Hsp70, inhibits GRLBD ligand binding (Figure 1). In this case, human GR was inhibited with bacterial Hsp70 and yeast Hsp40, demonstrating how universally conserved the chaperone system is. However, HtpG, the bacterial Hsp90, could not reverse the inhibition (not shown- Exp895). This provides a potentially interesting approach for understanding the important mechanistic features essential for Hsp90 to reverse the Hsp70 inhibition.

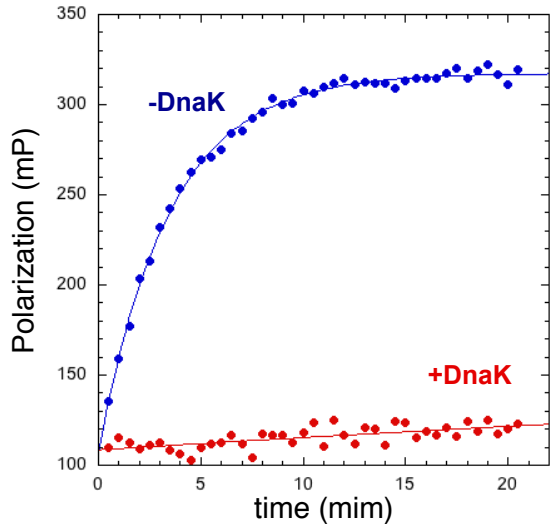

Figure 1. Bacterial Hsp70 (DnaK) inhibits GRLBD
GRLBD ligand binding kinetics of 20nM Dex-F to 1μM MBP-GRLB alone (blue) or with 2μM Hsp40 (Ydj1) and 15μM DnaK. DnaK was kindly provided by Daniel Elnatan. (Exp895)

The bacterial system also provides an interesting opportunity to explore the degree of coordination between HtpG and the bacterial NEF, GrpE. While it could be that the failure of HtpG to reverse the DnaK inhibition of GRLBD maybe due to the inability of HtpG to interact correctly with GRLBD, another possibility is that bacterial Hsp90 does not promote nucleotide exchange on Hsp70 as speculated for the human system. It could be that in the bacterial system, GrpE entirely controls client release through nucleotide exchange, while HtpG only provides a chaperone function upon Hsp70 release. If this is the case, the evolutionary loss of GrpE likely correlates with Hsp90's evolved ability to carry out the NEF function in addition to its chaperone function. More specialized NEFs in eukaryotes may have then emerged to work with Hsp90 to facilitate client release, but more as a mechanism for regulation to allow for fine-tuning and specific targeting of client release. If this is the case, it raises the question of what function ATP hydrolysis is carrying out on HtpG, which maybe a conserved function in the human system that is occurring after the initial ATP hydrolysis event on Hsp90 that releases Hsp70.

Role of Hsp40 J-proteins

In humans, there are 41 J-proteins that all contain the conserved J-domain that is necessary and sufficient for stimulating ATP hydrolysis on Hsp70. Outside of the J-domain, there is a very large degree of sequence and structural divergence, with this large variation making J-proteins drivers of functional specificity for the Hsp70 system (Kampinga and Craig, 2010). Like the human Hsp70, a J-protein is required for DnaK to inhibit GRLBD ligand binding (data not shown, Exp896). The

bacterial Hsp40, DnaJ, is able to carry out this function (personal communication, Daniel Elnatan). However, just the N-terminal J-domain sufficient for stimulating ATP hydrolysis on Hsp70 was not able to promote GRLBD inhibition by DnaK (data not shown- Exp896). This indicates that the C-terminal client-binding region on Hsp40 is essential for GR inhibition.

Conversely, in many biological contexts the J-domain is sufficient (Kampinga and Craig, 2010). The reason for why some circumstances necessitate a client binding region and others do not is not entirely clear, and raises the question of what exactly Hsp40 is mechanistically doing. It is emerging that the client binding regions are specifically important for promoting Hsp70's interaction with native like clients (Kampinga and Craig, 2010). For the DnaK client, σ^{32}, DnaJ was found to induce a local structural disruption in σ^{32} that was proposed to be responsible for exposing the Hsp70 binding site (Rodriguez et al., 2008). In contrast, the HDX-MS did not reveal any significant change in H/D exchange on GRLBD with just Hsp40, suggesting that this is not the case for GR.

Having a client-binding domain physically connected to a J-domain ensures more stringent coupling of ATP hydrolysis to client binding such that ATP hydrolysis occurs predominantly when the client is present, therefore promoting productive cycling. Moreover, Hsp40's mechanism may be more complex, with Hsp40 playing a more integral role in client unfolding. Hsp40 may be coupling its holdase function with the actions of Hsp70 to facilitate client unfolding. This would explain why the client-binding domain would be more essential for interacting with

more native like proteins, and not as important for clients already in the unfolded state.

In some cases, J-proteins have been implicated in playing a distinct role in the targeting of client proteins, with the determination of a client's fate between folding or degradation depending on the specific J-protein (DNAJB1 vs. DNAJB8) (Howarth et al., 2007; Kampinga and Craig, 2010). In support of this, a recent high-throughput assay designed to systematically characterize the chaperone-cochaperone-client interaction network revealed that a small subset of the J-proteins, DNAJB1 and DNAJB6, were classified as belonging to a small group of cochaperones that bridge the Hsp70 and Hsp90 subnetworks, suggesting that these specific J-proteins facilitate the transfer of clients between chaperones (Taipale et al., 2014). This connection is further supported by the synthetically lethal phenotype of Ydj1 and Hop (Flom et al., 2005). Together, it seems that Hsp40s maybe playing an overlooked aspect in Hsp70 client hand-off from in the GR system. Also, given the critical importance of Hsp40 in initiating the whole GR chaperone cycle, the mechanistic details associated with Hsp40 in this system may be worth further investigation.

Mechanism for GRLBD hand off from Hsp90 to Hsp70

One of the most significant concepts put forth by this work that was not fully investigated is the coupling of Hsp70's and Hsp90's ATP hydrolysis cycles as part of the mechanism for client transfer. The coupling should be evident in steady state ATP hydrolysis rates. Preliminary results indicated a synergistic stimulation of ATP

hydrolysis in the presence of both the Hsp70 and Hsp90 system not seen with hydrolysis dead Hsp90 (data not shown). However, these investigations proved challenging due to the low signal to noise resulting from the low ATP hydrolysis rates of the human proteins, and was further complicated by the number of cochaperones. For these reasons, the ATP hydrolysis experiments were not actively pursued at the time, but at this point are worth revisiting.

A more direct question that needs addressing is if Hsp90 is indeed promoting ADP release on Hsp70 to facilitate GRLBD release. This is the most likely explanation for how Hsp90 could be promoting client transfer. However, it should be noted that in a comparable study investigating the transfer of clients from Hsp70 to ClpB, it was found that while ClpB also promotes client release from Hsp70, the data suggested that it does not do so by promoting nucleotide exchange (Rosenzweig et al., 2013). Unfortunately, this investigation did not provide an alternative mechanistic explanation for how ClpB could be promoting client release. In the case of ClpB, the pulling force generated by the AAA ATPase ring of ClpB could provide a strong enough force to pry the client off Hsp70 while Hsp70 transiently samples an open state. If this is the case, it is unclear if Hsp90 could be generating a comparable force in the way ClpB does. Given the biological significance of the Hsp70 to Hsp90 hand off as a critical decision point in the targeting of clients to either folding or degradation, these are important mechanistic details worth further investigation.

The double Hsp70:Hop:Hsp90:GRLBD complex and implications for a processive unfolding mechanism

Ultimately, higher resolution of the cryo-EM reconstruction of the GR:Hsp70:Hop:Hsp90 complex would provide invaluable structural details that could help illuminate how the interaction between the ATPase domains is occurring and would help guide the design of future biochemical experiments that would more fully describe the mechanism of client hand off. In pushing for higher resolution of the complex, initial efforts for optimizing the sample included increasing the ATP levels during complex formation. It was determined biochemically in the ligand binding assay that excess ATP was required for optimal inhibition of GLRBD by Hsp70 (data not shown) and consequently was found to improve the incorporation of GRLBD into the complex (Figure 2A). Additionally, the ATP hydrolysis deficient Hsp90 mutants were investigated to facilitate stalling of the intermediate complex. While both the E47A and the D93N mutants prevent turnover of the complex, the D93N mutant is particularly interesting in that it allows for targeting of Hsp70's nucleotide binding pocket without interfering with Hsp90's cycle.

Unexpectedly, the hydrolysis deficient mutants promote the formation of the front shoulder peak which actually consists of a complex about twice the size of the $Hsp70_1$:Hop_1:$Hsp90_2$:$GRLBD_1$ complex (Figure 2A). The cross-linked 'single' and 'double' complex could be resolved by SDS-PAGE as distinct cross-linked species (Figure 2B). Negative stain EM by Zygy Roe-Zurz confirmed that the double complex looks like two of the single complexes associated to form a larger complex that is about twice the size of the original complex described in Chapter 4 (Figure 2D and 2E).

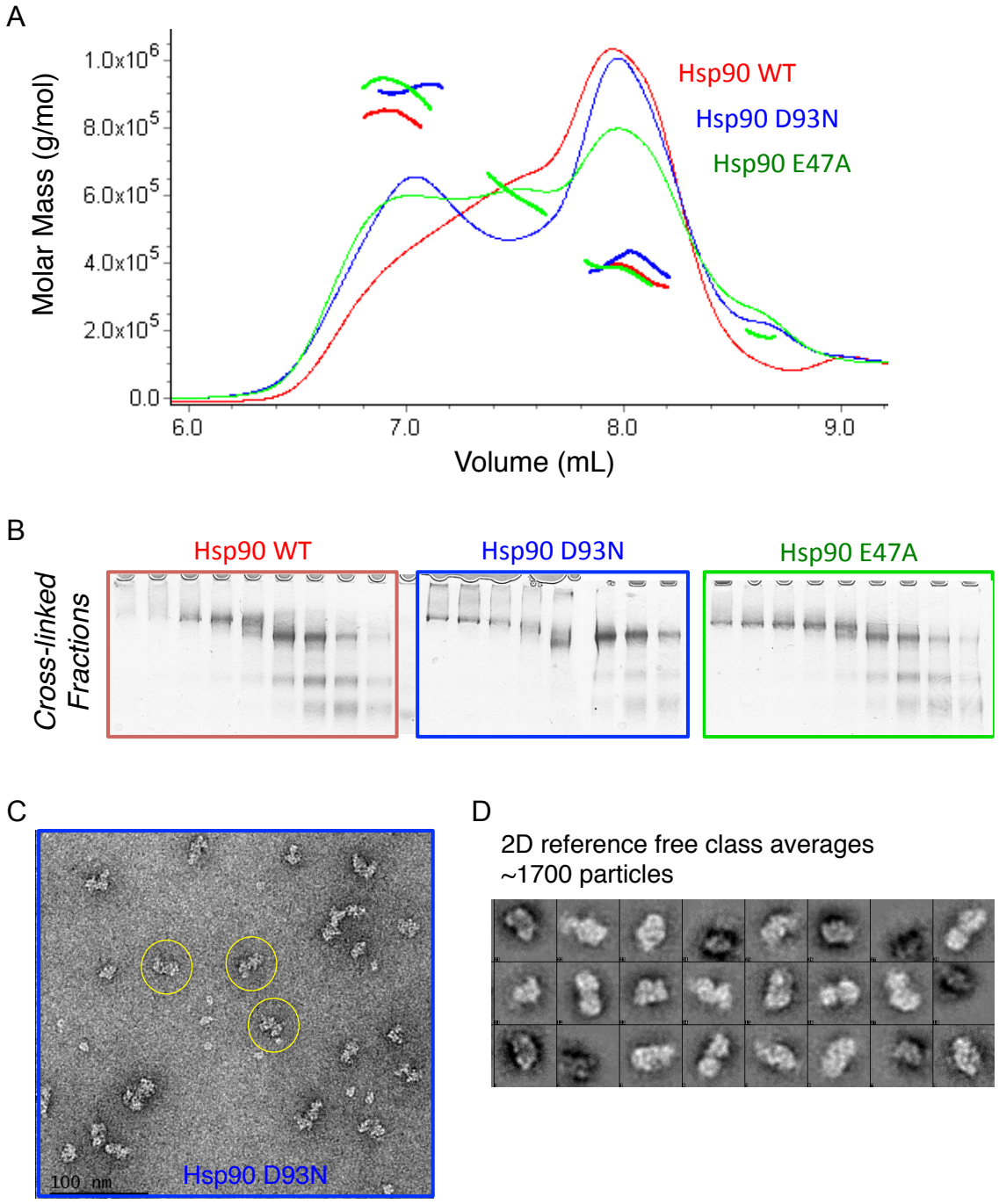

Figure 2. Hydrolysis dead Hsp90 mutants promote formation of a double Hsp70:Hop:Hsp90:GRLBD complex.
A) SEC-MALS of Hsp70:Hop:Hsp90:MBP-GRLBD complex with WT Hsp90 (red), nucleotide binding deficient Hsp90 mutant D93N (blue), and hydrolysis dead Hsp90 E47A (green). Complex was formed as described in Chapter 4 with 10μM Hsp90 dimer, 10μM Hop, 15μM Hsp70 (sf9), 20μM MBP-GRLBD, and 5mM ATP. Gel filtration running buffer contained 200μM ADP. (Exp617)

B) Cross-linked fractions from (A) resolved by SDS-PAGE. (Exp617)
C) Negative stain EM of front peak from complex formed with Hsp90 D93N (Data provided by Zygy Roe-Zurz).
D) Reference free 2D class averages of 1700 particles as in (C) (Data provided by Zygy Roe-Zurz).

The nature of the double complex and its functional relevance are currently very unclear. One possibility is that the double complex is an intermediate complex along a sequential pathway involving more than one Hsp70:Hsp90 complex, in which Hsp90 and Hsp70 collaboratively act to processively unfold a protein. In this proposed mechanism, the initial chaperone interaction with a single Hsp70:Hsp90 complex induces partial unfolding of the substrate, resulting in the exposure of a second Hsp70 site for a second chaperone complex to bind and induce further unfolding and so on. In this way, the chaperones could more completely unfold and refold a protein, with unfolding propagating from a domain that initiates the chaperone interaction into an adjacent domain that on its own would not necessarily interact with the chaperones.

Evidence for this processive unfolding mechanism was detected in the MBP-GRLBD pull-downs. With the entire chaperone system there is a reduction in the amount of MBP-GRLBD that is pulled down by the MBP affinity resin, suggesting that the chaperone system disrupts MBP's ability to recognize the amylose resin, presumably by unfolding the MBP domain (Figure 3). This loss of MBP binding was clearly seen upon titration of Hsp70 with fixed amount of the other chaperone components (Figure 3B). Intriguingly, the reduction of MBP binding was not observed with the Hsp90 hydrolysis deficient mutants, indicating that ATP hydrolysis on Hsp90 is required to disrupt MBP's interaction with the resin. Since

the chaperone complex is still bound with the hydrolysis dead mutants, it rules out steric hindrance from the bound chaperones to the resin.

Therefore, both chaperones likely work together, with ATP hydrolysis required on both chaperones, to carry out the inactivation of the adjacent MBP domain. This model begins to shed light onto how chaperones hold apo GR in an inactive state in which the GR DNA binding domain cannot bind DNA. More importantly, this model has significant implications as part of Hsp70's and Hsp90's mechanism for quality control, in which both chaperones could work collaboratively to more fully unfold and then refold a protein to consistently ensure proper folding, as discussed in Chapter 3.

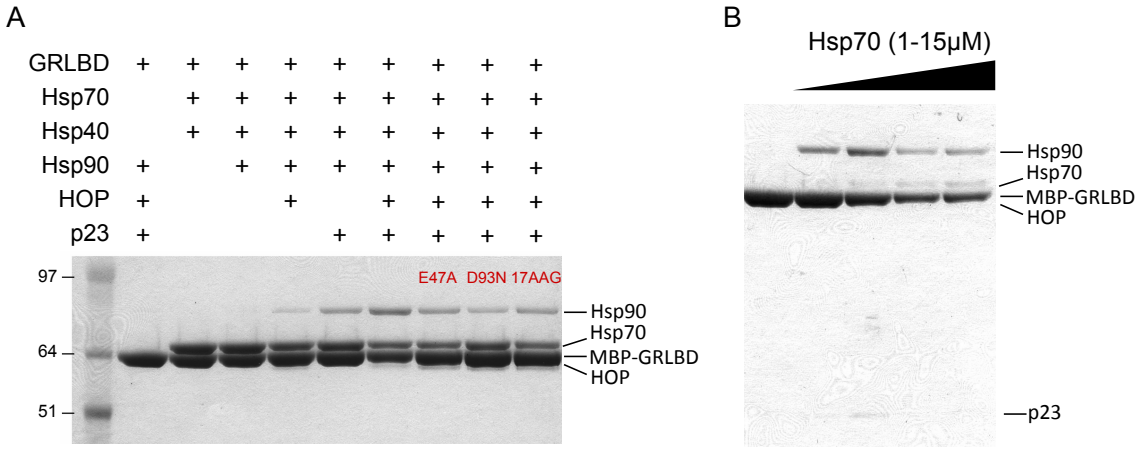

Figure 3. Evidence for processive unfolding of MBP-GRLBD by the combined actions of Hsp70 and Hsp90 in the MBP pull-down assay.
A) MBP-GRLBD pull-down as shown in Chapter 3, Figure 8 and 9B. Less MBP-GRLBD is detected in the presence of the entire system, but only with WT Hsp90 (Exp807)
B) Loss of MBP-GRLBD pulled down in the presence of the entire chaperone system is dependent on the Hsp70 concentration. Pull-down was carried out as in Chapter 3 with 5μM MBP-GRLBD, 15μM Hsp90 monomer, 7.5 μM Hop, 15 μM p23, and 0, 1, 5, 10, and 15μM Hsp70. (Exp796)

The role of p23 in the GR chaperone cycle

The structural work presented in Chapter 4 provides insight into why Hop is so important for the ligand binding recovery, in that it coordinates client hand off by promoting the direct interaction between Hsp90 and Hsp70. Conversely, the significance of the role of p23 is not as clear. Work by Pratt and co-workers indicate that p23 is not involved in the actual activation process, but allowed for the active state of GRLBD that is bound to Hsp90 to persist and thus the active state maintained (Dittmar et al., 1997; Dittmar and Pratt, 1997). Since our data clearly shows that GRLBD does not need to be associated with Hsp90 to bind ligand, in the context of the whole system p23 could be important for stalling rebinding of Hsp70 to GR, by slowing GR's off rate from Hsp90. Additionally, by competing with Hop rebinding, p23 could be imposing directionality, and would be consist with the requirement of stoichiometric amounts of p23 as apposed to the catalytic amounts of Hop (Kosano et al., 1998).

Related to this, it is still unclear what the state of GR is when bound to Hsp90 in the p23 bound closed Hsp90 complex and when exactly ligand binds. We propose that the persistent acceleration in the ligand binding with the whole chaperone system suggests that GRLBD is held in a high affinity ligand state after Hsp70 release, which is assumed to be partially unstructured. Based on thiol reactivity, early investigations by Pratt and co-workers indicated that the GRLBD ligand binding pocket is more solvent exposed in this state based (Stancato et al., 1996). However this is in contrast to the recent work from the Buchner lab which suggest that the fully folded GRLBD binds to the closed p23 bound Hsp90 complex (Lorenz

et al., 2014). Given how relatively crude the early thiol reactivity experiments were and in light of the new data from the Buchner lab, it would be helpful to have more direct probes for the state of GRLBD in the system in order to have a better understanding of how GRLBD conformational state is being modulated at every step of the cycle.

Chaperone are involved in multiple aspects of GR's functional cycle

It is becoming clear that chaperones play important roles in other aspects of steroid hormone receptor biology (Freeman and Yamamoto, 2001; Galigniana et al., 2001) (Figure 4). Hsp90 with FKBP52 are involved in the active translocation of GR to the nucleus (discussed in Chapter 6). Once in the nucleus, chaperones associate with GR transcriptional complexes and may be a significant factor that gets integrated into the complex process that results in specific transcriptional outcomes at different response elements. Furthermore, Hsp90 has been implicated in playing an important role in the disassembly of GR transcriptional complexes (Elbi et al., 2004; Freeman and Yamamoto, 2001; 2002; Liu and DeFranco, 1999).

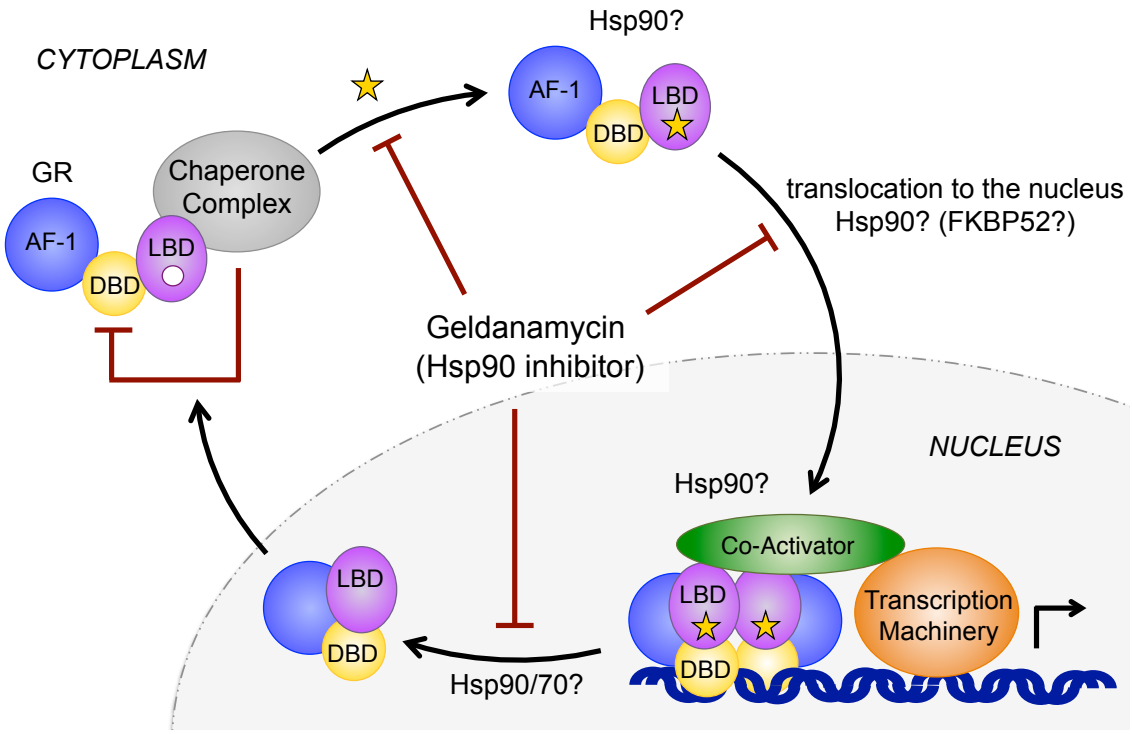

Figure 4. Model for chaperone involvement in all aspects of GR cycle. Monomeric apo GR resides in the cytoplasm associated with the Hsp70/Hsp90 chaperon complex through its LBD. In addition to regulating ligand binding, association with the chaperone complex results in the receptor existing in a repressed state that cannot bind DNA.

Chaperone regulation of GR transcriptional complexes

As conformational modulators of GRLBD, Hsp70 and Hsp90 likely influence GRLBD's interactions with co-regulators, which in turn connects GR to the transcriptional machinery. This suggests that the functional implications of the Hsp70 induced conformational changes likely extend beyond ligand binding. The region on GRLBD most disrupted by Hsp70 (helix 3) interacts directly with co-repressors and forms the important charge clamp interaction required for selective co-activator binding (Schoch et al., 2010). While it is still unclear what the state of GRLBD is while bound to Hsp90 in the p23 state, work from the Darimont lab

suggests that Hsp90 competes with co-activators, with Hsp90 utilizing the hydrophobic co-activator binding groove to bind to ligand bound GRLBD (Fang et al., 2006). This all suggests that both Hsp90 and Hsp70 modulate co-regulator interactions, and potentially carry out an important role in dictating the final transcriptional out come.

Chaperones have previously been proposed to be involved in the disassembly of transcription complexes (Freeman and Yamamoto, 2001; McLaughlin and Jackson, 2002). The rate of transcription complex disassembly is biological important since signaling complexes must be able to rapidly respond to decreases in cellular ligand concentration. *In vivo*, GR dissociates from DNA very rapidly ($t_{1/2}$~5-10 min), suggesting that something actively promotes receptor disassembly from the response element (Freeman and Yamamoto, 2001). Chaperones emerged as the likely cellular components facilitating disassembly since this ATP dependent process was shown to correlate with Hsp90, with the specific Hsp90 inhibitor, Geldanamycin, slowing the release of GR from DNA as well as inducing the loss of chaperone localization at the response elements (Kang et al., 1999; Liu and DeFranco, 1999; Stavreva et al., 2004).

More direct evidence for the role of chaperones in GR transcription complex disassembly came from the work of Freeman *et al*, who showed that localization of Hsp90 and p23 to a GR response element resulted in significant suppression of transcriptional activity (Freeman and Yamamoto, 2002). However, most of this work focused on p23, and at the time, p23's role as an important conformational modulator of Hsp90 was not well understood. While some evidence suggests p23

can act independently in this process, its actions are likely mostly indirect and result from its ability to stabilize the closed state of Hsp90 (Ali et al., 2006).

While previously, most of the attention has been centered around Hsp90 and p23 (Freeman and Yamamoto, 2002), our findings suggest that the role of Hsp70 in promoting the disassembly of GR transcriptional complexes has been over looked. For transcription activation, the DNA binding domains bind DNA cooperatively as a dimer, and not surprisingly dimer disruption has been shown to drastically accelerate DNA dissociation (Watson et al., 2013). While isolated GRLBD in solution are mostly monomeric, the LBD dimers form important structural contacts in the context of full length DNA bound complexes (Chandra et al., 2008; 2013; Lou et al., 2014). Intriguingly, the reported GRLBD dimer interface on GRLBD shown to be important for GR transactivation coincides with the second most disrupted region by Hsp70 (Bledsoe et al., 2002). Additionally the extensive contacts made on the Hsp70:Hsp90:Hop complex likely preclude dimerization. It is thus likely that chaperones promote DNA dissociation by disrupting receptor dimerization. Given the new insight provided by the findings presented in this body of work, the time is appropriate to revisit some of the other aspects of the GR cycle and to determine the unique role chaperones may be carrying out in gene regulation at the level of GR transcriptional complexes

References

Ali, M.M.U., Roe, S.M., Vaughan, C.K., Meyer, P., Panaretou, B., Piper, P.W., Prodromou, C., and Pearl, L.H. (2006). Crystal structure of an Hsp90–nucleotide–p23/Sba1 closed chaperone complex. Nature *440*, 1013–1017.

Aprile, F.A., Dhulesia, A., Stengel, F., Roodveldt, C., Justin L. P. Benesch, Tortora, P., Robinson, C.V., Salvatella, X., Dobson, C.M., and Cremades, N. (2013). Hsp70 Oligomerization Is Mediated by an Interaction between the Interdomain Linker and the Substrate-Binding Domain. PLoS ONE *8*, e67961.

Bledsoe, R.K., Montana, V.G., Stanley, T.B., Delves, C.J., Apolito, C.J., McKee, D.D., Consler, T.G., Parks, D.J., Stewart, E.L., and Willson, T.M. (2002). Crystal Structure of the Glucocorticoid Receptor Ligand Binding Domain Reveals a Novel Mode of Receptor Dimerization and Coactivator Recognition. Cell *110*, 93–105.

Chandra, V., Huang, P., Hamuro, Y., Raghuram, S., Wang, Y., Burris, T.P., and Rastinejad, F. (2008). Structure of the intact PPAR-gamma-RXR- nuclear receptor complex on DNA. Nature *456*, 350–356.

Chandra, V., Huang, P., Potluri, N., Wu, D., Kim, Y., and Rastinejad, F. (2013). Multidomain integration in the structure of the HNF-4α nuclear receptor complex. Nature *495*, 394–398.

Dittmar, K.D., Demady, D.R., Stancato, L.F., Krishna, P., and Pratt, W.B. (1997). Folding of the glucocorticoid receptor by the heat shock protein (hsp) 90-based chaperone machinery. The role of p23 is to stabilize receptor.hsp90 heterocomplexes formed by hsp90.p60.hsp70. J. Biol. Chem. *272*, 21213–21220.

Dittmar, K.D., and Pratt, W.B. (1997). Folding of the Glucocorticoid Receptor by the Reconstituted hsp90-based Chaperone Machinery. THE INITIAL hsp90 p60 hsp70-DEPENDENT STEP IS SUFFICIENT FOR CREATING THE STEROID BINDING CONFORMATION. Journal of Biological Chemistry *272*, 13047–13054.

Elbi, C., Walker, D.A., Romero, G., Sullivan, W.P., Toft, D.O., Hager, G.L., and DeFranco, D.B. (2004). Molecular chaperones function as steroid receptor nuclear mobility factors. Proceedings of the ….

Fang, L., Ricketson, D., Getubig, L., and Darimont, B.D. (2006). Unliganded and hormone-bound glucocorticoid receptors interact with distinct hydrophobic sites in the Hsp90 C-terminal domain. Proc. Natl. Acad. Sci. U.S.a. *103*, 1847–18492.

Flom, G., Weekes, J., and Johnson, J.L. (2005). Novel interaction of the Hsp90 chaperone machine with Ssl2, an essential DNA helicase in Saccharomyces cerevisiae. Curr. Genet. *47*, 368–380.

Freeman, B.C., and Yamamoto, K.R. (2001). Continuous recycling: a mechanism for modulatory signal transduction. Trends in Biochemical Sciences *26*, 285–290.

Freeman, B.C., and Yamamoto, K.R. (2002). Disassembly of transcriptional regulatory complexes by molecular chaperones. Science *296*, 2232–2235.

Galigniana, M.D., Radanyi, C., Renoir, J.M., Housley, P.R., and Pratt, W.B. (2001).

Evidence that the peptidylprolyl isomerase domain of the hsp90-binding immunophilin FKBP52 is involved in both dynein interaction and glucocorticoid receptor movement to the nucleus. J. Biol. Chem. *276*, 14884–14889.

Howarth, J.L., Kelly, S., Keasey, M.P., Glover, C.P.J., Lee, Y.-B., Mitrophanous, K., Chapple, J.P., Gallo, J.M., Cheetham, M.E., and Uney, J.B. (2007). Hsp40 molecules that target to the ubiquitin-proteasome system decrease inclusion formation in models of polyglutamine disease. Mol. Ther. *15*, 1100–1105.

Kampinga, H.H., and Craig, E.A. (2010). The HSP70 chaperone machinery: J proteins as drivers of functional specificity. Nat Rev Mol Cell Biol *11*, 579–592.

Kang, K.I., Meng, X., Devin-Leclerc, J., Bouhouche, I., Chadli, A., Cadepond, F., Baulieu, E.E., and Catelli, M.G. (1999). The molecular chaperone Hsp90 can negatively regulate the activity of a glucocorticosteroid-dependent promoter. Proc. Natl. Acad. Sci. U.S.a. *96*, 1439–1444.

Kosano, H., Stensgard, B., Charlesworth, M.C., McMahon, N., and Toft, D. (1998). The assembly of progesterone receptor-hsp90 complexes using purified proteins. J. Biol. Chem. *273*, 32973–32979.

Liu, J., and DeFranco, D.B. (1999). Chromatin recycling of glucocorticoid receptors: implications for multiple roles of heat shock protein 90. Mol. Endocrinol. *13*, 355–365.

Lorenz, O.R., Freiburger, L., Rutz, D.A., Krause, M., Zierer, B.K., Alvira, S., Cuellar, J., Valpuesta, J.M., Madl, T., Sattler, M., et al. (2014). Modulation of the Hsp90 Chaperone Cycle by a Stringent Client Protein. Mol. Cell *53*, 941–953.

Lou, X., Toresson, G., Benod, C., Suh, J.H., Philips, K.J., Webb, P., and Gustafsson, J.-Å. (2014). Structure of the retinoid X receptor α-liver X receptor β (RXRα-LXRβ) heterodimer on DNA. Nat. Struct. Mol. Biol. *21*, 277–281.

McLaughlin, S.H., and Jackson, S.E. (2002). Folding and stability of the ligand-binding domain of the glucocorticoid receptor. Protein Science *11*, 1926–1936.

Rodriguez, F., Arsène-Ploetze, F., Rist, W., Rudiger, S., Schneider-Mergener, J., Mayer, M.P., and Bukau, B. (2008). Molecular basis for regulation of the heat shock transcription factor sigma32 by the DnaK and DnaJ chaperones. Mol. Cell *32*, 347–358.

Rosenzweig, R., Moradi, S., Zarrine-Afsar, A., Glover, J.R., and Kay, L.E. (2013). Unraveling the mechanism of protein disaggregation through a ClpB-DnaK interaction. Science *339*, 1080–1083.

Rothnie, A., Clarke, A.R., Kuzmic, P., Cameron, A., and Smith, C.J. (2011). A sequential mechanism for clathrin cage disassembly by 70-kDa heat-shock cognate protein

(Hsc70) and auxilin. Proceedings of the National Academy of Sciences *108*, 6927–6932.

Schoch, G.A., D'Arcy, B., Stihle, M., Burger, D., Bär, D., Benz, J., Thoma, R., and Ruf, A. (2010). Molecular switch in the glucocorticoid receptor: active and passive antagonist conformations. J. Mol. Biol. *395*, 568–577.

Sharma, S.K., De Los Rios, P., Christen, P., Lustig, A., and Goloubinoff, P. (2010). The kinetic parameters and energy cost of the Hsp70 chaperone as a polypeptide unfoldase. Nat Chem Biol *6*, 914–920.

Stancato, L.F., Silverstein, A.M., Gitler, C., Groner, B., and Pratt, W.B. (1996). Use of the thiol-specific derivatizing agent N-iodoacetyl-3-[125I]iodotyrosine to demonstrate conformational differences between the unbound and hsp90-bound glucocorticoid receptor hormone binding domain. J. Biol. Chem. *271*, 8831–8836.

Stavreva, D.A., Müller, W.G., Hager, G.L., Smith, C.L., and McNally, J.G. (2004). Rapid Glucocorticoid Receptor Exchange at a Promoter Is Coupled to Transcription and Regulated by Chaperones and Proteasomes. Mol. Cell. Biol.

Taipale, M., Tucker, G., Peng, J., Krykbaeva, I., and Lin, Z.Y. (2014). A Quantitative Chaperone Interaction Network Reveals the Architecture of Cellular Protein Homeostasis Pathways. Cell.

Thompson, A.D., Bernard, S.M., Skiniotis, G., and Gestwicki, J.E. (2011). Visualization and functional analysis of the oligomeric states of Escherichia coli heat shock protein 70 (Hsp70/DnaK). Cell Stress Chaperones *17*, 313–327.

Watson, L.C., Kuchenbecker, K.M., Schiller, B.J., Gross, J.D., Pufall, M.A., and Yamamoto, K.R. (2013). The glucocorticoid receptor dimer interface allosterically transmits sequence-specific DNA signals. Nat. Struct. Mol. Biol. *20*, 876–883.

Appendix

Section 1: Protein Expression and Purification Procedures

Zwittergent 3-12 apo GRLBD

The double mutant of apo GRLBD (F602S/C628D) was expressed with an N-terminal thrombin cleavable GST-tagged in a pGEX-4T vector from the Fletterick lab. GST-GRLBD was bacterially expressed in BL21(DE3) cells. Cells were grown at 37°C and then cooled to 15°C before overnight induction at 0.6-0.8 OD_{600} with 0.25mM IPTG. Cells were lysed in 50mM Tris-HCl pH 8.0, 150mM NaCl, 0.1% Zwittergent 3-12, and either 5mM DTT, 1mM TCEP, or 2mM mono-thio-glycerol. The initial purification was performed using a GST column. Eluted GST-GRLBD was then cleaved overnight with thrombin in buffer supplemented with 2.5mM $CaCl_2$. GST tag was separated and GRLBD further purified on a 5mL HiTrap Q anion exchange column followed by size exclusion with a Superdex-200 column. Protein was concentrated and stored on ice for several day during which experiments were performed.

This protein purification procedure was developed by Sam Pfaff in the Fletterick lab. With this procedure, Sam was able to obtain apo GRLBD that was similarly behaved to the apo GRLBD reported by the Jackson lab, with comparable gel filtration behavior, a mostly helical circular dichroism spectrum, and extremely weak dex binding. Further details and characterization of zwittergent purified apo GRLBD can be found in Sam Pfaff's thesis, Chapter 3. While I was able to obtain apo GRLBD following this procedure, the yields were very low. Sam generously provided the large amount of apo GRLBD required for SAXS analysis.

Example purification: Exp22-25

Detergent free apo GRLBD

A synthetic gene for human GR was codon optimized for bacterial expression (GeneArt). The LBD fragment (521-777) containing the F602S mutation was cloned into a pMAL-c2X derivative with a N-terminal TEV cleavable 6x His-MBP tag. The construct was expressed in BL21 star (DE3). Typically, cells were grown in 37°C for 2-3 hour, and then the temperature was lowered to 16°C. When the OD_{600} reached about 0.8, dexamethasone was added to a final concentration of 180μM and then the cells were induced overnight with 1mM IPTG. Harvested cells were lysed by an EmulsiFlex-3C (Avestin) in 50mM Tris pH8, 300mM KCl, 10% glycerol, 20mM imidazole, 50μM dexamethasone, 0.5mM TCEP, 0.04% CHAPS and protease inhibitor pills (Roche). The lysate was clarified by centrifugation and the soluble fraction was batch bound to Ni-NTA affinity resin (QIAGEN) for 1-2 hours. The column was washed with lysis buffer with 5mM $MgCl_2$, and 2mM ATP and then eluted in 30mM Tris pH8, 50mM KCl, 0.5mM TCEP, 10% glycerol, 50μM cortisol, and 300mM imidazole. The eluted protein was flowed over a MonoQ 10/100 GL (GE Healthcare) ion exchange column in which GRLBD was collected in the flow through. The flow through was concentrated and dialyzed over night against 1 liter of ligand free buffer (30mM Tris 7.5, 150mM KCl, 0.5mM TCEP and 10% glycerol). The next morning, the protein was purified by size exclusion with a Superdex S200 16/60 (GE Healthcare) in 30mM Tris pH7.5, 500mM KCl, 0.5mM TCEP, and 10% glycerol. The purified protein was dialyzed against 1 L of storage buffer (30mM HEPES pH 7.5, 100mM KCl, 4mM DTT, and 10% Glycerol) overnight, and then further against the next day in 500mL of storage buffer for 5-8 hours to ensure

ligand removal. Purified protein was concentrated, flash frozen, and stored in aliquots at −80°C.

For WT MBP-GRLBD, MBP-GRLBD (F602S/C638D) separated by a 3C precision cleavage site was cloned into the pET-Duet vector multi-cloning site (MCS) 1 with the N-terminal 6xHis tag. Human Hsp90α was cloned into the second MCS, although due to a cloning error, Hsp90 lacked residue P2 (ΔP2). Site directed mutagenesis was used to change the F602S back to wild type. WT MBP-GRLBD was co-expressed with Hsp90 and FKBP52 and p23 on a second duet plasmid (pRSFDuet) with FKBP52 in the MCS1 and p23 in the MCS2, which was shown to reduce degradation (data not shown-Exp430). WT MBP-GRLBD was purified the same as above with the exception that 0.04% CHAPS was in all buffers.

Example purification: MBP-GRLBD (F602S)-Exp584, MBP-GRLBD WT- Exp646, GRLBD (F602S)- Exp890 and 522

Hsp90

Human Hsp90α was expressed in the pET151 bacterial expression plasmid with a Tev cleavable 6x His-tag. Proteins were expressed in bacterial BL21 star (DE3) strain. Cells were grown in LB at 37°C until OD_{600} reached 0.7-0.8, at which point cells were induced with 0.5mM IPTG overnight at 16°C. Cells were harvested and lysed in 50mM Phosphate-KCl pH8, 500mM KCl, 6mM β-mercaptoethanol (βME), 0.2mM PMSF and 5mM imidazole using a EmilsiFlex-C3 (Avestin). Lysate was centrifuged and the soluble fraction was affinity purified by gravity column with Ni-NTA affinity resin (QIAGEN). Protien was first batch bound to about 1mL resin per liter of culture for 2 hours, and the flow was removed

by gravity. The column was then washed with 2-4 column volumes of 30mM Tris pH8, 500mM KCl, 2mM ATP, 5mM $MgCl_2$, 0.1% Tween20, 6mM β-mercaptoethanol (βME), followed by 2-3 column volumes of 30mM Tris pH8, 500mM KCl, and 6mM β-mercaptoethanol (βME). The protein was eluted with 30mM Tris pH8, 50mM KCl, 6mM βME, and 300mM imidazole.

Eluted protein was then loaded onto an ion exchange column, MonoQ 10/100 GL (GE Healthcare) with 30mM Tris pH8, 50mM KCl, 6mM βME and eluted with a linear gradient of 50-500mM KCl over 8-10 column volumes. The MonoQ step is crucial for separating the full length Hsp90 from a degradation product. Full length Hsp90 elutes in the later of the two peaks. The 6x-His tag was cleaved off with TEV protease during the following overnight dialysis in 30mM Tris pH7.5, 150mM KCl, 6mM βME. Cleaved protein was further purified by size exclusion in 30mM Tris pH7.5, 500mM KCl, 6mM βME using a Superdex S200 16/60 (GE Healthcare). The purified protein was then dialyzed overnight into a storage buffer of 30mM HEPES pH 7.5, 50mM KCl, 1mM DTT, and 10% Glycerol, concentrated, flash frozen, and stored in aliquots at −80°C.

Example purifications: Exp631

Hsp40, Hop and p23

Human Hop, human p23, and yeast Hsp40 (Ydj1) were expressed in the pET151 bacterial expression plasmid with a cleavable 6x His-tag. Typically, proteins were expressed and purified by the following procedure. Proteins were expressed in bacterial BL21 star (DE3) strain. Cells were grown in LB at 37°C until OD_{600} reached 0.7-0.8, at which point cells were induced with 1mM IPTG for 3 hours at 37°C or overnight at 16°C. Cells

were harvested and lysed in 50mM Tris pH8, 300mM KCl, 6mM β-mercaptoethanol (βME), 0.2mM PMSF and 10mM imidazole using a EmilsiFlex-C3 (Avestin). Lysate was centrifuged and the soluble fraction was affinity purified by gravity column with Ni-NTA affinity resin (QIAGEN). The protein was eluted with 30mM Tris pH8, 50mM KCl, 6mM βME, and 300mM imidazole. Eluted protein was then loaded onto an ion exchange column, MonoQ 10/100 GL (GE Healthcare) with 30mM Tris pH8, 50mM KCl, 6mM βME and eluted with a linear gradient of 50-500mM KCl. The 6x-His tag was cleaved off with TEV protease during the following overnight dialysis in 30mM Tris pH7.5, 150mM KCl, 6mM βME. Cleaved protein was further purified by size exclusion in 30mM Tris pH7.5, 500mM KCl, 6mM βME using a Superdex S200 16/60 (GE Healthcare) or Superdex S75 16/60 (GE Healthcare) for p23. The purified protein was then dialyzed overnight into a storage buffer of 30mM HEPES pH 7.5, 50mM KCl, 1mM DTT, and 10% Glycerol, concentrated, flash frozen, and stored in aliquots at −80°C.

Example purifications: Hop-Exp603, p23-Exp602, Hsp40-Exp785

Hsp70

The gene for full length human Hsp70 (HSPA1A) was purchased from GeneCopoeia and cloned into the pET151 plasmid with the TEV cleavable 6x His-tag. Hsp70 was expressed and purified the same described with the following modifications. An extra wash step with 0.1% Tween20 and 2mM ATP was added to the Ni-NTA column and the elution was loaded straight onto an ion exchange column (Q Sepharose, GE Healthcare). The first of the two Hsp70 peaks was collected and TEV cleaved overnight. The cleaved protein was then purified on a Superdex S200 16/60 (GE Healthcare) and only the monomeric peak

was collected. The protein was buffer exchanged on a HiTrap desalting column (GE Healthcare) into storage buffer with 5mM $MgCl_2$. Since the presence of residue nucleotide was detected by the ratio of 260 vs 280 nm absorption, the protein concentration was determined by Bradford assay. While only the monomeric protein peak was pooled off the S200, investigation of the stored protein by analytical gel filtration with an inline multi-angel light scatter detector revealed the reappearance of the dimers in protein stocks (data not shown). While relative amounts of dimer varied slightly between purifications, there were no noticeable differences in the GRLBD ligand binding inhibition that correlated with the monomer and dimer distributions.

Example purification: Exp482

sf9 sp70 for Cryo-EM

For cryo-EM Hsp70 was purified from baculovirus infected Sf9 cell pellets expressing human Hsp70, which were produced at the Baculovirus/Monoclonal Antibody Facility at Baylor College of Medicine. Cells were lysed in 20mM Tris7.5, 20mM KCl, 1mM EDTA, and 1mM DTT and loaded onto an ion exchange HiPrep 16/60 Q FF column (GE Healthcare). Protein was eluted with a linear gradient of 20-500mM KCl, and then affinity purified by ATP agarose (N-6 attachment) gravity column (Sigma). Protein was eluted in 20mM Tris7.5, 20mM KCl, 1mM EDTA, 20mM ATP/$MgCl_2$ and 10mM βME, and then further purified as the bacteria expressed Hsp70 starting with the S200 SEC column.

Example purification: Exp553

Bag-1

The human gene for the Bag-1 isoform, Bag-1M (71-345), was obtained from the Protein Structure Initiative Material Repository (Cormier et al., 2010). The 26 kDa fragment corresponding to the Bag-1 isoform (116-345) was cloned into a modified pET28a vector with an N-terminal TEV cleavable 6x His tag. Protein was expressed and purified using a standard purification procedure as described for Hop.
Example purification: Exp690

Smyd2

A synthetic gene for human Smyd2 was codon optimized for bacterial expression (GeneArt) and cloned into the pET-151-D topo vector with a Tev cleavable 6x His-tag.
Example purification: Exp171

FKBP52 and FKBP51

A synthetic gene for human FKBP52 was codon optimized for bacterial expression (GeneArt) and the human gene for FKBP51 was obtained from the Protein Structure Initiative Material Repository (Cormier et al., 2010). Both FKBP51 and FKBP51 were cloned into the pET-151-D topo vector with a Tev cleavable 6x His-tag. Proteins were expressed and purified using a standard purification procedure as described for Hop.
Example purification: FKBP51-Exp477, and FKBP52- Exp243

References

Cormier, C.Y., Mohr, S.E., Zuo, D., Hu, Y., Rolfs, A., Kramer, J., Taycher, E., Kelley, F., Fiacco, M., Turnbull, G., et al. (2010). Protein Structure Initiative Material Repository: an open shared public resource of structural genomics plasmids for the biological community. Nucleic Acids Res. *38*, D743–D749.

Table 1. Chaperone and cochaperone constructs

Ref#	Chaperone Constructs	Mutations		Vector	Marker	Tag/Protease	Source	Lab Book Ref.
73	VECTOR			p28a derivative	Kan	His/Tev	L. Montabana (Agard)	EK6-p53
88	Hsp40 (YDJ1)	WT	y	pET151-D Topo	Amp	His/Tev	Dan Southworth	
87	Hsp70	WT	h	pET151-D Topo	Amp	His/Tev	Klim Verba (Agard)	EK6-111
90	Hsp70 SBD	SBD (390-641)	h	pET151-D Topo	Amp	His/Tev	EK	EK7-31
113	Hsp70	K112A	h	pET151-D Topo	Amp	His/Tev	EK	EK9-p103
114	Hsp70	K49A	h	pET151-D Topo	Amp	His/Tev	EK	EK9-p105
115	Hsp70	K102A/K108A/K112A	h	pET151-D Topo	Amp	His/Tev	EK	EK9-p105
5	p23	WT	h	pET151-D Topo	Amp	His/Tev	Dan Southworth	
79	HOP	WT	h	pET151-D Topo	Amp	His/Tev	Dan Southworth	
66	HOP	1b	h	pET151-D Topo	Amp	His/Tev	Dan Southworth	
67	HOP	2b	h	pET151-D Topo	Amp	His/Tev	Dan Southworth	
89	HOP	ΔTPR2B/DP2	h	pET151-D Topo	Amp	His/Tev	EK	EK7-21
119	HOP	ΔTPR1/DP1 (225-531)	h	pET151-D Topo	Amp	His/Tev	EK	EK10-105
94	Bag1	WT	h	pDONR201	Kan		DNASU-HsCD00081592	
107	Bag1-M	WT	h	pET28a	Kan	His/Tev	EK	
108	Bag1	WT	h	pET28a	Kan	His/Tev	EK	
109	HIP (St13)	WT	h	pENTR223	spectin.		DNASU-HsCD00073690	
6	FKBP52	WT	h	pET151-D Topo	Amp	His/Tev	Dan Southworth	
34	FKBP52	P199L	h	pET151-D Topo	Amp	His/Tev	EK	EK5-p24
78	FKBP51	WT	h	pDONR201	Kan		DNASU-HsCD00000271	
80	FKBP51	WT	h	pET151-D Topo	Amp	His/Tev	EK	EK6-p98
9	Smyd2	WT	h	pMK-RQ	Kan		GeneArt	
10	Smyd2	WT	h	pET151-D Topo	Amp	His/Tev	EK	EK3-p37
33	Smyd2	H341C	h	pET151-D Topo	Amp	His/Tev	EK	EK5- p21
35	Smyd2	S383C	h	pET151-D Topo	Amp	His/Tev	EK	
50	Smyd2	Y344C	h	pET151-D Topo	Amp	His/Tev	EK	EK5-128

h=human y=yeast r=rat

Table 2. Hsp90 constructs

Ref#	Hsp90 Constructs	Mutations		Vector	Marker	Tag/Protease	Source	Lab Book Ref.
4	Hsp90a	WT	h	pET151-D Topo	Amp	His/Tev	Dan Southworth	
7	Hsp90a-Mut2	M575A/I578D/L579A	h	pET151-D Topo	Amp	His/Tev	EK	EK2-p112
8	Hsp90a-Mut4	M610K/I613A/M614K	h	pET151-D Topo	Amp	His/Tev	EK	EK2-p112
25	Hsp90a-NM Domains	WT	h	pET151-D Topo	Amp	His/Tev	EK	EK3-p95
27	Hsp90a-MC Domains	WT-292-733	h	pET151-D Topo	Amp	His/Tev	EK	EK4-p35
29	Hsp90a- NTD	WT	h	pET151-D Topo	Amp	His/Tev	EK	EK4-p35
39	Hsp90a- CTD	569-732	h	pET151-D Topo	Amp	His/Tev	James Partrige (Agard)	
36	Hsp90a	K616A	h	pET151-D Topo	Amp	His/Tev	EK	
37	Hsp90a	T36A	h	pET151-D Topo	Amp	His/Tev	EK	
38	Hsp90a	T36E	h	pET151-D Topo	Amp	His/Tev	EK	
49	Hsp90a	E730C	h	pET151-D Topo	Amp	His/Tev	EK	EK5-128
91	Hsp90a	E47A	h	pET151-D Topo	Amp	His/Tev	EK	EK7-42
95	Hsp90a	D93N	h	pET151-D Topo	Amp	His/Tev	EK	EK8-28
97	Hsp90a	ΔMEEVD	h	pET151-D Topo	Amp	His/Tev	EK	EK8-42
116	Hsp90a	E527Q	h	pET151-D Topo	Amp	His/Tev	EK	EK9-p106
117	Hsp90a	Y528R	h	pET151-D Topo	Amp	His/Tev	EK	EK9-p117
118	Hsp90a	M610A/I613A/M614A	h	pET151-D Topo	Amp	His/Tev	EK	EK9-p115
28	NTD Chimera (N-y, MC-h)		h/y	pET151-D Topo	Amp	His/Tev	C. Cuningham (Agard)	
56	Chimera 6		h/y	pET151-D Topo	Amp	His/Tev	C. Cuningham (Agard)	EK5-p117
26	Hsp90b (codon opt.)	WT	h	pET151-D Topo	Amp	His/Tev	Dan Southworth	
105	Hsp90b (codon opt.)	E42A	h	pET151-D Topo	Amp	His/Tev	EK	EK8-138
106	Hsp90b (codon opt.)	D88N	h	pET151-D Topo	Amp	His/Tev	EK	EK8-138
68	Hsp90b Δ6C	cys free	h	pMK	Kan		GeneArt- (Dan S.)	
69	Hsp90b Δ6C	cys free, E70C	h	pMK	Kan		GeneArt- (Dan S.)	
70	Hsp90b Δ6C	cys free, Q397C	h	pMK	Kan		GeneArt- (Dan S.)	
71	Chimera6_ΔC	cys free	h/y	pMK-RQ	Kan		GeneArt- (Dan S.)	
72	Chimera6_ΔC	cys free, E70C	h/y	pMK	Kan		GeneArt- (Dan S.)	
74	Chimera6_ΔC	cys free, Q397C	h/y	pMK	Kan		GeneArt- (Dan S.)	
81	Hsp90b Δ6C	cys free	h	pET151-D Topo	Amp	His/Tev	EK	EK6-101
82	Hsp90b Δ6C	cys free, E70C	h	pET151-D Topo	Amp	His/Tev	EK	EK6-102
83	Hsp90b Δ6C	cys free, Q397C	h	pET151-D Topo	Amp	His/Tev	EK	EK6-104
84	Chimera6_ΔC	cys free	h/y	pET151-D Topo	Amp	His/Tev	EK	EK6-110
85	Chimera6_ΔC	cys free, E70C	h/y	pET151-D Topo	Amp	His/Tev	EK	EK6-95
86	Chimera6_ΔC	cys free, Q397C	h/y	pET151-D Topo	Amp	His/Tev	EK	
93	Hsc82	WT	y	pET151-D Topo	Amp	His/Tev	James Partrige (Agard)	
96	Hsc82	S51C	y	pET151-D Topo	Amp	His/Tev	EK	EK8-28
98	Hsc82	S51C/Q381C	y	pET151-D Topo	Amp	His/Tev	EK	EK8-55

Table 3. GR constructs

Ref#	GR Constructs	Mutations		Vector	Marker	Tag/Protease	Source	Lab Book Ref.
12	GR-gama (FL) (codon opt.)	F602S/C638D	h	pMK-RQ	Kan		GeneArt	
13	GR-alpha (FL) (codon opt.)	F602S/C638D	h	pMK-RQ	Kan		Miles P. (Yamamoto)	
40	GR-FL (human codons)	WT	h	pcDNA3	Amp		Miles P. (Yamamoto)	EK5-p116
1	VECTOR			pMal	Amp	His-MBP/3C	Kexin (Agard)	
14	HMBP-3C-GRLBD (521-777)	F602S/C638D	h	pMal	Amp	His-MBP/3C	EK	EK2-p31
16	HMBP-Throm-GRLBD (521-777)	F602S/C638D	h	pMal	Amp	His-MBP/Thromb	Miles P. (Yamamoto)	
15	HMBP-Tev-GRLBD (521-777)	F602S/C638D	h	pMal	Amp	His-MBP/Tev	Miles P. (Yamamoto)	
24	HMBP-Tev-GRLBD (521-777)	F602S/C638D/D626C	h	pMal	Amp	His-MBP/Tev	EK	
23	HMBP-Tev-GRLBD (521-777)	C638D/D626C	h	pMal	Amp	His-MBP/Tev	EK	EK3-p130
45	HMBP-Tev-GRLBD (521-777)	F602A/C638D	h	pMal	Amp	His-MBP/Tev	EK	EK5-126
46	HMBP-Tev-GRLBD (521-777)	F602L/C638D	h	pMal	Amp	His-MBP/Tev	EK	EK5-127
47	HMBP-Tev-GRLBD (521-777)	F602I/C638D	h	pMal	Amp	His-MBP/Tev	EK	EK5-127
58	HMBP-Tev-GRLBD (521-777)	C638D	h	pMal	Amp	His-MBP/Tev	EK	EK5-137
92	HMBP-Tev-GRLBD (521-777)	F602S	h	pMal	Amp	His-MBP/Tev	EK	EK7-p137
100	HMBP-Tev-GRLBD (521-777)	F602S/F606A	h	pMal	Amp	His-MBP/Tev	EK	EK8-p97
102	HMBP-Tev-GRLBD (521-777)	F602S/W557A	h	pMal	Amp	His-MBP/Tev	EK	EK8-p130
103	HMBP-Tev-GRLBD (521-777)	F602S/W610A	h	pMal	Amp	His-MBP/Tev	EK	EK8-p130
104	HMBP-Tev-GRLBD (521-777)	F602S/L669A	h	pMal	Amp	His-MBP/Tev	EK	EK8-p130
110	HMBP-Tev-GRLBD (521-777)	F602S/L532A	h	pMal	Amp	His-MBP/Tev	Zygy (Agard)	
111	HMBP-Tev-GRLBD (521-777)	F602S/V533A	h	pMal	Amp	His-MBP/Tev	Zygy (Agard)	
112	HMBP-Tev-GRLBD (521-777)	F602S/L532A/V533A	h	pMal	Amp	His-MBP/Tev	Zygy (Agard)	
17	H-3C-GRLBD (521-777)	F602S/C638D	h	pACYCDuet(Δ)	Cam	His/3C	Sam Pfaff. (Flett)	
18	H-Thromb-GRLBD (521-777)	F602S/C638D	h	pACYCDuet(Δ)	Cam	His/Thromb	Sam Pfaff. (Flett)	
30	H-Thromb-GRLBD (521-777)	F602S	h	pACYCDuet(Δ)	Cam	His/Thromb		
32	H-Thromb-GRLBD (521-777)	WT	h	pACYCDuet(Δ)	Cam	His/Thromb	EK	EK5-p19
31	H-Thromb-GRLBD (521-777)	F602S/C638D/M752I	h	pACYCDuet(Δ)	Cam	His/Thromb	Sam Pfaff. (Flett)	
101	H-Thromb-GRLBD (521-777)	F602S/F606A	h	pACYCDuet(Δ)	Cam	His/Thromb	EK	EK8-p97
63	His-Avitag-GRLBD (521-777)	F602S	h			His/Avitag	K. Kuchenbecker (Flett)	EK6-11
41	GR- GFP- DBD-LBD (385-777)	F602S/C638D	h	pET160	Amp	His-GFP/Thromb	Miles P. (Yamamoto)	EK5-p117-118
51	GR- GFP- DBD-LBD (385-777)	C638D	h	pET160	Amp	His-GFP/Thromb	EK	EK5-p129
54	GR- GFP- DBD-LBD (385-777)	F602S	h	pET160	Amp	His-GFP/Thromb	EK	EK5-130
42	GR- DBD-LBD (385-777)	F602S/C638D	h	pET28a	Kan	His/Thrombin	Miles P. (Yamamoto)	EK5-p119
52	GR- DBD-LBD (385-777)	C638D	h	pET28a	Kan	His/Thrombin	EK	EK5-p129
55	GR- DBD-LBD (385-777)	F602S	h	pET28a	Kan	His/Thrombin	EK	EK5-131
43	GR- MBP-DBD-LBD (440-795)	F602S(?)	rat	pET28a	Kan	His/Tev	Miles P. (Yamamoto)	
44	GR- GB1-DBD-LBD (440-795)	F602S	rat	pET41a	Kan	His-GB1/Tev	Miles P. (Yamamoto)	EK-p118
75	GR (27-777)	F602S/C638D	h	pET160	Amp	His/Thromb	Miles P. (Yamamoto)	
76	GR (27-777)	F602S/C638D	h	pET28a	Kan	His/Thromb	Miles P. (Yamamoto)	
77	GR	F602S/C638D	h	pET160	Amp	His/Thromb	Miles P. (Yamamoto)	
99	p2A/GRGZ- GR for yeast reporter	WT	rat		Amp		Mikko- Lindquist Lab	

Table 4. Co-expression Constructs

Ref#	Duet Expression Constructs	Mutations		Vector	Marker	Tag/Protease	Source	Lab Book Ref.
2	VECTOR			pETDuet-1	Amp		Kexin (Agard)	
3	VECTOR			pRSFDuet	Kan		Kexin (Agard)	
19	p23(MCS2)	WT	h	pRSFDuet	Kan		EK	EK2-p96
20	FKBP52 + p23	WT	h	pRSFDuet	Kan		EK	EK2-p118
21	Hsp90a (MCS2)	ΔP2	h	pETDuet-1	Amp		EK	EK2-p140/EK5-p139
62	Hsp90a (MCS2)	WT	h	pETDuet-1	Amp		EK	EK5-p142
22	HMBP-3C-GRLBD + Hsp90a	F602S/C638D (90-ΔP2)	h	pETDuet-1	Amp		EK	EK2-p44/p140
53	HMBP-3C-GRLBD + Hsp90a	F602S (90-ΔP2)	h	pETDuet-1	Amp		EK	EK5-p130
64	HMBP-3C-GRLBD + Hsp90a	WT (90-ΔP2)	h	pETDuet-1	Amp		EK	EK6-p31
48	HMBP-3C-GRLBD + Hsp90a	F602I/C638D (90-ΔP2)	h	pETDuet-1	Amp		EK	EK5-128
57	HMBP-3C-GRLBD + Hsp90a	F602A/C638D (90-ΔP2)	h	pETDuet-1	Amp		EK	EK5-p137
59	HMBP-3C-GRLBD + Hsp90a	F602L/C638D (90-ΔP2)	h	pETDuet-1	Amp			EK5-p140
60	HMBP-3C-GRLBD + Hsp90a	F602L (90-ΔP2)	h	pETDuet-1	Amp			EK5-p140
61	HMBP-3C-GRLBD + Hsp90a	F602S (90-ΔP2)	h	pETDuet-1	Amp		EK	EK5-p141
65	HMBP-3C-GRLBD + Hsp90a	WT (90-ΔP2)	h	pETDuet-1	Amp		EK	

Section 3: Attempts at identifying Hsp70 binding site on GRLBD

Preface

The crystal structure of Hsp70 SBD bound to a substrate peptide revealed the structural basis for Hsp70's preference for hydrophobic hepatapeptides. In the crystal structure, the seven amino acid NRLLLTG substrate peptide binds in a completely extended conformation with the central fourth peptide residue (L^4) buried in a deep hydrophobic pocket in the binding site (Zhu et al., 1996). The binding interaction is then mostly mediated by hydrophobic interactions between the other central hydrophobic residues. Additionally, the substrate binding site is flanked with negatively charged patches, resulting in a preference for hydrophobic residues flanked with positively charged residues.

Peptide screen- hydrophobic core 4-5 residues flanked with residues enriched with basic residues.- allowed for prediction algorithm (Rüdiger et al., 1997)
In the most recent iteration of binding site prediction algorithm, LIMBO, combines sequence information from peptide binding experiments with structural parameters obtained from homology modeling (Van Durme et al., 2009).

Summary

The sequence for GRLBD was analyzed with LIMBO, and seven sites above the stringent threshold were predicted to be Hsp70 binding sites (Figure 1A). Of these, the two highest scoring binding regions were picked for experimental investigation. Of particular interests was the region in the core of the GRLBD that consists of three overlapping binding sites, two of which contain the F602 residue.

A

LIMBO Results for GRLBD

	Position	Sequence	Score
*	557-563	WRIMTTL	18.3
*	600-606	WMFLMAF	19.0
	601-607	MFLMAFA	15.3
	605-611	AFALGWR	19.0
	668-674	TLLLLSS	14.1
	688-694	EIRMTYI	13.0
	770-776	KKLLFHQ	16.4

B

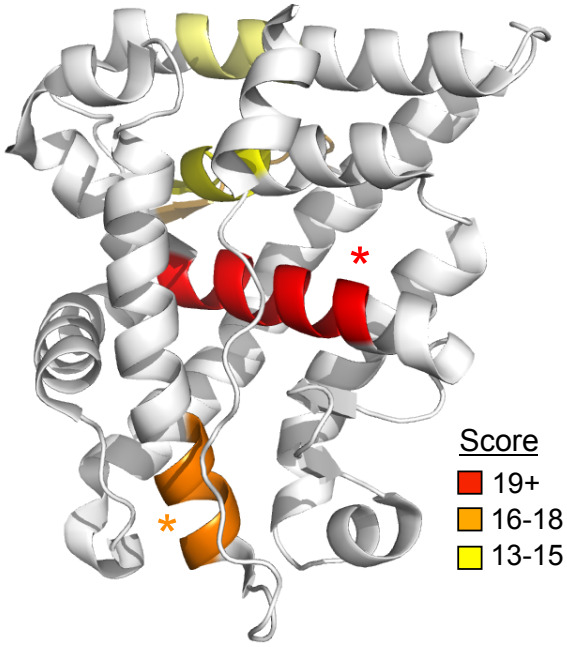

Figure 1. LIMBO predicted Hsp70 binding sites on GRLBD.
A) LIMBO scores for predicted Hsp70 binding sites on GRLBD
B) Predicted Hsp70 binding sites from (A) mapped onto the crystal structure of GRLBD (pdb 1M2Z) with color code according to the score as indicated.

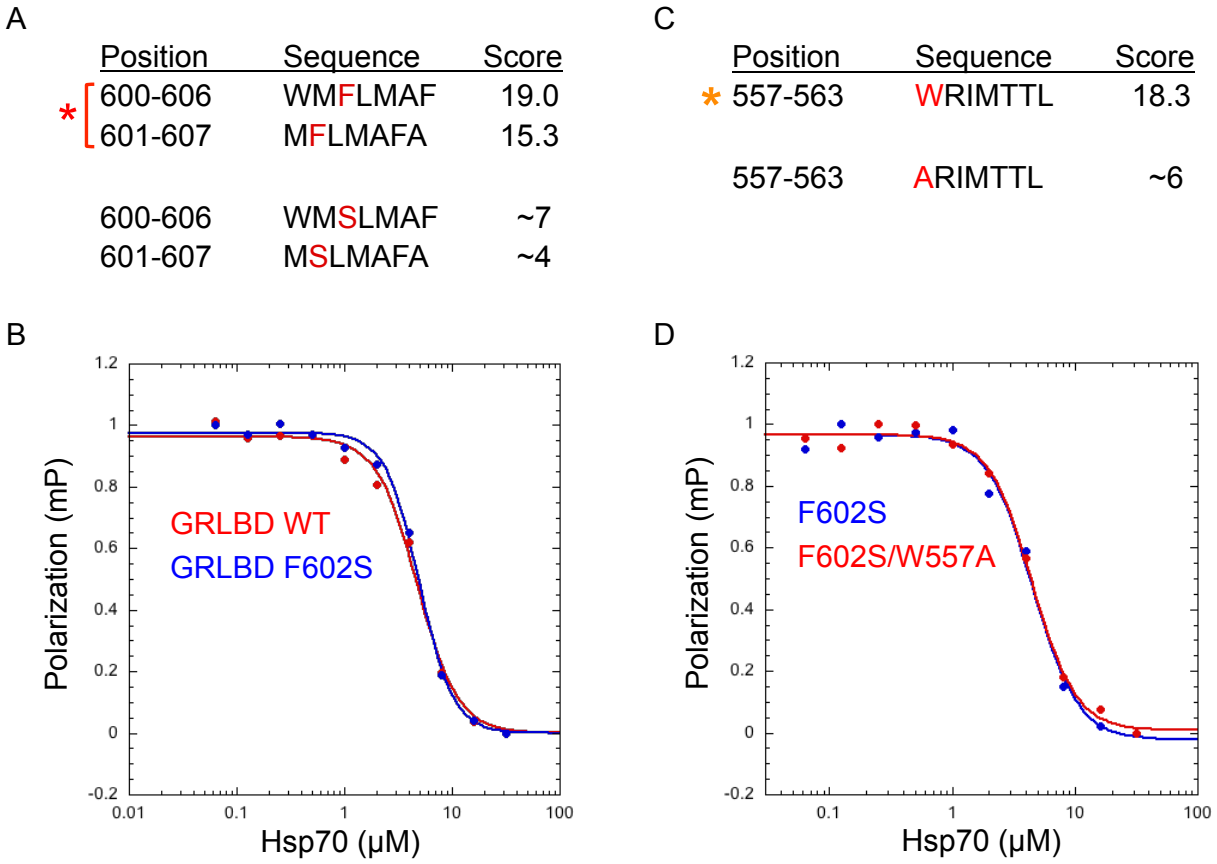

Figure 2. Mutations to the top two LIMBO Hsp70 binding sites have no effect on Hps70 inhibition of GRLBD.
A) Top scoring site consists of two overlapping Hsp70 binding sites, both of which contain the F602, with the F602S mutation significantly impacting the Hsp70 binding score, with the WT predicted to have a very favorable interaction, and the F602S mutation disfavoring Hsp70 binding.
B) IC_{50} curve for GRLBD ligand binding inhibition by Hsp70 for GRLBD F602S (blue) and WT (red). Assay conditions: 1μM MBP-GRLBD, 20nM F-dex, 2μM Hsp40, and varying concentrations of Hsp70. Inhibition curve fit to a cooperative competitive binding model. (Exp651)
C) Second highest scoring Hsp70 binding region on GRLBD (557-563). W557A mutation was predicted to significantly inhibit Hsp70 binding to this site.
D) IC_{50} curve for GRLBD ligand binding inhibition by Hsp70 for GRLBD F602S (blue) and F602S/W557A (red). Same conditions as in (B). (Exp709)

References

Rüdiger, S., Germeroth, L., Schneider-Mergener, J., and Bukau, B. (1997). Substrate specificity of the DnaK chaperone determined by screening cellulose-bound peptide libraries. Embo J. *16*, 1501–1507.

Van Durme, J., Maurer-Stroh, S., Gallardo, R., Wilkinson, H., Rousseau, F., and Schymkowitz, J. (2009). Accurate Prediction of DnaK-Peptide Binding via Homology Modelling and Experimental Data. PLoS Comput. Biol. *5*, e1000475.

Zhu, X., Zhao, X., Burkholder, W.F., Gragerov, A., Ogata, C.M., Gottesman, M.E., and Hendrickson, W.A. (1996). Structural Analysis of Substrate Binding by the Molecular Chaperone DnaK. Science, New Series *272*, 1606–1614.

Section 4: Unusual GRLBD behavior observed from 2009 to 2010

Summary

From when I first obtained workable apo MBP-GRLBD that was expressed with ligand in February 2009 until March 2010, the apo MBP-GRLBD exhibited an unusual ligand binding behavior. For the ligand association kinetics there was a lag phase observed at lower GRLBD concentrations, which suggested a two-step binding model (Figure 1A). Additionally, the equilibrium ligand binding fit a cooperative binding model with a Hill coefficient of about 2 (Figure 1C). Intriguingly, addition of Hsp90 had a dramatic effect on this GRLBD ligand binding behavior. For the association kinetics, Hsp90 accelerated the ligand association by removing the lag phase such that a single-phase association curve was observed (Figure 1B). For GRLBD ligand binding equilibrium, Hsp90 enhanced the K_D and converted the cooperative binding curve to a regular single-site binding model (Figure 1C).

This ligand binding behavior could be explained by a model in which GRLBD existed in at least two distinct states, in which only one of the states is active and able to bind ligand, referred to as the GR* state (Figure 1D). The lag phase observed for GR alone could be explained by the time required for the conversion of the inactive GR molecules to the active GR* state. Due to the low concentration of ligand compared to the GRLBD

concentration, at higher concentrations of GRLBD there would be a sufficient amount of the active GR* population compared to ligand such that the inactive population would be negligible and a lag phase would not be detected. The loss of the lag phase in the association kinetics observed with Hsp90 could be explained by Hsp90 acting to convert the inactive GR molecules to the active GR* state. The cooperativity in the equilibrium ligand binding for GRLDB alone is intriguing as it suggested that GRLBDs could dimerize, with the dimerization interaction resulting in the conversion of an inactive GRLBD to the active GR* state. Given that trace amounts of GRLBD dimers could then (and now) be detected (Chapter 2, Figure 3), this seemed a possible explanation.

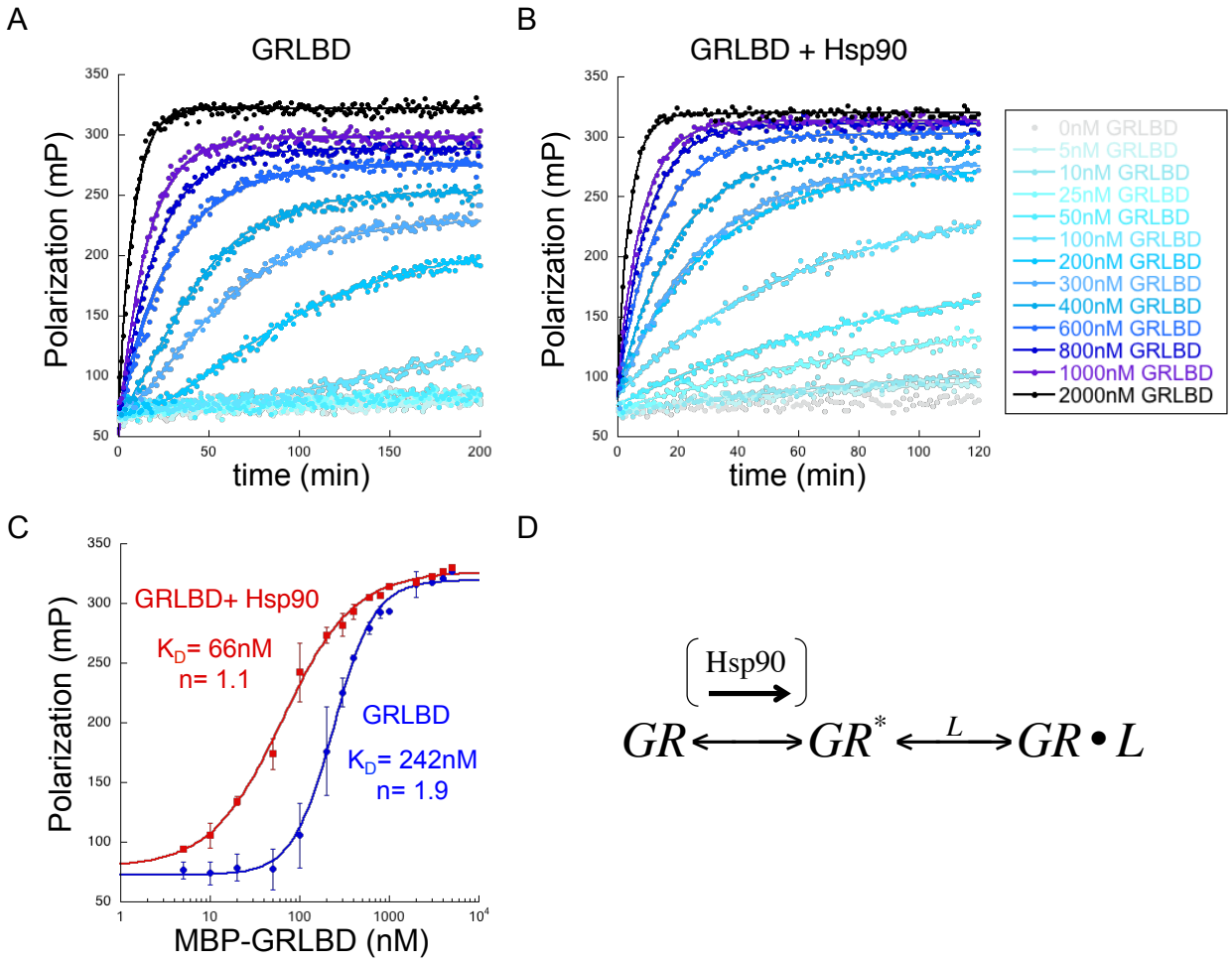

Figure 1. Hsp90 dramatically changes GRLBD ligand binding behavior.
A) GRLBD ligand association kinetics of 20nM F-dex to varying MBP-GRLBD concentrations. (Exp215)
B) GRLBD ligand association kinetics as in A, but with 1μM Hsp90. (Exp215)
C) GRLBD equilibrium ligand binding to 20nM F-dex at varying MBP-GRLBD concentration for GRLBD alone (blue) and with 1μM Hsp90. Curves were fit with a two site binding model. Not only does Hsp90 improve GRLBD ligand affinity by 3-4 fold, but also changes the binding mode from a cooperative binding mode with a hill coefficient of ~2 to a non-cooperative binding mode with a hill coefficient of ~1. (Exp264)
D) Mechanistic model that fits the unusual GRLBD binding behavior. GRLBD exists in at least two states in which only one specific state can binding ligand (GR*). Hsp90 converts the inactive GR population to the GR* state that can bind ligand (L).

The affinity range for the Hsp90 effect was considerably tight, titrating around 200-300nM (Figure 2). Additionally, this effect was specific to the human Hsp90 homologue, with the yeast Hsp90 homologue (Hsc82) being significantly less effective than human, and the bacterial homologue (HtpG) showing no detectable enhancement in GRLBD ligand binding (Figure 3A). Exploiting the significant difference in the observed effect between the human and yeast Hsp90s, the yeast and human chimera constructs designed and created by Christian Cunningham (Figure 3C) were utilized to determine that mostly the MD and partially the CTD of Hsp90 were responsible for the difference, with the NTD chimera behaving identical to the WT human Hsp90 (Figure 3B).

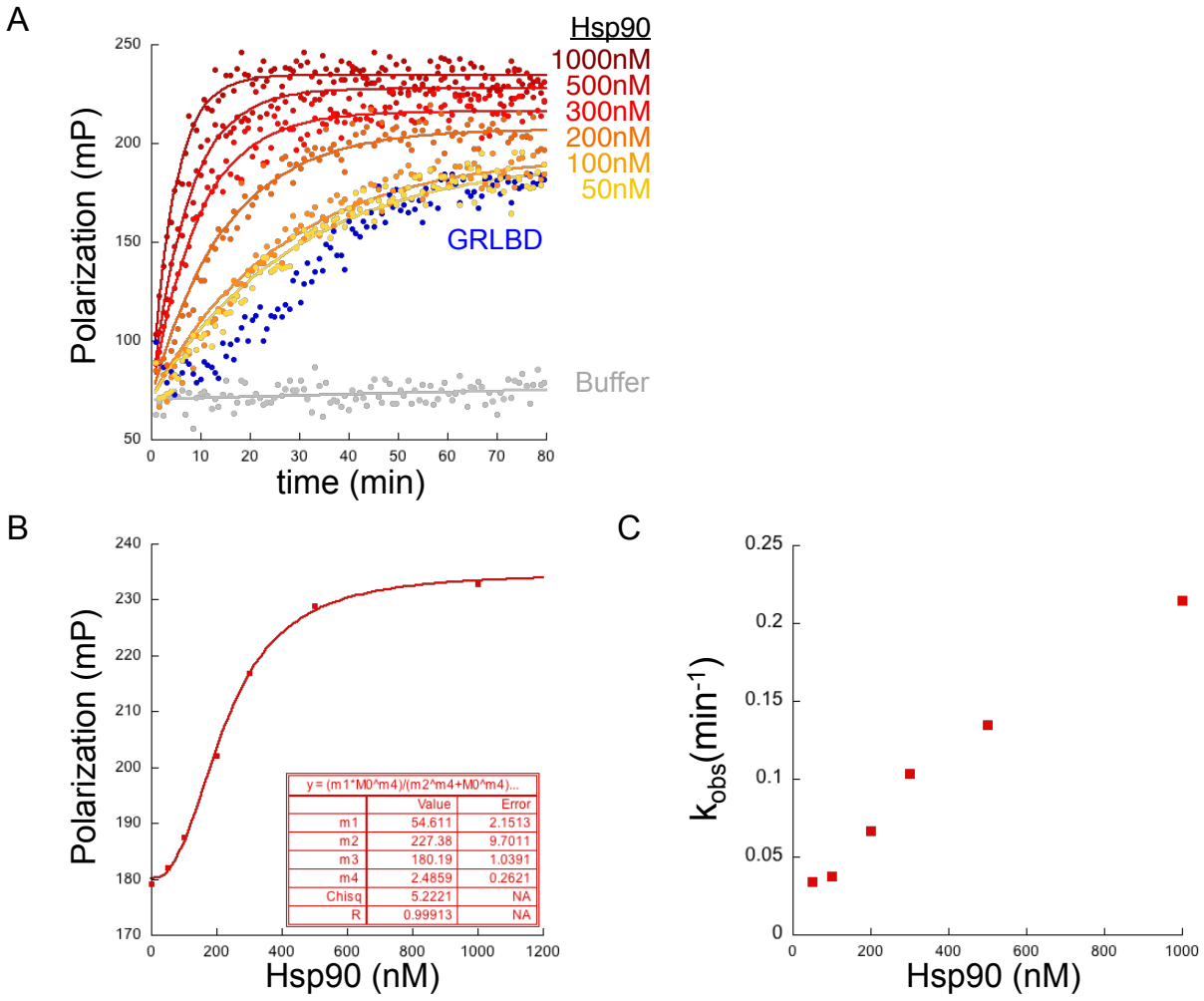

Figure 2. Hsp90 concentration dependence for modulation of GRLBD ligand binding behavior.

A) GRLBD ligand association kinetics of 20nM F-dex to 300nM MBP-GRLBD alone (blue) and with varying concentrations of Hsp90. (Exp97)

B) Plateau values from A plotted against Hsp90 concentration. Curve is fit with a half-maximal binding model indicating an approximate K_D of 230nM.

C) Association rates (k_{obs}) from A plotted against Hsp90 concentration.

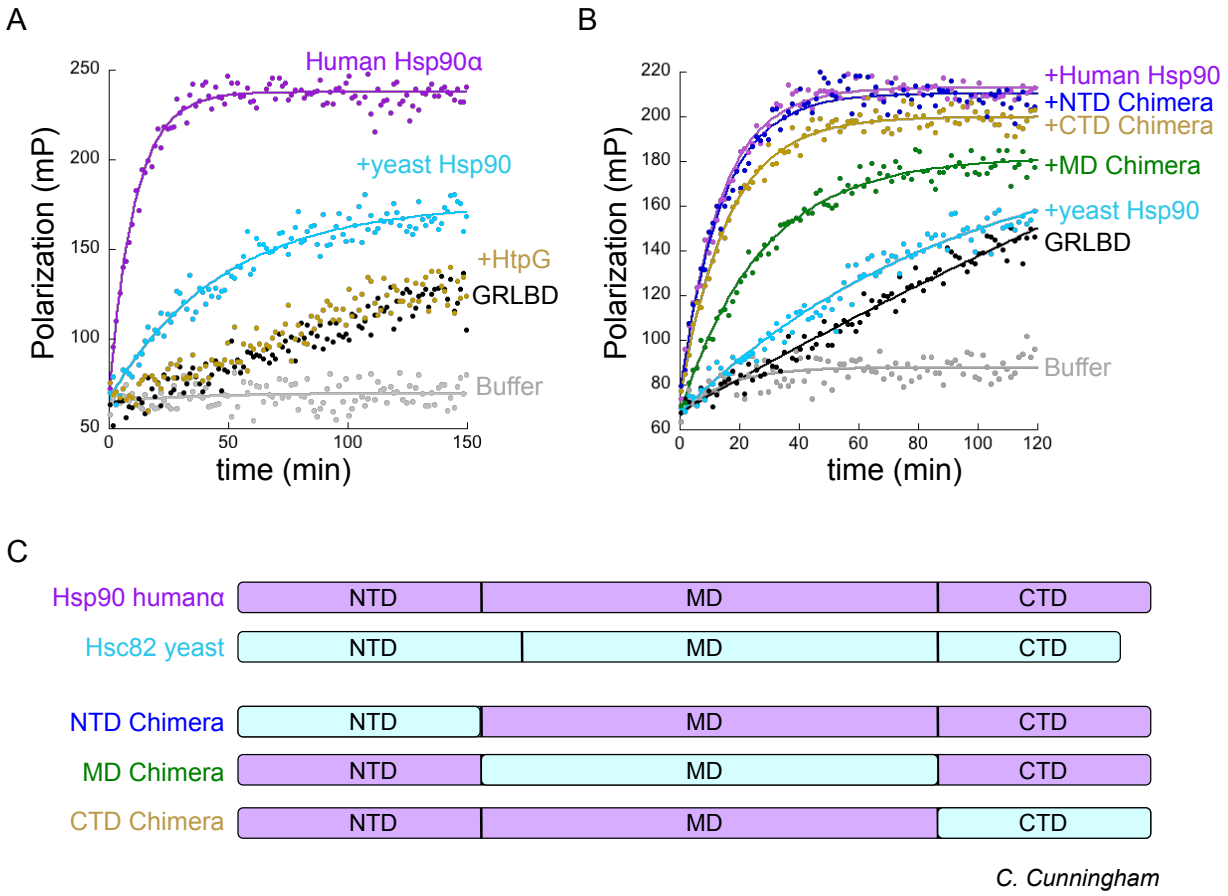

Figure 3. Modulation of GRLBD ligand binding behavior is specific to human Hsp90.
A) GRLBD ligand association kinetics of 10nM F-dex to 100nM MBP-GRLBD alone (balck) and with 1μM bacterial Hsp90 (HptG) in tan, yeast Hsp90 (Hsc82) in blue, and human Hsp90 (Hsp90α) in purple. (Exp175)
B) GRLBD ligand association kinetics of 20nM F-dex to 100nM MBP-GRLBD alone (balck) and with yeast Hsp90 WT (light blue), human Hsp90 WT (purple), NTD chimera (dark blue), MD chimera (green), and CTD chimera (tan). Hsp90 chimeras were provided by Christian Cunningham. (Exp190)
C) Diagram indicating domain composition of the yeast/human Hsp90 chimeras used in B. The NTD chimera contains the NTD of yeast with the MD and CTD of human. The MD chimera contains the MD of yeast with the NTD and CTD of human. The CTD chimera contains the CTD of yeast with the NTD and MD of human.

Surprisingly, I was unable to detect any significant difference in the Hsp90 effect upon the addition of nucleotides or 17AAG, indicating that this effect was entirely independent of ATP hydrolysis or the nucleotide state (data not shown). Furthermore,

while several proteins such as HtpG and p23 had no effect even at high protein concentrations, I began to discover that some proteins other than Hsp90 that included Hop, FKBP52 and Smyd2, had a similar effect, although with varying potencies that were less than human Hsp90 (data not shown).

Nevertheless, very suddenly, the unusual GRLBD behavior ceased, with GRLBD by itself behaving as it did when Hsp90 was around, such that there was no longer an Hsp90 effect. Essentially, it was as if there was no longer any inactive GR and that all the GR now existed in the GR* state. Unfortunately, I was never able to determine what the origin of this unusual behavior was. Since the change was observed using the same frozen protein stocks, it could not have been due to the protein source itself, and had to have been due to some other factor that was either causing a shift in the GR population to the inactive GR state or was causing some sort of unusual experimental artifact that was effected by more general physical properties of some proteins but not others.

Publishing Agreement

It is the policy of the University to encourage the distribution of all theses, dissertations, and manuscripts. Copies of all UCSF theses, dissertations, and manuscripts will be routed to the library via the Graduate Division. The library will make all theses, dissertations, and manuscripts accessible to the public and will preserve these to the best of their abilities, in perpetuity.

Please sign the following statement:

I hereby grant permission to the Graduate Division of the University of California, San Francisco to release copies of my thesis, dissertation, or manuscript to the Campus Library to provide access and preservation, in whole or in part, in perpetuity.

Elaine C Kirschke
Author Signature

01/08/2015
Date